Investigations for an improved Large Scale Topographic Mapping in Indonesia

Winhard Tampubolon

Vollständiger Abdruck der von der Fakultät für Informatik der Universität der Bundeswehr München zur Erlangung des akademischen Grades

Doktor Ingenieur (Dr.-Ing.)

genehmigten Dissertation.

Gutachter:

1. Univ.-Prof. Dr.-Ing. Wolfgang Reinhardt

2. Prof. Dr.-Ing. Franz-Josef Behr

Die Dissertation wurde am 14.11.2019 bei der Universität der Bundeswehr München eingereicht und durch die Fakultät für Informatik am 08.01.2020 angenommen. Die mündliche Prüfung fand am 22.01.2020 statt.

Abstract

The recent legislation Act Nr.4/2011 about Geospatial Information in Indonesia gives exclusive authority to the Geospatial Information Agency of Indonesia (BIG) as the only responsible institution providing the official topographic map of Indonesia. It must cover 1.9 million square kilometers land area of Indonesia which is approximately more than 5 times the land area of Germany. This governmental act opens an opportunity and a challenge for the geospatial data production especially to support the economic development in Indonesia. In that case, the appropriate technologies and methodologies have to be integrated and synchronized to speed up the huge topographic mapping volume in particular for Large Scale Topographic Mapping (LSTM) i.e. equal or larger than 1:10,000.

Space borne radar is a reliable technology nowadays to provide base data for topographic mapping. Its flexibility and weather independency make radar data more attractive in comparison with the traditional airborne data acquisition. On the other hand, the Unmanned Aerial Vehicle (UAV) data is also widely used as a potential source to produce high resolution geospatial data. These aforementioned advantages emplace both radar and UAV data as alternative sources for many applications including LSTM.

Currently, the available TerraSAR-X add on Digital Elevation Model X (TanDEM-X) Intermediate Digital Elevation Model (IDEM) from German Aerospace Center (DLR) as one useful global scientific data set however still complies with High Resolution Terrain Information (HRTI) level 3 only. The accuracy of the end product of pairwise bi-static TanDEM-X data in a what so called the Interferometric Synthetic Aperture Radar (InSAR) data processing can be improved by some potential measures such as the incorporation of Ground Control Points (GCPs) and Digital Elevation Model (DEM) reference taken from UAV.

Therefore it is necessary to find the optimal solution for the InSAR DEM generation with a proper adjustment model. In this dissertation, a new algorithm using both, UAV and TanDEM-X radar data is introduced to process the bi-static TanDEM-X datasets and to investigate how this method improves the accuracy of the generated DEM. As InSAR data processing relies on accurate GCPs and/or DEM reference data, the Indonesian Geospatial Reference System (SRGI) is used as a national framework of the investigations.

Subsequently, the DEM generated using the Sentinel Application Platform (SNAP) desktop, is the main product used for LSTM. This DEM has to be assessed using Independent Check Points (ICPs) derived e.g. from conventional airborne data acquisition using metric camera and the accuracy is compared also with the accuracy of the IDEM. Summarized, this dissertation aims on an improvement of LSTM by using UAV and TanDEM-X data e.g. through the introduced linearized model of InSAR data processing.

Kurzfassung

Das Gesetz Nr.4/2011 über Geodaten in Indonesien gibt der Indonesischer Geodatenagentur (BIG) als einziger verantwortlicher Stelle das Recht, offizielle topografische Kartendaten Indonesiens zur Verfügung zu stellen. Die Landfläche Indonesiens umfasst ca 1,9 Millionen Quadratkilometer, was ungefähr dem Fünffachen der Landfläche Deutschlands entspricht. Dieses Regierungsgesetz eröffnet der Geodatenproduktion eine Chance und Herausforderung, insbesondere, um die wirtschaftliche Entwicklung in Indonesien zu unterstützen. In diesem Fall müssen die richtigen Technologien und Methoden integriert werden, um das äußerst umfangreiche topografische Kartenprogramm in verschiedenen Kartenmaßstäben zu beschleunigen, und zwar speziell für topografische Karten in großem Maßstab (Large Scale Topographic Mapping, LSTM), d. h. gleich oder größer als 1: 10,000.

Radaraufnahmen von satellitengetragenen Sensoren sind eine mögliche zuverlässige Technologie zur Bereitstellung von Basisdaten für die topografische Kartierung. Aufgrund seiner Flexibilität und Wetterunabhängigkeit sind Radardaten im Vergleich zur herkömmlichen Datenerfassung in der Luft attraktiver. Andererseits werden unbemannte Luftfahrzeugdaten (Unmanned Aerial Vehicle, UAV) auch häufig als potenzielle Datenquelle zur Erzeugung der geneue Geodaten verwendet. Diese vorgenannten Vorteile stellen sowohl Radar- als auch UAV-Daten als alternative Quellen für viele Anwendungen einschließlich LSTM dar. Das verfügbare TerraSAR-X add on Digital Elevation Model-X Band (TanDEM-X) Intermediate Digital Elevation Model (IDEM) des Deutschen Zentrums für Luft- und Raumfahrt (DLR) als ein nützlicher globaler wissenschaftlicher Datensatz entspricht jedoch weiterhin der High Resolution Terrain Information (HRTI) Level 3.

Die Genauigkeit des aus den paarweisen bi-statischen TanDEM-X-Daten abgeleiteten Endprodukts kann durch einige potenzielle Maßnahmen verbessert werden, z. B. durch die Verwendung von Passpunkten (Ground Control Points, GCPs) und DEM-Referenzen aus partiellen UAV-Aufnahmen bei der InSAR (Interferometric Synthetic Aperture Radar)-Daten-prozessierung. Daher ist es notwendig, die optimale Lösung mit einem geeigneten Auswertemodell zu finden. In dieser Dissertation wird ein neuer Algorithmus unter Verwendung von UAV- und TanDEM-X-Radardaten vorgestellt, um die bistatischen TanDEM-X-Datensätze zu verarbeiten und zu untersuchen, wie dies die Genauigkeit der generierten Geländemodelle verbessert. Da die interferometrische Radardatenverarbeitung auf genauen GCPs und-/-oder Geländemodell-Referenzdaten beruht, wird für die Untersuchungen das Indonesian Geospatial Reference System (SRGI) verwendet.

Anschließend ist das mit dem Software-Werkzeug SNAP-Desktop (Sentinel Application Platform) generierte Geländemodell das Hauptprodukt für LSTM. Dieses Geländemodell muss anhand von Kontrollpunkten bewertet werden, die z.B. aus der konventionellen Luftdatenerfassung mit einer metrischen Kamera abgeleitet wurden. Die erreichte Genauigkeit wird mit der Genauigkeit des IDEM verglichen. Zusammenfassend zielt diese Dissertation auf eine Verbesserung des LSTM durch Verwendung von UAV- und TanDEM-X-Daten ab.

Table of Contents

List of Figures

List of Tables

Abbreviations

AGL	Above Ground Level
BIG	Geospatial Information Agency of Indonesia
CE	Circular Error
CORS	Continuous Operating Reference System
Co-SSC	Coregistered Single-look Slant-range Complex
CMAS	Circular Mapping Accuracy Standard
DEM	Digital Elevation Model
D-InSAR	Differential Interferometric Synthetic Aperture Radar
DLR	German Aerospace Center
DM	Disaster Management
DSM	Digital Surface Model
DTM	Digital Terrain Model
GCP	Ground Control Point
GIS	Geographical Information System
GNSS	Global Navigation Satellite System
GPS	Global Positioning System
GSD	Ground Sampling Distance
HOA	Height of Ambiguity
HRTI	High Resolution Terrain Information
ICP	Independent Check Point
IDEM	Intermediate Digital Elevation Model
Ina-SDI	Indonesian Spatial Data Infrastructure
InSAR	Interferometric Synthetic Aperture Radar
LE	Linear Error
LSTM	Large Scale Topographic Mapping
MSL	Mean Sea Level
NMA	National Mapping Agency
NMAS	National Mapping Accuracy Standard
NSDI	National Spatial Data Infrastructure
NSSDA	National Standard for Spatial Data Accuracy

ORRI	Ortho Rectified Radar Imagery
PDF	Probability Density Function
PU	Phase Unwrapping
RMSE	Root Mean Square Error
SNAP	Sentinel Application Platform
SOP	Standard Operating Procedure
SRGI	Geospatial Reference System of Indonesia
SRTM	Shuttle Radar Topographic Mission
TanDEM-X	TerraSAR-X add on Digital Elevation Model-X Band
TEWS	Tsunami Early Warning System
TLM	Tile Line Map
UAV	Unmanned Aerial Vehicles
VHRS	Very High Resolution Satellite

1 Introduction

This chapter introduces the background of the dissertation based on the requirements for geospatial data in developing countries such as Indonesia. In many applications, the topographic maps are the most authoritative, principal and fundamental type of geospatial data. Therefore this dissertation is mainly focused on the topographic mapping. At first the conventional topographical mapping and its characteristics are explained and why the concentration on large scale topographic mapping has been predefined as a use case in the dissertation. Afterwards, the research objectives and the structure of the dissertation are described.

1.1 Problem definition and motivation

In December 26th, 2004, a 9.1-9.3 magnitude earthquake caused the following tsunami which swept the coastal area of many Asian nations including Bangladesh, Sri Lanka, India, Malaysia, Indonesia, Myanmar, Thailand, and Singapore and it brought the unprecedented natural disaster of this century. As the epicenter of this earthquake was west of the coast of Sumatera, Indonesia, it produced the elevated sea waves approximately up to 5 km from the local coastlines of the province capital city of Banda Aceh. Within the context of the following Disaster Management (DM) to rehabilitate and reconstruct the impacted area, the international communities have initiated a lot of projects.

One initiative was a cooperation between German and Indonesian government in the so called “German Indonesia Tsunami Early Warning System” (GITEWS). Later on, GITEWS was handed over and became a part of Indonesian Tsunami Early Warning System (InaTEWS) in 2011. For this purpose, geospatial data played an important role to support the different levels of DM. The National Coordinating Agency for Surveys and Mapping of Indonesia (BAKOSURTANAL) at that time contributed in providing the official topographic map data as a part of the National Spatial Data Infrastructure (NSDI) for GITEWS development as well as supporting the system with real time access to the tide gauges station within the Indonesian coastal territory. Unfortunately the recent topographic map data for the disaster area dated back to 1976 with a scale of 1:50,000.

Even though these old topographic datasets provided helpful information especially with regard to the local contents such as administrative boundaries, geographical names, etc., the quality and resolution were still not adequate enough for the technical level. With this coarse map scale, it was difficult to perform a detailed analysis based on Geographical Information System (GIS) as a part of a Decision Support System (DSS). Therefore, immediate mapping activities for a larger map scale were initiated in the form of a project granted by Norway, Australia and France in the middle of 2005. Based on BAKOSURTANAL’s request, the Norwegian Agency for International Development (NORAD) initiated an aerial digital metric camera data acquisition campaign to provide the orthophotos in 25, 50 cm resolutions as well as the Topographic Line Map (TLM) with the map scale of 1:10,000 and 1:5,000 for the partial coastal area of Aceh (Kidd, et al., 2009).

As one of the vulnerable countries around a disaster prone area, Indonesia really needs sophisticated seamless topographic map data for a better disaster preparedness and a quick emergency response. Topographic maps are essential because they contain basic geospatial features including terrain information with respect to their proper geometrical accuracy.

Normally, in order to provide high resolution three dimensional (3D) geospatial data, Large Scale Topographic Mapping (LSTM) needs an input from conventional airborne campaigns which is in Indonesia bureaucratically complicated especially due to legal administration procedures i.e. security clearance from the military/defense ministry. This often causes additional time delays besides technical constraints such as weather and limited aircraft availability for airborne campaigns. Due to the high costs of airborne data acquisition, the topographic maps derived from digital metric camera, Light Detection and Ranging (LiDAR) or Interferometric Synthetic Aperture Radar (InSAR) are often not completed in time to catch the dynamic changes in the built areas, which is the common area of interest (AOI) in LSTM.

1.2 Spatial data for disaster management in Indonesia

Since 2000, the International Charter on Space and Major Disaster[1] has established an agreement by coordinating the involved agencies all around the globe to initialize an effective system collaboration of spatial data acquisition for providing remote sensing data within affected regions during disaster situations. Initiated by the French Space Agency (CNES) and the European Space Agency (ESA), the members of that charter now are 23 institutions either from private or governmental sector providing widely used space borne remote sensing data for disaster preparedness and emergency response. Under this charter, the provided space borne imagery data shall be distributed by the participating agencies on a voluntary basis without any direct funding and payment during the period of natural or man-made disasters in any part of the globe. This important breakthrough has triggered awareness of the other potential institutions to participate in this mutual cooperation such as United States Geological Survey (USGS) since 2005, German Aerospace Center (DLR) since 2010, etc. The most prominent instance was activated at the end of 2004 when the already mentioned earthquake followed by a tsunami has hit the Indian Ocean region. At that time, the high resolution imageries were freely given to the public through authorized users immediately.

For disaster and emergency situations, earth observation in form of geospatial data plays an important role to be used within Decision Support Systems (DSS) to strengthen the DM analysis (Percival, et al., 2012). One fundamental component of the geospatial datasets is the Digital Elevation Model (DEM), which is mandatory in order to enable Geographical Information System (GIS) analysis within quite a number of societal challenges. Such models (DEMs) play an important role within all DM phases.

[1] https://disasterscharter.org (last accessed 05.03.20)

Hence, for such a huge archipelagic country with a great potential of disasters like Indonesia the DEM generation from satellite data is very important.

Especially within Earthquake / Tsunami events it is a challenging task to derive an up to date and not too costly terrain representation through DEMs. Satellite-based radar data are very well suited to fulfill such needs. A wide coverage and flexible data acquisition modes make radar satellite-based data very interesting also for DEM generation especially for large monitoring areas. The main reason for this is the weather independence and high orbit altitudes which can avoid local restrictions and limitations e.g. security clearance, survey permission, etc.

Beside global satellite data acquisition other methodologies are also potential to generate geospatial data for DM purposes. For instance, Unmanned Aerial Vehicle (UAV) is used more and more nowadays in particular for smaller areas with high resolution requirements. Related to the processing of UAV images, Structure from Motion (SfM) is the common approach nowadays to provide 3 dimension (3D) information of an object especially by using non metric cameras. This approach can provide the camera position as well as the object geometries without any knowledge of parameters like the 3D position of the camera or the camera calibration. In order to guarantee the necessary height accuracy, UAV data processing however must be supported by ground segment data i.e. Ground Control Points (GCPs) which refers to the national geodetic and geodynamic reference network.

Today, UAV platforms are brought and introduced massively on various interesting applications such as monitoring, security and mapping, obviously. On the other hand, the satellite based platforms have the advantage for national or even global monitoring with on-demand very high resolution data. The idea of integrating valuable information from those alternative data resources of often non-restricted data is obviously challenging. However, two questions arise: “Is the accuracy in fact sufficient for LSTM requirements?” and if so, “How can it be integrated into the LSTM data processing in a more efficient way?” In the scope of this dissertation mainly these two different sources of geospatial data for LSTM in Indonesia will be considered and further investigated.

1.3 Research objectives and use case

One of the most important advantages of digital technology nowadays is the improving sensor resolution with relatively affordable price even for personal purpose. The challenging task is how to evaluate the achievable current quality with respect to the LSTM purpose. From this point, the main goal of this dissertation is to define alternative efficient procedures for LSTM in the context of emergency response and disaster preparedness in Indonesia and to investigate if and how the necessary accuracy and other requirements can be met.

The main focus is put on the global satellite-based monitoring data e.g. optical sensor (QuickBird, SPOT6) and radar sensor TerraSAR-X add on Digital Elevation Model-X Band (TanDEM-X) as well as the rapid UAV-based monitoring data. In particular, the absolute phase offset determination in the radar data processing based on reliable height

references is discussed in depth, since a linear algorithm has been introduced and a new approach referring to the more precise national reference datum has been implemented i.e. Geospatial Reference System of Indonesia (SRGI).

The hypothesis of this dissertation is:

> Through the usage of state-of-the art Remote Sensing data and corresponding processing methods the situation related to the availability of high quality Geoinformation in Indonesia can be improved considerably. For specific areas where a more detailed information with higher accuracy is needed, UAV-technology can play an important role.

If and how that can be reached has to be investigated in the dissertation. This relates to the testing and further development of processing methods / software as well as to the assessments of the quality – specifically the geometric accuracy – of the products derived from the data sources. Such important products are DEMs and orthoimages.

In consequence, the satellite-based data sources in a form of Very High Resolution Satellite (VHRS) like Quickbird, SPOT6, TanDEM-X as well as UAV data are evaluated. In general an important focus of the investigations lies in the question if and how the quality-requirements like accuracy and completeness can be reached.

Further it has to be investigated how the data from aforementioned sources can be combined and/or integrated into existing data processing workflows in order to increase their geometrical product accuracies.

In more detail, the specific goals of this dissertation are the following:

1. Analysis of the current state of the art for LSTM.
2. Investigation of available alternative data sources, related methods and the potential drawbacks.
3. Development of a concept to improve the geometric accuracy of the used data sources by performing technical investigations on:
   - Stereo radargrammetry and stereo optical method for satellite-based data;
   - InSAR data processing for satellite-based radar data;
   - High resolution DEM generation with UAV data by GCP support and local knowledge (building structures).
4. Geometric accuracy investigations within 4 different areas, representing the various terrain conditions of Indonesia.
5. Investigations for DM purposes i.e. related to volcano eruptions and the Tsunami Early Warning System (TEWS) in Indonesia.

1.4 Structure of the dissertation

This dissertation is structured as follows. At first, the characteristics of LSTM, the potential data sources and the development of concepts for the Indonesian use case in

Part I (chapter 2-4) and the investigations for LSTM and DM purposes in Part II (chapter 5-6) are discussed. The investigations try to be as general as possible for different topographical situations, starting from flat terrains which allow for a DEM generation with reliable accuracy and extending with mountainous terrains where usually a derived DEM has larger uncertainties. The general overview of this dissertation is visualized in Figure 1. The generated DEMs are validated against field GCPs, reliable datasets, TanDEM-X Intermediate Digital Elevation Model (IDEM), and Shuttle Radar Topography Mission (SRTM).

In more detail, for Part I: chapter 2 gives an outline for the scope of LSTM in a specific case of Indonesia. The conventional data acquisition system is introduced in section 2.2 with a large focus on the DEM generation algorithms, since a significant portion of DEM errors are produced in this stage. The DEM standards, in terms of accuracy, are described in section 2.4. Though they are created for LiDAR and optical systems, an expansion to the InSAR and UAV context is also relevant. The main advantages and drawbacks of potential data sources and processing methods are described in chapter 3. Subsequently, the more detailed technical settings for the developed concepts have been elaborated in chapter 4. For Part II: chapter 5 further discusses the proposed LSTM data processing to provide orthoimages and DEMs and their quality assessment results for four test areas. Subsequently, chapter 6 is dedicated for the DM purpose, by the test scenario on 2015's eruption of Mount Sinabung and 2018's tsunami of Sunda Strait.

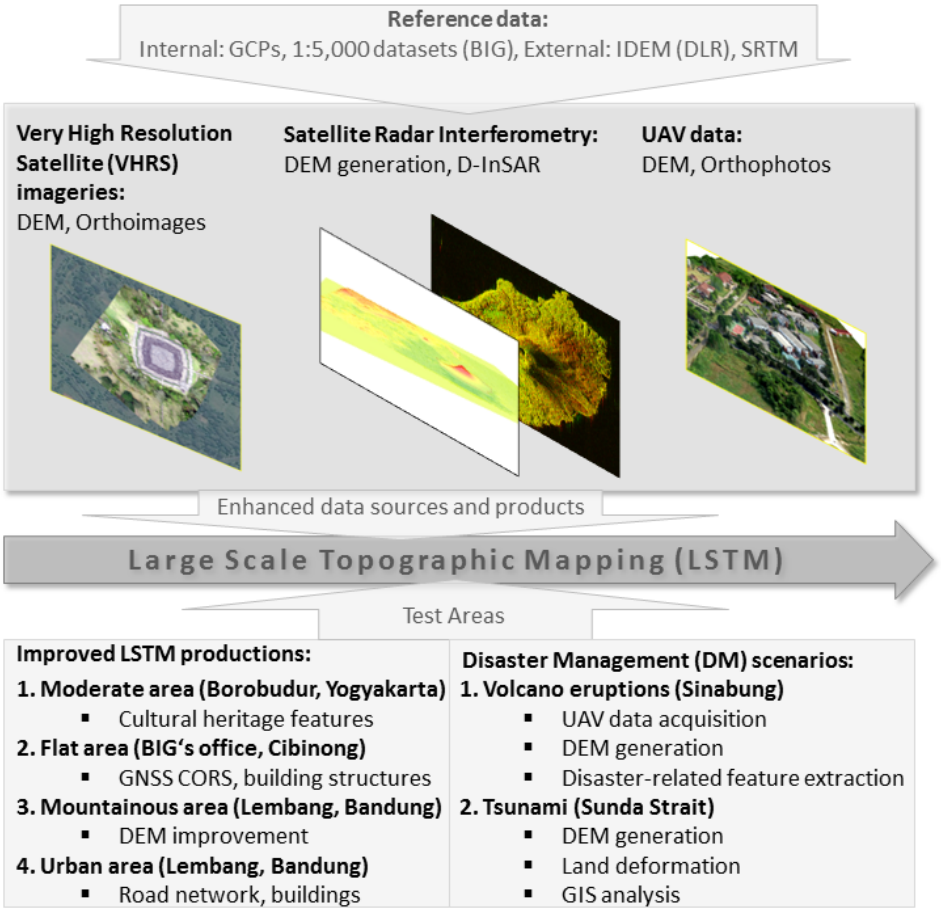

Figure 1: Overview about LSTM data sources and test areas

2 Large Scale Topographic Mapping in Indonesia

This chapter explains the current LSTM procedure as applied in Indonesia by discussing the conventional LSTM methodologies with respect to the requirements and specifications. The huge LSTM volume is a challenging task when relying only on conventional methods as discussed in 2.1 - 2.3. Therefore, the LSTM acceleration program is a necessity in order to accommodate the dynamic nature of LSTM topographic features such as buildings, infrastructure, etc. Finally, the accuracy assessment procedure and standards used to evaluate the quality of geospatial data will be discussed in 2.4.

2.1 Background

Knowledge about the topography and the infrastructure is an essential pre-requisite for disaster analysis. Hence, topographic maps are a visualization of models of the earth which show both natural and man-made objects e.g. vegetation, infrastructure, etc. The building structures are also one of the important components included in topographic maps.

DEM as an essential component of the LSTM can be produced with various technologies such as stereo photogrammetry, with airborne InSAR or digital metric cameras, or with Light Detection and Ranging (LiDAR). As a national mission, LSTM is applicable to map each square meter of Indonesia's land. Thus, all the typical topographic map features are included and reconstructed based on DEMs. As explained in the following chapter 3.1.1.2, InSAR DEM accuracy depends on the terrain conditions which are subjected to both the orbital sensors and the topographical correction.

Table 1: Topographic mapping aspects in + as one advantage unit (Infoterra, 2009)

System	Cloud independence	Suitability for		Cost Efficiency	DEM	GCP independence	Interpretability
		1:50K	1:25K				
TerraSAR-X	+++	+++	++	+++	++	+++	++
Airborne InSAR	+++	+++	+++	+	+++	+	++
High-res. Optical satellites	+	+++	+++	++	++	+	+++

Topographic maps are considered as quite expensive with respect to production time and cost. There are a number of possible methods available for the production of topographic maps, as explained further in this section, but also radar data are very well suited to fulfill these needs as it can be seen in Table 1. Almost in every aspect as evaluated in Table 1, satellite-based radar data indicates some prominent advantages namely cloud independence, cost efficiency, and GCP independence. The main reason for this is the necessity to provide the DEM as a three dimensional component of LSTM

which allocates a lot of resources and efforts both in data acquisition and data processing stages.

In the period of 2011-2014, BAKOSURTANAL has been transformed into Geospatial Information Agency (BIG) based on the Act which was ratified on March 2011. Not only the name itself, but the role of BIG is becoming more important in the context of geospatial data acquisition, production and dissemination.

By the above mentioned regulation only BIG is responsible for the provision of fundamental information as the basic geospatial references e.g. Horizontal Geodetic Network (JKG), Vertical Geodetic Network (JKH) and Topographic Base Map in Indonesia. Consequently, the expected geospatial data accuracy shall follow certain standards to fulfill the requirements of the users (see 2.4 for more details).

Under the recent legislation Act No. 4/2011 about Geospatial Information in Indonesia (Act of Republic of Indonesia, 2011), the Geospatial Information Agency of Indonesia (BIG) takes responsibility to provide topographical maps which shall cover 1.9 million square kilometer land area of Indonesia. For that purpose, the proper technologies and methodologies shall be implemented in order to accelerate the huge topographic mapping activities in various map scales especially for large scale topographical mapping i.e. ≥ 1:10,000.

Table 2: Overview of Indonesian topographic maps (2018)

	Map scale (1:M)	**Map coverage (length×width) in km**	**Map-sheets (Numbers)**	**Availability (%)**
1	1,000,000	668 × 442	37	100
2	500,000	334 × 221	103	100
3	250,000	167 × 111	309	100
4	100,000	55.6 × 55.6	1,245	100
5	50,000	27.8 × 27.8	3,899	62
6	25,000	13.8 × 13.8	13,020	14
7	**10,000**	**4.6 × 4.6**	**91,547**	**0.7**
8	**5,000**	**2.3 × 2.3**	**379,014**	**0.06**
9	**2,500**	**1.15 × 1.15**	**880,206**	**0**
10	**1,000**	**0.58 × 0.58**	**2,729,319**	**0**

Table 2 gives an overview of the topographic map scales used in Indonesia with respect to the coverages, number of map sheets and the availability related to the year 2018. As an example for the 1:5,000 map scale which is the interest of a detailed spatial planning, the numbers of single map-sheets covering an area of 2.3 by 2.3 km is 379.014 (Table 2 number 8). Such detailed maps are not necessary for the whole country, but only for prioritized areas such as big cities and/or heavily built areas. Even

though reduced by aforementioned prioritization, the LSTM volume estimations are still indicating a large number of 15,000 map-sheets (by only around 5% from the total coverage) as visualized in Figure 2. Unfortunately the normal capacities for the annual production of the 1:5,000 topographical maps are only 100-200 map-sheets. Thus, without any acceleration, the whole 1:5,000 topographic mapping of Indonesia will be completed in 75-150 years.

Commonly the combination of Light Detection and Ranging (LiDAR) and digital aerial metric camera has been utilized for map production by using airborne platforms. In practice, the problem is not only to deal with the technology itself but also with bureaucratic problems such as security clearance, which needs a lot of administrative terms and conditions in Indonesia both from defense ministry and air force institutions.

Nowadays, there are quite a number of satellite based data sources available, partly in very high resolution. However, the high resolution is not always correlated with a sufficient geometric accuracy for LSTM. Therefore in this dissertation it has to be investigated which of the data sources are fulfilling the requirements.

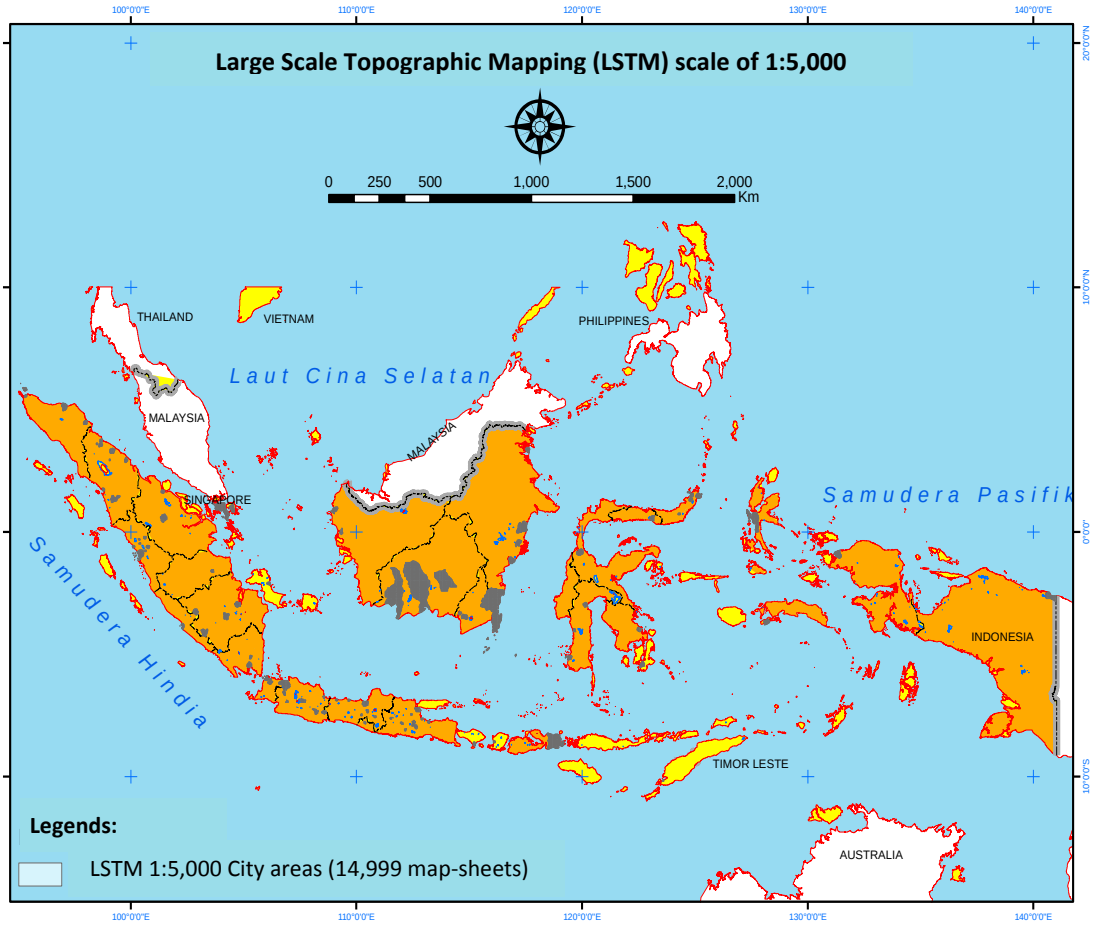

Figure 2: Prioritized areas 1:5,000 LSTM of Indonesia ca. 15,000 map-sheets (grey colour)

Based on the aforementioned legislation act in Indonesia, there are four map scales which are classified as LSTM, namely 1:10,000; 1:5,000; 1:2,500 and 1:1,000 (see Table

2 number 7-10, bold sections), and therefore the focus in this dissertation is brought to the requirements of these map scales.

2.2 Data acquisition and topographic mapping workflow

Geospatial data acquisition is the primary component to be considered as essential in the whole LSTM production chain. It takes a lot of resources especially in the context of airborne data acquisition. Based on the current technical specification of BIG as National Mapping Agency (NMA) in Indonesia, the primary approach to produce LSTM is by using airborne data acquisition either with passive sensors (optical digital metric cameras) or active sensors (InSAR, LiDAR).

Höchle, 2012 has concluded that for example the Leica RCD30, a medium format camera can be used for the generation of city models and automated Digital Surface Models (DSM) with a comparable quality to the large-format photogrammetric camera. From this point of view, the use of a medium format camera in Indonesia is adequate.

Figure 3: Aircraft and cameras used (upper: Cessna 206t with Trimble P65+, lower: Cessna 402b with Leica RCD30)

As the test case in this dissertation, airborne campaigns using Leica RCD30 and Trimble Phase One (P65+) cameras have been performed in May 2013 and August 2011 to provide an aerial photogrammetric data as depicted in Figure 3. This acquisition used Cessna aircraft fully equipped by Gyro-stabilizer as well as with an Inertial Measurement Unit (IMU) and an Inertial Navigation System (INS) to support an accurate direct georeferencing. Table 3 describes the details of the three flight missions to produce LSTM data including the UAV data acquisition.

By using this type of aircraft, the altitude during acquisition can be set up to 500 m Above Ground Level (AGL) to acquire photogrammetric data with the best possible

resolution. Therefore it is sufficient to use this photogrammetric data as a source to derive the building structures (see 4.4.1 for more details) mentioned by digitizing them. In addition, this reliable dataset will be used as a reference data for accuracy assessments as well as for height reference data in the InSAR DEM generation.

Table 3: Acquisition details for BIG office (example)

	UAV Canon S100	**Leica RCD30**	**Trimble Phase One (P65+)**
Altitude	268 m AGL	500 m AGL	793 m AGL
Aircraft	Skywalker 1680	Cessna 402b	Cessna 206t
Focus	5.712 mm	53 mm	51.407 mm
Date	12 June 2014	9 May 2013	22 August 2011
On-board Navigation	GPS Camera	Leica IPAS20 (IMU/INS)	Applanix POS AV (IMU/INS)
GPS/IMU Accuracy	Position: 10-20 m	Position: 0.05-0,3 m Roll&Pitch: 0.008° Heading: 0.015°	Position: 0.5-2 m Roll&Pitch: 0.03° Heading: 0.28°

Figure 4 gives an overview of the LSTM workflow in Indonesia from establishing a GCP network, mainly by using Global Navigation Satellite System (GNSS) or Global Positioning System (GPS) technologies, to providing georeferenced image data (airborne and/or satellite-based) to deriving the end products, mainly orthophoto and DEM. Basically, there is a clear separation between data acquisition tasks and feature compilation tasks in order to produce LSTM on a map-sheet base.

DEM can be divided into two different types of digital model namely Digital Surface Model (DSM) and Digital Terrain Model (DTM). A DSM is a representation of the earth surface including manmade and natural structure above ground (off-terrain) in three dimensional (3D) coordinates while a DTM only represents the bare earth surface (on-terrain). In addition, the Ortho Rectified Imagery (ORI) or orthophoto must be produced as the terrain corrected image data by taking into account the DSM or DTM input.

All in all, the main assumption here is that only airborne data acquisition with sophisticated sensors e.g. InSAR/IFSAR, digital metric camera, LiDAR can fulfill the LSTM technical specifications as further explained in 2.4. Unfortunately the airborne data acquisition allocates a lot of resources such as time, cost in the form of administrative bureaucracy (security clearance), flight operation and sophisticate sensor/equipment provision such as metric camera, InSAR/IFSAR, LiDAR, IMU, INS. The focus of this dissertation is put on the data acquisition since the geometric accuracy of the GIS vector and the cartographic data as the final output will be determined (Figure 4).

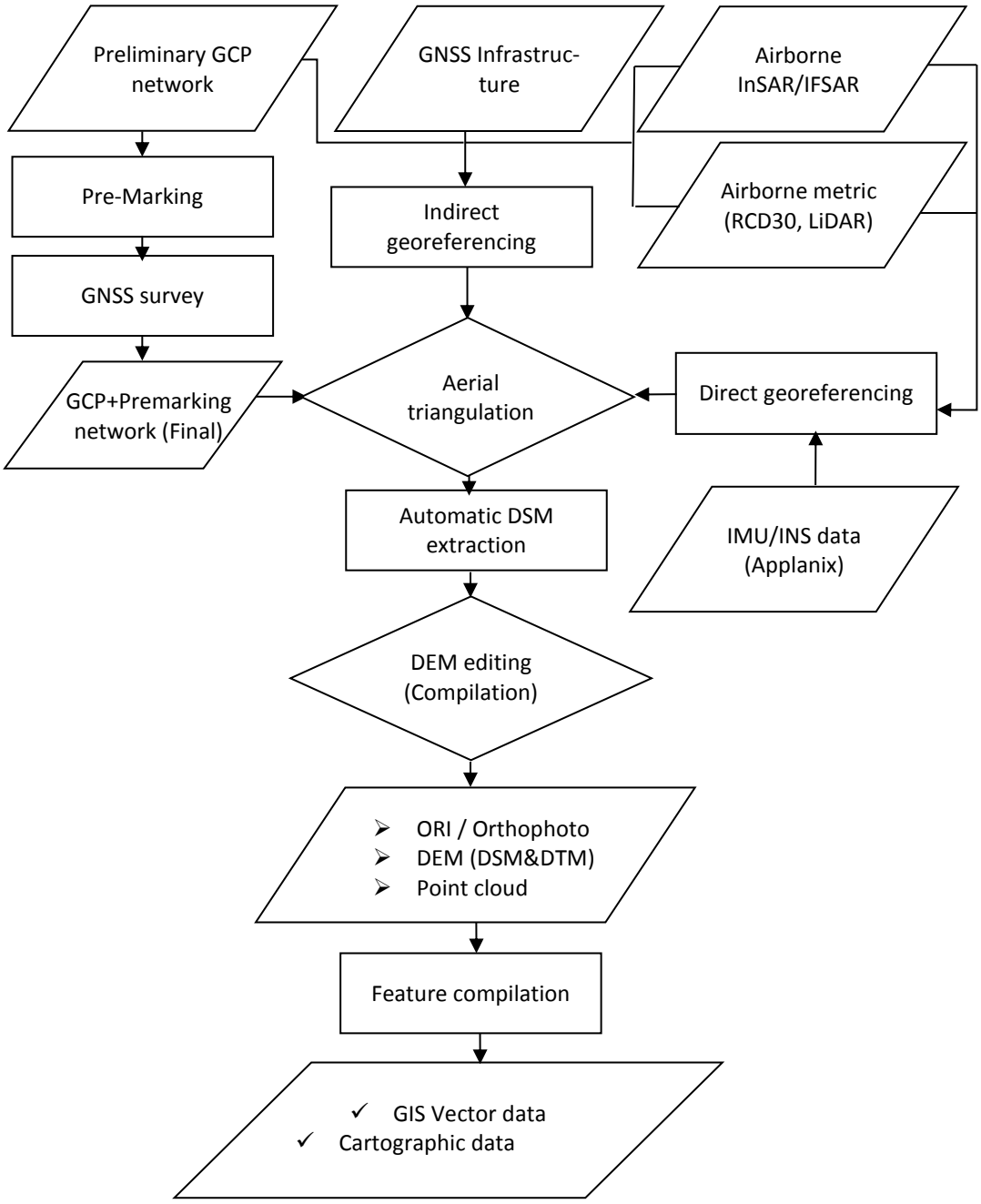

Figure 4: Workflow of conventional LSTM

2.3 GIS and map production

The involvement of Geographical Information Systems (GIS) in this dissertation is mainly related to the vector data production from both orthophotos and DEM. In this case, the quality of geospatial data sources is the key performance indicator for the overall output or end product as it will be used in the subsequent topographic mapping step. For this reason, the end product will be evaluated based on the correctness and consistency during feature compilation. Normally, topographical features are compiled by using stereo working stations.

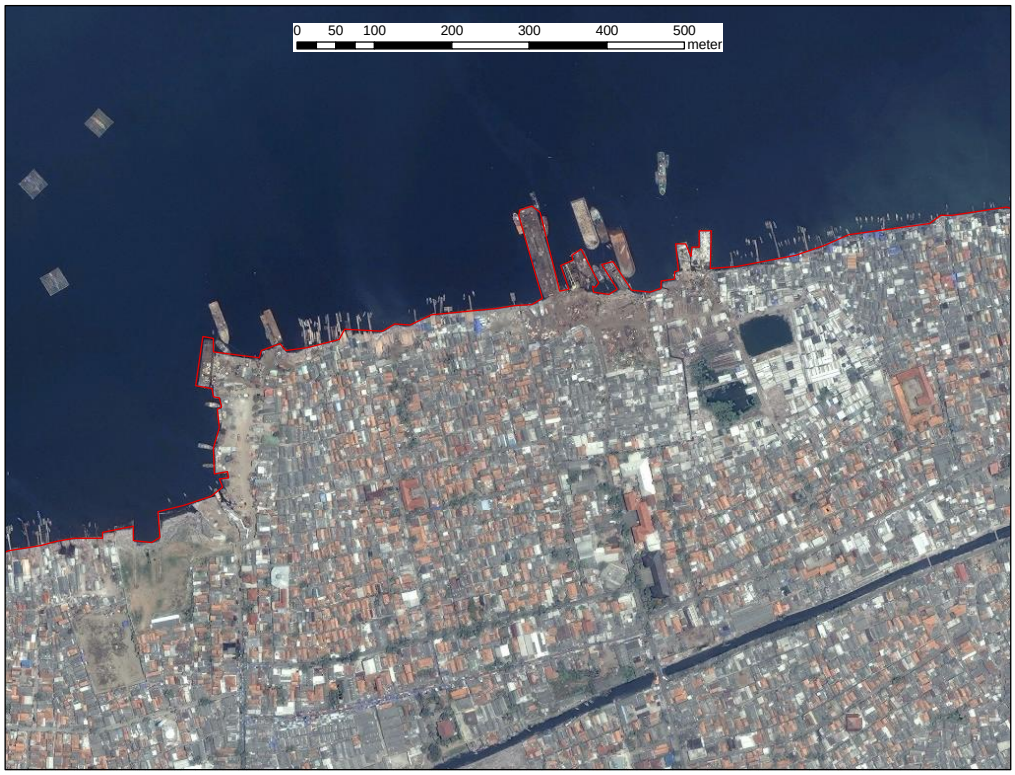

Figure 5: Coastal area of Jakarta in the 1:5,000 map scale

Based on the official regulation in Indonesia (legislation Act Nr.4/2011) as implemented in the technical specification, there are 8 different themes/layers involved in the topographical mapping:

1. Coastline, represents imaginary lines as the boundary between land and water area as depicted in Figure 5.
2. Hypsography, represents earth terrain by mass points, spot heights and breaklines (related with DTM production) as depicted in Figure 6.
3. Hydrology, represents watershed or water network.
4. Geographical name (Toponym), represents the topographical feature identification based on standardized naming conventions.
5. Administration boundaries, represent feature delineation between different regions of authorities.
6. Transportation and utilities, represent the network of manmade objects to interconnect.
7. Building and public facilities, represent topographical features related with human activities.
8. Land cover (not land use), represents coverage types and classifications based on the actual situation in the field.

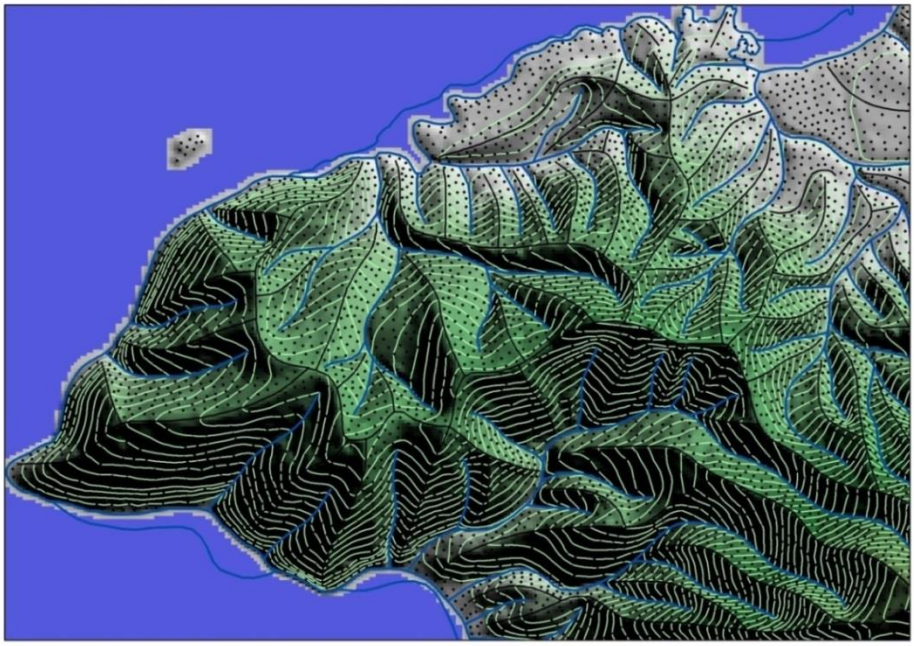

Figure 6: The components of hypsography

The accuracy of the interpolated DTM in the GIS data production depends on the compilation quality of the hypsography features as depicted in Figure 6. Hypsography consists of masspoints, spot heights, breaklines in GIS format and the interpolated DTM in grid format. Therefore the DEM quality as an end product also can be evaluated referring to the hypsography features in 2.5 D format.

In LSTM, almost every object can be compiled in a 1:1 relationship in the GIS as well as in the cartographic products. For example a port/jetty and the road segments as depicted in Figure 7 are compiled referring to the actual form and size in reality.

Figure 7: Feature compilation using stereo-plotting equipment

2.4 Accuracy assessments

As already explained in 2.2, the focus of this dissertation is basically related to the geospatial data sources as a mandatory input to the whole LSTM production chain. Therefore for the geospatial data source evaluations only the data quality elements (ISO, 2013) prominently correlated with geometric aspects will be evaluated: completeness and positional (geospatial) accuracy.

In order to pose the geospatial data quality, the comparison method must be defined. Accuracy aspects play an important role for an objective comparison both in a qualitative and a quantitative manner.

The important question addressed in the accuracy assessment is how to select appropriate reference datasets comparing to the evaluated datasets. In this case, the reference datasets have been selected based on the assumption that they have a better quality than the evaluated alternative geospatial datasets (FGDC, 1998).

2.4.1 Completeness

In the framework of the European Committee for Standardization (CEN)/TC287/WG02 (Langaas and Tveite, 1995) completeness is defined as presence and absence of geospatial features in the evaluated dataset by comparing them with the specifications. Quantitatively, three possible measures are suggested to indicate the completeness. These are omission, commission and coverage ratio, represented by the following metrics:

- Omission : percentage of absence of geospatial features relative to the specification,
- Commission: percentage of presence of geospatial feature that is not included in the current specification yet,
- Coverage ratio: number of occurrences of one variable per geospatial unit.

For ISO 19113 as described in ISO, 2013, only the first two metrics exist to evaluate the completeness aspect. Practically, completeness can be defined as the measure of the lack of the data (Haklay, 2010). Simply it means the assessment of the objects covered in the evaluated datasets comparing to the reference data which is assumed to be correct and complete.

This can be achieved by a comparison of a reference dataset against the dataset to be examined. This assessment needs to define the measurement unit as a basis for quantifying the result by using GIS analysis. All GIS operations such as overlay, calculate geometry, dissolve, etc. will be performed in the Universal Transverse Mercator (UTM) coordinate system. Therefore it is a mandatory to have both the evaluated and reference data on the aforementioned projected metric coordinate system i.e. UTM.

As an example, two different approaches of completeness evaluation have been applied for the actual large scale topographical dataset of Jakarta, Indonesia in order to proceed with further evaluation as the following:

1) Tile based

Tile based uses the fixed object with regular size, for example the map index (tile) as a unit for measuring the geometrical aspect of the features (length, area, etc.) covered in each dataset (Figure 8). The map tile will be used as a reference for calculating each feature consistently with minimum discrepancy. Similarly to the indexing approach in the geodatabase, this approach will divide seamless objects into different region tiles, therefore it can be considered as an intermediate map unit as well.

The size of the map-sheets as included in Table 2 column 3 will determine the assessment results. For a single map-sheet of 1:10,000 as shown in Figure 8, it covers an area of approximately 4.6 by 4.6 km. The larger the size of the map-sheets, the harder the completeness evaluation can provide a meaningful result.

This approach is suitable for areas with regular density of objects since it will quantify the amount of the objects as equal as possible. Considering the data density, the tile size can be changed by a balance between the performance and the intended level of detail in the completeness evaluation.

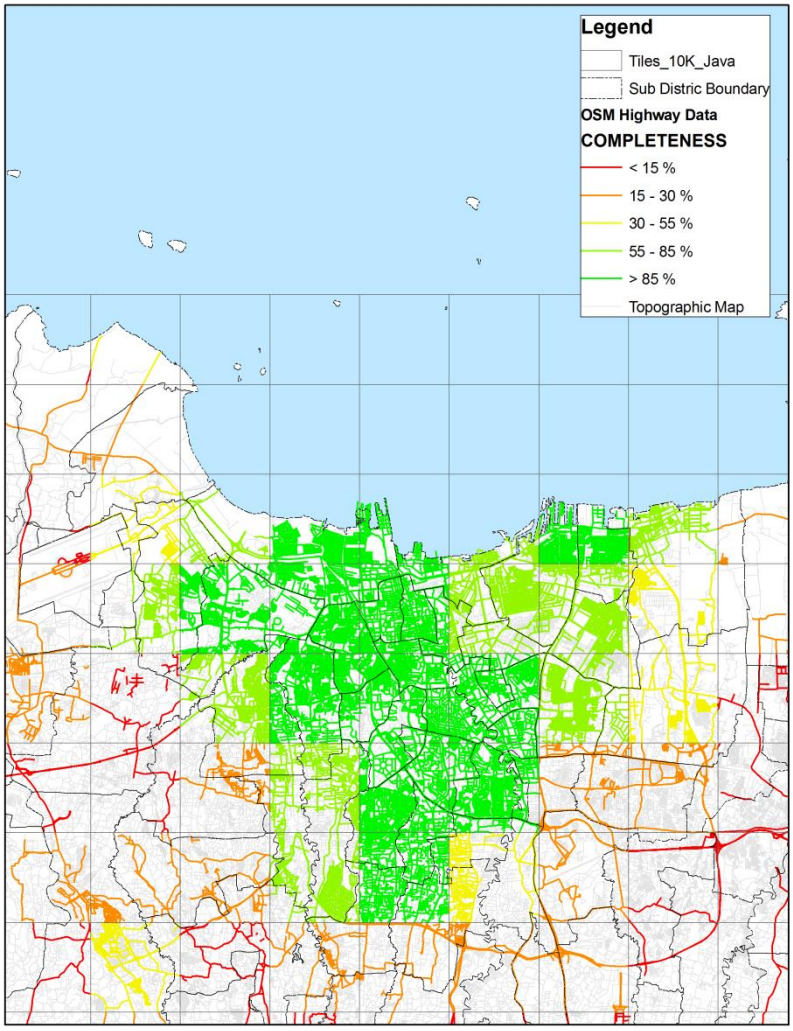

Figure 8: Map tile unit based approach

2) Administration boundary based

Administration boundary is one important theme in topographic maps as already discussed in 2.3 that can be used both as a technical mapping unit and coordination management unit (Figure 9). Non-technical aspects such as political aspects also can be identified by using this theme to indicate the progress of local or regional development. For example in an administration boundary area which is extensively developed, the completeness aspect also can be used to indicate the dynamic nature of topographic feature in LSTM.

Using administration boundary as the reference for dissolving the topographical features can indicate the completeness factor with respect to the development progress in the corresponding area. Unfortunately in term of performance, this operation needs a longer time and heavier operation, since the clipping function will involve such an irregular polygon and not a simple bounding box like in the tile based operation.

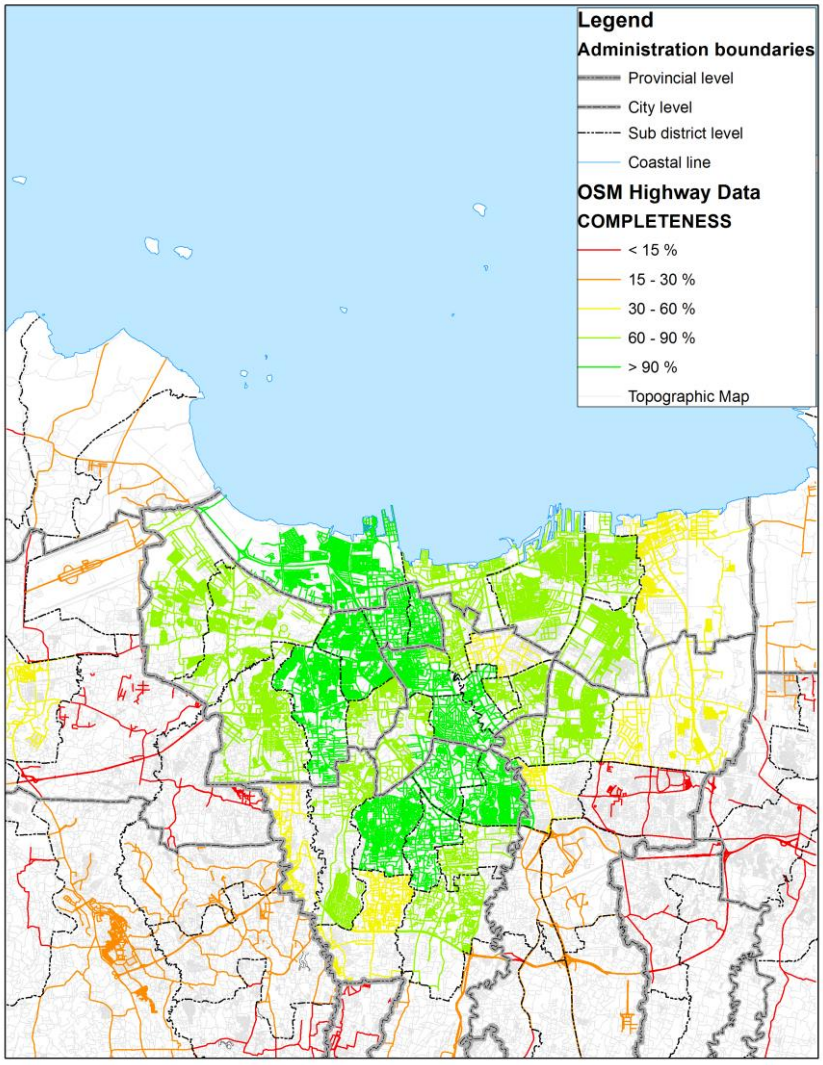

Figure 9: Administration unit based approach

2.4.2 Positional accuracy

Considering positional accuracy, the evaluation method called National Standard for Spatial Data Accuracy (NSSDA) has been applied for consistency checking (FGDC, 1998). The main objective of this method is the detection of blunders from an input data set and the derivation of a statistical model based on Root Mean Square Error (RMSE).

The NSSDA proposes to use RMSE for assessing the positional accuracy of the evaluated datasets. RMSE is the square root of the average of the set of squared differences between dataset coordinate values and coordinate values from the reference data for identical objects.

The NSSDA accuracy is reported in ground differences (deviations) for each axis at a 95% level of confidence. It means that 95% of the positions in the dataset will have an error with respect to the true ground position that is equal to or smaller than the reported accuracy value. The reported accuracy value reflects all uncertainties, including those introduced by geodetic control coordinates, introduced by the acquired data, the compilation, and final computation of ground coordinate values in the product.

The planimetric (X,Y) RMSE can be calculated by the following equation 2.1-2.3 (FGDC, 1998) for each corresponding object i in the different datasets i.e. between the evaluated data and the reference data. The examination focuses on the point features since the involved spatial data are assumed to deal with different resolutions and various acquisition methods.

$$RMSE_x = \sqrt{\frac{\sum(XCheck_i - XRef_i)^2}{n}} \tag{2.1}$$

$$RMSE_y = \sqrt{\frac{\sum(YCheck_i - YRef_i)^2}{n}} \tag{2.2}$$

$$RMSE_r = \sqrt{RMSE_x{}^2 + RMSE_y{}^2} \tag{2.3}$$

where:

$RMSE_x$ = Root Mean Square Error in x axis direction

$RMSE_y$ = Root Mean Square Error in y axis direction

$RMSE_r$ = Planimetric (X,Y) Root Mean Square Error

($XRef_i$, $YRef_i$) = Coordinates of common points i in the reference dataset

($XCheck_i$, $YCheck_i$) = Coordinates of common points i in the evaluated dataset

On the other hand, based on the National Mapping Accuracy Standard (NMAS), the planimetric required RMSE can be seen in Table 4. Differently to the NSSDA accuracy, the NMAS introduced a circular error at 90% level of confidence which is more moder-

ate than 95% of NSSDA. This 90% area (circle) of the possible position can be estimated with the so called Circular Map Accuracy (CMAS) as put in Eq.2.4.

$$CMAS_r = 1.5175 * RMSE_r \quad (2.4)$$

The NMAS defines a planimetric accuracy in Circular Error (CE) and a vertical accuracy in Linear Error (LE) at 90% level of confidence. In terms of elevation data for 1:10,000 topographic mapping, it means that 90% of spot elevations must be within 8.5 m of their true planimetric position and 90% measured vertical elevation shall be within 2 m (half of the contour interval) of the absolute height.

In addition, the comparison between NMAS and NSSDA as included in Table 4 shows different strictness levels. For planimetric accuracy, NSSDA is more stringent than NMAS while for height accuracy is the other way around. Nevertheless, there is an accuracy measure that can be used more flexible in the comparison purposes namely "required RMSE". Indeed, the required RMSE value indicates level of accuracy among different datasets.

Table 4: Required RMSE based on NMAS vs. NSSDA (FGDC, 1998 & ASPRS, 1990)

Standard / Map scale	National Mapping Accuracy Standard (NMAS)					National Standard for Spatial Data Accuracy (NSSDA) for class I maps (ASPRS)			
	publication scale (hard-copy maps) in mm	Required RMSE (planimetric) in m	Accuracy (CE90) in m	Required RMSE (height) in m	Accuracy (LE90) in m	Required RMSE (planimetric) in m	Accuracy (CE95) in m	Required RMSE (height) in m	Accuracy (LE95) in m
1:10,000	0.85	5.60	8.50	1.22	2.00	2.50	4.33	1.33	2.61
1:5,000		2.80	4.25	0.61	1.00	1.25	2.16	0.67	1.31
1:2,500		1.40	2.13	0.30	0.50	0.63	1.08	0.33	0.65
1:1,000		0.56	0.85	0.12	0.20	0.25	0.43	0.13	0.26

Based on the Indonesian use case as predefined by the Regulation of Head of BIG No. 15/2014 updated by the No. 6/2018 about the technical guidance for topographical base map accuracy, the geospatial qualities of LSTM can be divided into three different classes with respect to their required RMSE as included in Table 5. As above mentioned, the required RMSE can be used to show that Indonesian topographic map specification requires stricter conditions beyond NMAS and NSSDA requirements.

Table 5: Required RMSE based on Indonesian topographic map specifications

Map scale	Required RMSE for class I maps		Required RMSE for class II maps		Required RMSE for class III maps	
	Planimetric (m)	Height (m)	Planimetric (m)	Height (m)	Planimetric (m)	Height (m)
1:10,000	1.98	1.22	3.95	1.82	5.93	2.43
1:5,000	0.99	0.61	1.98	0.91	2.97	1.22
1:2,500	0.49	0.30	0.99	0.46	1.52	0.61
1:1,000	0.20	0.12	0.40	0.18	0.59	0.24

For DEM specifications, there are standards as defined by the National Geospatial-Intelligence Agency (NGA) or former National Imagery and Mappping Agency (NIMA) and the USGS given in Table 6. HRTI stands for High Resolution Terrain Information, while DTED stands for Digital Terrain Elevation Data). In order to get a better accuracy, HRTI will be stored as 4-byte (32-bit) in a case that elevations can be stored in real numbers instead of integers. However, this will also double the file size compared to using 16-bit data. Currently, HRTI can only be produced by using an airborne InSAR platform.

The height accuracies included in Table 5 and Table 6 can be calculated from RMSE as also defined by FGDC, 1998 for vertical/height component (3D) following Eq. 2.5. It means that 90% of the measured elevation will have a deviation less than the given accuracy for each respected DEM class.

$$RMSE_Z = \sqrt{\frac{\sum(ZCheck_i - ZRef_i)^2}{n}} \tag{2.5}$$

$$Accuracy_Z(LE\ 90\%) = RMSE_Z * 1.6449 RMSE_x \tag{2.6}$$

where:

$RMSE_Z$ = Root Mean Square Error for vertical/height component (3D)

$ZRef_i$ = height of common points i in the reference dataset

$ZCheck_i$ = height of common points i in the evaluated dataset

Table 6: NGA/NIMA and USGS Digital Elevation Data specifications (Heady, 2009 & D'Errico, 2013)

DEM class (Level of details)	Post spacing (arc-sec)	Post spacing (m)	Accuracy measures in m			
			Required RMSE (planimetric)	Accuracy (CE90)	Required RMSE (height)	Accuracy (LE90)
DTED level 0	30.00	1,000	32.95	50	18.24	30
DTED level 1&DEM 1°	3.00	100				
DTED level 2	1.00	30	15.16	23	10.94	18
HRTI level 3/HREG	0.40	12	9.88	15	6.08	10
HRE08	0.27	8	6.59	10	4.86	8
HRTI level 4	0.20	6	5.27	8	3.65	6
HRE04	0.14	4	3.29	5	2.43	4
HRTI level 5/HRE01	0.04	1	1.32	2	0.61	1

3 State of the art

This chapter describes available geospatial data sources related to the whole dissertation work as well as the data processing methods. The focus is on the DEM generation using different technologies that aim for acceptable accuracy in the context of LSTM in Indonesia.

Some sections of this chapter explain the importance of absolute phase offset linearization by using partial accurate DEM reference which will be further discussed in chapter 4. Some ideas to introduce the concept of alternative geospatial data processing are also discussed.

3.1 Potential data sources

A study conducted by ISPRS and United Nation Global Geospatial Information Management (UNGGIM) identifies the status of topographic maps availability including the potential data sources to be used as a basis for the topographic maps production (Konecny et al., 2015). For range I (≥ 1:25 000), which is the focus of this dissertation only Europe, the Russian Federation, Turkey, Japan and the continental USA are well covered by the topographic mapping program. The large scale topographic map availability as explained in chapter 2 confirmed the above mentioned study for the Indonesian use case.

The on-going development of new technologies from the space (GNSS, VHRS, SAR), digital aerial mapping, GIS attracts not only NMA but also private organizations/companies to map the world topographically. The potential data sources were also listed that have been used as a part of the questions for the questionnaire (Konecny et al., 2015) e.g. aerial photogrammetry, satellite imageries, geodetic control survey, others (LiDAR, radar, etc.). However, it is interesting that the UAV data is not mentioned as a potential data source in the aforementioned study. In addition, from the NMA's perspective the utilization of satellite imageries to produce official topographic maps is relatively infrequent, while private companies such as Google, Microsoft are giving more effort to the production of orthoimages from VHRS.

As explained in 2.4.2 in particular about the Indonesian topographic map specifications, the focus is about the geometrical quality of the output instead of specific technology pre-requisite as an input to the LSTM work chain. However, there was a guidance and standard of the geospatial data collection as regulated in the Regulation of Head of BIG No 2/2012 that mentioned about the acceptable methodologies:

(a) Survey and acquisition using sensor based on land, marine, air or space vessels;
(b) Census;
(c) Other methods following the trend of technology.

Based on the aforementioned regulation, available data acquisition technologies are listed in Table 7 to identify the potential data sources for LSTM.

Presidential Instruction No. 6/2012 about Provision, Utilization, Quality Control, Processing and Distribution of High Resolution Satellite Imageries constitutes the definition of Orthorectified Very High Resolution Satellite Imageries (CTSRT) with a resolution ≤ 4 m. This type of data must be produced by the National VHRS Imageries Orthorectification project in BIG with a government (national) license that enables further utilization among other departments or institutions. The mandatory input sources for the aforementioned program are the GCPs and DSM (or DTM) from radar satellite-based data.

The airborne data acquisition by using InSAR, LiDAR and Metric Camera are listed as the conventional method for LSTM with a limited productivity since they are costly and time consuming method for LSTM. Lengthy security clearance and insufficient available airborne equipment are the major constraints which undermine the productivity.

On the other hand, the tremendous utilization of UAV/Drone offers many interesting applications in geospatial data production by using various sensors and equipment as will be discussed in 3.1.2. Finally the most accurate data acquisition is the terrestrial (field) survey by using theodolite, Electronic Distance Measurements (EDM), GNSS/GPS receivers or Terrestrial Laser Scanner (TLS) though limited only to a small coverage area.

Table 7: Potential data sources for LSTM (Act of Republic of Indonesia, 2011)

<table>
<tr><th rowspan="2">Data source</th><th rowspan="2">Processing</th><th colspan="2">General accuracy (m)</th><th rowspan="2">Coverage</th><th rowspan="2">Administrative aspect</th></tr>
<tr><th>CE90%</th><th>RMSE</th></tr>
<tr><td>Optical satellite-based</td><td>National ortho-rectification</td><td>3.79</td><td>2.5</td><td rowspan="2">Global</td><td>National license</td></tr>
<tr><td>Radar satellite-based</td><td>End product</td><td>13.66</td><td>9</td><td>Exclusive license</td></tr>
<tr><td>Airborne InSAR</td><td rowspan="3">Complicated</td><td>0.76</td><td>0.5</td><td rowspan="3">Regional-based</td><td rowspan="3">Security clearance</td></tr>
<tr><td>Airborne LiDAR</td><td>0.30</td><td>0.2</td></tr>
<tr><td>Aerial metric camera</td><td>0.46</td><td>0.3</td></tr>
<tr><td>UAV/Drone</td><td rowspan="2">Customized</td><td>0.76</td><td>0.5</td><td rowspan="2">Small AOI-based</td><td rowspan="2">Survey permit</td></tr>
<tr><td>Terrestrial survey</td><td>0.15</td><td>0.1</td></tr>
</table>

3.1.1 Space borne data

Although has been used for several decades for mapping projects, there is still no actual instance of topographical mapping relied only on remote sensing or satellite-based data as the primary geospatial data source. From NMA perspectives, (Holland et al., 2006) addresses the potential of high resolution satellite imageries for the topographic map updating in Ordnance Survey, Great Britain. This approach intends to make updating process more efficient since the feature change in the case of Great Britain area is usually only focused on small details such as a single building, road, etc.

For the case of Indonesia in which is still extensively developing its territories, the topographical feature changes are more massive and dynamic especially in the big cit-

ies and urban areas. The plan to move the capital city of Indonesia from Jakarta to East Kalimantan in 2024 is the actual instance of LSTM demand that must be provided in a very efficient way. Indeed, satellite-based platform is always interesting with its (very) high resolution data, frequent temporal datasets and local/regional bureaucracy cut-off prior to the data acquisition.

3.1.1.1 Optical sensors

The utilization of optical sensor-based imagery for topographic mapping purposes have been tested since latest 1990's by introducing automatic DEM extraction and orthoimage generation. Al-Rousan et al., 1997 emphasized that satellite-based data can be used to perform small scale topographic mapping up to scale of 1:100,000. This approach has been tested using SPOT Level 1B data and verified by comparison with current 1:250,000 topographic map at that time. At this point, the role of current topographic maps derived from photogrammetric acquisition had an important role to verify the new satellite-based technology.

Table 8: VHRS stereo optical satellites (Jacobsen, 2013 and Astrium, 2013)

Satellite	Processing	Geometric quality (m)			Data Provision
		Acc.CE90%	RMSE	GSD	
IKONOS	Rational Polynomial Coefficients (RPC)	15	9.9	0.81	Commercial
QuickBird		23	15.2	0.62	
Orbview-3		25	16.5	2.3	
Worldview-1		5	3.3	0.5	
Worldview-2			3.3	0.46	
GeoEye-1			3.3	0.41	
Pleiades 1B			3.3	0.7	
Cartosat-1		15	9.9	1	
KOMPSAT-2		80	52.7		
SPOT-6		35	23.1	1.5	

Nowadays, the development of geospatial data acquisition by using space borne platforms is proliferated rapidly to present a tremendous data resolution of optical satellite imagery which is improving dramatically. This phenomenon triggers the massive utilization of Very High Resolution Satellite (VHRS) imageries worldwide i.e. web-based imageries application (Goudarzi and Landry, 2017). People tend to use this kind of interesting geospatial data source to answer their geospatial awareness demand.

Onboard ephemeris and attitude of satellite geolocation based on Rational Polynomial Coefficients (RPCs) is the most common and generic method to provide georeferenced satellite imageries without any GCP. However, high resolution is not always correlated with reliable geometric accuracy. As included in Table 8, the geometric accuracies of

VHRS images processed by RPCs are within 5-80 meter of CE 90% though the Ground Sampling Distance (GSD) is less than 2.5 m. In order to improve the geometric accuracy, it is mandatory to remove bias and systematic errors contended by the RPCs. Indeed, some approaches to compensate aforementioned bias and systematic errors do exist for example by using the local polynomial modelling (Shen, et al., 2017) or DEM (Alidoost et al., 2015).

One specific example of VHRS imagery widely used is WorldView imagery product which has a geospatial accuracy depending on the processing scheme as published by Digital Globe, 2016. This product can be delivered on the basis of Area of Interest (AOI) scheme by using square kilometer as a unit price. Even though the WorldView panchromatic imagery has a 0.46 m resolution, the absolute accuracy for CE 90% is within the range of 4.2 m to 25.4 m or almost 10 times resolution to the utmost i.e. orthorectified without any GCP (Table 9).

Table 9: WorldView product level (Digital Globe, 2016)

<table>
<tr><th rowspan="2">Product type</th><th rowspan="2">Processing</th><th colspan="2">Absolute Accuracy (m)</th><th rowspan="2">Geographic Availability</th></tr>
<tr><th>CE90%</th><th>RMSE</th></tr>
<tr><td>System-Ready (Basic)</td><td rowspan="8">Radiometric & Sensor Corrected</td><td rowspan="5">5</td><td rowspan="4">2.3</td><td rowspan="5">Worldwide</td></tr>
<tr><td>System-Ready (Basic stereo)</td></tr>
<tr><td>View-Ready (Standard)</td></tr>
<tr><td>View-Ready (Ortho ready standard)</td></tr>
<tr><td>View-Ready (Ortho ready stereo)</td><td>3.3</td></tr>
<tr><td>Map-Ready 1:5,000 (Ortho)</td><td>4.2</td><td>2.0</td><td rowspan="3">Worldwide, need a fine DEM</td></tr>
<tr><td>Map-Ready 1:12,000 (Ortho)</td><td>10.2</td><td>4.8</td></tr>
<tr><td>Map-Ready 1:50,000 (Ortho)</td><td>25.4</td><td>11.8</td></tr>
</table>

Another example of VHRS data is SPOT 6/7 satellite imageries (see Table 10), that provide a geospatial information intended for civil and military mapping as well for disaster monitoring. These products are also well coordinated with radar data acquisition i.e. TerraSAR-X and TanDEM-X under the same project management at least until 2024 and afterwards. As reported in Astrium, 2013, the technical specifications about the geometric modeling are included and described in details to support further advance investigations related with the image product. In addition, the integration between optical and radar data can complement each other such as by pan-sharpening (fusion) the TerraSAR-X radar data with SPOT5 optical data (Klonus and Ehlers, 2008).

Table 10: SPOT6 product level (Astrium, 2013)

Product Level	Processing	Absolute Accuracy (m)		Geometry
		CE90%	GSD	
Primary product	Radiometric and sensor corrected	35	1.5	Sensor
Standard ortho	Radiometric, sensor corrected and Ortho corrected	10		Map projection with standard GCPs and DEM
Tailored ortho		On demand		Map projection with customized GCPs and DEM

A more advanced approach is applied by the investigation of stereo pair data from optical sensor imageries. The satellites jitter effect was introduced as a significant systematic error in the image orientation model (Jacobsen, 2018). Even though this error can be located in the order of 0.1-0.4 pixels, it is rather only validation with available high resolution DSM/DTM. In other words, the high accuracy only can be achieved by stereo pair data with a support from high resolution (accuracy) DEM. The calibration procedure as implemented by using GCP data only is not suitable for this stereo pair data because the aforementioned errors could differ from one part to another part of the image/scene.

3.1.1.2 Radar sensors

As radar stands for radio detection and ranging, distance measurements are the main component to be utilized by detecting time delay between transmitting and receiving active energy from detected objects of interest. In that sense, the basic components which shall be further taken into consideration are the range/distance (R) with a corresponding object as well as the reflectance based on its characteristics. Range can be calculated by using equation 3.1 in which c is the speed of light (299,792,458 m/s) and t is the measured time delay in second.

$$R = \frac{c\,t}{2} \tag{3.1}$$

In general, space-borne radar sensors record earth object based on three basic modes (Wang, 2008):

1. Stripmap, which records along track with fixed elevation angle;
2. ScanSAR, which records across track with varying elevation angle;
3. Spotlight, which records one object (area) from multiple elevation angle.

Table 11: Radar-based data available for DEM generation[2]

Data source	Data provision	Acquisition	Wavelength / λ (cm)	Resolution (m)
RadarSAT	Commercial	Repeat pass	5.5 (C-band)	3-100
TerraSAR-X/TanDEM-X	Commercial / Scientific	Single/Repeat pass	3.1 (X-band)	1.25 – 30
Sentinel 1A/1B	Free	Repeat pass	5.5 (C-band)	14
ALOS PALSAR	Commercial		24 (L-band)	6.25
SRTM-X	Free	Single pass	3.1 (X-band)	30
Cosmo-SkyMed	Commercial	Single/Repeat pass		3-5
ASAR ENVISAT	Free	Repeat pass		9
ERS-1/2			5.5 (C-band)	12

Radar data acquisition is a reliable technology to provide base data for topographic mapping. Its flexibility and weather independency makes radar data more attractive in comparison with traditional airborne data acquisition. This advantage emplaces radar data acquisition as an alternative method for many applications including LSTM. LSTM i.e. larger or equal than 1:10,000 map scale requires the data sources with an adequate spatial resolution i.e. better than 4 m (Digital Globe, 2016; Jacobsen, 2013).

The major drawbacks of repeat pass acquisition are the temporal decorrelation and the atmospheric constraints (Krieger et al., 2004). Single pass radar interferometry can avoid such cases by measuring the earth object simultaneously from two positions (antennas) at the same time. The Shuttle Radar Topography Mission (SRTM) is the prominent successful example of single pass interferometry to obtain a global DEM with uniform high resolution and quality (Hoffman and Walter, 2006). Hence, only data with single pass acquisition will be further evaluated in this dissertation (see Table 11).

$$A_R \approx \frac{\lambda R}{L} \qquad (3.2)$$

Following the approximation equation 3.2, in order to get 10 m azimuth resolution A_R for TerraSAR-X constellation which has a range measurement R to the earth about 580-680 km, the size of the antenna (L) shall be 1.8-2.1 km long. This type of antenna does not exist in reality because no such fuselage can operationally carry it.

Synthetic Aperture Radar (SAR) presents an alternative way to provide high resolution radar images without having such large antenna size. By synthesizing more than one

[2] https://earth.esa.int/web/guest/data-access/browse-data-products (last accessed 05.03.20)

real aperture radar in one 4.784 by 0.704 m phased-array antenna, the azimuth resolution up to 1.1 m can be achieved (DLR, 2013).

Since June 21st, 2010, TanDEM-X as a complement to the earlier TerraSAR-X is in its orbit to generate the earth surface data measurements such as phase, amplitude, etc. by using interferometric approach simultaneously. In particular, this TanDEM-X and TerraSAR-X close formation in bi-static mode aims on providing the global DEM by using Integrated TanDEM-X Processor at DLR (Breit et al., 2012). The three above mentioned modes are also applied in the TerraSAR-X and TanDEM-X data acquisition. From this point, further deeper research will identify the accuracy of this first innovative bistatic X-band Radar data acquisition in the context of LSTM activity in Indonesia.

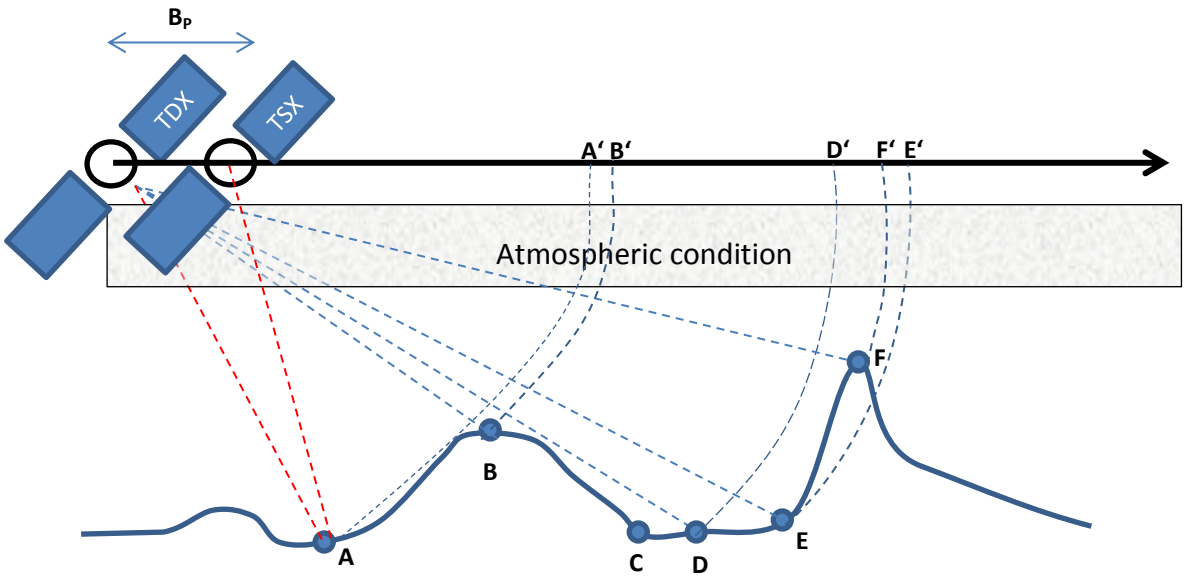

Figure 10: TanDEM-X bi-static radar data acquisition

As for the general radar data acquisition, three major error sources have to be considered in the TanDEM-X radar data processing namely foreshortening, layover, and shadow. Figure 10 shows the shrinkage of distance A'-B' named as foreshortening that happens because of the slope effect towards the radar sensor. This distortion makes the distance A'-B' look shorter than B'-D' in the slant range projection. In fact, both distances A-B and B-D shall have the same dimension in the ground coordinates. Subsequently, the layover distortion can be seen as well in Figure 10 as the projection of F' is between D' and E' in the slant range projection though in the ground coordinates the point E is located between D and F. And even worse, the point C cannot be illuminated in the side looking radar because it lies on the other side of the hill or shadowed area. For the first type of distortion, it can be corrected in the geocoding process by using a DEM. While the second also can be corrected by taking into account echo delay in the ground range coordinates, only the last type of error presents blank area in the radar image as there is no recorded data value from the radar illumination.

The advantages of TanDEM-X data acquisition as also included in Figure 10 are the elimination of the atmospheric distortion and the consideration of bi-static data measurements. Basically, the simultaneous measurements of TerraSAR-X and TanDEM-X

remove the atmospheric phase component included in the whole interferometric phase differences. An approach to effectively take an advantage from the elimination of an atmospheric effect will be explained in 3.2.2.

The bi-static radar measurement had a strategic value as Inertial Measurement Unit (IMU) and hence in the early development stage was implemented only for military purposes. In the early 20th century, it was still forbidden to export IMU equipment to Indonesia. Bi-static radar as visualized in Figure 10 adds one dimension between two monostatic distance measurements (red dotted line). Since the monostatic radar distance measurement is very accurate in the level of 3.1 cm for one cycle of X-Band electromagnetic wave, additional measurements from its tandem will enable very accurate DEM generation consequently. However this approach requires the accurate time synchronization and antenna pointing between transmitter, target and receiver (Cherniakov, 2008).

Moreover the bi-static SAR imagery is also less spiky than the monostatic one (Willis and Griffiths, 2007). In that sense, it will be less fringed by the salt and pepper effects as handled by the Speckle filtering. Hence the generated DEM based on bi-static measurements technique has an advantage to have not only better geometric accuracy but also a smoother generated relief.

The accurate perpendicular baseline B_P value (see Figure 10) is also influencing the accuracy of bi-static radar measurements. Therefore in this dissertation, a robust algorithm to provide accurate B_P values will be presented. More details about the contribution of B_P will be discussed in 3.2.2.

In addition, after the successful launch of the next complementary generation of German TanDEM-X satellite, this ambitious project will hopefully provide worldwide DEM in a resolution of 10 m in a similar way as the SRTM global DEM provision in 2000. This global DEM is already published.

However, the available IDEM from German Aerospace Center (DLR) as one useful global scientific data set still complies with High Resolution Terrain Information (HRTI) Level 3 with 10 meter (LE90%) absolute accuracy only (Weber and Herrmann, 2006).

3.1.2 UAV/Drone based data

Since the last decade, UAV technologies have shown a tremendous increase in the application, providing a basis to develop new alternative platforms for analyzing and monitoring earth surfaces. Among the available technologies, the UAV platform has a significantly rising number of applications and innovations.

At a first glance, UAV appears as a breakthrough which can combine interesting high resolution data acquisition with relatively simple and cheap platforms in comparison with conventional airborne campaigns (Neitzel, 2011). By flying on low altitude, the captured UAV photos depict the geospatial objects in high details and full color. On the other hand, the complicated regulations/restrictions in Indonesia for conventional aerial/airborne mapping survey are still somehow endorsing people to

alternatively choose UAV technology that can fly away without significant legal limitation (at least in Indonesia).

UAV as a complementary platform for geospatial data acquisition offers potentials because of its flexibility and practicability combined with low cost implementations. After all, the high resolution data collected from UAV platforms have the capabilities to provide a quick overview of one region. Nevertheless, there are some limitations that shall be taken into account in the UAV data processing for topographic mapping. One prominent drawback is that the UAV platform is only effective for relatively small areas.

In order to guarantee the necessary height accuracy, UAV data processing must be supported either by direct georeferencing using differential GPS (dGPS) and Inertial Measurement Unit (IMU) or using ground segment data i.e. Ground Control Points (GCPs) which refer to the national geodetic and geodynamic reference network. The combination between those two methods is frequently used as the optimal solution (Carrivick et al., 2016). However, GCPs are always an issue with regards to the geometric accuracy and hence the project costs (Forlani et al., 2018). Synchronizing GCP measurements can presumably increase the project efficiency without reducing geometric accuracy.

With respect to other geospatial data sources i.e. VHRS, the UAV technology can be synchronized in order to avoid project inefficiency especially in the scope of GCP requirements. Therefore the concept of a synergy between GCP and orthorectification projects is also considered in order to achieve optimum geometric accuracy with minimum redundancy.

Figure 11: Sensor platform (left), Sony NEX7 (upper right), Canon S100 (lower right)

For a UAV flight from around 200 m Above Ground Level (AGL), there is no need for specific weather conditions i.e. cloud constraints are not significantly preventing a mission. However very often, wind factors lead to difficulties for stabilizing the flimsy fuselage during the data acquisition.

Data acquisition related to this dissertation has been done using Skywalker Condor with wingspan 1880 mm (Figure 11). This platform is capable enough to carry the digital cameras used for the orthophoto productions, either Canon S-100 or Sony NEX-7 including the necessary power sources during the campaign.

In general, the Sony NEX7 has a more suitable specification for LSTM than Canon S100 especially in the image resolution which usually indicates better performance (see Table 12).

Table 12: Camera specification for UAV data acquisition

Camera	Sony NEX7	Canon S100
Weight	400 g	198 g
Resolution	24 Mpixels	12 Mpixels
Focal length	18 - 55 mm	24 -120 mm
Optical zoom	1.5 times	5 times
Sensor size	23.5 × 15.6 mm	7.44 × 5.58 mm
Image size	± 7.75 Mb	± 3.5 Mb

3.2 Processing methods

The focus on DEM generation is essential since the DEMs will be used as an input to derive both planimetric (2D) in what so called the orthorectification and the height components (3D) for each topographic feature within the scope of LSTM. For SAR-based data, there are two processing methods available to generate DEM i.e. stereo radargrammetry and interferometry techniques. In general, these two methods require also GCPs in order to solve their model parameters. On the other hand, for small/partial area the Structure from Motion (SfM) algorithm can derive 3D models in a high resolution manner without any field GCP. Finally, the standard to evaluate the generated DEM accuracy must be defined in order to be able to detect and mitigate error sources.

3.2.1 Stereo compilation

The basic principle of stereo techniques is the parallax shift measurements of brightness value (optical) or amplitude (radar) of common objects between one image to another (Crosetto and Aragues, 2000). Therefore this technique uses images pair acquired for the same areas simply from different positions or incidence angles. The stereo-pair approach for the radar and optical data solves collinearity problems by using GCPs and tie points measurements.

3.2.1.1 Stereo-pair DEM generation

The stereo-optical method is the most classical way to model the object especially for the 3D visualization purpose. This approach can be described simply at best by the stereo viewing system of human eyes. In this case, depth perception can be established if there are two perspectives available.

As also explained in the next section, the stereo-pair DEM generation provides epipolar images for each stereo-pair image in order to extract the elevation components. The difference is only in the data input, and its difficulties to identify the GCP location in the images. For manual interpretation, it is easier to locate the GCP in optical image than in the radar image.

At least 4 sets (coordinates and identifications) of GCPs are required to improve the RPCs from the sensor model correction as already explained in 3.1.1.1. However, as investigated by (Perko et al., 2018), the usage of 10 GCPs improves both planimetric (2D) and height (3D) accuracy significantly up to 1 pixel (planimetric) and 0.5-1 m (height) for Pleiades images with 0.7 m resolution.

Once the DEM has been generated, the VHRS orthorectification can be implemented in order to produce the image with the correct location on the ground by also considering the terrain condition. This aforementioned orthorectification has been selected as a mathematical solution to reconstruct remote sensing data including VHRS imagery by combining planimetric (GCPs) and terrain aspect (DEMs) of the earth surface in order to get more accurate results (Tampubolon and Reinhardt, 2015).

3.2.1.2 Stereo radargrammetric approach

The additional available measurements to be taken into account in the stereo-radargrammetric are the range and the Doppler equations. The range equation can be applied to estimate the satellite position X_S, Y_S, Z_S by using polynomial transformation with polynomial coefficients a_i, b_i, c_i and measured time delay t_R for each pixel:

$$X_S = a_0 + a_1 \cdot t_R + a_2 \cdot t_R^2 + a_3 \cdot t_R^3 \quad (3.3)$$

$$Y_S = b_0 + b_1 \cdot t_R + b_2 \cdot t_R^2 + b_3 \cdot t_R^3 \quad (3.4)$$

$$Z_S = c_0 + c_1 \cdot t_R + c_2 \cdot t_R^2 + c_3 \cdot t_R^3 \quad (3.5)$$

$$R_G = \sqrt{(X_S - X_G)^2 + (Y_S - Y_G)^2 + (Z_S - Z_G)^2} \quad (3.6)$$

By taking into account the input from GCPs (X_G, Y_G, Z_G), the range equation 3.6 for both left and right images can be solved in order to derive the polynomial coefficients as included in equation 3.3 – 3.5. Once the polynomial coefficients are solved using least square adjustment, the coordinates for the whole pixels can be calculated.

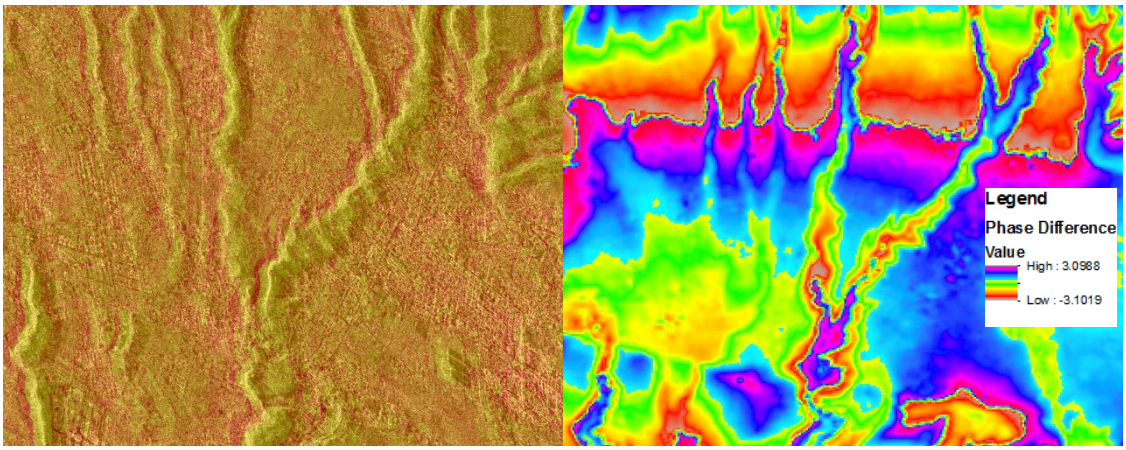

Figure 12: TerraSAR-X/TanDEM-X data of hilly Lembang, Indonesia in stereo radargrammetric method (left) and interferometric method (right)

The general workflow from stereo SAR imageries to generate DEM is described in Figure 13 and already implemented in OrthoEngine of PCI Geomatics (Toutin, 2012). As also tested by (Toutin, 2012), the generated DSMs from Radarsat-2 stereo data were validated against 0.2 m LiDAR elevation data. Whilst, Hybrid Toutin Model (HTM) without GCPs presented the LE90% (see 2.4.2 about the NMAS specifications) accuracy of 7 m, Toutin Model (TM) with 8 GCPs gave the LE90% accuracy of 6.25 m.

The concept of epipolar geometry in optical image pairs is adopted for the SAR image pairs in order to be implemented in the stereo radargrammetric approach of TerraSAR-X DEM generation workflow (Gutjahr et al., 2014). Differently to the situation in using optical satellite data, the stereo radargrammetry is not harmed by the cloud coverage. This method is suitable especially for the mountainous areas which are covered by the cloud most of the time. As investigated by (Kiefl et al., 2010), TerraSAR-X DSM generation for Alpine regions with combination of different looking direction and higher disparity angle gives the best result i.e. 3.1 m LE90%.

As depicted in Figure 12 (left), in the stereo radargrammetric method, the parallax shift resulted from both amplitudes and range measurements provides direct 3D visualization of the earth terrain. Simply by using 3D glasses, the undulations of the terrain can be seen once the geolocations and orientations for both image pairs were solved.

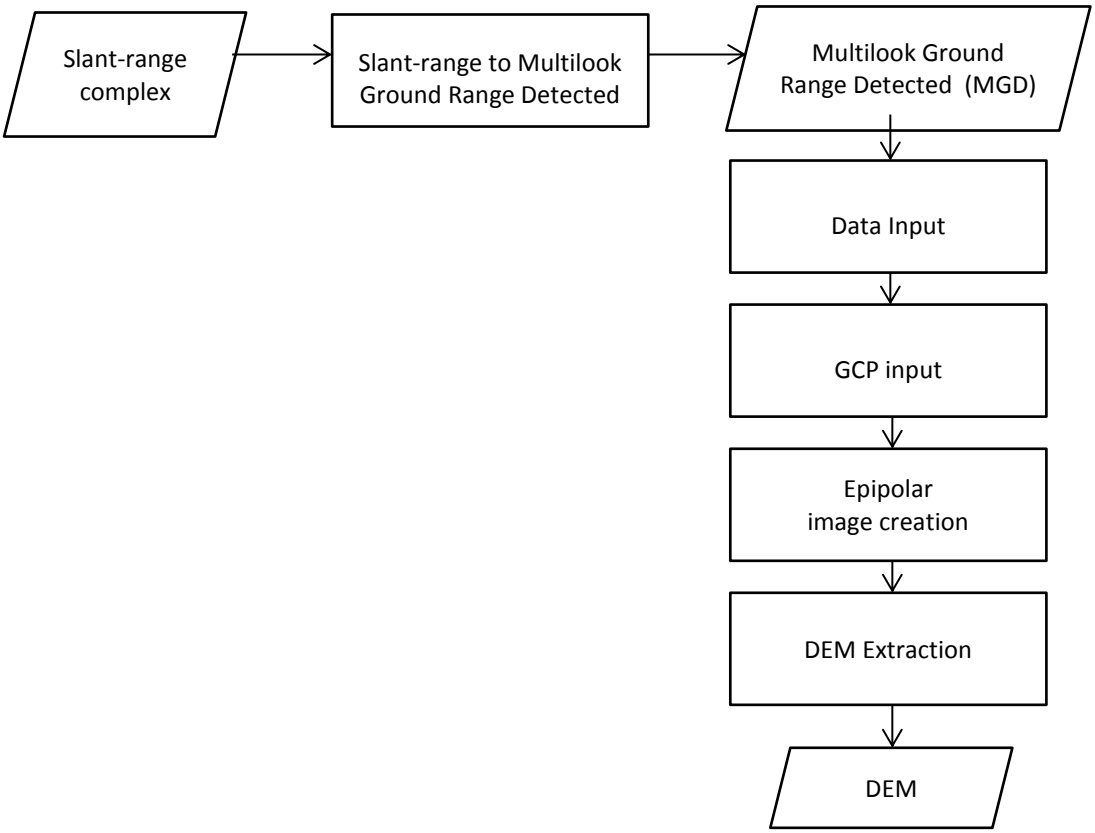

Figure 13: Stereo radargrammetry workflow

3.2.2 Interferometric SAR (InSAR)

The Interferometric SAR (InSAR) method is defined as the employment of complex valued images by reconstructing the phase value of the SAR signals (Bamler and Hartl, 1998). As depicted in Figure 12 (right), the phase differences in a form of fringes between two complex valued images are the primary output of the SAR interferometry.

In addition, the interferogram is derived by cross-multiplying one image (master) with the other image (slave). Basically, the interferogram consists of the amplitude multiplication of both images and phase differences between two complex valued images (Richards, 2007). The phase differences can be elaborated into 5 components as included in equation 3.7.

$$\Delta\Phi = \Delta\Phi_{\text{flat}} + \Delta\Phi_{\text{height}} + \Delta\Phi_{\text{differential}} + \Delta\Phi_{\text{atmosphere}} + \Delta\Phi_{\text{noise}} \quad (3.7)$$

In single pass radar interferometry as implemented by TanDEM-X bi-static data acquisition (Figure 14), $\Delta\Phi_{\text{atmosphere}}$ and $\Delta\Phi_{\text{differential}}$ can be neglected due to the same atmospheric condition and no ground displacements between master and slave scenes acquired at the same time. However, the differential phase $\Delta\Phi_{\text{differential}}$ can be further exploited to detect the ground displacement detection as will be discussed in section 6.3.

On the other hand, the phase error ($\Delta\Phi_{noise}$) depends on coherence and number of looks (DLR, 2015). The flat earth phase ($\Delta\Phi_{flat}$) due to the earth curvature also can be removed from the interferogram using a polynomial function. Once the $\Delta\Phi_{flat}$, $\Delta\Phi_{atmosphere}$ and $\Delta\Phi_{noise}$ have been removed, the remaining phase differences can be used to generate the DEMs using equation 3.8:

$$\Delta\Phi_{height} = -\frac{\Delta h \cdot B_P \cdot 4\pi}{\sin\theta \cdot R_G \cdot \lambda} \quad (3.8)$$

From equation 3.8, the height variations (Δh) can be calculated as a function of phase differences ($\Delta\Phi_{height}$), incidence angle (θ), slant range (R_G), wavelength (λ), and perpendicular baseline (B_P). More details about height variation including also the consideration of each component in the proposed DEM generation algorithm will be further discussed in 4.3.2.2.

Strictly speaking, one of the parameters affecting the DEM generation is the perpendicular baseline value (B_P) between bi-static satellites (see Figure 10). In the interferometric approach, orbital information is essentially used for the sub sequential process aiming at the DEM reconstruction, such as the co-registration step and the final absolute phase offset determination step. Referring to the analysis in Krieger et al., 2007, an error in the perpendicular baseline determination leads to a significant DEM error in a sub meter level, for more details see Cherniakov, 2008.

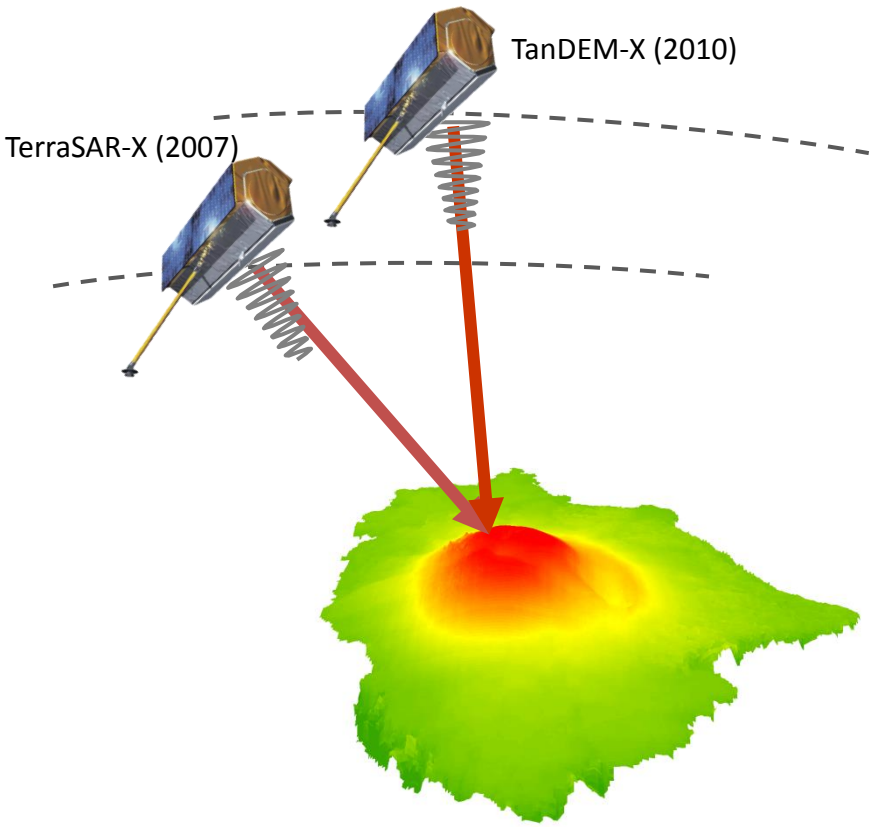

Figure 14: TerraSAR-X and TanDEM-X data acquisition

3.2.3 Structure from Motion (SfM)

Structure from Motion (SfM) is one of the prominent approaches to provide the full three-dimensional structure of an object viewed from a wide range of positions by taking into account the sensor movement along its trajectory (Westoby et al., 2012). Beforehand, a robust algorithm to produce rough 3D point clouds by using internet photographs from crowdsourcing was developed in order to implement the SfM approach (Snavely et al., 2008).

This approach can provide the relative camera position as well as the object geometries without any absolute positional (geospatial) reference as required in the conventional softcopy photogrammetric methods such as the 3D position (X,Y,Z) of the camera or a set of GCPs with a mandatory camera calibration data to perform the bundle adjustment. The terms of self-calibration techniques has been implemented to estimate the unknown camera calibration. However the value of an accurate focal length and geolocation as usually included in Exchangeable Image File Format (EXIF) tags are mandatory in order to produce better 3D point clouds (Brown and Lowe, 2005). Another important tag is the geolocation provided by the GPS camera that will be further used in georeferencing procedures and elaborated in 4.4.1.

Carrivick, 2016 et al. also has defined SfM as a method to generate 3-D information from images produced by consumer grade non-metric camera. For the purpose of producing the point cloud in the earth-reference based coordinates instead of local/arbitrary coordinates, it requires either:

- Minimum 3 set (coordinates and identifications) of GCPs,
- Direct Georeferencing (DG) equipment with kinematic dGPS and IMU,
- The hybrid combination between GCPs and DG.

Photos collected from a UAV are usually captured from low altitude. Under this circumstance, there normally is a significant occlusion surrounding the elevated objects such as high buildings, skyscrapers, towers, etc. This situation usually brings a tedious work in the data processing, especially during mosaicking tasks. However, these elevated objects can be useful if we use their 3D shapes and forms as a reference model to precisely extract image orientation parameters. As already presented by (Zhang et al., 2004), the elevated objects such as buildings and other man-made objects can be used to extract precise camera parameters for sequential images.

At this point, the camera parameters are an essential input to adjust sensor orientation from the GPS and IMU/INS equipment. Agisoft PhotoScan is one example of a software which can improve the SfM method with a more advanced feature matching algorithm in which the GCPs also can be used to achieve a good absolute accuracy (Agisoft, 2019).

Overall, SfM has an advantage as a simple technique to produce 3D geospatial data in a resolution comparable with other existing topographic data production methods. However due to the altitude limitation which is nowadays restricted i.e. less than 150 m Above Ground Level (AGL) for the Indonesian use case, the SfM method is effectively applied for relatively small areas.

3.2.4 Methods of DEM quality assessment

To evaluate the DEM quality, each mapping institution usually has its own standard operating procedure depending to the local and natural contents. For tropical area like Indonesia, there is no extreme weather change such as winter, autumn determining the seasonal land cover. By this condition, the utilization either DTM or DSM to evaluate the DEM quality is considered appropriate.

According to the NSSDA in FGDC, 1998, the reference data must fulfill two certain aspects: independence and higher accuracy. Independence means that the reference dataset is not used in the data processing or calibration. Higher positional accuracy in LSTM requires that the reference datasets are well derived by the LiDAR, Aerial Photogrammetry and point-based GNSS measurements.

Reference data is a very important part in the evaluation of geospatial data quality since it will influence the statistical descriptors from available (limited amount) datasets i.e. a sample. The selection of proper reference data prior to the description of quantitative analysis e.g. geometric accuracy, completeness, etc. is fundamental for the scientific investigation. Reference posteriori is a way to update the prior statistical analysis once the probability function e.g. the accuracy assessment takes into account the new data or information (Bernardo, 2005). Thus the reference posteriori (a posteriori) can be used to predict the appropriateness of reference datasets in a form of Probability Density Functions (PDF).

The reference posteriori is simply the deviation measures of an evaluated datasets with respect to the reference dataset, while reference prior is the first assumption for the expected accuracy. For example in the context of the orthorectification purpose, there is a possible blunder error in the GCP identification that is also used in the accuracy assessments. By measuring an a posteriori deviation of each GCP e.g. planimetric (X,Y) as calculated in Eq. 2.1 to 2.3 (section 2.4.2), the blunder errors can be identified with respect to the expected accuracy (image resolution).

In this case, the appropriateness of the reference prior is very important especially for the comparison of geometric accuracy between different datasets. In more detail, if the discrepancy for a GCP exceeds the reference prior (threshold), this GCP will be removed from the orthorectification process. The approach employed to apply the usage of reference posteriori (a posteriori) will be further explained in 5.2.2.

Taking representative samples is very important in the stochastic model for error investigation. Simple random sampling is the common method to represent population with the equal selection chance (Singh, 2003). For the purpose of DEM evaluation there are two aspects that have to be considered namely resolution and accuracy.

While the resolution of data from optical sensor depends on the flight altitude, the resolution of radar sensor data depends on the bandwidth (Bamler, 1998). The optimal resolution or GSD reflects the relative horizontal quality and level of detail of the DEMs. The DEM resolution of the evaluated data also can be used as an indicator to determine the appropriateness of reference data for the quality assessment. As an example, it is not proper to use SRTM data in 30 m resolution for the purpose of TanDEM-X data quality assessment with 8 m resolution.

Since DEM represents the earth surface in a discrete value (Z) for each pixel (X, Y) or grid point, the simple random sampling with replacement method is suitable to assess the accuracy. One example of simple random sampling in the field of digital geospatial data evaluation is the ICP selection. The accuracy test guidelines of FGDC, 1998 define a minimum of well distributed 20 ICPs to fulfil the 95% confidence level for each dataset. For the insufficient number of ICPs (< 20), additional measures such as deductive estimation, internal evidence recognition or source comparison must follow (FGDC, 1998).

3.3 Summary

For the following investigations in this dissertation, this chapter summarizes the available and potential data sources as well as the suitable data processing scheme to be implemented. These aforementioned data sources will be extensively discussed to present the so called alternative LSTM development concept in the next chapter.

Firstly, with a huge area like Indonesia, it is obvious that the suitable data sources for 1:10,000 LSTM are optical and radar spaceborne data. The VHRS imagery for example QuickBird in 60 cm resolution is selected as the use test case for its large ratio between resolution and accuracy (Table 8). In this case, it will be further investigated how the influence of GCPs and DEMs can improve the accuracy of the QuickBird data. In addition, it was expected that QuickBird imagery can fulfill the planimetric (2D) required RMSE given in 2.4.2 (Table 5) for 1:5,000 LSTM (class II maps) i.e. 1.98 m or three times the above mentioned resolution. The synchronized orthorectification and GCPs measurements program is considered essential in particular for mountainous/hilly area. In this context, the reliable and up to date DEMs are mandatory.

Secondly, in a comparison with the stereo optical method, stereo radargrammetry is a more advanced and comprehensive solution to overcome the weather constraint as well as to achieve better geometric accuracy. By using an active sensor, the stereo radargrammetry has taken into account the slant range measurements in addition to the acquired amplitude values.

Finally, the DEM quality assessment procedures are the last but not the least component to evaluate the compliance of proposed approach with respect to the LSTM technical specification in Indonesia. The direct comparison with reference datasets based on the NSSDA procedure is selected but with a stepwise solution to identify the potential error in the DEM generation process. For example the layover, foreshortening and shadow area must be taken into account as explained in 3.1.1.2 before further proceed with the DEM quality assessment.

4 Development of Concept

In this chapter the concepts developed in relation with the goals of this dissertation are presented. As will be discussed in 4.1, UAV data, VHRS imagery and InSAR data processing rely on accurate local height reference data using the Indonesian Geospatial Reference System (SRGI) for the whole investigations. Sec. 4.2 discusses the selected data as potential sources for LSTM. As a comparison with the more accurate approach in the subsequent section, the stereo radargrammetry approach using GCPs was also applied as explained in 4.3.1. The development of more robust approach in the DEM generation by using GCPs and DEM reference is briefly explained in 4.3.2. Finally, Sec. 4.4 deals with the specific purposes of UAV based data.

4.1 Generation of GCPs

Even though there are a lot of tremendous improvements in remote sensing sensor capabilities to produce geospatial data without any field data, the question about their positional (geospatial) accuracy is always interesting. In order to address that question, many tasks in LSTM rely mostly on GCP data, not only for geospatial data calibration but also for accuracy validation at the end.

4.1.1 GNSS/GPS measurements

The GNSS/GPS survey to provide the representative GCP network with a good spatial distribution over the whole test areas addressed two main objectives: (1) to check the quality of the acquired photograph including photo orientation and (2) to establish an accurate GCP network for orthorectification purpose.

During the data acquisition, all GCPs have been measured using geodetic GPS double frequency L1/L2 with representative distribution covering the AOI. Implementing rapid static differential positioning method, every GCP has been measured not less than 30 minutes as a pre-condition in order to get centimeter accuracy as expected by the UAV data resolution.

In addition to the rapid static measurements, additional points i.e. *Independent Check Points* (ICPs) have been measured utilizing the *Continuous Operating Reference System* (CORS) service method for elevation accuracy assessment purpose only. These measurements also enable the synchronization of the positional reference between static and real time modes which are in the range below 1 m accuracy. Hence it will ensure the consistent positioning reference both for UAV data processing and accuracy assessment.

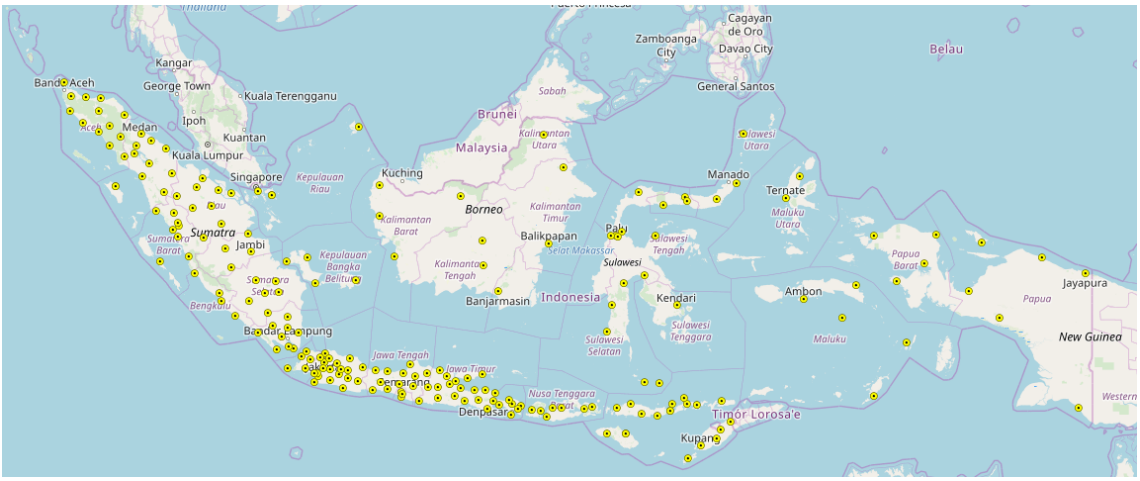

Figure 15: CORS station distribution in Indonesia (courtesy of BIG, 2019)

Related with GCP measurements, there are two types of fundamental geospatial data which shall be used as a reference for thematic or general spatial purposes. Those basic geospatial data determine overall geospatial accuracy in order to support a "One Map" policy in Indonesia. This policy restricts any thematic geospatial users to refer on fundamental geospatial datasets e.g. topographic map, coastal map and national sea map.

The first component is the topographical map itself which will be provided in the *Indonesian Spatial Data Infrastructure* (Ina- SDI). This type of reference frame must be used as the official reference for both the content and the positional (geometrical) aspect. Second is the geodetic and geodynamic control network which can be considered as Indonesian Geospatial Reference System (SRGI). As a main core component, this official network mainly establishes reference stations serving different kind of users including topographical map producers. The question about availability is always raised regarding to the reference control network (Figure 15).

In the context of the technical implementation, there are 4 options used to process GPS/GNSS data:

1. Near fix reference
   As an example for Borobudur test area (5.2), GNSS measurements refer to the nearest available CORS operated by BIG which is located in Magelang city (CMGL), around 14 km north of the AOI as an example for one specific test area. This CORS station can deliver GPS raw data in the highest resolution i.e. up to 1 second interval time. In particular, the GNSS reference point was put in the center of the Borobudur Temple test area as indicated by blue benchmark (Figure 17) in order to support more accurate rapid static measurement of each surrounding GCP.

2. Precise Point Positioning (PPP)
   PPP is an online application for GNSS data post-processing that allows users to submit raw GNSS data via internet and receive data with enhanced positioning precisions within a global reference frame, based on precise GNSS orbit and clock information.

3. Absolute positioning
   The measurement is performed independently without any reference station consideration.

4. Far fix reference
   GPS measurements refer to the CORS operated by BIG which is located in BIG office (BAKO), around 400 km from the AOI for the worst case.

GNSS measurement schemes can lead to the proper field data collection and processing methodology with respect to the accuracy requirement. As a compromise, PPP brings reliable solution independently from the reference network coverage despite of its sub-meter accuracy.

Figure 16: GNSS survey

4.1.2 GCP identifications

GCP selection has been performed in the field by defining points which can be identified clearly in the photo or VHRS imagery with high certainty. Suitable examples of this regular form features are the building edge, the statue and the tile objects (Figure 16). The point selection has to be done by extracting point objects from regular form features within the minimum size of 2 times photo resolution i.e. 10 cm for 5 cm GSD (Figure 17).

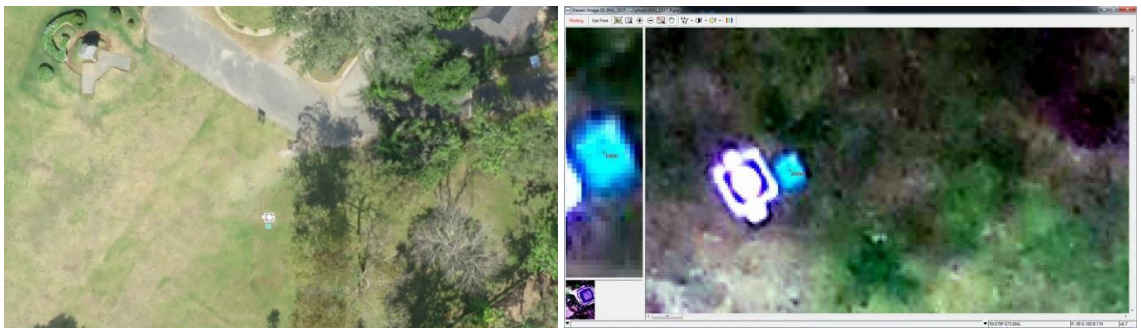

Figure 17: GCP identification from the raw photo (left) and orthophoto (right)

At the first place, orthorectified VHRS imagery with planimetric accuracy in the level of 1.7-2.1 m (CE90) as further emphasized in 5.2.2 has been used as the reference image to be used as the GCP sources of UAV data. Certainly it requires elevation data in which it can be extracted from radar space borne data i.e. TanDEM-X DEM. Currently, this radar space borne data has just been used for the medium scale topographic mapping e.g. up to 1:25,000. By using this approach, the provision of DEM from UAV data presented a potential solution for LSTM i.e. 1:5,000.

4.2 Data sources

The selected data sources based on recommendation in 3.3 are:

- VHRS imageries (QuickBird, SPOT6, TanDEM-X)
- UAV data captured by consumer grade cameras (Sony NEX7, Canon S-100)

The space borne optical data recommended in this dissertation are pan-sharpened SPOT 6 with a resolution of 1.5 m and pan-sharpened Quickbird with a resolution of 0.6 m (see Table 10 for more detail about available SPOT 6 data specification). Related to these imageries, there are two types of processing levels which shall be compared. A primary standard product is used for customized orthorectification by using GCPs and DEM data while Standard ortho product has been geometrically corrected by encountering viewing angle and ground effects.

The evaluation of national orthorectification program by using selected VHRS in particular for the provision of data sources for LSTM is intended. For that case, it shall fulfil 5 m planimetric accuracy (CE90). Hence, to fulfill the requirements, the comparison between different DEMs as a mandatory input for orthorectification is necessary.

It has also been investigated how services provided in the context of the Services and Applications for Emergency Response (SAFER) project can be used to produce virtual GCPs from more accurate reference images, which lead to useful results (Schneiderhan et al., 2010). In this context, the integration of optical (SPOT 6) and radar (TanDEM-X) data for LSTM has been implemented for the Digital Elevation Model (DEM) generation process.

In addition to the above mentioned orthorectification purpose, space borne radar data also has an important contribution to the topographical mapping workflow as it requires DEM. This DEM is used as a basis for creating terrain information including contour lines and other hypsographic components such as spot heights, breaklines, etc.

The advent of TanDEM-X with a bi-static interferometry aims on providing HRTI level 3 global DEMs which has an accuracy within 10 m absolute horizontal (circular error) and 10 m absolute vertical (linear error) at 90% level of confidence. TanDEM-X generation implemented data acquisition using bi-static InSAR approach (DLR, 2012). The basic principle is performing the simultaneous measurement of the same scene and identical doppler spectrum by using two sensors, thereby avoiding temporal decorrelation.

Specifically, IDEM released by TanDEM-X scientific service in 2014 has found its way to comply with the HRTI level 3 specifications (DLR, 2018). While using interferometric approach in the DEM generation, the height calibration still relies on the GCP from Ice, Cloud and Land Elevation Satellite (ICESat) though. This scientific data has

been used to verify the DEM generation process using stereo radargrammetry approach.

By the advent of the revolutionary single pass bi-static TanDEM-X InSAR data, the accuracy of generated DEMs can be improved not only to comply with HRTI level 3 as mentioned above but also up to the HRTI Level 4. Since the temporal decorrelation and atmospheric influence are no longer significant issues for DEM generation using single pass TanDEM-X data, the synchronized absolute phase offset and baseline adjustment is the only major constraint to be solved for more accurate InSAR DEM generation. Currently, this data source is only used for medium scale topographic mapping up to the 1:25,000 map scale. For larger map scales the integration with GCPs or high resolution DEM from UAV data is assumed as a potential solution especially in order to improve the absolute accuracy of elevation data. The selection of UAV data as a partial DEM reference data is feasible and also time efficient especially in the context of LSTM and DM procedures.

4.3 DEM Generation using TanDEM-X data

In this section, the InSAR DEM generation for the selected test area using TanDEM-X Coregistered Single-look Slant-range Complex (CoSSC) data is briefly explained. The extension of the linear model is intended to provide the accurate perpendicular baseline as discussed in section 3.1.3, presents the usage of high resolution height references e.g. UAV DEM, LiDAR DEM, Airborne metric camera DEM, GCP data.

4.3.1 Stereo radargrammetry using GCPs

As depicted in Figure 18, the GCPs have been selected from optical dataset into radar dataset based on feature extraction from Ortho Rectified Imagery (ORI). At the first place, orthorectified SPOT-6 data with a planimetric accuracy of 4.7 m has been used as the reference image for the first orthorectification of radar data. Certainly it requires elevation/height information that can be extracted from radar space borne acquisition i.e. TanDEM-X DEM.

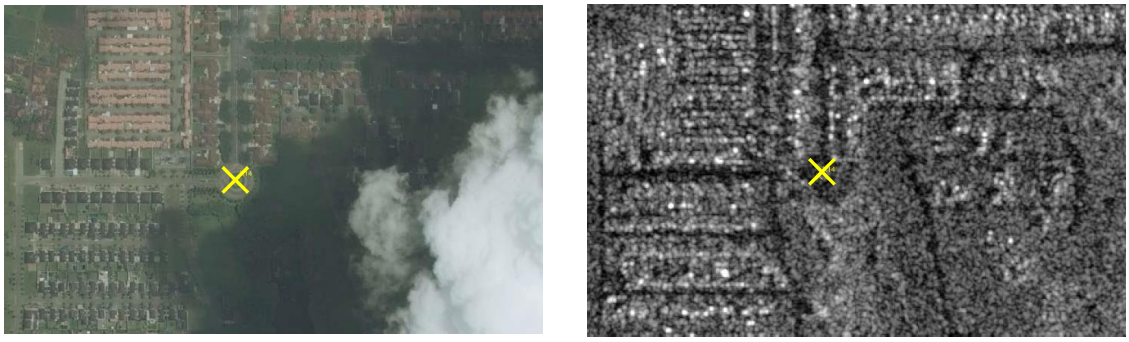

(a) GCP in the optical imagery (b) GCP in the Radar Imagery

Figure 18: Common GCP both in optical and radar Imagery

By implementing GCP transfer from an optical to a radar dataset, DEM enhancement can be achieved in order to provide a reliable space borne dataset. In this case, planimetric position of GCPs in optical imagery (Figure 18 (a)) can be projected to the Orthorectified Radar Imagery (ORRI) resulted from the first initial orthorectification (Figure 18 (b)). Subsequently, these transferred GCPs are used for the improved DEM generation process. This process is continuously running until the expected accuracy for 1:10,000 map scale namely < 4.33 m (CE95) as included in Table 4. is reached.

The final GSD has been defined in ≤ 6 m for DEM and 1.5 m for optical satellite imagery to fulfill the geometric accuracy and specification of HRTI-4 (Table 6) and 1:10,000 LSTM (Table 4). This resolution allows that during digitation, object patterns with optimal zooming can be recognized in the stereo plotting environment.

In order to minimize radar data distortion, three pairs of both TerraSAR-X Multilook Ground range Detected (MGD-SE) ascending and descending scenes have been used in the stereo-radargrammetric processing. This radargrammetric approach provides DEM in 6 m resolution which is essentially better than IDEM data.

4.3.2 InSAR extension in SNAP Desktop

For further development of a more reliable and adaptable approach in InSAR DEM generation, the open source Sentinel Application Platform (SNAP) from ESA which is the next generation of the Next ESA SAR Toolbox (NEST) focusing on radar interferometry and polarimetry is selected as the processing software. Obviously the TanDEM-X CoSSC format which is the focus of the investigations can be processed already by the SNAP desktop.

4.3.2.1 InSAR DEM generation workflow

The interferometric phase differences between two radar measurements from slightly different looking angles enable the height (altitude from Height Reference) derivation once ground references are known (ESA, 2007). The higher coherence and more precise coregistration between master and slave interferograms are the prominent advantages to generate more accurate DEM (Richards, 2007). For its single pass data acquisition as explained in 3.2.2, the TanDEM-X platform has some advantages related with the quality of CoSSC data as the raw data for DEM generation. Therefore TanDEM-X data will be used for all different test areas in the investigations.

Figure 19 visualizes the general steps for InSAR DEM generation in SNAP desktop by using TanDEM-X CoSSC (TDM) with a more detailed elaboration as follows (explained from stepwise task in Veci, 2016):

1. Interferogram formation of the CoSSC data (TDM format)

   This step provides an interferogram from the pair wise bi-static data acquisition. In order to get only the topographical phase, the flat earth phase must be subtracted.
2. Goldstein filtering

   The objective of the Goldstein filtering is to reduce the number of inaccurate fringes from the interferogram.
3. Multilooking

The interferogram multilooking step is necessary to increase the positional accuracy of the intensity and wrapped phase by increasing the number of looking views of the CoSSC data. Normally, 2-5 looking views are the optimal solution to produce effective ground range pixels.

4. Export to SNAPHU[3] (Statistical-Cost Network-Flow Algorithm for Phase Unwrapping)

   Currently, the complicated phase unwrapping built-in step is still not provided by the SNAP desktop. Nevertheless, SNAP has an export functionality to hand over the task to the SNAPHU platform.

5. Phase unwrapping in SNAPHU (Linux-based)

   Phase unwrapping using SNAPHU consumes a lot of Random Access Memory (RAM) during processing. Therefore as a rule of thumb, it is necessary to subset the whole area into a size of less than 20 megabyte of Wrapped phase interferograms.

6. Unwrapped phase to elevation

   The Elevation (height) calculation in SNAP is mainly based on a DEM reference e.g. SRTM 1 Arc Second as an existing topographic phase reference. Hence, the absolute phase offset is determined by the DEM reference accuracy.

7. Geocoding

   The geocoding in SNAP considers the terrain correction as well as the GCPs input if available. However, only planimetric (X,Y) information from the GCPs can be taken into account in the geocoding step.

However, the generated DEM as derived by applying the above mentioned steps is not accurate enough for the LSTM requirements. As a preliminary test in our test area, we get 10.97 m (95 % height accuracy) of the generated DEM from S01 dataset (Descending-30-01-2012) which is out of the level of the HRTI-3 specification. The main missing part in SNAP desktop is the height calibration based on GCP input. Currently the GCPs are only involved in the geocoding step (step 7) and not in the absolute phase offset estimation (step 6).

[3] https://web.stanford.edu/group/radar/softwareandlinks/sw/snaphu/ (last accessed 05.03.20)

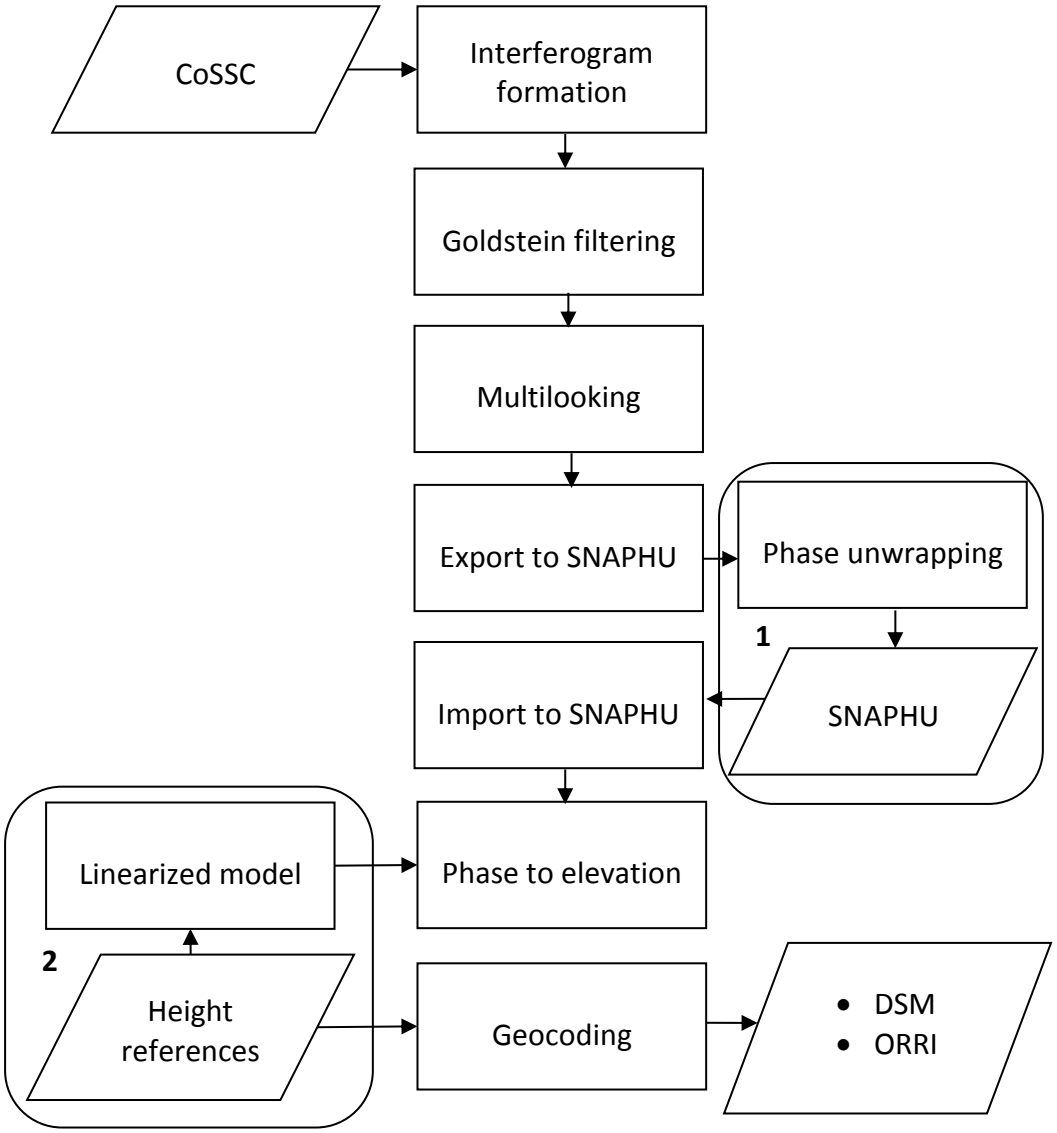

Figure 19: DEM Generation workflow using CoSSC data

4.3.2.2 InSAR DEM generation with a linearized model

In order to produce an effective overlap of each doppler spectra, TanDEM-X InSAR DEM requires an along track baselines less than 2 km with an across track baselines in the range between 300 m - 1 km (Krieger et al., 2007). On the other hand, an alternating acquisition mode is also available which allows the simultaneous interferogram generation with single and double baseline of the radar systems (ping pong). The accurate baseline information thereby is really mandatory to produce a high quality DEM.

In addition, errors in the baseline estimation induce a low frequency modulation of the generated DEM. Hence they contribute significantly to the relative and absolute height accuracy. Especially for absolute height accuracy, HRTI level 4 requirement is stricter and requires an accuracy of 6 m at a 90% level of confidence (see Table 6). In general, radar interferometry requires precise (scientific) orbital information measured from

on-board sensors in order to provide georeferenced data without any field GCP. Unfortunately, due to some errors during data acquisition it is mostly not possible to reach the required accuracy without any field GCPs. Specifically for radar data, the important component is the height itself and not the 2 D (X,Y) location of GCP as stressed for the orthorectification purpose. Even though on board GNSS in TanDEM-X platform usually can determine the satellite location very precise up to 1-2 mm, the baseline error estimation contributes significantly to the generated DEM (Cherniakov, 2008).

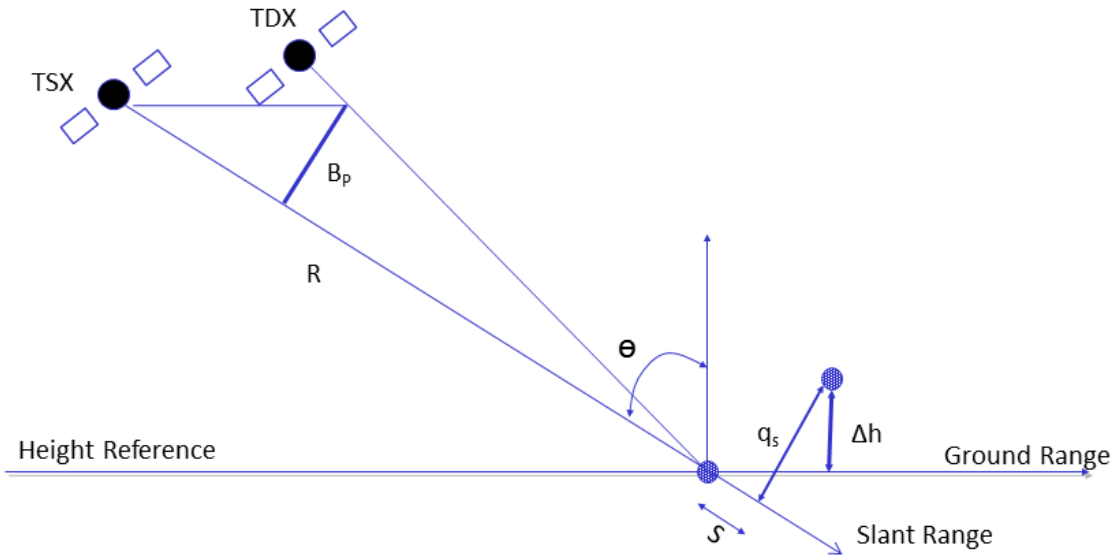

Figure 20: Height calculation consideration in the linear model

For the InSAR DEM generation, the interferometric phase difference is correlated with the elevation difference in the corresponding measured object on the ground. From this point, the focus lays on the exploitation of phase difference measurements in single pass radar interferometry to generate a DEM with least square adjustment approach. Hence as depicted in Figure 20, the known parameters from TanDEM-X CoSSC data are:

- Range R is the slant range distance between radar sensor (master) and object on the ground in meter
- Incidence angle θ is the angle between normal and the slant range distance pointing to the radar sensor (master) in degree
- Resolution S is the capability of radar measurement to distinguish objects on the ground in meter
- Slant range elevation q_S is the elevation perpendicular to the slant range in meter

Where the unknown parameters are:

- Height reference h_{ref} is the imaginary flat plain to be used as the zero height to each detected object in meter
- Perpendicular baseline B_P is the distance between TerraSAR-X and TanDEM-X perpendicular to the slant range in meter
- Relative height Δh is the height difference between detected object and the height reference in meter

From Figure 20, the basic equation for the InSAR height calculation can be developed in equation 4.1 with additional known parameters from the radar sensor or measure-

ments: wavelength λ in meter, t in second and constant speed of light C_0 in meter/second, measured phase difference Φ in degree, time delay in second. The second term in equation 4.1 includes a very important indicator for radar interferometry i.e. Height of Ambiguity (HOA) as will be further explained in 5.2.3. As depicted in Figure 20, HOA will determine the relative terrain height (Δh) in which it decreases along with increasing perpendicular baseline length (B_P). Therefore in principal the smaller the HOA the more sensitive or more accurate is the InSAR DEM generation. Once the h_{ref} and Δh are solved, the height above ellipsoid h_{ell} for all part h_n of the interferogram can be calculated.

In order to comply with the HRTI Level 3 standard, it shall be noted that the height ambiguity must be in the order less than 40 m (Krieger et al., 2004). In most cases, it is difficult to fulfill this requirement including for the dataset used in this dissertation as will be explained in section 5.2.3, 5.3.2, and 5.4.2.1.

$$\boldsymbol{h_{ell}} = \boldsymbol{h_{ref}} + \frac{\boldsymbol{\Phi}.\lambda.C_0.t.\sin\theta}{8\pi\ .B_P} \tag{4.1}$$

$$\boldsymbol{f}\ (\boldsymbol{t}) = \boldsymbol{f}(\boldsymbol{a}) + \boldsymbol{f}\ `(\boldsymbol{t}-\boldsymbol{a}) + \frac{f^n}{n!}(\boldsymbol{t}-\boldsymbol{a})^n \tag{4.2}$$

Taylor series linearization based on equation 4.2 of equation 4.1 yields:

$$\begin{bmatrix} \boldsymbol{h_{ell}} \\ \vdots \\ \boldsymbol{h_n} \end{bmatrix} = \begin{bmatrix} \frac{\Phi\ \lambda.\mathrm{t}.C_0.\sin\theta}{8\pi\ .B_P} \\ \vdots \\ \frac{\lambda.t_n.C_0.\sin\theta_n}{8\pi\ .B_P} \end{bmatrix} + \begin{bmatrix} \mathbf{1} & \frac{\lambda.C_0.t.\sin\theta}{8\pi\ .B_P} & -\frac{\Phi.\lambda.C_0.t.\sin\theta}{8\pi\ .{B_P}^2} \\ \vdots & \vdots & \vdots \\ \mathbf{1} & \frac{\lambda.C_0.\sin\theta_n}{8\pi\ .B_P} & -\frac{\Phi.\lambda.C_0.t.\sin\theta_n}{8\pi\ .{B_P}^2} \end{bmatrix} \begin{bmatrix} \boldsymbol{h_{ref}} \\ \Delta\Phi \\ \Delta\boldsymbol{B_P} \end{bmatrix} \tag{4.3}$$

From equation 4.3, there are three main parameters namely height reference h_{ref}, phase offset ΔΦ and corrected baseline ΔB_P to be solved in a linearized model. With this lightweight linear function, the parameter can be solved and convergent after 4-5 iteration. As an initial input (values), the effective baseline and phase offset from CoSSC metadata are available. Important is the correct sign (-/+) of the effective baseline to provide the convergent results in the adjustment. The proposed linear model is implemented in the unwrapped phase to elevation step as already explained in 4.3.2.1.

4.3.2.3 Height calibration algorithm with reliable reference data

As already presented by Zhou et al., 2011, the ICESat data can be used to calibrate the residuals in InSAR DEM generation. In addition, the TanDEM-X project is also designed to support the DEM production on a local scale (DLR, 2018). At this point, certainly more accurate field GCPs based on local datum i.e. SRGI will increase the DEM accuracy. The accurate height from GCP is used as an input to adjust the main parameters in InSAR DEM generation namely height reference h_{ref}, absolute phase offset ΔΦ and perpendicular baseline B_P value.

The absolute phase offset ΔΦ, emphasized in Mura et al., 2012 and Lachaise et al., 2014, is a very essential parameter in SAR interferometry. The main reason is that it allows the geocoding algorithm to find a solution for the phase to height as a part of

the DEM generation. Error estimation for the phase offset produces shift and noise in the generated DEM. Therefore it is a mandatory to overcome these offset in order to provide a correct estimation. By performing this calibration with an accurate height reference data, the absolute circular and linear error can be increased significantly.

The baseline phase offset estimation result using phase offset functions (POF) as investigated by Mura et al., 2012 indicated a vertical accuracy in the level of 3 meter (2.768 m) by using OrbiSAR X-Band data. From this result, it will be possible to improve the vertical accuracy of TanDEM-X data by taking into account GCP data in the subsequent linear phase offset estimation using SNAP desktop as already discussed in 4.3.2.1.

In addition, several drawbacks have been counted in radar sensor platform due to its basic principle of range measurements on space (Richards, 2007). As explained in 3.1.1.2, layover and foreshortening are the most significant problems for radar measurements. In principal, radar anomalies e.g. foreshortening, shadow and layover can be minimized in the radar data by using multi data set (from different looking directions) and the secondary data such as DEM.

The main advantage of TanDEM-X data acquisition is the capability to provide on-demand very high resolution data independent from weather conditions with high coherence. Frequently, InSAR uses active sensors aiming at DEM as well as orthoimage generation. In this section, the aim on extending the method of InSAR DEM generation to provide a sufficient accuracy for LSTM by only using a minimum amount of GCPs is introduced. For this purpose, a linearization of phase offset estimation as explained in the previous section (4.3.2.2) has been selected as a potential solution to increase the height measurement accuracy based on more accurate (reliable) reference data.

Therefore, the height calibration algorithm by taking into account the unwrapped phase as well as the height information from the GCPs was developed. As depicted in Figure 19, the focus on two components which are SNAPHU phase unwrapping (1) and the extension of InSAR in phase to elevation step (2) is addressed.

There are some pre-condition and consideration for the proposed algorithm:

- The input parameters: unwrapped phase, effective (perpendicular) baseline and initial phase offset from TDM metadata.
- The constants : wavelength λ, speed of light C_0
- The phase offset functions : from equation 4.3
- The GCP data provide accurate height reference on a local scale based on the Indonesian Geospatial Reference System (SRGI)
- Linear adjustment of 3 parameters : height reference h_{ref}, absolute phase offset $\Delta\Phi$, and baseline ΔB_P
- Output : unwrapped phase, final height reference and adjusted baseline
- Unwrapped phase to elevation: calculated height based on adjusted parameters.

The linear adjustment has been selected because of the flat earth consideration. Finally, the implementation of a least square adjustment on linear height model provides height for the whole interferogram which is already discussed in section 4.3.2.2.

Those three above mentioned parameters are considered to be essential within the DEM generation process. Therefore it is necessary to find the optimal solution within the aforementioned adjustment model. In the proposed approach, the linearized

model is selected, as discussed in section 4.3.2.2, to process the bi-static TanDEM-X datasets and investigate how this improves the accuracy of the generated DEM.

The proposed approach needs precise GCP data from GNSS measurements referring to the local height reference system. The focus of the investigation also put to incorporate the role of existing phase difference consideration into the height derivation method. The main goal is to present a more robust approach for the DEM generation based on linear equations to accurately provide the above mentioned main parameters.

In this approach, the height reference is fixed as a basis for the absolute height determination within the height derivation model. In addition to the flat earth model, the main reason of this selection is that the height reference has its height system locally to the SRGI ground coordinates. This national (local) framework minimizes the height error contribution to the proposed algorithm in order to improve the generated DEM accuracy from TanDEM-X CoSSC StripMap data at the end.

To evaluate the approach, the comparison with different height references namely GCP, DEM used for the absolute phase offset estimation is proposed. From this step, the selection of the appropriate height reference which is adequate enough for the linear model implementation will be investigated. In order to evaluate the results, it is necessary to compare the generated DEM data with the other available DEM sources. Finally the influences of height reference to the whole DEM generation process such as the coverage of the height reference and its accuracy will be also briefly discussed.

4.3.2.4 Differential InSAR for Disaster Management (DM)

The Indonesian Tsunami Early Warning System (InaTEWS) is the built-in system handed over by the former Government to Government (G-G) cooperation initiated after the 2004 Indian Ocean Tsunami in a so called German Indonesian Tsunami Early Warning System (GITEWS). Technically it consists of land and sea monitoring components as depicted Figure 21. The land monitoring part is equipped by mainly GPS/GNSS and broadband seismometer units while the sea monitoring part is equipped by buoy, tide gauge and ocean bottom units. As the corresponding legislation Act Nr.31/2009 stated that Meteorology and Climatology Agency of Indonesia (BMKG) is responsible to deliver the tsunami early warning, InaTEWS is well maintained essentially by BMKG.

The existing InaTEWS has not yet integrated the volcanic eruption detection system in which it also can be a potential source for a tsunami event as occurred at the end of 2018 in Indonesia (Tampubolon and Reinhardt, 2019). Therefore it is necessary also to improve the current InaTEWS with Differential InSAR (D-InSAR) technique especially for volcanic islands such as Anak Krakatau, Gamalama, etc. This improvement enables more accurate DM analysis for a better disaster preparedness in the future.

On the contrary to the DSM generation purpose, a single TanDEM-X data acquisition is not intended for Differential InSAR to detect phase differences contribution as an earth deformation component. Since earth deformation occurs for a long time period, multi temporal datasets are more suitable for this purpose.

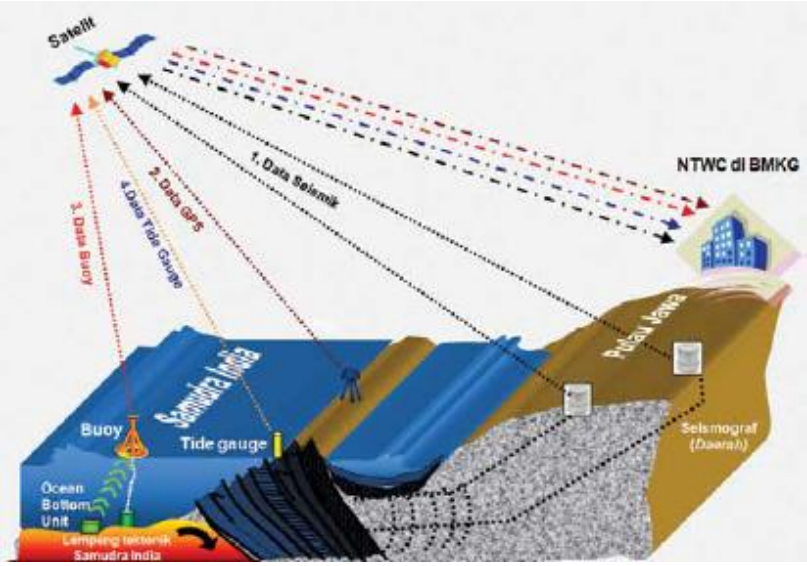

Figure 21: InaTEWS components (BMKG, 2012)

$$\Phi = \Phi_{flat} + \Phi_{height} + \Phi_{differential} \tag{4.4}$$

From equation (4.4), the differential phase component can be subtracted from unwrapped phase ($\boldsymbol{\Phi}$) if the flat earth phase and height phase are known (Richards, 2007). Afterwards the deformation (d) in meter from multi temporal datasets can be calculated using equation (4.5), where $\boldsymbol{\lambda}$ = wavelength (X Band) = 0.03106658 m with a frequency of 9649.999293 MHz.

$$d = \frac{\lambda \, \Phi_{differential}}{4\pi} \tag{4.5}$$

Differential InSAR can be applied by using time series radar data to detect earth surface deformations up to a precision within a few millimeter levels especially in the situation where accurate DEM references and/or GCP are available. However in the disaster area it is sometimes difficult to provide actual DEM and/or GCPs data. Therefore the new height calibration algorithm in the linear model as explained in 4.3.2.3 contributes in the differential phase depending on the DEM reference accuracy. The deformation can be detected in a degraded centimeter level accuracy for the case where SRTM 1 arc second is used as DEM Reference as presented in 6.3.

4.4 UAV-based data for specific purposes

In this section, the UAV-based data processing using common (cheap) fuselage and consumer grade cameras is briefly explained. The UAV-based data processing is intended to provide high resolution data as discussed in section 3.1.2 by presenting the usage of building structures to reduce the number of GCPs. In addition, classification methods of UAV data for disaster feature extraction are also further explored.

4.4.1 UAV data georeferencing using building structure model

The results of UAV data investigations from Javernick et al., 2014 indicate georeferencing errors in the level of decimeter (0.04 m) for planimetric and centimeter (0.10 m) for elevation in a non-vegetation area. This result endorses us to improve the orientation parameters from SfM software (Agisoft PhotoScan) by taking into account the building structures in the subsequent bundle adjustment using conventional photogrammetric software (PCI Geomatica).

The simple building structures play a significant role in such a way that local geometrical knowledge can help to add more conditions in the computational equations. Some instances are the orthogonality of the building's wall/rooftop and the local knowledge of the building orientation in the field.

In this specific task, the mosque has been selected as a building reference object for orientation parameter determination. In addition to the orthogonality of the rooftop, the main reason of this selection is that the mosque has its regular building orientation towards city of Mecca as visualized in Figure 22 (right). This regularity makes also an exclusive input to the algorithm without any necessary measurement on the field.

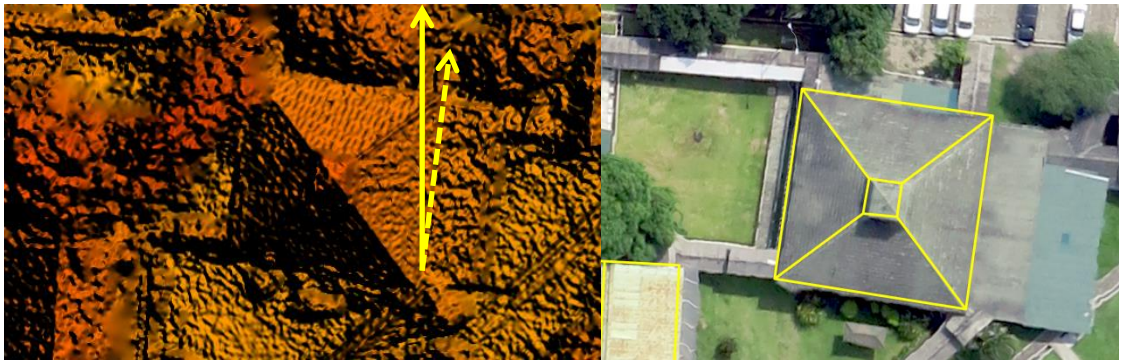

Figure 22: The building orientation of the mosque (point cloud: left, orthophoto: right)

The building outlines as depicted in Figure 22 (right) are manually digitized using 3D stereo working station (Summit Evolution) in mm height resolution to be used for the orientation parameters improvement. The absolute accuracy of these data, captured from the Leica RCD30 imagery, is 1.55*GSD = 7.75 cm. As an example for the mosque, the 8 edge points of the rooftop with additional 4 orthogonal lines and 4 edge lines were compiled.

Agisoft PhotoScan is an image processing software that can be used to apply SfM. This software implements a robust feature matching algorithm across the images. Initially, Agisoft PhotoScan detects points in the source images which are relatively stable from different viewing points as well as lighting sources including their descriptors. Finally, these descriptors are used to reconstruct the structures across the sequential images (Agisoft, 2019).

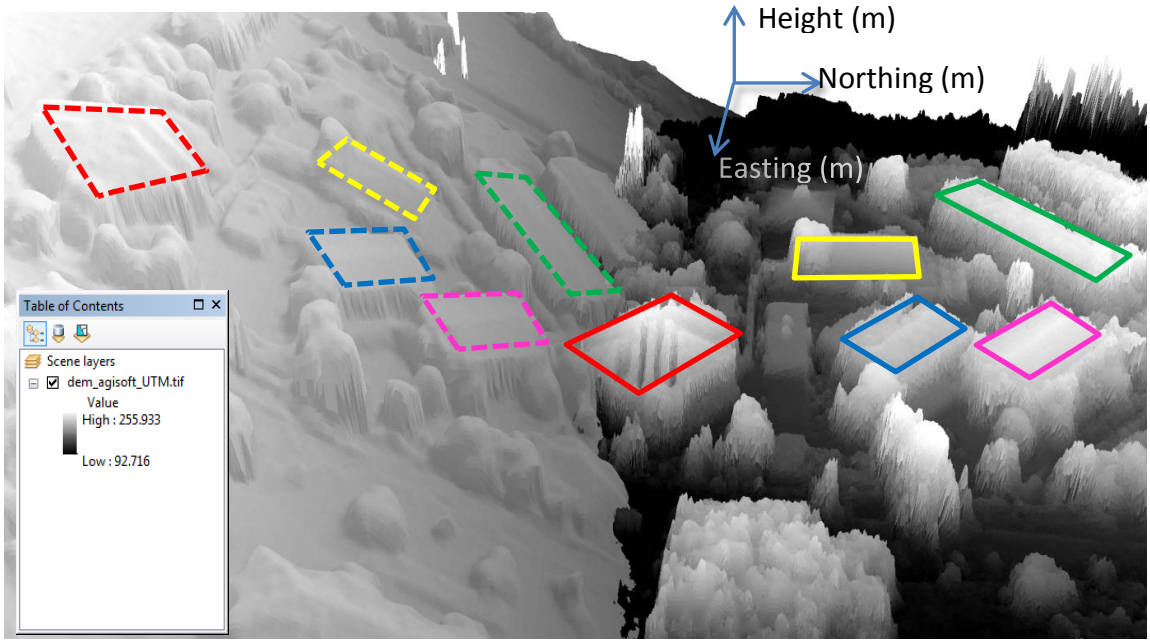

Figure 23: Inaccurate georeferencing of UAV data using GPS camera (left: uncorrected, right: corrected)

The first step to derive a DSM from the UAV data is the internal orientation estimation by using Agisoft PhotoScan within some sequential images. The GPS tag camera as read from Exchangeable Image File Format (EXIF) metadata is used as an approximate principal point to perform initial bundle adjustment for self-calibration of camera parameters. Hence, the 3D model for each building structure in a rough absolute coordinates has been extracted from some pairs of images by using Agisoft PhotoScan. Nevertheless, the building orientations to the local normal as depicted in Figure 23 are incorrect due to the inaccurate GPS camera positioning especially for the height (elevation) component despite the success of DEM generation.

In the next step, a mosque is considered in a simple building form and direction in order to estimate the elevation of the other buildings within the test area by taking into account the relief displacements. This height estimation is used to improve the external orientation of the camera of each image. For this purpose PCI Geomatica can be used to manually extract the set of tie points on each edge of the building structure (Figure 24). Hence, this manual process focuses only on building structures instead of other objects.

Figure 24: Simple building consideration

4.4.2 UAV for rapid mapping activities

Rapid mapping is a procedure to provide geospatial data by combining an immediate data collection and processing with a certain contextual aspect in order to give a quick overview about certain earth phenomena. This term is frequently used in the context of disaster preparedness and emergency response e.g. for presenting earth observation data (Percival et al., 2012).

UAVs can provide non-metric camera data (images) as well as hyperspectral data which can be increasingly utilized to support decision-making processes within disaster context situations. In this section, the UAV platform ability to provide geospatial data with sufficient accuracy as a pre-requirement for disaster-related feature extraction was demonstrated (Tampubolon and Reinhardt, 2015). For this purpose, a proper georeferencing approach must be defined at first.

Based on the previous investigation presented in Tampubolon and Reinhardt, 2014, the georeferencing procedure uses GCPs (2D) from Microsoft Bing in combination with globally available DEM data which delivers the height component for the GCPs (3D). In this context, the usage of GCPs by manually selecting identified objects such as road intersection, building corner, pond, etc. is sufficient to achieve a better geometric accuracy. For the purpose of independent validation of horizontal accuracy, additionally ICP measurements were conducted using GNSS in centimeter accuracy.

A conventional airborne mission using Star-3i platform has been performed in August 2011 to provide IFSAR Type II data (Table 13). A Digital Surface Model (DSM) is a representation of earth surface including manmade and natural structure above ground in three dimensional (3D) coordinates. The derived product of DSM which

reflects the bare earth information is called Digital Terrain Model (DTM). In addition, the Ortho Rectified Radar Imagery (ORRI) can be produced as the ground projected object data by taking into account DSM or DTM data. With this Star-3i technology, the altitude during acquisition can be increased up to 10,000 m by still keeping the geometric accuracy in the level below 1 m. Therefore it is reasonable to use this IFSAR data as an elevation source for geo-referencing purpose of the UAV data.

Table 13: IFSAR (airborne) product type (Mercer, 2009)

Product Type	DSM (in m)		DTM (in m)		ORRI (in m)	
	RMSE	Resolution	RMSE	Resolution	RMSE	Resolution
Type I+	0.5	5	0.7	5	< 2	0.625
Type I	0.5	5	0.7	5	< 2	1.25
Type II	1	5	1	5	2	1.25
Type III	3	5	-	-	-	1.25

In order to determine any significant accuracy of elevation improvement provided by the use of IFSAR DEM reference in the geo-referencing procedure, a comparison was performed by using two types of software. Subsequently, the generated DEMs have been evaluated against the ICP data and IFSAR DEM. At the end, the best available existing DEM was used as the elevation reference.

The main objective is to extract relevant disaster-related features for supporting rapid mapping activities. In many cases, it is hard to estimate the actual disaster impact in the field. For example, if there was a broken bridge detected in the UAV orthophoto after a certain disaster, it is presumably suspected as an impact of disaster occurrence. Therefore in this section, two approaches have been introduced for feature extraction. The first approach uses geometrical analysis on time series topographical data while the second implements unsupervised classification from UAV data (Li, 2008). The combination between those two approaches aims its way to extract relevant features in a quite simple implementation but with sufficient accuracy for DM analysis.

Basically, the main reason for using the best available DEM to define the elevation reference is the 3D analysis requirement to detect geometrical changes between different data acquisitions. In other words, it must be ensured that the DEM differences between IFSAR and UAV data reflect geometrical changes from different acquisitions over time. However, for rapid mapping activities, it is necessary to detect only changes due to the disaster occurrence.

The proposed approach for the feature extraction has four key steps. First, the extraction of a gridded DEM from UAV DEM and IFSAR DEM in 11 cm resolution for the smaller study area (350 x 450 m) and a calculation of the differences. Second, the height accuracy from the assessment that is used to group the DEM differences between UAV DSM (evaluated data) and IFSAR DSM (reference data) are used to determine the threshold value and submitted as a seed file to the unsupervised classifica-

tion. Third, the parameters of the fuzzy classes i.e. the seed file were used to classify all cells on the basis of their brightness value thereby creating classified disaster class maps of smaller contiguous areas. Fourth, the comparison of manually classified data with the unsupervised classification result can be performed in order to evaluate the influence of the seed file as a starting predictor of classification types.

For that purpose, the comparison of three different approaches for unsupervised classification were performed namely Isodata, K-Means and Fuzzy K-Means. Unsupervised classification has been selected because it can reduce field measurement and ground truth data. Normally, those aforementioned data are difficult to get during disaster period.

The main difference between the K-Means and the Fuzzy K-Means algorithm is the assignment approach for each cluster with respect to its centroid (Rahmani et al., 2014). Fuzzy K-Means considers the degree of ownership in the cluster assignment, thereby getting an input from DEM analysis yields more accurate results for mud flows feature extraction. In this case, the assumption of Fuzzy K-means classification is suitable for the feature extraction purpose were validated. This is mainly because of its accuracy and extrapolation capability for other extended areas of interest especially in the case of a disaster (emergency). Finally, more detailed results will be presented in section 6.2.3.

5 Investigations on Large Scale Topographic Mapping (LSTM)

As explained in the two previous chapters, the combination of satellite borne (optical and radar) data and UAV data with consumer grade camera is the potential complementary solution for LSTM especially in cases where time constraints are decisive e.g. disaster, emergency, or dynamic situations. It is inevitable that the geospatial data resolution generated from the aforementioned data is tremendously dense nowadays (< 1 meter GSD). Nonetheless, the concern of mapping agencies i.e. BIG is not only the resolution but also the absolute accuracy.

Hence, the motivation of this chapter is to determine the achievable geometric accuracy of above mentioned geospatial data sources with respect to the reference data. Referring to the conventional data from airborne data acquisition (2.2), it will be further investigated how appropriate is the above mentioned data with regard to the LSTM specifications as explained in 2.4.2. Since the GCPs (Toutin, 2012) and DEM reference (Tampubolon and Reinhardt, 2019) are essential for a reliable geospatial data production namely VHRS orthorectification (3.1.1.1) and InSAR DEM generation (4.3.2.3), their influences and specifications must also be investigated in the context of LSTM in Indonesia. The necessary number of GCPs and its appropriateness for VHRS orthorectification, UAV data processing and TanDEM-X DEM generation is the intended result of this investigation.

Finally, both orthophoto and DSM/DTM compliant with LSTM specification (as discussed in 2.4.2) must be provided promptly not only because of DM requirements but also of the dynamic nature of features covered by LSTM (building, utilities, infrastructures, etc.) in developing countries like Indonesia. In addition, the analysis of the supporting infrastructure such as the Continuous Operating Reference System (CORS) to accelerate the LSTM will also be presented. With respect to the error sources and the available aforementioned infrastructures, it is mandatory to take into account the potential constraints from the field. Therefore, the selection of the test areas must represent the actual necessities for different infrastructure and terrain conditions as will be explained in the next section.

5.1 Research questions and the corresponding LSTM use case areas

For the LSTM investigations, three types of terrain conditions are defined: (1) Almost flat, (2) moderate terrain area that consists of an earth surface with gentle slopes, frequently including man-made objects such as building, road network, etc., (3) mountainous or hilly terrain that consists of earth surface with steep slopes which is sometimes not suitable for man-made objects.

The following sections describe the investigations for LSTM related to the geometric accuracy improvement of the output products derived from above mentioned geospatial data sources. Hence, the research questions for the investigations in this chapter were:

1. Is the planimetric accuracy of VHRS compliant with the LSTM technical specification in Indonesia and if yes how can it be achieved?

   The achievable geometric i.e. planimetric accuracy of VHRS imageries for LSTM data provision is investigated and explained in 5.2.2 for moderate terrain using QuickBird data and in 5.4.2.4 for mountainous terrain using SPOT6 data. The currently achievable VHRS planimetric accuracy will be identified by using two reliable reference data namely ICPs from GNSS and ICPs from orthophotos.

2. How many GCPs and which DEM are needed for orthorectification of VHRS data to fulfill the LSTM accuracy?

   Initially, the detailed investigation on the contribution of the GCPs and the DEM accuracy to the geometric accuracy (planimetric) of VHRS imagery will be performed in 5.2.2.1. Different number of GCPs and various DEMs will be combined in the orthorectification process in order to fulfill the required RMSE for LSTM of 1:5,000 map scale. Finally, the effective number of GCPs and DEM (with reliable accuracy) must be tested in a more advanced investigation for mountainous (sec. 5.4.1) and urban areas (sec. 5.4.2) in Bandung.

3. Can the orthorectified VHRS imagery be used as a sufficient source to provide GCP for UAV data processing?

   The usage of appropriately orthorectified VHRS provided beforehand will be also exploited as a reference image for the high resolution data derived from UAV data acquisition. In addition, more detailed investigations on Borobudur Temple Area will be performed to define the Standard Operating Procedures (SOP) of orthorectification for moderate undulated terrain by using UAV data and VHRS data in order to comply with the required RMSE.

4. Which height reference data is necessary to derive an HRTI level 4 DEM from TanDEM-X data?

   The InSAR DEM generation by using only an insufficient amount and/or an inaccurate height reference data is not applicable to produce more accurate DEM than HRTI level 3 as fulfilled by DLR's IDEM. In particular for TanDEM-X StripMap data, the DEM resolution will also increase to keep the interferometric phase error low (DLR, 2018). The details about how to handle accuracy and resolution issues will be explained in 5.2.3. In addition to the GCPs from GNSS as height reference, the role of partial DEM references will be also further investigated in 5.2.3.1 in order to improve the DEM accuracy.

   Specifically, the investigation on BIG office in Cibinong is intended to test the algorithm suitability for an area with the ideal situation where accurate GCPs and DEM references are available. The improved TanDEM-X DEM generation for an area composed by flat terrains with small slopes (< 20°) will be explained and tested in chapter 5.3. For this type of area, the height accuracy is normally very high since the geometric distortions and phase unwrapping errors are not dominant.

5. Can building structures improve the UAV data georeferencing procedures?

For the case of UAV platforms without INS/IMU equipment, the potential of self-calibrated data will be exploited to achieve a better accuracy. In addition, the role of building structures in the high resolution UAV data processing will be investigated also in 5.3.3.1.

The interest in man-made objects is important for the scope of the LSTM workflow. As discussed in 2.3, the topographical features such as road, jetty, etc. in LSTM are mostly compiled on their original physical size and related with man-made objects. For example the road features are compiled in the form of double line with a real size on LSTM instead as a single center line on the smaller map scales. From this point, the test area selection must take into account the existence of topographic features availability for LSTM such as body of the road (pavement areas). The road features are important in the investigations since they will be used to interpolate the DEM as the reliable reference data as well. Therefore the different types of terrain have been selected to investigate if the terrain types are influencing the achievable accuracy for example of the DEMs derived from TanDEM-X data.

As depicted in Figure 25, there are four test areas reflecting different earth terrain conditions. The first test area with a size of 6 by 8 km, Borobudur Temple in Jogjakarta is representing moderate terrain. The second test area with a size of 0.5 by 0.1 km, BIG office in Cibinong represents built-up area with low elevation (above Mean Sea Level (MSL)) and flat undulated terrain. Finally, for the Bandung test area, the coverage of two map sheets of 1: 5,000 scale LSTM (2.3 by 2.3 km) as explained in Table 2 are selected as high elevation (above MSL) mountainous (Mount Tangkubanperahu) and urban (Lembang) areas.

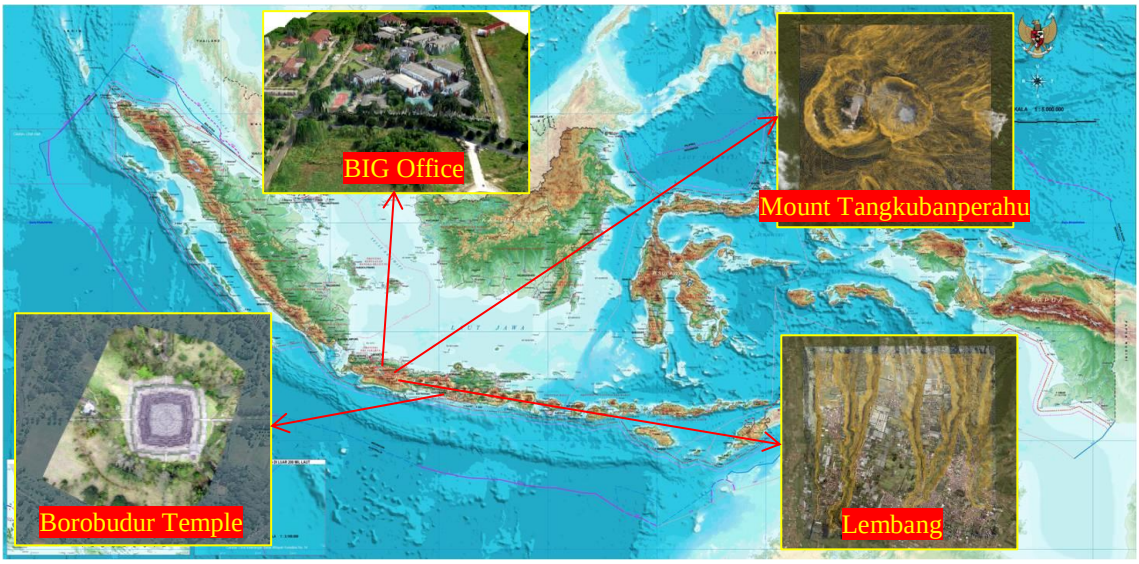

Figure 25: Test areas for LSTM investigations

5.2 Investigation on moderate terrain (Borobudur Temple)

The Borobudur temple, a Buddhist temple which was constructed within 8th and 9th centuries, the biggest and the most popular archeological site in Indonesia, is located in the southern part of Central Java Island as depicted in Figure 25. This temple is also well known as one of the preserved UNESCO's world heritage sites[4].

The surrounding National Strategic Area of Borobudur temple includes some villages elongated in a North East – South West direction covering approximately 2,700 hectares (Figure 26). Basically the terrain condition of the study site is classified as medium undulated without any steep slopes.

As a prominent archeological site, the Borobudur temple and its surroundings are important for tourism but also considered as a preserved area. Therefore this area is prioritized by the stakeholders for a detailed spatial planning over above mentioned National Strategic area. For this purpose, it is mandatory to perform 1:5,000 LSTM in order to establish a reliable framework at the first place. The investigation with geospatial data sources from radar, optical space borne, and UAV data in this section is aimed to find an alternative solution in areas where large scale topographic maps do not exist.

The massive development of space-based remote sensing technologies enhances both spatial and spectral resolution of the geospatial data sources used for topographic mapping. Indeed, it has accelerated the production of National DEM (DEMNAS) in order to develop the high end Indonesian Spatial Data Infrastructure (Ina-SDI)[5]. Therefore, for the detailed spatial planning in moderate terrain of Borobudur area, it will be further investigated how the combination between space borne and UAV data can provide the geospatial data sets namely orthophotos, orthoimages and DEMs as the reliable solutions that fully comply with the LSTM specifications in Indonesia.

The Borobudur temple consists of three different major tiers/components: (1) the pyramidal base with five concentric square terraces, (2) the conical trunk with three circular platforms, (3) a monumental stupa located at the top. For their openness (not obstructed by any other object) and unique structures (always preserved) these temple can be potentially used as the height reference with high accuracy and coherency especially in the context of TanDEM-X InSAR DEM generation.

[4] http://whc.unesco.org/en/list/592 (last accessed 05.03.20)

[5] http://tanahair.indonesia.go.id/portal-web (last accessed 05.03.20)

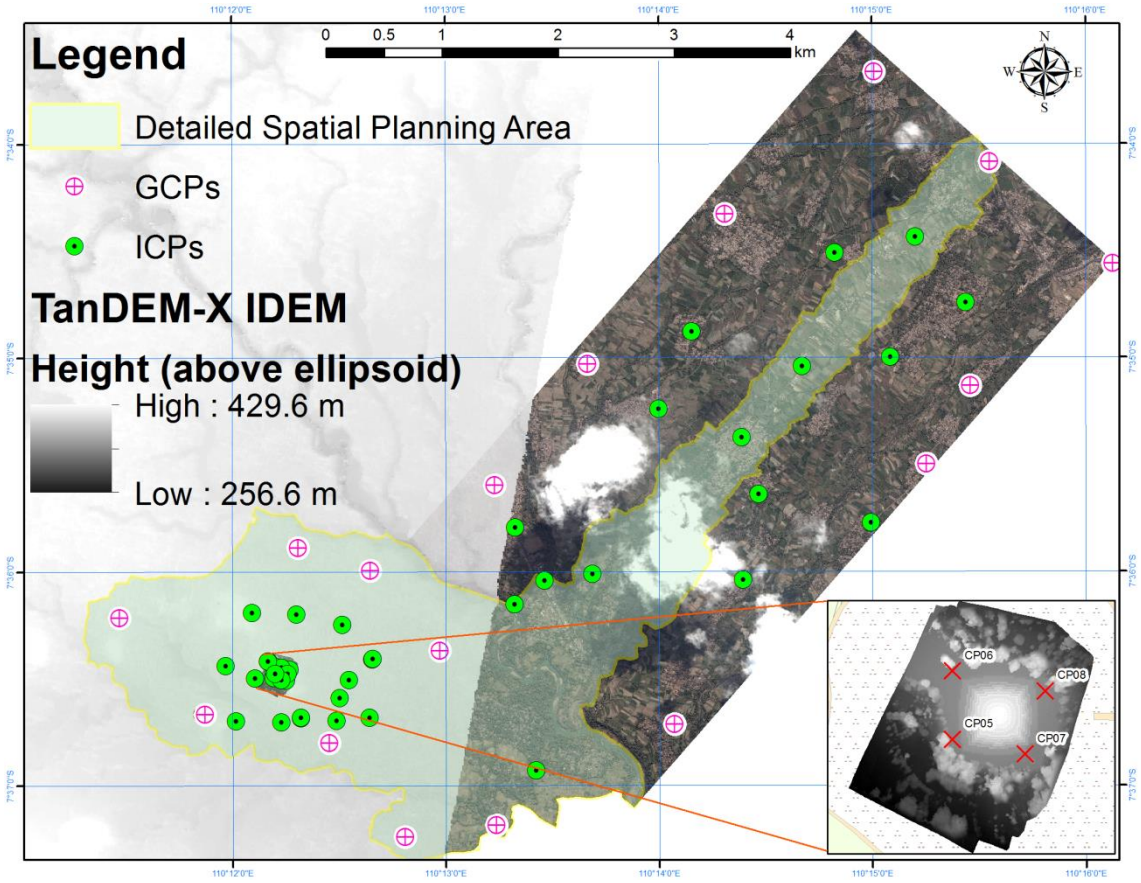

Figure 26: Area of interest in Borobudur national strategic region

Basically its walls and balustrades are decorated with fine low reliefs, covering a total surface area of 2,500 m^2. There are 72 openwork stupas around the circular building platform (Figure 27). Each of it contains a statue of the Buddha. Fortunately for the preservation act, the monument was restored in the 1970s by UNESCO's support.

The detailed investigation focusing on the Borobudur temple has been planned under the assumption that the temple structure is always preserved as a cultural heritage or conservation site. Therefore, the temporal issue related with the usage of GCP data in the calibration and/or validation procedure involving multi datasets from different time of acquisitions can be neglected.

Figure 27: Test area of Borobudur temple

5.2.1 GCP measurements

Considering the spatial resolution of QuickBird imagery (60 cm), it is required to conduct measurements with a positional accuracy in the order of 10-20 cm (Toutin, 2002). Hence the GNSS measurements were conducted either by using rapid static positioning (Figure 28) or Real Time Kinematic (RTK) GNSS positioning. Rapid static positioning requires at least one pair of baselines from two positions which usually needs 30-45 minutes per baseline.

Since the object planned as a GCP is selected currently from recently available VHRS imagery, it is often called post-marking GCP. The drawback of this post-marking method is related with the nature of geospatial objects which are dynamically changing over time. In this case, the time stamp is an issue which should be taken into account. It is necessary to make sure that every selected object is less dynamic and therefore some changes in the actually selected GCP object is allowed within a given tolerance. Despite the aforementioned required positional accuracy is in the level of decimeter, the GNSS campaign is designed for centimeter level of accuracy in order to reduce object discrepancies. However, the GNSS measurements should be supported by picking reliable and fixed objects in the field. Otherwise, the GNSS centimeter level of accuracy is not worth for the accuracy of the end products. The actual examples will be explained in 5.2.2.

Using a SOUTH STAR S86T Integrated RTK GNSS dual frequency receiver, every planned GCP was measured accurately by aiming on centimeter level accuracy just to ensure that the decimeter level (GCP picking) as above mentioned is reached. In rapid static position-

ing the minimum measurement time was about 30 minutes per GCP while with RTK only less than 5 minutes were needed to get fixed positioning.

Figure 28: Example of GCP measurements by using rapid static GNSS

In addition to the GNSS measurements, it is also important to take some photos of GCP locations from at least 4 different directions (see Figure 28). Such documentation supports the GCP identification in the orthorectification step with the highest level of confidence. The acquired photographs ensure a more exact identification in the VHRS imagery in order to increase the accuracy. Supporting this aim, additional measurements are also necessary e.g. the diametrical size of the object, distance to other objects, etc. as also included in the documentations.

As explained in 4.1.1, GNSS measurement schemes can lead to a proper field data collection and processing methodology with respect to the accuracy requirement. As a compromise, the PPP method (see p.39) delivers sufficient results independently from the reference network coverage despite of its decimeter accuracy (Table 14).

Table 14: GNSS accuracy for GCP measurements

GCP_ID	Near Fix Reference (m)	PPP (m)	Far Fix Reference (m)	Absolute Positioning (m)
BR04	0.073	0.032	3.745	2.471
BRB1	0.021	0.417	7.520	11.048
BRB2	0.030	0.204	0.698	4.068
BRB3	0.038	0.407	8.004	8.210
BRB4	0.015	0.033	3.283	0.670
E000	0.037	0.422	3.538	2.413
Accuracy	**0.069**	**0.521**	**8.755**	**10.279**

5.2.2 Investigations on the planimetric accuracy of VHRS imagery

As already stated in chapter 2, the geospatial information in topographic maps as a basic reference is mandatory to support many development activities especially for regional planning. From this point, the national government of Indonesia encourages rapid mapping activities in a scale of 1:5,000 by local communities. This so called "village mapping" (Regulation of Head of BIG No. 3/2016) requires VHRS orthorectified imageries (CSRT) as a primary data source produced not only with high resolution but also high accuracy. Therefore, the synchronized national orthorectification program is the only solution by taking into account the GCPs and fine DEM data (Astrium, 2013; Digital Globe, 2016).

Noticeably, it is necessary that the VHRS orthorectified imagery in a resolution < 4 m (see section 3.1) as a geospatial data source must comply with 1:5,000 LSTM specifications required by the detailed spatial planning regulation. The goal of this section hence is to investigate the achievable planimetric accuracy of QuickBird data based on various GCP configurations and DEM inputs in the orthorectification tasks.

Datasets used The space borne optical data used is QuickBird data with a resolution of 0.6 m which has specifications as included in Table 9: WorldView product level (Digital Globe, 2016). For the orthorectification purpose, there were three used DEMs namely SRTM 1 Arc Second, ASTER DEM (free) and Radargrammetric TerraSAR-X DEM (commercial). In this case, the claim from the image provider is also validated against the planimetric accuracy investigation results in this section.

Reference datasets The GCP datasets from GNSS rapid static as described in 5.2.1 were used as the reference data in the accuracy assessments. To detect the influences of GCPs (from GNSS survey) and different DEM data on planimetric accuracy, the ICPs (also from GNSS survey) were used to validate the orthorectification results.

5.2.2.1 VHRS orthorectification

The investigation in this section was conducted by combining theoretical (Jacobsen, 2018) and empirical (Digital Globe, 2016) studies in order to provide proper geospatial data sources i.e. VHRS imagery for 1:5,000 map scale of the detailed spatial planning in an efficient way (Figure 29). As the satellite jitter effect only can be corrected by using either stereo pairs and/or GCP data, it is obvious that the VHRS data rectified with RPC only (Table 8) is not sufficient to achieve 1.25 m required RMSE by the LSTM specification. This is also confirmed by the image providers. Digital Globe, 2016, stated that the best geometric accuracy result is 4.2 m (2.0 m required RMSE) with fine DEM input as a pre-requisite (Table 9).

Orthorectification has been applied in this section for VHRS imagery (QuickBird) covering the National Strategic Area of Borobudur by using GCPs and DEMs as three dimensional components (Tampubolon, 2012). As explained in 3.1.1.1, this VHRS investigation intends to prove the insufficiency of the RPC geocoding approach to fulfill the LSTM re-

quirements and to provide other solution from the adequate GCPs and DEM data as well. By putting focus on GCPs and DEM, it is the main objective of this step to achieve the best possible geometric accuracy in the level of 4 times of QuickBird image resolution i.e. 60 cm*4 = 2.4 m respectively.

Initially, the QuickBird image with RPC-Standard Ortho is used as a reference for 38 units of GCPs and ICPs measurements planning as depicted in Figure 26. By following this GCP planning network, a Rapid Static and RTK GNSS campaign as explained in 5.2.1 has been done as well as GCP pricking over the VHRS image for being used in the subsequent orthorectification step.

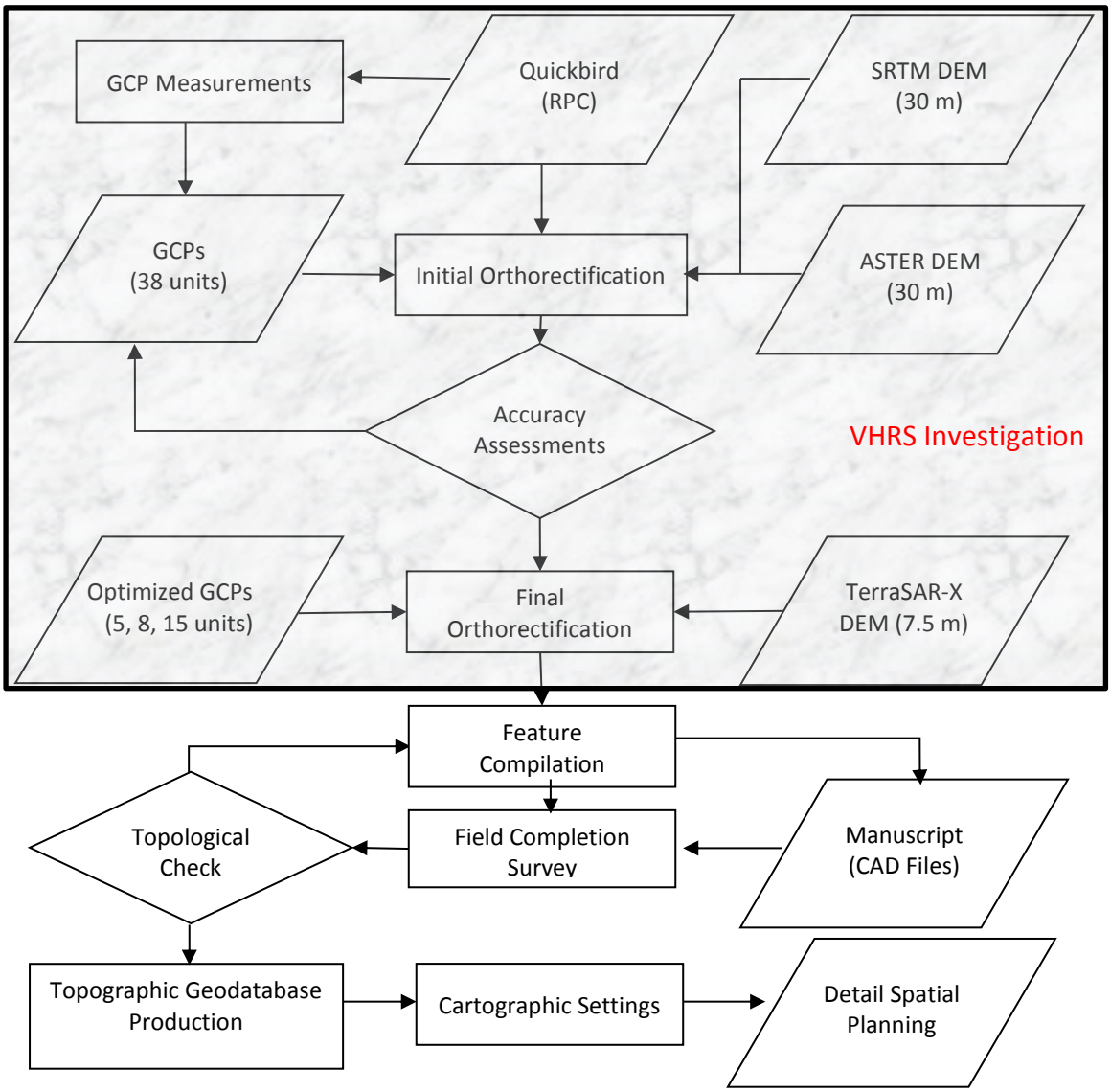

Figure 29: VHRS investigation workflow (large box) as a part of detail spatial planning in map scale of 1:5,000

For this section, the focus was put on the orthorectification task that is mainly determined by GCPs and DEM as mandatory inputs. By using both free downloadable SRTM DEM in a medium resolution of 1 arc second (30 m) and measured GCPs, first initial orthorectification has been done subsequently to produce QuickBird orthorectified image-

ry for further accuracy assessment analysis. In this case, an assessment has been performed in order to identify the planimetric accuracy of the orthoimages.

The next steps of orthorectification were done iteratively by an increasing numbers of GCPs i.e. 5, 8 and 15 until it saturates within the specified required RMSE according to the NSSDA and the NMAS. From this point, the optimized numbers of GCPs have been identified for a further improvement in the Standard Operating Procedure (SOP) of orthorectification.

In the next step, by using DEM generated from TanDEM-X data with a better resolution and accuracy as will be discussed in 5.2.3, the final orthorectification has provided the reliable geospatial data source to be used in feature compilation using GIS desktop software. A geodatabase has been used as a geospatial data warehouse with the necessary cartographic setting afterwards. At the end, the detailed spatial planning in 1:5,000 map scale can be provided to govern the National Strategic Area in a proper way (Figure 29).

Using PCI Geomatica 2012 (Figure 30), all of the measured GCPs were taken into account for orthorectification process to provide first orthorectified QuickBird imagery by using both Shuttle Radar Topography Mission (SRTM) DEM and ASTER DEM as DEM input. In this initial stage, the GCP elevation was extracted from SRTM DEM and ASTER DEM as a free DEM data. In order to enable blunder detection as will be explained in 5.2.2.3, the identification of each GCP (Figure 30) is pricked in the image as the documentation shows without any effort to modify it.

In order to obtain a proper statistical analysis and to avoid misleading results in the accuracy assessment, the assumptions have been used in the investigations as follows:

- Rapid static positioning for GCP measurements provides coordinates in centimeter level accuracy;
- Operator ability to prick the GCP points in the VHRS image is 2 times image resolution = 0.6*2 = 1.2 m.

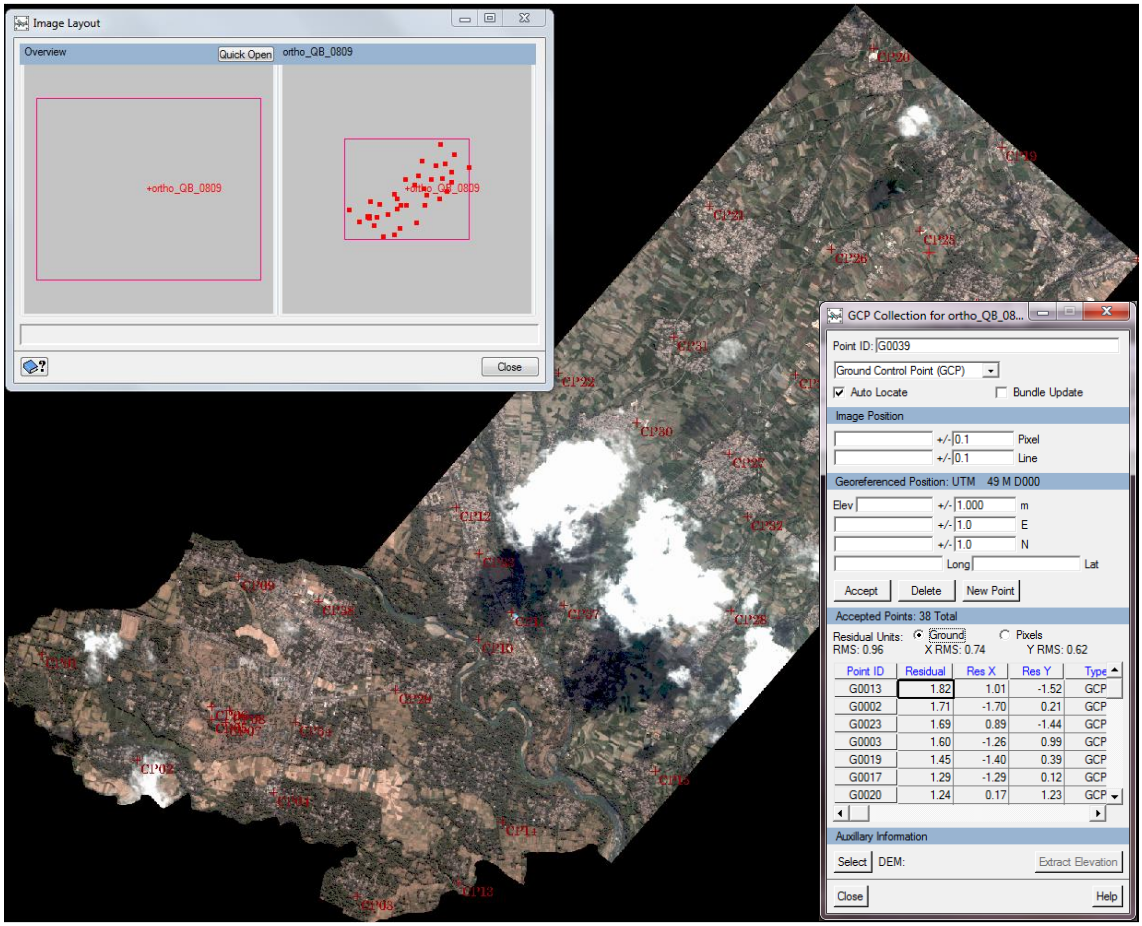

Figure 30: Orthoimage with 38 GCPs

Subsequently, the number of GCPs was decreased deliberately from 38 to 15, 8 and 5, thus there are some orthorectified imageries produced to be further investigated. Four different schemes of GCP networks (Figure 31) have been used to identify the appropriate GCP setting and configurations for fulfilling the 1:5,000 LSTM accuracy requirements.

The 38 total amount of GCPs is divided into two types of control points: (1) GCP used for orthorectification and (2) Independent Check Point (ICP) used for validation. In this case, ICPs must not be used in the orthorectification process as they are only used for the accuracy assessments. Consequently, the numbers of ICP is equal to the subtraction of total numbers of GCPs with the maximum numbers of selected GCP scheme.

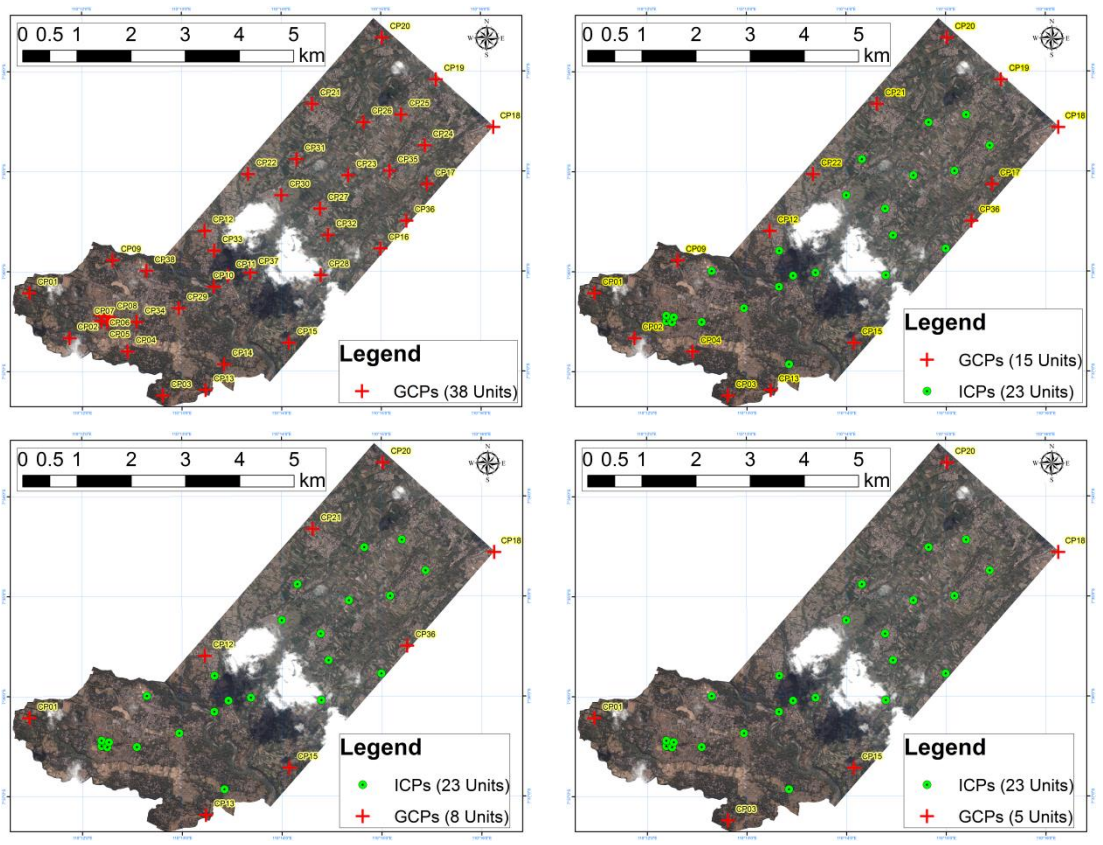

Figure 31: GCP network distribution (upper-left: 38 GCPs, upper-right: 15 GCPs, lower-left: 8 GCPs, lower-right: 5 GCPs)

The GCP distributions shown in Figure 31 have been defined using 15, 8, and 5 GCPs with a fixed numbers of 23 ICPs within the GCP's perimeters. For a proper assessment of the results, the number of ICP is fixed in order to keep the same weight of ICPs in the statistical analysis.

As explained in 2.4.2, NSSDA and NMAS use RMSE to indicate the required positional (planimetric) accuracy of the evaluated datasets. RMSE can be calculated by using eq. 2.1 - 2.3 by taking into account the coordinates (X,Y) of GCPs from GNSS vis-à-vis from orthoimages. To ensure more certain identification, the position of 15 GCPs and 23 ICPs were digitized manually in the orthoimages based on the photographic documentations as described in 5.2.1.

Figure 32: Manual GCP identifications in VHRS orthoimages (left: corner path in Borobudur Temple, right: edge of the roof) with respect to the LSTM tolerances (red circle)

5.2.2.2 VHRS investigation results

With respect to the RMSE value as an important statistical indicator in the orthorectification, it is usual to restrict the RMSE not more than half of pixel size i.e. 30 cm as the predefined threshold. However in this investigation, there is no minimum threshold to be applied. Instead, it is better to use the GCP data from GNSS processing and pricking identification without any modification to fulfill the threshold. Specifically, as described in Figure 30, the provided RMSE in PCI Geomatica 2012 by using 38 GCPs was 96 cm with $RMSE_X$ = 74 cm and $RMSE_Y$ = 62 cm, though the image resolution is 60 cm. This approach was applied in order to enable blunder detection in the GCP pricking.

Table 15: VHRS planimetric accuracy for the whole Borobudur National Strategic Area

No	GCP amount	RMSE (m)		NSSDA-95% (m)		NMAS-90% (m)		Required RMSE (m)
		SRTM (30 m)	TSX-DSM (7.5 m)	SRTM (30 m)	TSX-DSM (7.5 m)	SRTM (30 m)	TSX-DSM (7.5 m)	
1	RPC (0 GCP)	7.2		12.5		10.9		1.25
2	5	2.3	1.2	4.0	2.1	3.5	1.8	
3	8	1.4	1.1	2.5	2.0	2.1	1.7	
4	15	1.4	1.2	2.5	2.1	2.1	1.8	

Table 15 summarizes the different accuracy standards. The NSSDA with 95% level of confidence was also included to increase the certainty level of accuracy assessment results even though in general the NMAS (CE-90%) is sufficient and commonly used e.g. by DLR, BIG, NGA as already discussed in 2.4.2. As included in Table 15, the calculated pla-

nimetric accuracy of VHRS orthorectified imagery using RPC can be seen by the GCP position of black cross that lie outside the required accuracy of red circle in Figure 32. Therefore, the VHRS orthorectified imagery using RPC is not adequate enough to fulfill the required RMSE either defined by NSSDA (CE95) or NMAS (CE90).

5.2.2.3 VHRS investigation discussions

In order to validate the orthorectification results, the reference prior (a posteriori) provision as explained in 3.2.4 was defined not also for blunder error detection but also for planimetric accuracy investigations. The importance of a posteriori is suitable for the data driven analysis (Bernardo, 2005). The validation procedure focuses on the output i.e. orthorectified imageries those are considered as the sample data to analyze the appropriateness of reference data i.e. the ICPs. Iteratively by using "Near" functionality in ArcGIS, the statistical analysis provided the sort of an a posteriori RMSE which can detect the misguided GCP pricking over the VHRS imagery.

In other words, the first initial orthorectification plays an important role to detect blunder errors which often occur because of the incorrect GCP pricking in the images. For that purpose, each GCP position at the orthorectified image was compared to the GCP position from GNSS measurement. By measuring the deviation, an a posteriori RMSE for the first orthorectification can be calculated and so forth until the constant RMSE is reached.

Therefore, the incorrect GCP identification can be detected from above mentioned blunder detection in order to provide the final orthorectified image. Findings from GCP02 and GCP27 as described in Figure 33 show incorrect GCP pricking which are mainly caused by two actual examples:

- Wrong street corner identification (CP02);
- Wrong building corner identification (CP27).

Figure 33: Blunder error detection (+: field identification, x: from orthorectification)

At first, the investigation has identified the actual planimetric accuracy of QuickBird imagery (RPC-standard ortho) against GCP measurements using GNSS survey with a 10-20

cm level accuracy. The claimed accuracy in the QuickBird product level (Table 8) as stated by the image provider can be confirmed.

It is inevitable that without any GCP the planimetric accuracy does not fit with the LSTM requirements i.e. 10.9 m (23 m from Jacobsen, 2013, see Table 8) for NMAS or CE90. With GCPs, the planimetric accuracies were within accuracy tolerance of 2.5 m as long as adequate DSM i.e. TerraSAR-X DSM is used in the orthorectification process. Nonetheless, orthorectification using 8 GCPs has better accuracy (2.0 m) and is thus selected as optimal number of GCPs for the whole of orthorectification step. However, the GCP positional quality and the GCP identification must not be ambiguous in the field as well as in the image.

The VHRS investigation using the QuickBird imagery was focused on finding the optimized number of GCPs to fulfill the requirements by using different amounts of GCPs. Practically, this kind of procedure is capable to detect possible errors from GCP measurements as well as misinterpretation of picking the correct objects in the image. Without orthorectified VHRS imagery by using GCPs, the detailed spatial planning features will be shifted significantly as depicted in Figure 34. Noticeably, this investigation has presented the significant geometrical improvement of VHRS imagery by the implementation of the national orthorectification mechanism.

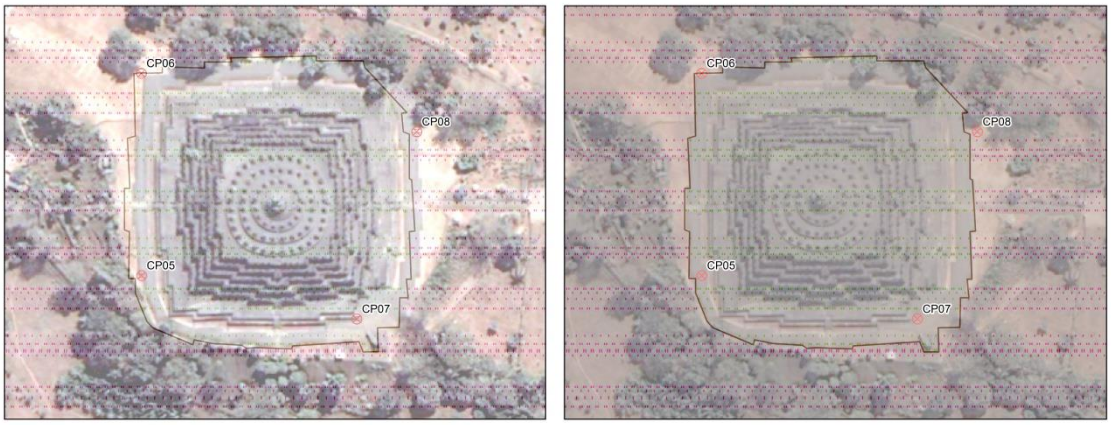

Figure 34: The geometric accuracy effect of different orthorectification methods (left: GCP-ortho, right: RPC-ortho)

5.2.3 Investigations on TanDEM-X data for moderate terrain area

For moderate terrain area, the GCPs and DEM in the orthorectification improved significantly the planimetric accuracy of VHRS as discussed in 3.1.1.1. The primary product of SPOT6 in 35 m accuracy (LE90) can be improved to 10 m accuracy (LE90) by the support of GCPs and DEM (Table 10). Unfortunately, the widely and globally used SRTM DEM however is not sufficient for producing the adequate orthorectified VHRS as a data source for LSTM in. 1:5,000 map scale. As already discussed in the previous section (Table 15), a reliable DEM is needed to fulfill the LSTM planimetric accuracy. In addition to SRTM and ASTER DEM, the generated DEM from TanDEM-X also has been evaluated to provide significant planimetric accuracy improvement of the orthorectified image.

Weber, 2006 has already identified the potential of generated DEM from TanDEM-X as a global satellite reconnaissance for orthorectification purpose. This section investigates further how a more accurate DEM from TanDEM-X CoSSC by using the interferometric approach can be generated. The generated TanDEM-X DEMs were validated and compared with other DEM against ICP data from GNSS. The influence of an improvement in data processing by an introduction of partial DEM reference as already discussed in 4.3.2 will also be presented.

Datasets used The TanDEM-X CoSSC data from different looking direction (see Table 16) were used to generate a DEM. For DEM Geocoding purpose as explained in 4.3.2.1 (Range-Doppler terrain correction in SNAP desktop), SRTM 1 arc second was selected.

Table 16: TanDEM-X CoSSC data (*height of ambiguity) for Borobudur area

Scenes	HOA* / Baseline (m)	Adjusted parameters		Incident angle / Range to DEM Reference area (°/m)	Looking direction	Acquisition date
		B_P (m)	ΔΦ (°)			
S01	64.527/ 119.500	124.070	78.3228	45.36035 / 704038.754	Ascending	20-03-2014
S02	-39.178/ 162.344	-156.535	-43-7457	39.37564 / 647221.816	Descending	18-09-2012

Reference datasets The UAV data acquisition on 29 October 2013 using Sony NEX7 and Canon S100 cameras was performed to successfully produce the ortophotos and DEM with a resolution of 5 and 10 cm respectively. In this case, both orthophotos and DEM were selected as the partial DEM reference for their reliable geometric accuracy with the support of GNSS data (see 5.2.4). The Borobudur temple area (inset map in Figure 26) has been selected by taking into consideration the preserved building structures as the DEM reference data for InSAR DEM generation. Differently to the other investigations, only ICP data were used as the reference data for the accuracy assessments.

The goal of TanDEM-X data investigation in Borobudur area was to check whether the proposed linear model leads to an accuracy improvement of the generated DEM as discussed in 4.3.2.2. TanDEM-X Science Service from DLR provided some TanDEM-X CoSSC Stripmap as described in Table 16. In addition, the IDEM is used as a comparable data provided by DLR as well.

The number of the looks is crucial in determining the azimuth and range resolution in TanDEM-X radar data acquisition (DLR, 2015). As shown in Eq.5.1, the number of independent looks n is determined by the number of independent looks in range direction n_{rg} and number of independent looks in azimuth direction n_{az}. By global DEM generation e.g. IDEM at DLR, the number of looks are varying from 15-32.

$$n = n_{az}.n_{rg} \quad (5.1)$$

On the other hand, the interferometric phase error is determined by the coherence and number of independent looks. In principal, the higher the coherence and the number of independent looks the less is the interferometric phase error. For instance, IDEM selected 3×5 (15) or 5×5 (25) number of looks in order to generate a 12 m resolution (0.4 arc second) DEM (DLR, 2018). From this point, it is somehow challenging to generate DEMs in higher resolution along with higher accuracy.

$$HOA = \frac{\lambda R \sin\theta}{B_P} \quad (5.2)$$

The Height of ambiguities (HOA) is the most important indicator representing the height measurement sensitivity of one cycle wavelength (2π) as described in Eq. 5.2. In this case, HOA is determined by the wavelength λ, slant range R, incidence angle θ and perpendicular baseline B_P.

Unfortunately the available IDEM covered only some part of National Strategic Area of Borobudur as depicted in Figure 26. However in this case, it is still possible to perform the geometric accuracy investigation only on the surroundings of the Borobudur temple area. The focus was put on the archeological site of Borobudur temple, under the assumption that basically the temple structure is not changing over time, i.e. Borobudur Temple as a data reference for geometric accuracy assessment is valid for different acquisition times.

5.2.3.1 Linear model implementation for moderate terrain area (the strategies)

To detect the contribution of different height references in the generated DEM accuracy, the moderate terrain area was selected. In this type of terrain, the error sources already exist for some tilted areas. For TanDEM-X InSAR DEM generation in this section, two strategies were developed:

1. Using 3 - 8 perimeter GCPs as height calibration reference data

   In this case the UAV DEM was used for validation. More details about the quality of UAV DEM will be explained in 5.2.4. The most important aspect is that the spatial resolution of UAV DEM i.e. 5 cm is far better than the generated InSAR DSM. The comparison with IDEM which was generated using the same data source i.e. TanDEM-X StripMap is also helpful to evaluate the effectiveness of the proposed strategy. In addition, IDEM plays an important role to recognize the contribution of the linear model for the geometric accuracy by using different height reference data. As explained in 4.3.2.1, the whole step for DEM generation was done with a stressing on the baseline and phase offset improvement to produce more accurate results.

2. Using preserved features of Borobudur temple as DEM reference

   To adjust the parameters in the linearized model the UAV DEM was used as the height calibration data. In addition, the UAV DEM reference is also used in the geocoding step for the partial area of Borobudur temple. Hence the extracted gridded points as depicted in Figure 35 have a high planimetric accuracy and can be used as height reference model. The advantage of this approach is the relatively small area

of height reference over the whole generated DSM area in the so called partial height reference data. As depicted in Figure 26, to generate reliable TanDEM-X DEM for whole 2,700 hectares of Borobudur National Strategic Area, the partial height reference coverage is only 300 m by 400 m or 12 hectares in size. Thus the coverage or distribution of the height reference data is not an important issue for the proposed linear approach. The most determining factor is the geometric quality of the partial height reference i.e. UAV DEM. For the investigations in this section, as further discussed in 5.2.4, the height accuracy of UAV DEM was in the level of 1-1.3 m (LE90) with a resolution of 5 cm. The selected high flight altitude of 200 m above ground level contributed mainly to the aforementioned low level of height accuracy. As a cultural heritage area, it is not allowed to fly lower than 150 m over the Borobudur temple.

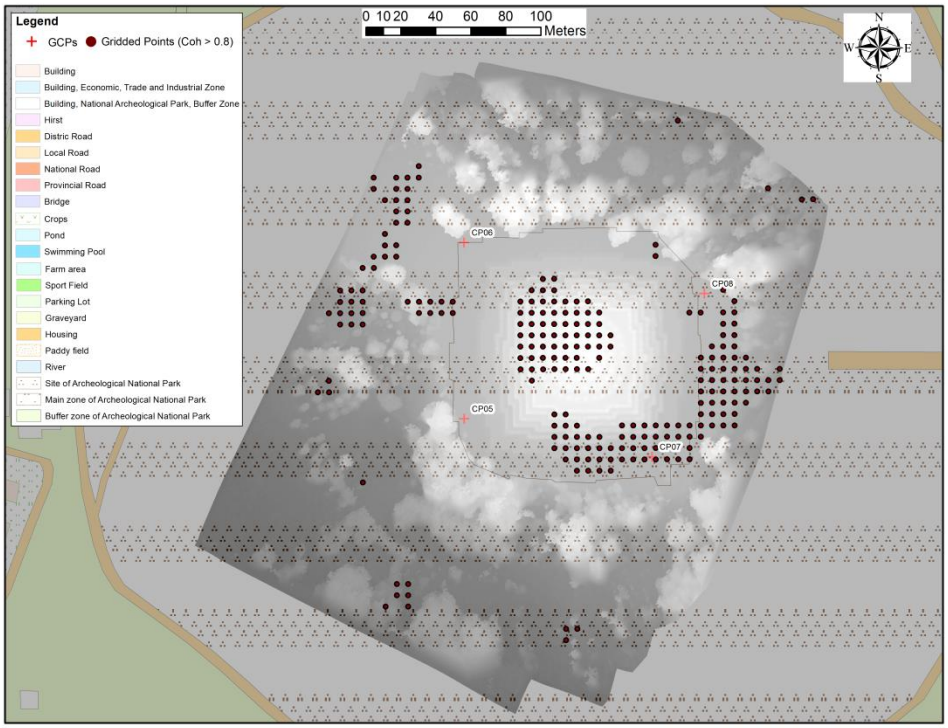

Figure 35: Reference points from UAV data with coherence > 0.8

The Phase Unwrapping (PU) step is always challenging mainly because of the occurrence of phase discontinuities especially with respect to the earth barrier objects such as rivers, waterbodies, etc. Chen, 2002 already noted that the subset of the large interferogram into separate tiles can be a subject to the isolated phase unwrapping area. For solving this problem, it is necessary to supply the PU task with a local adjusted baseline value with respect to the subset of the large interferogram. For two aforementioned strategies, every baseline value has to be adjusted with the linear model by some inputs those were generated from an initial unwrapped phase interferogram. Iteratively, the adjusted baseline value will improve the PU results especially in an area where phase discontinuities do exist.

As explained in 4.3.2.1, the heavy and resource consuming PU task using SNAPHU must be run separately in the linux-based platform as currently SNAP desktop has not been

yet equipped with a PU tool. In order to proceed, the major input values related with the proposed linear model are perpendicular baseline value B_P and wavelength $\boldsymbol{\lambda}$. For the TanDEM-X bi-static data processing, also the single antenna transmit mode must be selected in order to get better unwrapped phase results. By default, SNAPHU reads only the required values from the TanDEM-X metadata, but it can be manually edited if necessary.

One concrete example in this investigation is the subset of the whole TanDEM-X CoSSC data by the river or hydrology features as depicted in Figure 36. Phase unwrapping artifacts resulted from river features as a barrier producing the surface discontinuity as shown in the lower part of Figure 36 still remain if the DEM generation uses only the original baseline value from the TanDEM-X metadata. This barrier contributes to some significant errors in the DEM generation on two major aspects.

First, a visual inspection on the river feature in the middle of the scene as depicted in the lower part of Figure 36 shows that the terrain has two height references as an adjusted parameter in the linear equation 4.3: one for the western side of the river, and one for the eastern side of the river. Hence, height reference as one parameter in the height calibration algorithm as explained in 4.3.2.3 is unable to provide one linear equation for the whole areas separated by the river. There must be one linear equation for the eastern part and one for the western part which cannot be applied at the same time for the whole coverage. In addition, without any accurate height reference data to adjust the baseline value, the unwrapped phase degrades consequently.

Second, an inaccurate PU step will also affect the generated DEM orientation results as best visualized in the eastern part of the river with the existence of jumping height as indicated by bright white color in the lower part of Figure 36. Along with this finding, Krieger, 2007 has already denoted the effect of the baseline errors to the DEM orientation in the form of an equation:

$$\mathrm{DEM}_{\mathrm{tilt}} = \frac{\Delta \mathrm{h}}{\Delta \mathrm{s}} = \frac{\Delta \mathrm{B}_{\mathrm{ll}}}{\mathrm{B}_{\mathrm{P}}} \tag{5.3}$$

From Eq. 5.3, the DEM tilt is affected by the height error Δh (see eq. 5.4), the ground range distance to the reference points Δs, the baseline estimation errors in the line of sight ΔB_{ll} and perpendicular baseline B_P. Again, one parameter in the proposed linear model i.e. perpendicular baseline B_P, determined the DEM orientation in a significant error portion. As also explained in Krieger, 2007, the baseline offsets (errors) contribute to the DEM orientation due to the vertical displacement and tilt of adjacent swaths.

According to Table 16, the perpendicular baseline value included in the metadata is -162.344 m. By adding only 3 GCPs as the height reference data, the adjusted perpendicular baseline value i.e. -156.535 m has removed the phase unwrapping artifacts as shown in the upper part of Figure 36. Since the Integrated TanDEM-X Processor (ITP) at DLR uses no external reference data either for PU or height calibration (DLR, 2018), the remaining error in the form of artifacts can still be present for some extents or cases especially within certain complex terrain conditions.

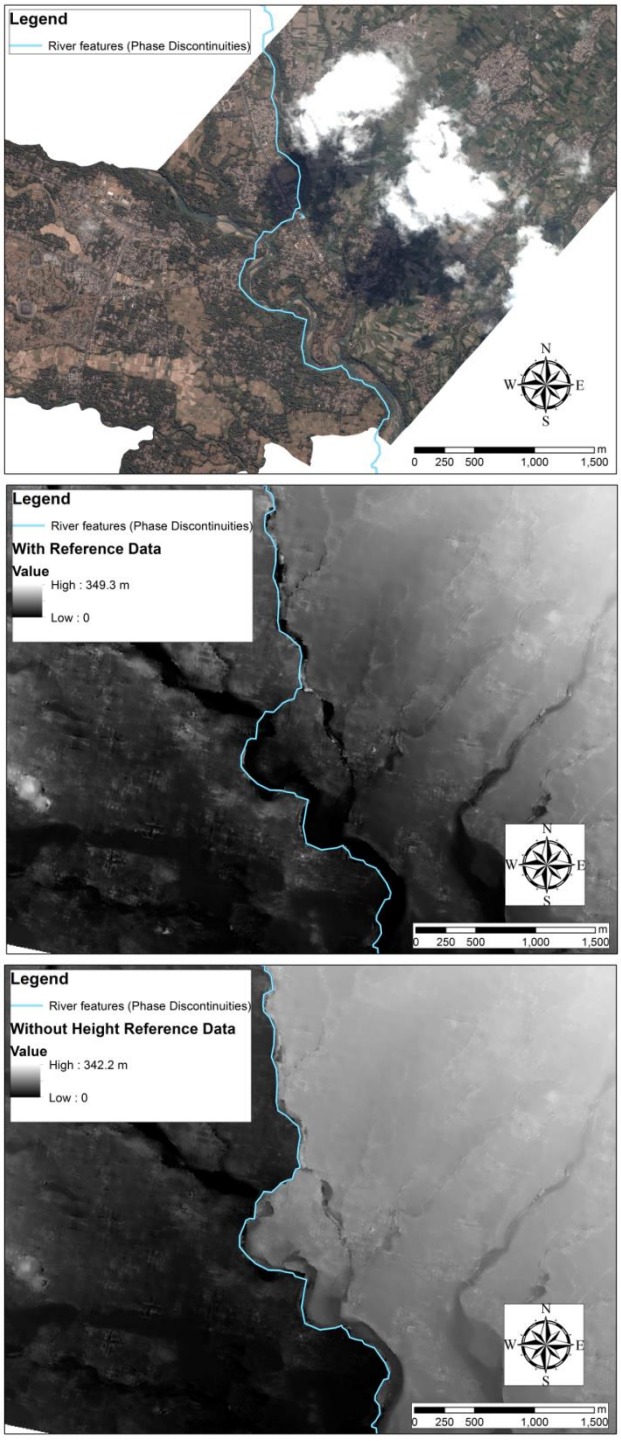

Figure 36: Phase discontinuity problems (upper: river features in QuickBird, middle: with corrected baseline, lower: with original baseline from metadata)

The discussion about TanDEM-X configurations as one prominent bi-static SAR mission example in Cherniakov, 2008 and Krieger et al., 2007 also emphasized that the baseline estimation errors will lead to a height error as inferred in Eq. 5.4. Using this equation for Borobudur Temple area (topographical height (h) around 275 m above MSL, ΔB_P = -156.535-(-162.344) m = -5.809 m) contributes to the significant height error of 9.84 m. This height error value is approximately equal to the terrain height differences between

the eastern sides of the river (brighter area) in lower part of Figure 36 i.e. around 302 m above MSL, and the cross over western sides of the river (darker area) i.e. around 281 m above MSL.

$$\Delta h = \frac{h\,\Delta B_{perp}}{B_{perp}} \tag{5.4}$$

5.2.3.2 Investigation results on the height accuracy for moderate terrain area

For the purpose of the investigations on height accuracy, in addition to the $RMSE_Z$ as discussed in 2.4.2, two other important statistical values have to be evaluated simultaneously namely Standard deviation σ_Z and Mean error μ_Z. The RMSE itself is not sufficient to indicate the geometric quality of geospatial data because it is still mixed with the blunder errors and different positional reference (datum). As calculated by using Eq. 5.5, the μ_Z reflects how success is the proposed algorithm in TanDEM-X DEM calibration based on the height reference data (see section 4.3.2.3). Subsequently, the μ_Z determines also the σ_Z as calculated by using Eq. 5.6.

$$\mu_Z = \frac{\sum(ZCheck_i - ZRef_i)}{n} \tag{5.5}$$

$$\sigma_Z = \sqrt{\frac{\sum((ZCheck_i - ZRef_i) - \mu_Z)^2}{n-1}} \tag{5.6}$$

Indeed, ASPRS, 1990 stated explicitly for LSTM that the σ_Z value must be equal or less than one-third of $RMSE_Z$ value. Hence the condition that the μ_Z value must be close to zero is normally not sufficient to reflect better geometric accuracy. In addition, the condition about the $\sigma_Z \approx RMSE_Z$ must be fulfilled as well in order to get fair judgment for the evaluated datasets. Therefore, the closer the $RMSE_Z$ value to the σ_Z indicates the better the geometric quality of the evaluated datasets.

Table 17 shows the DEM accuracy assessment results using different ICPs numbers and coverages. It is always a question which amount and distribution of ICPs will be sufficient to represent the geometric accuracy analysis. The minimum 20 well distributed ICPs as required by FGDC, 1998 is presumably not sufficient for more comprehensive comparison on different schemes, variables and aspects of evaluations. More specific for the LSTM case, these numbers are insufficient for the evaluation of the relative and absolute accuracy as indicated by the values of σ_Z and $RMSE_Z$ (ASPRS, 1990).

For the investigation area, the different numbers and distributions of ICPs were compared for the small area (35 units) and the whole area (60 units) as depicted in Figure 26. As mentioned above, due to the IDEM data availability the different schemes must be defined in order to provide reliable accuracy assessments. Since the available ICPs for the small area are only 35 units, the additional 25 units must be added in order to get more meaningful statistical values of μ_Z, σ_Z, and $RMSE_Z$.

Table 17: DEM accuracy (in meter) for Borobudur area

Data Sources	ICPs small area (35 Units)				ICPs whole area (60 Units)			
	μ_Z	σ_Z	$RMSE_Z$	LE90	μ_Z	σ_Z	$RMSE_Z$	LE90
SRTM	3.43	3.45	4.86	7.99	3.51	3.23	4.77	7.84
IDEM	-0.93	3.58	3.70	6.08	-	-	-	-
TDM90	0.88	3.67	3.78	6.21	1.40	3.02	3.34	5.49
S01	**TDM Lin-DEM (ascending)**							
UAV DEM	0.11	2.83	2.84	4.67	0.14	2.94	2.95	4.85
3 GCPs	-3.01	3.78	4.84	7.96	-3.47	3.43	4.87	8.02
8 GCPs	-2.18	3.79	4.37	7.19	-2.93	3.56	4.61	7.58
S02	**TDM Lin-DEM (descending)**							
UAV DEM	-0.14	2.93	2.94	4.84	0.11	2.99	2.99	4.92
3 GCPs	-1.74	2.93	3.42	5.62	1.38	5.19	5.38	8.84
8 GCPs	-1.82	3.24	3.72	6.12	-2.14	3.33	3.97	6.52

There are 4 datasets which were evaluated in this section as follows (Table 17):

1. SRTM 1 arc second in 30 m resolution;
2. IDEM 0.4 arc second in 12 m resolution;
3. TanDEM-X DEM 3 arc second in 90 m resolution (TDM90);
4. TanDEM-X generated DEM by using linearized model (TDM Lin-DEM) in 6 m resolution i.e. S01 (ascending) and S02 (descending).

As specified by DLR, 2018, even though the resolutions of IDEM and TDM90 are different but they have the same absolute height accuracy i.e. < 10 m of LE90 (HRTI level 3 as included in Table 6). Therefore, in case where IDEM is not available as found for the whole National Strategic Area of Borobudur (see Table 17 and Figure 26), it can be substituted by the comparable TDM90.

5.2.3.3 Discussions

As investigated by Hoffmann, 2006, SRTM DEMs derived from X-Band and C-Band had an error of σ_Z between 3.4 – 3.99 m in test area of Northern Alps and moderate terrain of South America. The investigation presented in this section indicates also a similar σ_Z of 3.23 – 3.45 m for the SRTM DEM. Interestingly, there is no significant difference of σ_Z values between the scheme of 35 ICPs (3.45 m) and the scheme of 60 ICPs (3.23 m) as the validation data. It means for the SRTM DEM, the number of ICPs has no significant impact to the height accuracy assessments.

Looking into more details about the minimum and maximum height deviations for all 35 ICPs (span of height accuracy) as depicted in Figure 37, it must be noted that for all of the evaluated DEMs they have more or less the same values (max-min = 13.6 – 16.9 m). Also reported by Hoffmann, 2006, the HOA of X-Band SRTM is 168 m (with the baseline of 60 m length) while HOA for the two TanDEM-X datasets in this investigation are 64.527 m and 39.178 respectively. Consequently, the aforementioned span of height accuracy is already within the expected result namely below the HOA.

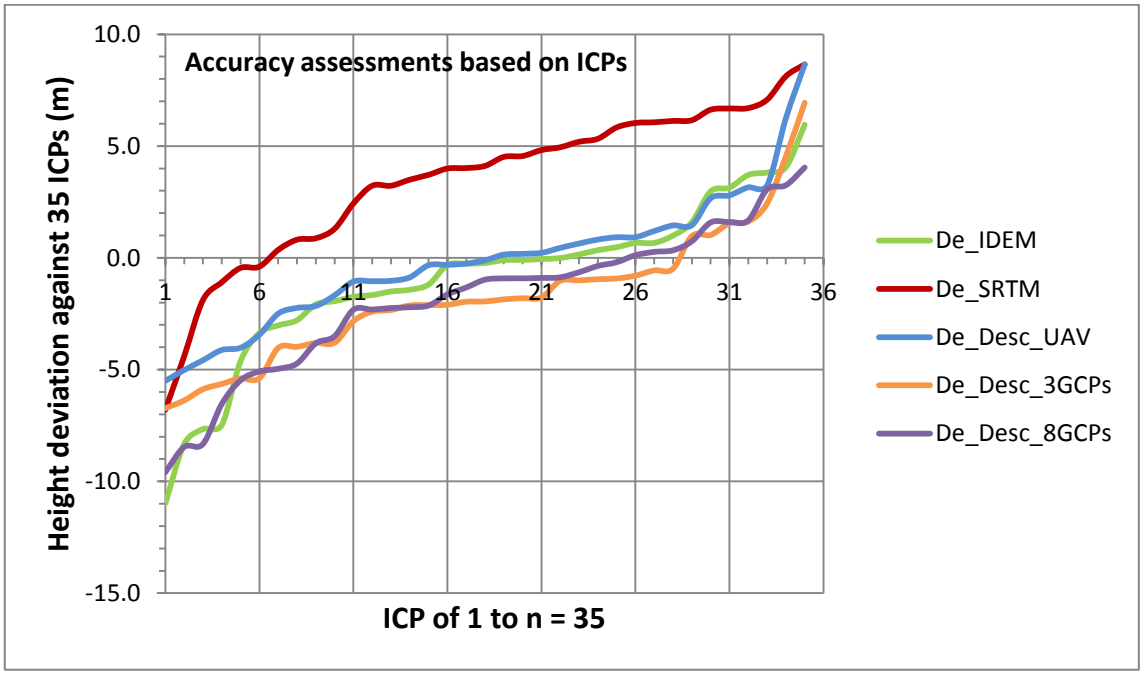

Figure 37: Height deviations for 35 well distributed ICPs

Hence, the PU steps for all evaluated datasets were done successfully without any significant height error at least on the ICP random samples. However, a more robust PU algorithm in SNAPHU shall be also supported by an accurate phase to height conversion module in order to precisely determine the remaining absolute phase offset for DEM generation (Lachaise et al., 2014).

The determined accuracy values as included in Table 17 however, are not sufficient to ensure the reliability of the investigation results. As already explained in 3.2.4, there shall be a further evaluation to take a good sample representing the population of geospatial data. In addition to the geospatial sample distribution, the number of the sample i.e. ICPs is evaluated by using more advanced statistical analysis. Consequently, the calculated values of statistical descriptors themselves are not enough to provide objective assessment results.

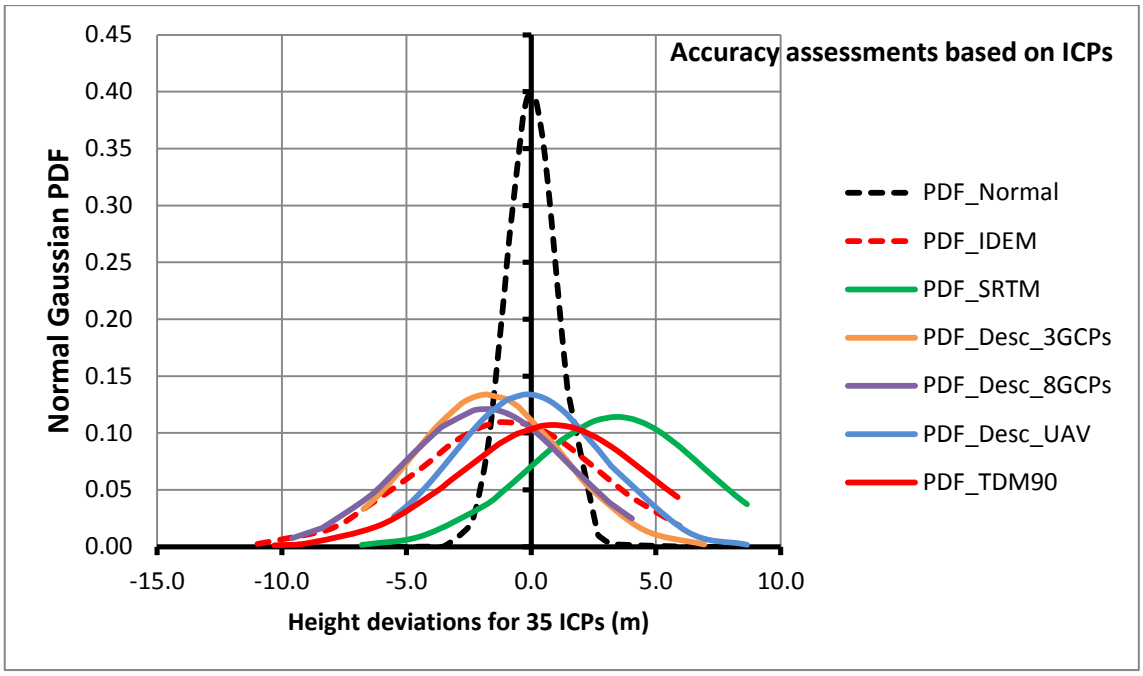

Figure 38: PDF plots for small area around Borobudur temple

For a more detailed analysis on geometric accuracy, the additional Probability Density Function (PDF) plots of the ICP samples in this dissertation have been created by using statistical function of Gaussian normal distribution in Microsoft Excel to recognize the error sources such as PU errors, geometric distortion, etc. The inputs for developing PDF are the height deviation for each ICP, mean value μ_Z and standard deviation σ_Z respectively. An important assumption is that the histograms of height differences between the evaluated DEM and the ICPs shall follow the normal distribution. By this assumption, how appropriate the number of sampling points and how suitable the normal distribution for the accuracy assessments have been evaluated.

At the first place, the presented height deviation for 35 ICP samples does not form a complete normal distribution curve for all evaluated DEM as shown in Figure 38. The insufficient number of ICPs is presumably the main reason of those incomplete curves. It shall be noted that the entire PDF plots except for SRTM and TDM90 have negative sample mean value μ_Z as they lie on the left side axis of the reference normal curve. Since the resolutions of both SRTM (30 m) and TDM90 (90 m) are coarser than the others, it tends to have a higher elevation value than the other evaluated DEMs (≤ 12m).

It is obvious that TDX-Descending using UAV DEM as height references (Desc_UAV) in the blue curve shows the best geometric accuracy indicated by the steeper shape with more center oriented shape to the Y axis. In other words, it has a narrower distribution as indicated by smaller σ_Z and a μ_Z closer to zero. As presented by the σ value showing in PDF plot, it is likely that the Desc_UAV (blue curve) and TDX-Descending using 3GCPs as height references (Desc_3GCPs: orange curve) indicated the same geometric qualities.

Noticeably, SRTM and IDEM have an almost similar curvature as indicated by the similar σ_Z value (SRTM=3.45 m, IDEM=3.63m) although with different μ_Z. On the other hand, all the TanDEM-X descending data have lower σ = 2.93 - 3.24 m. As indicated by HOA values, TanDEM-X DEM shall have a better height accuracy in a comparison with SRTM DEM. It means that for the investigation area IDEM accuracy (12 m resolution) does not indicate the expected relative accuracy in a comparison with SRTM DEM (30 m resolution) even though IDEM is better calibrated as shown by the smaller value of μ_Z =-0.93 m. The absence of reliable height reference contributes to the TanDEM-X DEM inaccuracy especially in the height scaling and DEM tilting factors of the generated DEM.

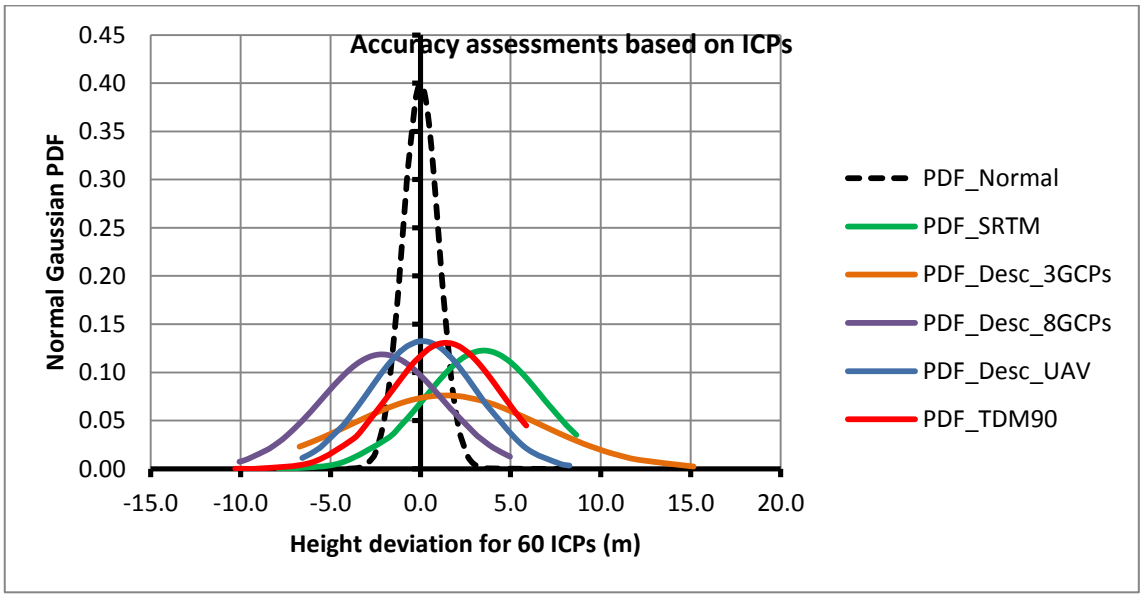

Figure 39: PDF plots for the whole of Borobudur National Strategic Area

Subsequently, PDF plots including the additional 25 ICPs for the whole area to get more representative sampling points are visualized in Figure 39. Differently to the previous PDF plots, the PDF plots for 60 ICPs showed almost a fully normal distribution curve for all the evaluated DEM. Unfortunately, the IDEM data is not available for further comparison with other evaluated DEMs. However, the aforementioned TDM90 as discussed in 5.2.3.2 was used as a substitute DEM in order to evaluate the other results. As included in DLR, 2018, the height accuracies of IDEM and TDM 90 (Table 17) also indicated similar results (IDEM=3.63m, TDM90=3.67 m).

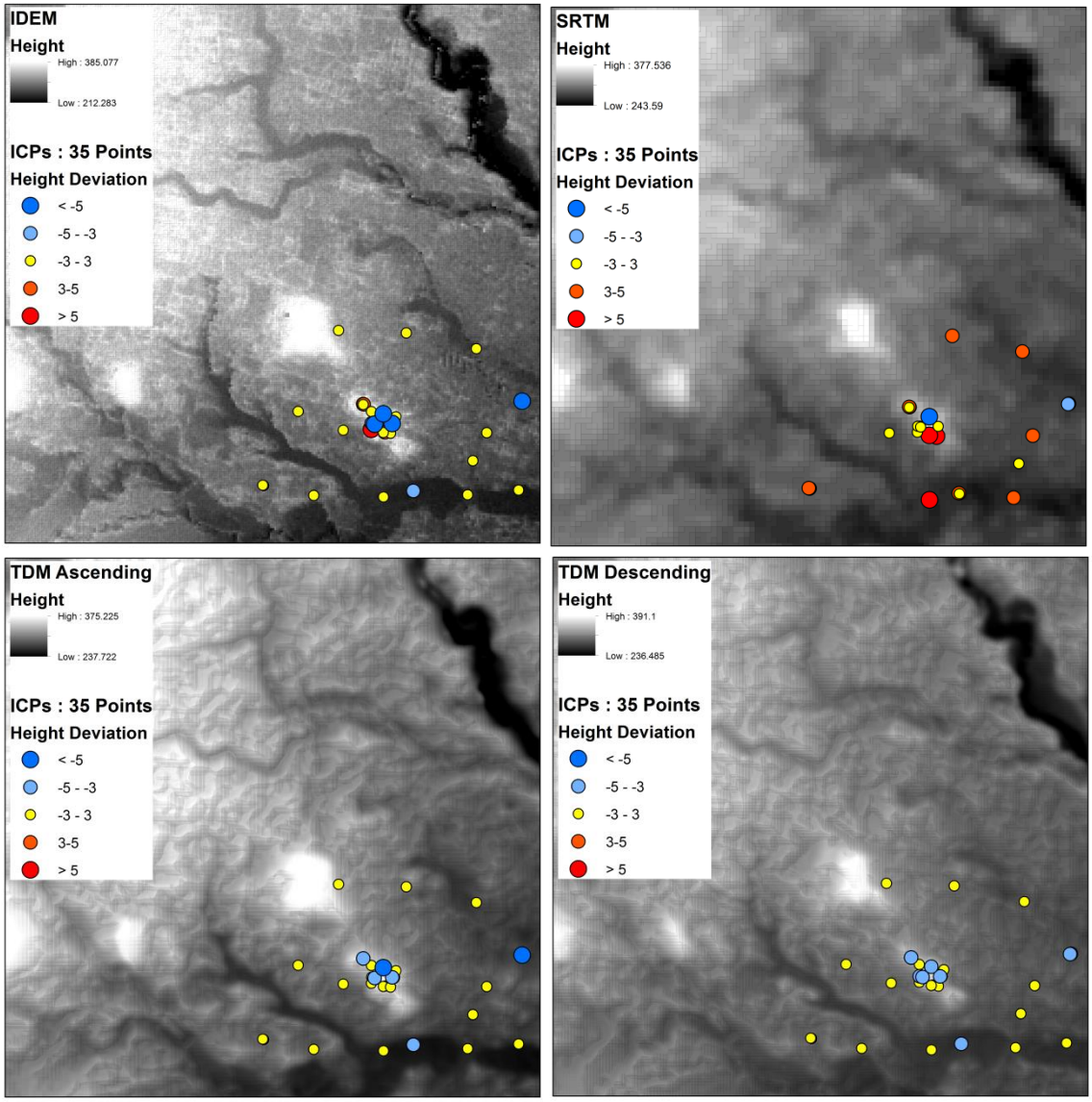

Figure 40: Shaded relief for different DEM with respect to the height deviation

By a visual inspection on the different DEMs as shown in Figure 40, the DEM quality of both generated TanDEM-X ascending and descending data are smoother without losing important details. All in all, the height deviation of 35 ICPs for TDX-Ascending and TDX-Descending are mostly in the range of -3 – +3 m without any removal of the outlier data. The observation on PDF plots confirms that all the errors are consistently normally distributed, with two major types of error. The first is an error towards higher terrain features due to the presence of vegetation, buildings and any other off-terrain objects. The latter is the outlier in conjunction with the PU errors which occurs more frequent than normal distribution can predict. However, the former height deviation from Normal Gaussian distribution is of no particular interest for a relative comparison of different DEMs.

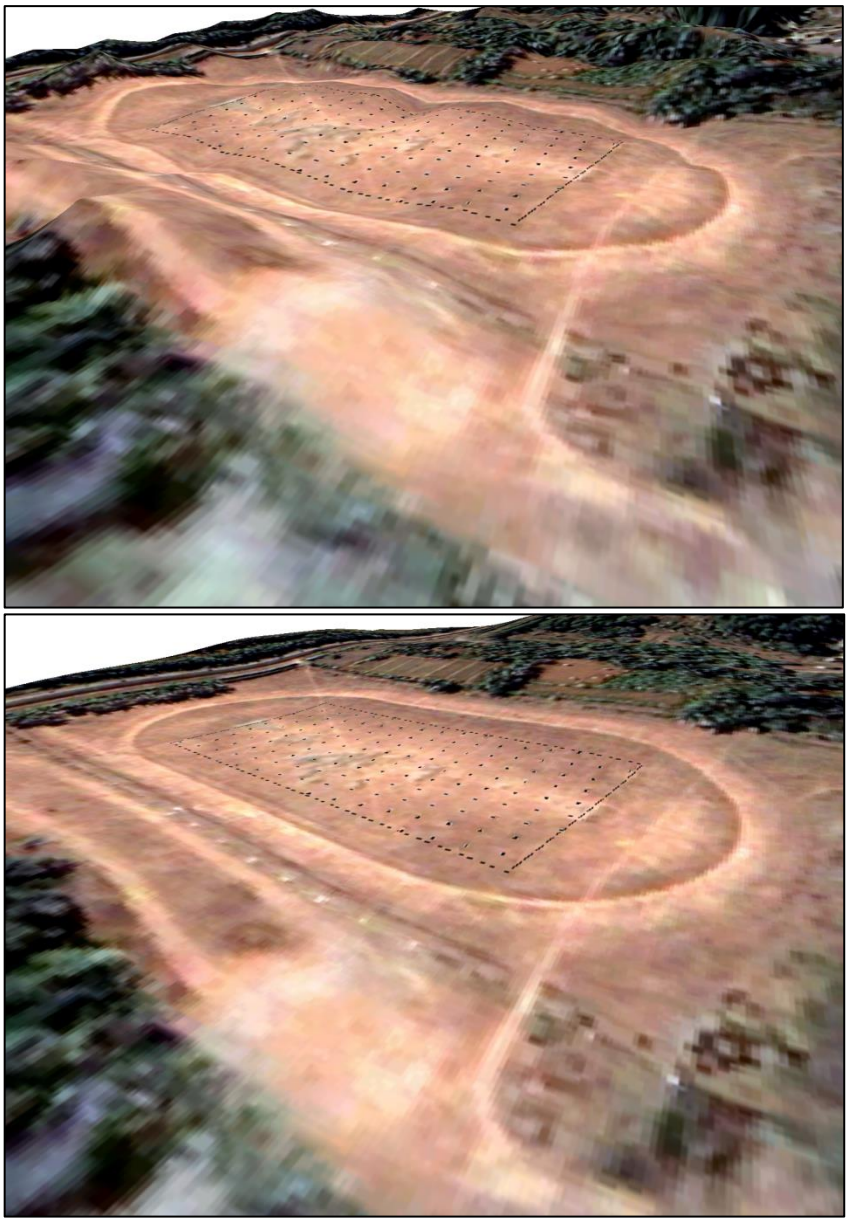

Figure 41: DEM visual rendering on VHRS (Quickbird) for the flat soccer field area (upper: IDEM, lower: TanDEM-X descending)

An additional evaluation of the geometric quality has been depicted in Figure 41 for the relative height accuracy assessments of the flat area (soccer field). By calculating point to point statistical errors as recommended by Howard, 1994 on flat area, the PDF plots has been created.

Visually, unlike the TanDEM-X Lin-DEM (descending), the IDEM exhibits bumpy terrain that shall not be the case for a flat soccer field as shown in Figure 41. For a 5,822 m^2 flat area of the soccer field, the statistical errors for each gridded point was also plotted in a form of PDF as depicted in Figure 42. The sample standard deviation σ_Z and ($RMSE_Z$) for IDEM, SRTM and TanDEM-X descending are 0.97 (0.96) m, 0.69 (0.69) m and 0.56 (0.56)

m respectively. Refer to PDF Plot in Figure 42, it is clear that the best relative geometric accuracy (point to point) goes to the TanDEM-X descending for this particular area as visualized by the steepest normal distribution curve to the local mean (green line). In addition, only TanDEM-X descending is sufficient enough to fulfill the relative accuracy requirements for HRTI Level 4 (< 1m) i.e. 0.92 m (LE90) as discussed in 2.4.2 by multiplying the RMSE value to the factor of 1.6449.

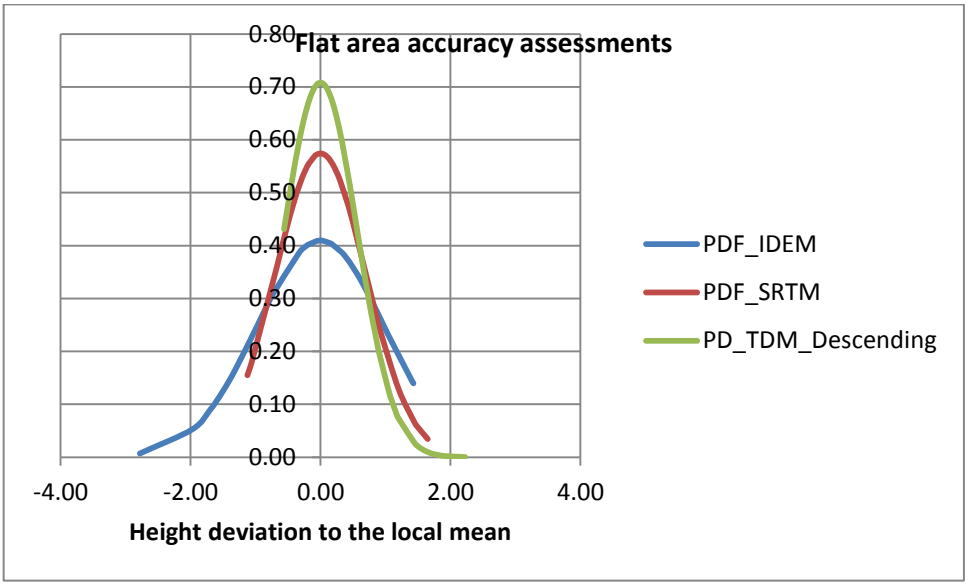

Figure 42: PDF plot for flat area (soccer field)

5.2.4 Investigations on UAV data for moderate terrain area

The main objective of this section is to provide a standard procedure for UAV data processing in the context of the LSTM purpose. By comparing UAV data acquired from different sensors, the geometrical accuracy of the end product can be estimated before the mission (Tampubolon and Reinhardt, 2014). With respect to other geospatial data sources i.e. VHRS, the UAV data can be consolidated in order to avoid project inefficiency especially in the scope of GCP measurements. Therefore this section demonstrates the synchronization amongst UAV data, VHRS and GCPs in order to achieve an optimum geometric accuracy with minimum redundancy measures.

At the end, recommendations for a proper usage of UAV technology for a complementary LSTM in the special case of Indonesia are given. It includes the GCP requirements as well as the processing schemes based on certain assessment standards in the context of LSTM in Indonesia.

Datasets used The UAV data acquisition with flying height of 200 m (AGL) on 29 October 2013 using Sony NEX7 and Canon S100 cameras was performed to produce ortophotos and DSM with a resolution of 5 and 10 cm respectively.

Reference datasets The GCP datasets from GNSS rapid static as described in 5.2.1 were used as the reference data in the accuracy assessments. To detect the influences of GCPs (from GNSS survey) and different DEM data on planimetric accuracy, the additional ICPs (also from GNSS survey) were used to validate the in-house orthorectification results by using Agisoft PhotoScan.

5.2.4.1 UAV data processing by using different GCP sources

The GPS/GNSS survey was providing the representative GCP network with a good spatial distribution over the Borobudur Temple (Figure 43).

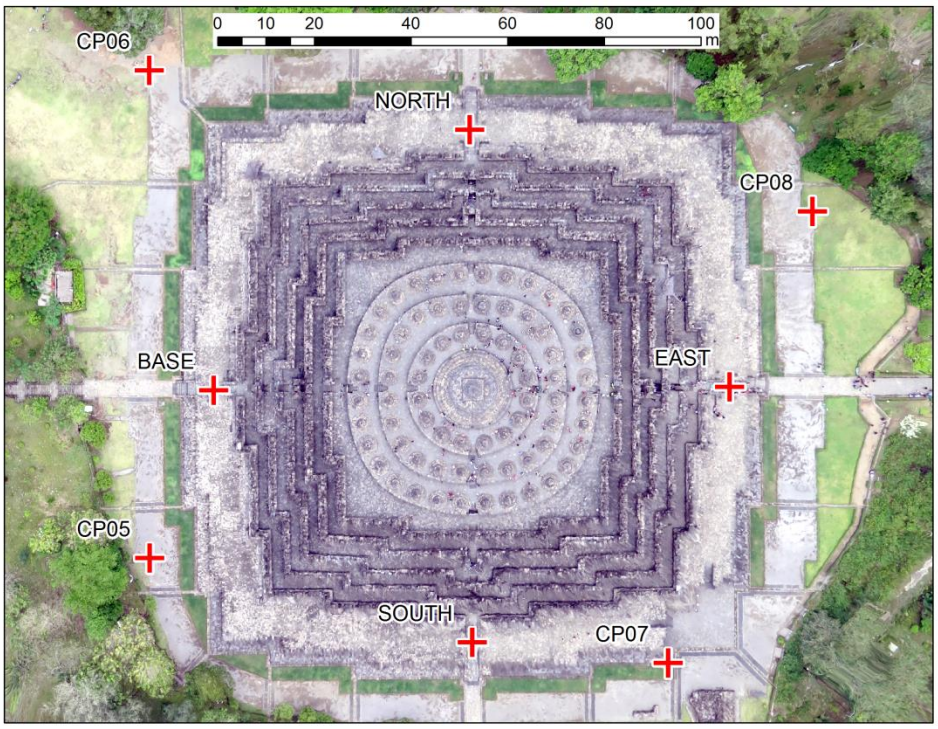

Figure 43: GCPs from GNSS survey

Alternatively, as already discussed in 5.2.2.2 the VHRS imagery with planimetric accuracy of 1.1 m (RMSE) has been used as the reference image for orthorectification of UAV data (Figure 44). Certainly the aforementioned orthorectification requires elevation data in which it can be extracted from radar space borne data (TerraSAR-X) as applied in the VHRS orthorectification.

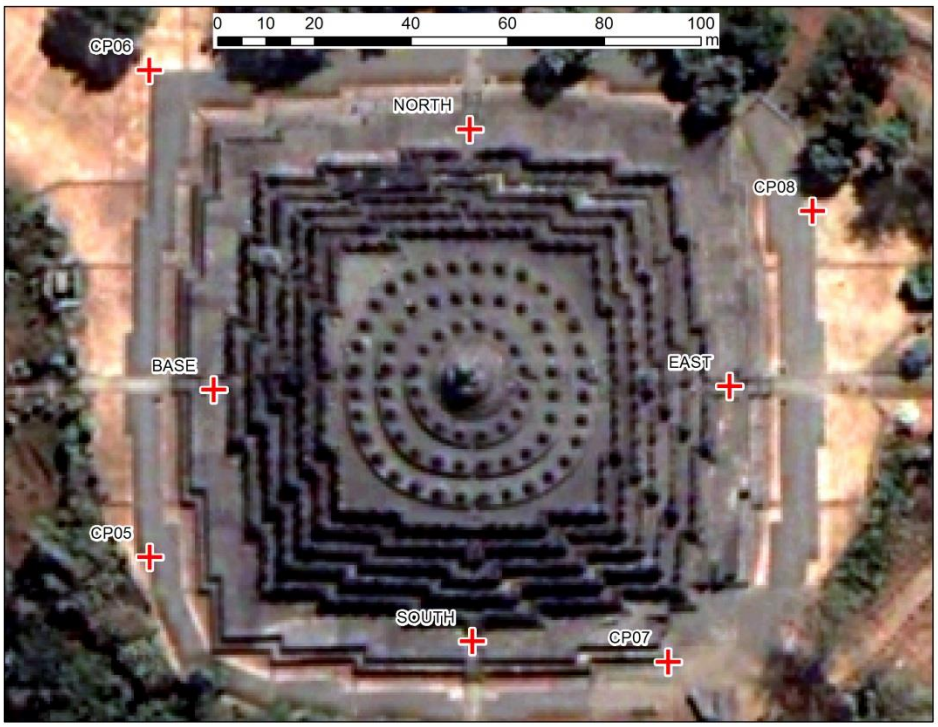

Figure 44: GCPs from VHRS imagery

Currently, this radar space borne data has just been used for the medium scale topographical mapping e.g. up to 1:25.000. By using this approach, the provision of DEM from UAV has presented a potential solution for LSTM i.e. 1:5,000. As depicted in Figure 45, orthorectification of UAV data using 5 GCPs from GNSS measurements has produced the orthophoto in 1:1,000 LSTM accuracies.

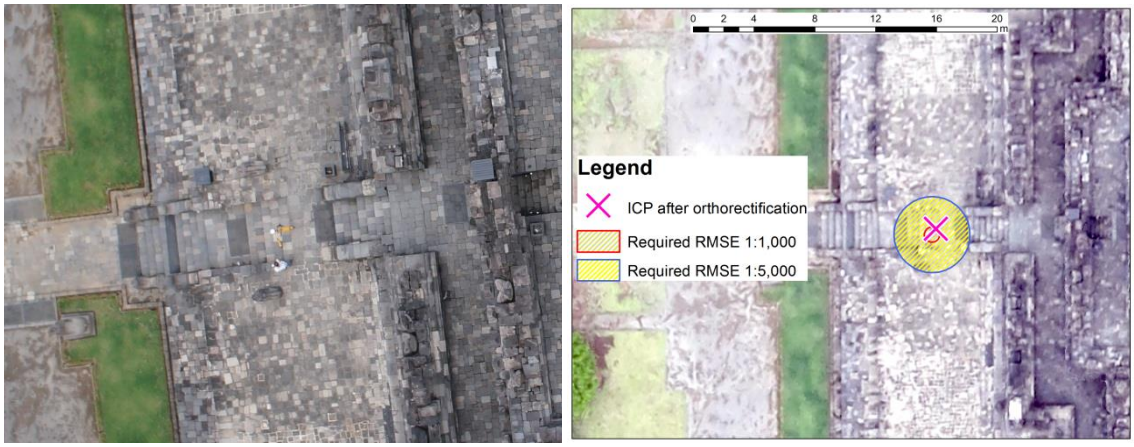

Figure 45: GCP from GNSS survey (left) in Sony NEX7 photo (right)

During the UAV campaign, 23 new GCPs have been measured using geodetic GNSS/GPS double frequency L1/L2 with a good distribution covering the AOI (Figure 45: left part). Implementing rapid static differential positioning, every GCP must be measured not less than 30 minutes in order to get sub centimeter accuracy. These 23 GCPs in favor of orthorectification and accuracy assessment, can be considered as GCP or ICP (Figure 46).

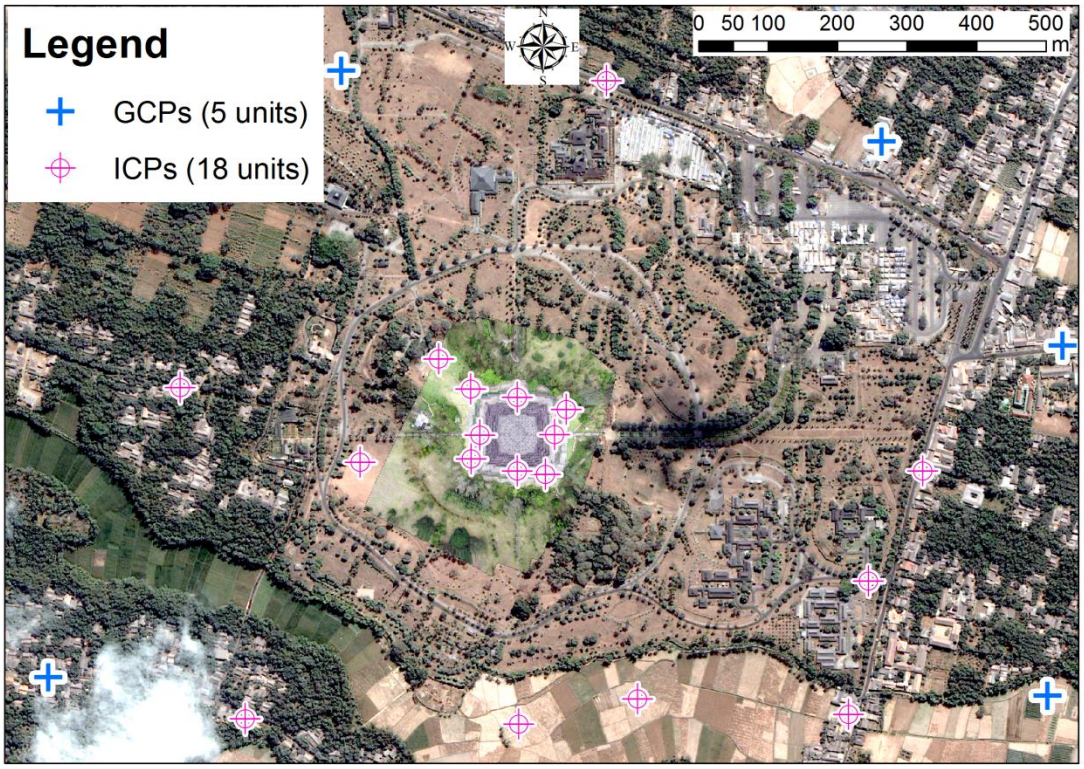

Figure 46: GCPs and ICPs network distribution

5.2.4.2 UAV investigation results on moderate terrain

Based on ICPs as depicted in Figure 46, the digitization of each point was manually done in an orthophoto to calculate the $RMSE_r$ by using eq. 2.3. By multiplying with factor 1.5175 as inferred in equation 2.4, the planimetric accuracy of Circular Error 90% (CE90) for each data acquisition with respect to its GCP scheme was included in Table 18. To get the height component of each aforementioned ICP, the Extract Values to point (ArcGIS toolbox) was used. $RMSE_z$ was calculated by using eq. 2.5 in order to yield height accuracy of Linear Error 90% (LE90) with eq. 2.6 (see also Table 18).

In addition to the default flying height i.e. 200 m AGL (see section 3.1.2), fortunately the UAV data acquisition with lower altitude i.e. 50 m focusing on Borobudur temple (Figure 46) has been performed only by using the Sony NEX7 camera. However for this acquisition, since all the 8 GCPs around Borobudur Temple were used as the ICPs, the possible GCP scheme is only by using GCP from VHRS. For this specific area, the height of GCP from VHRS was extracted from TanDEM-X Lin-DEM in order to detect their influences in the absolute accuracy as included in Table 18.

Table 18: RMSE of UAV data acquisition

	Using GCP from VHRS		Using GCP from GNSS	
	Planimetric (m)	Height (m)	Planimetric (m)	Height (m)
NEX7 (TanDEM-X) (h = ± 50 m AGL)	0.38	0.49	-	-
NEX7 (TanDEM-X) (h = ± 200 m AGL)	0.59	0.82	0.50	0.65
S-100 (TanDEM-X) (h = ± 200 m AGL)	0.65	1.14	0.62	0.49

5.2.4.3 Discussions

In this section, a hybrid orthorectification has been selected as an optimal solution to reconstruct remote sensing data including a UAV survey campaign by combining planimetric and terrain aspects of the earth surface from VHRS. The investigation has identified the absolute geometric accuracy of the outputs by using a manual approach from different cameras and GCP schemes.

An inaccurate camera calibration gives more significant geometric deviation in NEX7 rather than S100. It is also confirmed by the ratio between planimetric and vertical accuracies RMSE in Agisoft Photo Scan. As included in Table 18, S100 gives 0.62/0.49, where NEX7 gives 0.50/0.65.

By flying lower to 50 m (AGL) leads to orthophoto and DEM with better resolution and absolute accuracy respectively as included in Table 18. However, the lower the flying height it requires a heavier workload on the data processing especially for generating the dense point cloud as well as for mosaicking the orthophotos.

This result has shown the significant geometrical improvement of UAV photo data processing in comparison with GPS camera only (see 4.4.1) by implementing an integration mechanism with VHRS imagery appropriate for 1:2,500 planimetric accuracy. The aforementioned mechanism by using only 5 GCPs either from QuickBird imagery or GNSS has reached a RMSE within 1.25 m as required for 1:5,000 LSTM.

However for the generated DEM, it is still necessary to use 5 GCPs from GNSS in order to comply with 1:5,000 LSTM accuracy. On this level of geometric accuracy, Precise Point Positioning (PPP) method as explained in 4.1.1 is sufficient to fulfill the GCP accuracy requirements i.e. 1 meter accuracy and hence can reduce time, cost and reference station dependency.

The final Ground Sampling Distance (GSD) has been selected to 7 cm both for DEM and orthophoto (Figure 47). This resolution allows that during digitization object patterns with optimal zooming can be recognized and a high accuracy can be reached in the end.

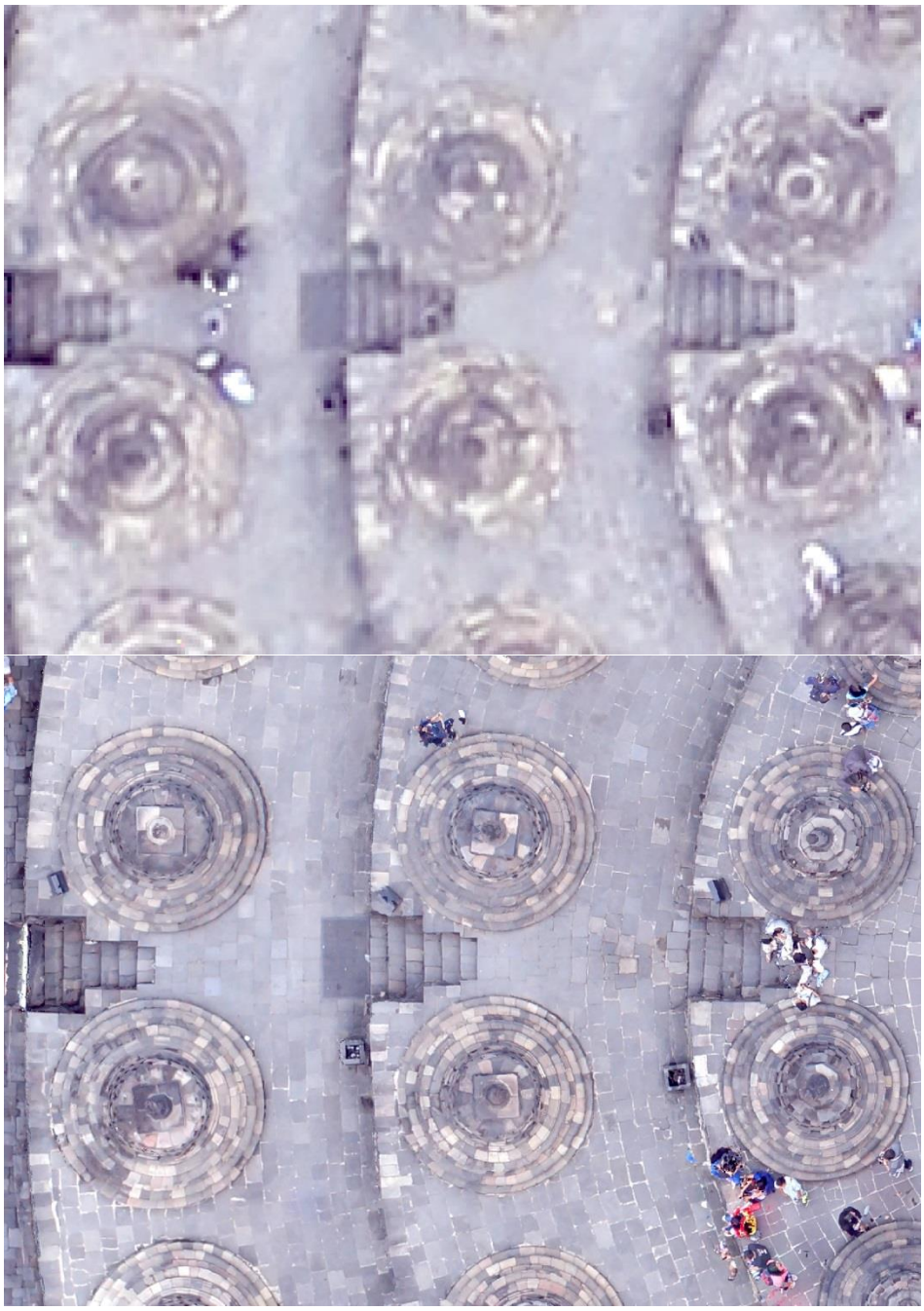

Figure 47: Visual comparison on orthophotos (upper: 7 cm GSD of Canon-S100 and lower: 1 cm GSD of Sony NEX7)

5.3 Investigation on flat terrain (BIG office)

The selection of the test area at the BIG office in Cibinong is mainly because of the availability of supporting data inputs, including the geodetic reference network infrastructure i.e. CORS with reliable accuracy (Tampubolon and Reinhardt, 2018).

In general, the test site covers an urban area of approximately 15 km^2 which has an approximate elevation of 140 meters above MSL. The terrain condition of the study

area is classified as medium undulated urban region surrounded by a lot of hills with small slopes and vegetation areas. For those conditions, the investigations in this section are aimed on the TanDEM-X DEM generation as well as the UAV data processing by using GCP data (CORS) only.

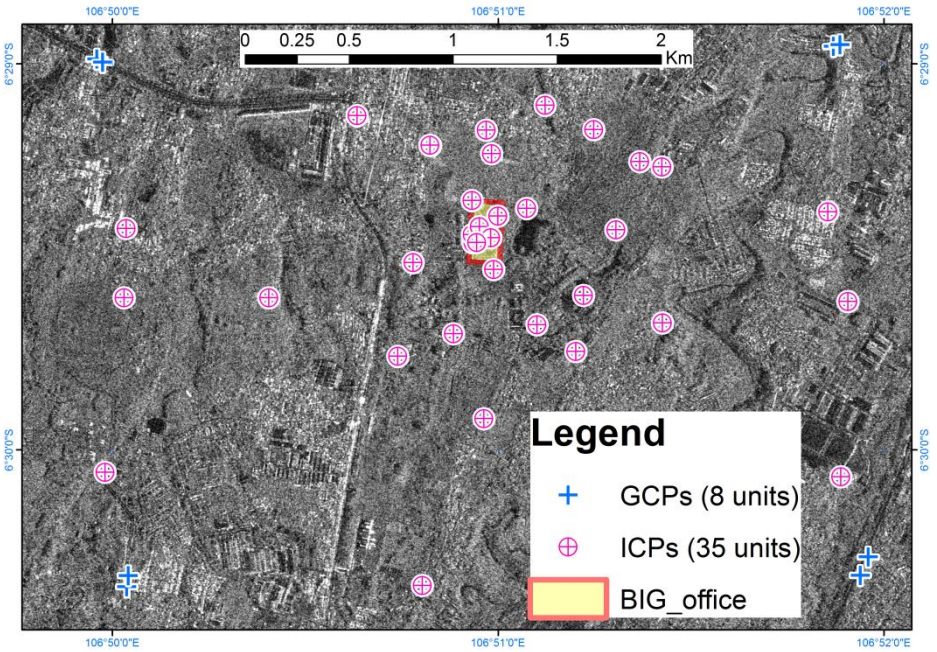

Figure 48: BIG office investigation area

Datasets used The TanDEM-X data used in this investigation are CoSSC data with a maximum resolution of 2 m (one look). Therefore with respect to the achievable resolution, the TanDEM-X data for this flat area presumably produce better DEM than the other test areas. To enable the detail investigation on geometric accuracy aspect, there are two type of processing schemes which shall be compared.

For the test area "BIG office", TanDEM-X products i.e. Coregistered Singlelook Slant-range Complex (CoSSC) data have been used as a raw dataset to generate a reliable DEM using the interferometric approach (Table 19). Indeed, the influence of the HOA value to the geometric accuracy can be neglected due to the flat terrain condition as well as the low orthometric height (150-200 m above MSL) of the test area.

Reference datasets The airborne data acquisition from 2012 by using Leica RCD30 and Trimble Phase One (P65+) cameras were performed to produce the ortophotos and DEM with a resolution of 5 and 10 cm respectively. In this case, both orthophotos and DEM were selected as the reference for accuracy assessments because of their reliable geometric accuracy supported by the aerial metric cameras as described in 2.2. The BIG office area (red rectangle in Figure 48) has been selected by taking into consideration the GCP coverage and the building structures. Differently to the previous investigation, only GCP data (see next section) were used as an input to the geospatial data processing i.e. InSAR DEM generation, UAV data processing.

Table 19: TanDEM-X CoSSC data (*Height of Ambiguity) for BIG office area

Scenes	HOA* / Baseline (m)	Looking direction	Acquisition Date
S01	135.280 / 40.394	Descending	30-01-2012
S02	34.090 / 146.064	Descending	31-10-2012
S03	61.715 / 95.550	Ascending	09-01-2013
S04	120.747 / 52.689	Ascending	11-10-2013

5.3.1 GCP measurements for flat terrain area

Since the proposed algorithm uses a linear approach to adjust the parameters, the design of GCP distributions were using only 4 and 8 GCPs configurations around the perimeter of the area (Figure 48). In this case, the assumption is that the GCP distribution has a significant influence in the parameter adjustment result for the InSAR DEM generation (height calibration) as well as for the UAV data processing (orthophoto and DEM generation). However, this aforementioned assumption is not always valid as will be further explained in 5.4.1.1. The most important factor is the GCP's accuracy itself as already explained in 4.1.

Figure 49: Geodetic control (CORS) at BIG office (left : BAKO, right: BAK1)

The main reason to use the GNSS monitoring stations (Figure 49) as the positional reference in this dissertation is to ensure the 3D accuracy as above mentioned. In this case, the utilization of a Global Navigation Satellite System (GNSS) infrastructure through the so called the Continuous Operating Reference System (CORS) for the global monitoring service is mandatory, hence the positional accuracy is in the range of millimeter. Obviously, their 2D positions as well as their heights above ellipsoid or MSL

using precise geoid model and the related documentations can also be freely accessed online at http://www.srgi.big.go.id.

The aforementioned CORS infrastructures establish a framework that can be used to improve and to reach the proper accuracy as explained in 4.3.2.3. This accurate positioning in combination with precise orbital information can provide a robust and sophisticated IFSAR data georeferencing. There are two types of georeferencing methods applied for the investigation in this section:

- For georeferencing of all field (in-situ) data, the geodetic and geodynamic control of NMA's reference system i.e. Indonesian Geospatial Reference System (SRGI) was nationally used;
- For on-board georeferencing of the radar data, the precise/scientific orbital information was globally used.

5.3.2 Investigations on TanDEM-X data for flat terrain area

The IDEM which was also generated from TanDEM-X StripMap data is sufficiently used for topographic mapping only up to the 1:25,000 map scale with its respected HRTI 3 level of geometric accuracy (Fiedler et al., 2008). For larger map scales, it is possible to improve the accuracy because TanDEM-X StripMap has basically high resolution i.e. 2-12 m (DLR, 2018). However, some potential improvements e.g. filtering, multilooking and more accurate phase unwrapping as explained in 4.3.2.1 shall be applied to increase the geometric accuracy with respect to the available local datum or ground segment in a form of GCPs.

In addition, InSAR DEM generation with the above mentioned improvements can provide topographic information with elevation accuracies comparable to the stereophotogrammetric approach (Tampubolon and Reinhardt, 2015). The sufficient and valid topographic information from the field in a form of height reference is considerably important for a reliable InSAR DEM generation. Indeed, the generated DEM without applying the above mentioned improvements is not accurate enough for fulfilling the LSTM requirements.

5.3.2.1 Processing strategies for the application of the linearized model in flat terrain

As a preliminary test using SNAP desktop without height reference data, the generated DEM achieved only 10.97 m (LE95 height accuracy) of the generated DEM from S01 dataset (Descending-30-01-2012) which is out of the level of the HRTI-3 specification (Tampubolon and Reinhardt, 2018). Therefore in this section, the DEM reference is only used for Geocoding step in a so called Range-Doppler terrain correction (SNAP Desktop in 4.3.2) since the GCP data as a height reference is considered sufficient to achieve HRTI level 4 accuracy for flat terrain such as BIG office area.

Nowadays, the worldwide user survey among societies has significantly shown that many applications require improved accuracy corresponding to the emerging HRTI standard and hence comparable to the similar DEM generated by an airborne Synthetic Aperture Radar (SAR) platform (Weber and Herrmann, 2006). The utilization of Tan-

DEM-X data on this matter is suitable for its single-pass acquisition and X-Band configurations which enable a more accurate DEM generation.

By using the TanDEM-X CoSSC dataset, the interferogram between master and slave channel has been generated directly (DLR, 2012). Nonetheless, if the coregistration quality is not adequate, there is no chance to modify the transformation parameters of the slave data. Low coherence indicating poor InSAR performance is the prominent factor that affects the coregistration result (Krieger et.al, 2007). Ideally, the coherence value must be more than 0.8 especially for the height reference area as also applied in the whole of the investigation (see section 5.2.3).

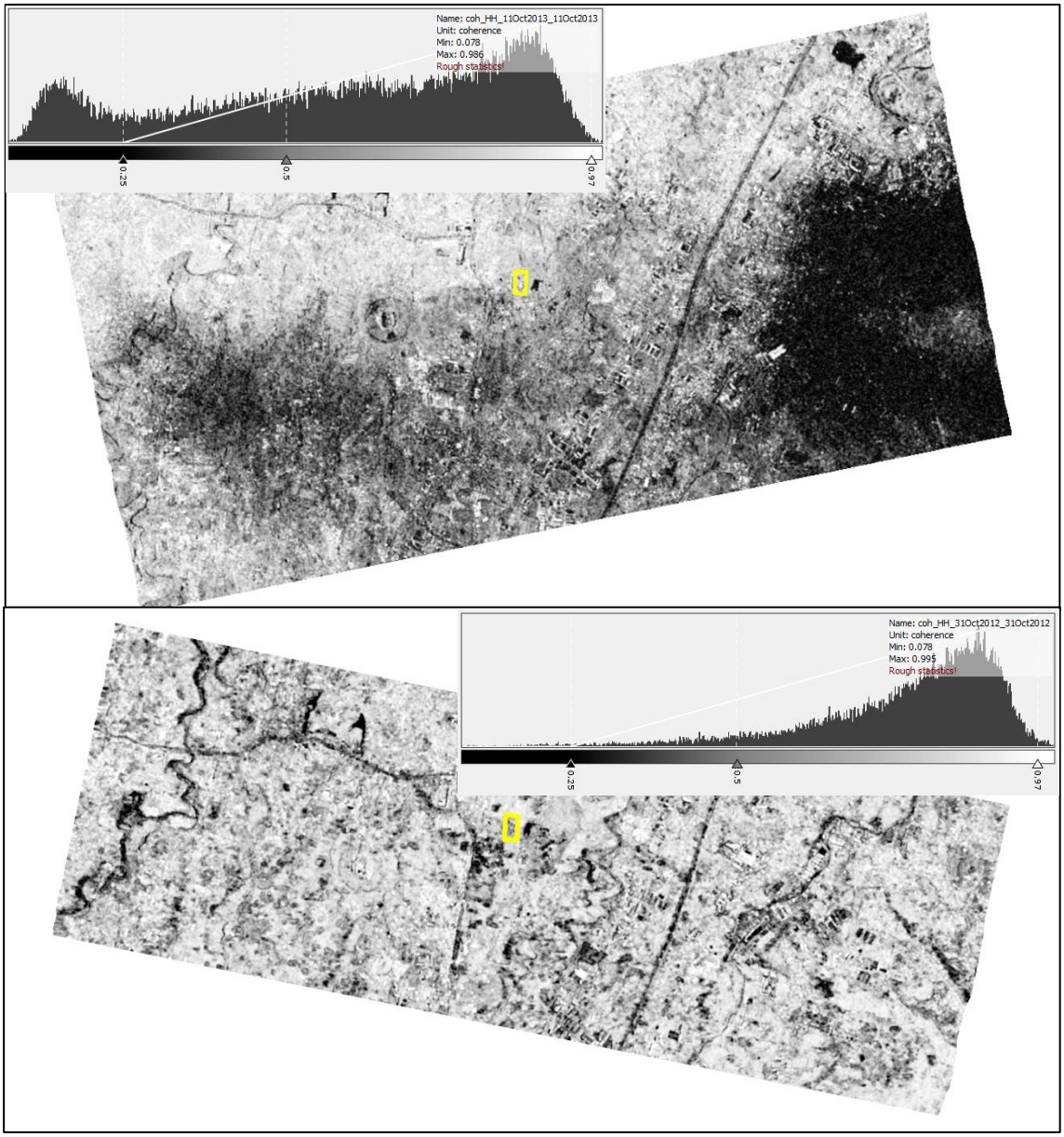

Figure 50: Coherence factor of TanDEM-X CoSSC data, yellow box indicates the BIG office area (upper: Ascending-S04 (11-10-2013), lower: Descending-S02 (31-10-2012))

For instance in the TanDEM-X ascending (S04) dataset, there are a lot of regions with low coherence indicated by black color i.e. in the eastern part of the scene (Figure 50: upper). The coherence values for TanDEM-X ascending (S04) are spread with a lot of portion in the range less than 0.25 (Figure 50: upper, left corner).

As it will be presented in the next section, the geometric accuracy of the generated DEM degrades along with the poor coregistration quality of the S04 dataset. Hence the influence of the poor coregistration result to the InSAR performance can be visually seen on the generated DEM for S04 dataset (upper part of Figure 52). Not only some details are loose but also some spikes and artifacts are present. However, the focus of the investigations in this dissertation does not deal with the improvement of the coregistration results.

5.3.2.2 Investigation results on the height accuracy for flat terrain area

Initially, the reference data generated from aerial metric cameras must be assessed by using GNSS measurements (cm level of accuracy) in a so called ICP level 1. ICP level 1 is intended to assess the geometric accuracy of conventional airborne data acquisition of RCD30 and Trimble P65 cameras (see 2.2) by using 10 ICPs. In this first level, the absolute accuracy assessment for 2D (planimetric) and 3D (elevation) components were calculated which cover the test area of BIG office as included in Table 20. For a Direct Georeferencing (DG) from airborne acquisition, there is no GCP used, while for either the Indirect Georeferencing (IG) or the combined method three GNSS CORS and 5 post marking GNSS rapid static measurements are used as 8 GCPs in the photogrammetric data processing. From this step, the more accurate reference data can be determined.

Table 20: RMSE by using 10 ICP level 1 for aerial metric cameras (DG: Direct Georeferencing, IG: Indirect Georeferencing, Co: Combined DG-IG)

Camera	Planimetric Accuracy (m)			Elevation Accuracy (m)		
	DG	IG	Co	DG	IG	Co
RCD30	0.14	0.15	0.09	0.17	0.18	0.11
Trimble Phase One	0.34	0.27	0.24	0.30	0.29	0.22

Since the DG method is not always free from systematic errors such as GPS/INS-camera misalignment, GPS time shift, camera calibration, etc, the combined method using both GPS/INS data and GCPs was also applied. To ensure the accuracy, all available aforementioned GCPs were used in the combined method. By performing ICP level 1 assessment, the orthophoto and DEM derived from Leica RCD30 camera as explained in 2.2 with the combined georeferencing method indicated the best geometric accuracy of 0.09 m (planimetric) and 0.11 m (height). For this reason, the Leica RCD30 products have been selected as the reference dataset.

For a further appraisal purpose, the TanDEM-X DEMs were compared directly with the aforementioned DEM obtained by conventional airborne data acquisition using a Leica RCD30 metric camera (Table 21). Subsequently, the generated DEM must be assessed by using ICP derived from the aforementioned reference data i.e. Leica RCD30 in a so called ICP level 2. This appraisal needs the ICP level 2 that is dedicated to assess the geometric accuracy of TanDEM-X related data.

Table 21: RMSE by using ICP level 2 from Leica RCD30 DEM in 0.1 m GSD

	IDEM (m)	TanDEM-X DEM (m)			
		S01	S02	S03	S04
Without GCP	3.41	5.60	6.27	8.90	12.08
4 GCPs	-	2.23	2.38	2.42	4.33
8 GCPs	-	2.51	2.54	2.43	4.86

In addition, the subsequent ICP level 2 accuracy assessments by using Leica RCD30 data and 35 ICPs as the reference data have been done. The generated DEMs of IDEM and 4 TanDEM-X CoSSC were validated against Leica RCD30 data within the corresponding resolution. For example to assess the IDEM with 12 m resolution, the gridded points in 12 m i.e. 814 points are created and interpolated using ArcGIS tool Extract Values with respect to the reference points from raster data of Leica RCD30 DEM (0.10 m resolution).

5.3.2.3 Discussions

To check the influence of the linearized model in the so called TanDEM-X Lin-DEM products, the final assessment by using ICP level 2 was performed as included in Table 21. In this case, the TanDEM-X results were evaluated in order to detect the geometric accuracy improvements.

First of all, the IDEM has shown the better result than the expected specification of HRTI level 3 (see section 3.1.1.2) as indicated by the RMSE value of 3.41 m which also fulfills the HRTI level 4 specifications (Table 6).

Obviously, the geometric accuracy as indicated by RMSE of TanDEM-X Lin-DEM using 4 or 8 GCPs as height references has improved significantly in a comparison with TanDEM-X without GCP (Table 21). Moreover, the comparison reveals that the TanDEM-X Lin-DEM is capable of fulfilling the HRE04 specifications with required RMSE ≤ 2.43 m as included in Table 6. The results from Table 21 also show that the linear model provides better results on a fewer number of GCPs. Hence, it also confirms the linearity condition of the model perfectly.

In addition as depicted in Figure 51, a profile of the building area in BIG office can be better represented in the generated TanDEM-X Lin-DEM rather than IDEM. However, since the DEM resolution is only 5 m, it is still not sufficient for a full building extraction

purpose in order to provide an input requested by the subsequent UAV data processing (see section 4.4.1).

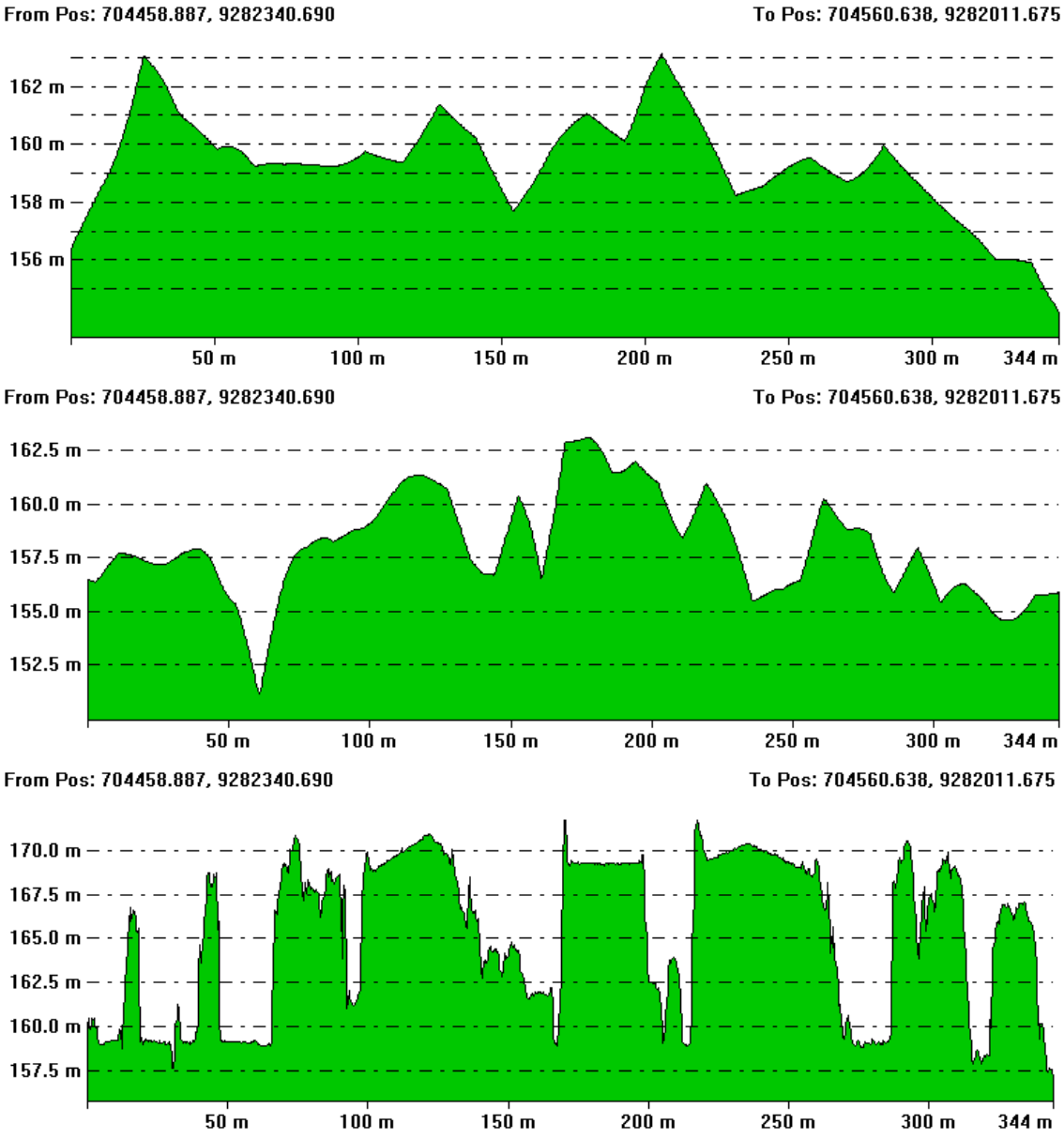

Figure 51: Profile cut in BIG office: IDEM (upper), generated DEM (middle) and Leica RCD-30 DSM (lower)

Finally, as depicted in the middle part of Figure 52, the appropriate DEM details of the S02 dataset improved significantly by performing the correct settings of Goldstein adaptive filtering, Speckle filtering and Multilooking by factor of 2 by 2 range and azimuth resolution. In addition, the visual quality of aforementioned generated DEM is smoother without losing any important detail compared to DLR's IDEM (lower part of Figure 52). Especially in the part of the BIG office (magenta rectangle) and its surrounding, the objects are sharp having better height accuracy as already discussed beforehand.

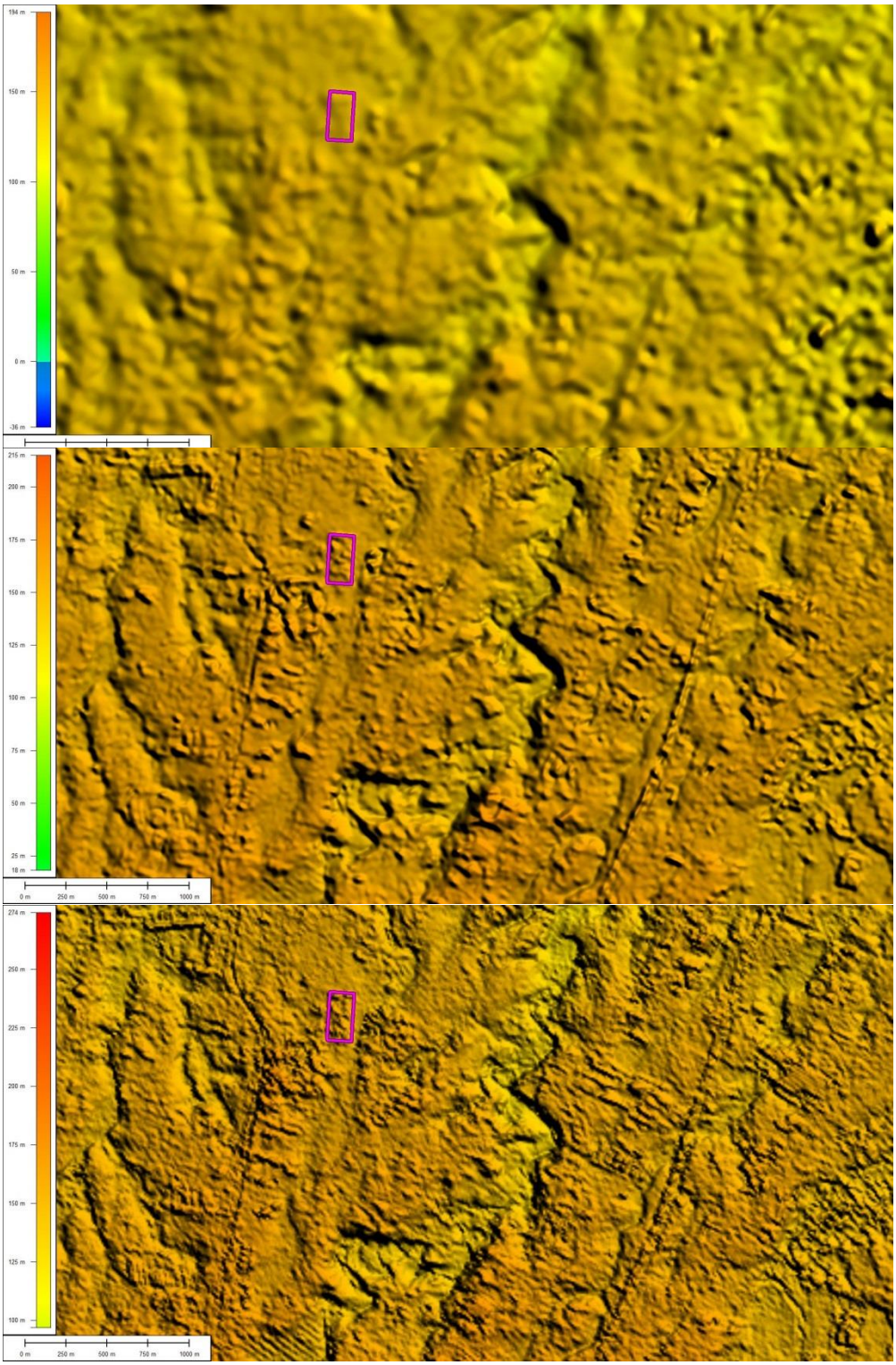

Figure 52: DEM visualization (upper: S04 dataset in 5 m resolution, middle: S02 dataset in 5 m resolution, lower: IDEM in 12 m resolution)

5.3.3 Investigations on UAV data for flat terrain area

In this section, the processing of UAV data to derive topographic map products is presented. It applies SfM and also investigates the usage of building structures to determine the orientation parameters.

5.3.3.1 Inclusion of building structures for flat terrain area (the strategies)

The approach for the calculation of orientation parameters has four key steps as follows:

- First, by using Agisoft PhotoScan a set of image orientation parameters (X_0, Y_0, Z_0, Omega, Phi, Kappa) of the UAV data in the local coordinate system is generated and subsequently the differences with indirect georeferencing method (using GCPs) are calculated.
- Second, the image orientation parameters by using building objects e.g. orientation to the normal, direction (of the mosque) are manually extracted by using PCI Geomatica as explained in section 4.4.1, and iteratively the difference with indirect georeferencing method (using GCPs) is calculated as well.
- Third, the combination between the image orientation parameters from building object and the indirect georeferencing method is done to improve the accuracy.
- Fourth, the comparison between the direct georeferencing method with the indirect georeferencing method (using GCP) is performed in order to evaluate the influence of the building structure model for the final bundle adjustment.

5.3.3.2 Investigation results on the geometric accuracy for flat terrain area

In this section, ICP level 1 is intended to assess the geometric accuracy of the UAV data acquisition by using Canon S-100 camera in addition to the airborne mission by using RCD30, Trimble P65 aerial metric cameras as explained in 5.3.2.1. For this purpose, the absolute accuracy assessment for 2D (planimetric) and 3D (elevation) components have considered 10 ICPs provided from GNSS surveys which cover the test area of the BIG office as included in Table 22.

Table 22: RMSE by using 10 ICP level 1 for Canon S-100 (DG: Direct Georeferencing, IG: Indirect Georeferencing, Co: Combined DG-IG)

Camera	Planimetric Accuracy (m)			Elevation Accuracy (m)		
	DG	IG	Co	DG	IG	Co
Canon S-100	-	0.26	0.22	-	0.26	0.21

The generated orthophotos and DEMs from airborne Trimble Phase One and UAV Canon S-100 were validated against Leica RCD30 data. As also performed in 5.3.2.2, the ICP level 2 from Leica RCD30 data were used to assess the UAV data using a Canon

S-100 camera. To investigate the influence of the building structures a final assessment using ICP level 2 was performed in which the results from the above mentioned approach were directly compared with the reference accuracy from the DG method.

For the combined method (DG with GPS camera and IG with 3 GCPs) of UAV Canon S-100 data, the RMSEs of 52 ICPs manually selected from the orthophoto and DEM of Leica RCD30 are 0.2 m (planimetric) and 0.19 m (height) respectively. To detect the influence of building structures, all the 52 ICPs were deliberately selected outside the GCP perimeter. In addition, as also depicted in Figure 53, the usage of 10 building structures in the orientation parameter calculations using the combined method for each Trimble Phase One (lower-left part) and Canon S-100 (lower-right part) has improved the RMSE (planimetric) in the range below 50 cm. Obviously, the results of the geometric accuracy assessment in Table 23 show that there is a significant improvement if the building structures as an additional reference to calculate the external orientation parameters were used.

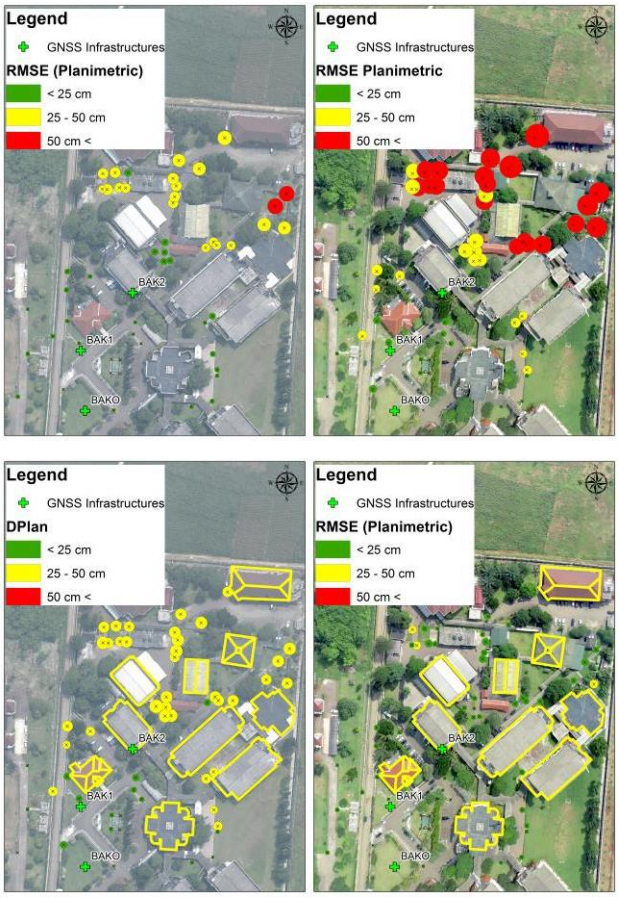

Figure 53: Accuracy assessment: DG Trimble Phase One (upper-left), combined Canon S-100 (upper-right), combined (10 Buildings) Trimble Phase One (lower-left) and combined (10 buildings) Canon S-100 (lower-right)

Table 23: RMSE by using 52 ICP level 2 (DG:Direct Georeferencing, IG:Indirect Georeferencing, Co:Combined DG-IG)

Approach	Trimble Phase One		Canon S-100	
	2D (m)	3D (m)	2D (m)	3D (m)
DG	0.32	0.33	-	-
IG (3 GCP)	0.44	0.44	0.38	0.38
IG (8 GCP)	0.39	0.35	0.27	0.25
Co (1 Building)	0.26	0.24	0.24	0.23
Co (10 Buildings)	0.20	0.20	0.20	0.19

5.3.3.3 Discussions

Obviously, the geometrical accuracy of the building structure is a pre-requisite for performing 3D analysis on high resolution data (Zhang et al., 2004). Therefore, the orientations of building structures have been used as a reference to improve the poor external orientation parameters from inaccurate GPS camera. Initially, the deviations of external orientation parameters given by the GPS/INS equipment for each camera were included in Table 24. In this case, the orientation parameters generated using the DG method were compared with the orientation parameters generated using IG (8 GCPs) method. As explained in 5.3.3.1, the first comparison has been done by calculating the deviation of the orientation parameters (X_0, Y_0, Z_0, O, P, K) for each dataset.

To evaluate the accuracy of the orientation parameters, two overlapping images/photos for airborne acquisition (Trimble Phase One and Leica RCD30) and four overlapping images/photos for UAV acquisition (Canon S-100) were used.

Table 24: The deviations of external orientation parameters (DG)

Orientation parameters	RCD30	Trimble Phase One	Canon S-100
dX_0 (m)	0.008	0.135	33.843
dY_0 (m)	0.011	0.140	10.069
dZ_0 (m)	0.017	0.062	10.532
dO (degree)	0.003	0.009	-
dP (degree)	0.003	0.009	-
dK (degree)	0.009	0.002	-

Since only GPS camera is used, the rotation parameters (O,P,K) of the UAV data are not available. However, as explained in 3.2.3, the generated DEM is tilted with respect to

the inaccuracy of GPS camera. Table 24 shows this result by the higher deviation values of dX_0, dY_0, dZ_0 of the Canon S-100 in the order of dozens of meters.

The comparison with Table 25 shows that the proposed approach has significantly improved the DG accuracy for the UAV data (Canon S-100). In specific, the DG using a GPS camera that is improved by the simple building structures approach has provided 1-3 meter for sensor position accuracy and a maximum of 0.309 degree for the sensor orientation accuracy (Table 25).

Table 25: External orientation parameters (combined with building structures)

Orientation Parameter	RCD30	Trimble Phase One	Canon S-100
dX_0 (m)	0.033	6.808	1.122
dY_0 (m)	0.011	1.885	0.272
dZ_0 (m)	0.030	1.506	2.893
dO (º)	0.009	0.183	0.237
dP (º)	0.041	0.362	0.309
dK (º)	0.022	0.012	0.137

Finally, as included in Table 23, the improvement of the external orientation parameters has presented a more accurate DEM by using the combined method with the inclusion of 10 building structures. As also depicted in Figure 54, the DEM details of Canon S-100 UAV data (upper) are now comparable with the Leica RCD30 medium-format camera (lower).

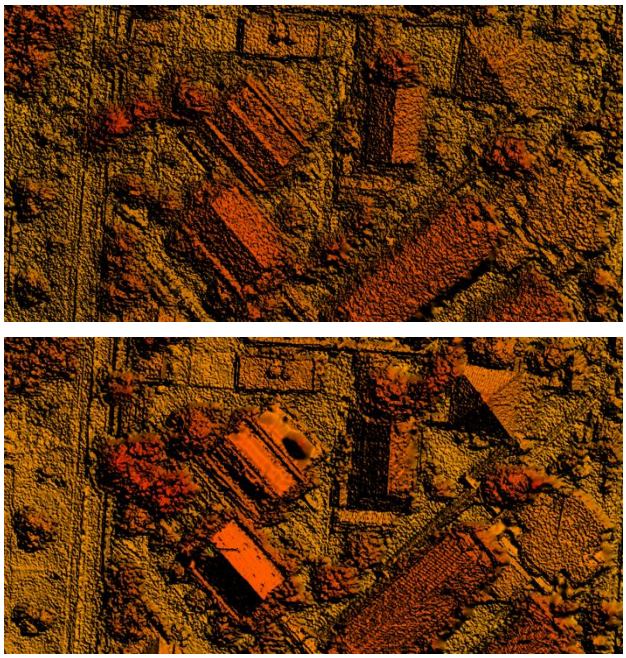

Figure 54: DSM in 10 cm GSD of BIG's office: UAV Canon S-100 (upper) and Airborne RCD30 (lower)

5.4 Investigation on mountainous terrain (Bandung area)

The test area "Bandung" was selected based on the mountainous terrain complexity and the supporting data availability, including the geodetic reference network infrastructure. The main objective of the investigations in Bandung area is to provide an integration of optical and radar space borne data processing in the context of LSTM.

With respect to other geospatial data projects in BIG i.e. VHRS image orthorectification of SPOT6, the DEM generation process can be improved in order to increase the resolution and accuracy of the output (Tampubolon and Reinhardt, 2015). By using GCPs as an important input, the planimetric and elevation accuracy of satellite-based data shall be improved in order to comply with LSTM requirements especially for mountainous area. Therefore this investigation synchronizes the local/national GCPs data measurements with global satellite-based data (Optical and Radar) acquisitions in order to achieve an optimum geometric accuracy with minimum GCPs. The role of DEM reference (in specific DTM) to the TanDEM-X DEM generation as introduced in 5.2.3.1 will also be tested for mountainous area.

Finally, the other goal of this investigation is to give recommendations for a proper usage of space borne data for an improved data processing chain in the special case of mountainous and urban areas. It includes the GCP requirements as well as the processing schemes based on certain assessment standards in the context of LSTM.

Datasets used The optical space borne data used in this investigation is a stereo pair of SPOT6 data with a resolution of 1.5 m. To enable the investigations on the geometric accuracy aspect, there are two type of processing levels which shall be compared. Primary standard product (Table 10) is used for in-house orthorectification by using GCPs and DEM data while Standard Ortho product has been geometrically processed by encountering viewing angle and ground effects as already explained in 3.1.1.1 (see Table 10). In this case, the DEM generated from stereo pair of SPOT6 data was also compared with the generated DEM from InSAR method.

Table 26: SPOT6 data for Bandung area

Scenes	Product Type	Viewing angle (°)	Processing	Planimetric accuracy in m (CE90)	Acquisition Date
SP1	Primary product	18.1400	Radiometric & Sensor corrected	-	19-04-2013
SP2	Primary product	14.0053	Radiometric & Sensor corrected	-	01-08-2013
SP3	Standard ortho	18.2431	Radiometric, Sensor corrected & Ortho corrected	7.548	19-04-2013

In addition, TanDEM-X data (see Table 27) also play a role for the above mentioned orthorectification purpose. On the other hand, the LSTM requires DSM as an input

for creating terrain information including contour lines and other hypsographic components. Therefore the generated InSAR DEM was also a subject for the accuracy assessments.

Table 27: TanDEM-X CoSSC data for Bandung area (*Height of Ambiguity)

Scenes	HOA* / B_P (m)	Adjusted Parameters		Incident Angle / Range in DSM Reference Area (°/m)	Looking Direction	Acquisition Date
		B_P' (m)	ΔΦ (°)			
B01	99.363 / 73.613	74.382	107.5868	43.48246 / 682861.771	Ascending	31-01-2013
B02	60.471 / 120.535	119.345	158.2498	44.20491/ 689683.224	Descending	28-11-2012

Reference datasets The airborne data acquisition in 2012 by using Trimble Phase One (P65+) camera was done to produce the GIS vector data of 1:5,000 LSTM. In this case, the DEM reference area has been selected by taking into consideration the coverage and the type of the objects. Differently to the previous investigation, the DEM reference was partially selected from the adjacent 1:5,000 DTM map sheet number 12093139B (red rectangle in the middle of Figure 55).

5.4.1 Investigations on Bandung valley area

Mountainous areas mostly consist of earth terrain with steep slopes that are susceptible for geometrical errors such as relief displacements in optical data as well as the layover, foreshortening, and shadow in radar data. However since the focus in the work presented here is put on the LSTM which usually concentrates on the compilation of features such as roads, building, utilities, etc., the selected test area must represent a built-up or non-homogenous mountainous area.

In more detail, it is not the focus of this dissertation to investigate the mountainous area that does not contain any relevant topographical object/feature for LSTM purpose. For instance, the top of the mountain and its surrounding area will not be mapped in LSTM details i.e. larger than or equal with 1:10,000 map scale. The selection of Lembang area which is located in the southern part of Mount Tangkubanperahu as depicted in Figure 55 was intended to ensure that the produced geospatial data sources for mountainous area fulfill the geometric accuracy requirements.

In this one 1:5,000's map sheet number 12093139A (DTM in Figure 55) of Lembang mountainous areas, there are tea plantations, settlement areas, and road networks with the slope mostly more than 10° and even in some part more than 30°.

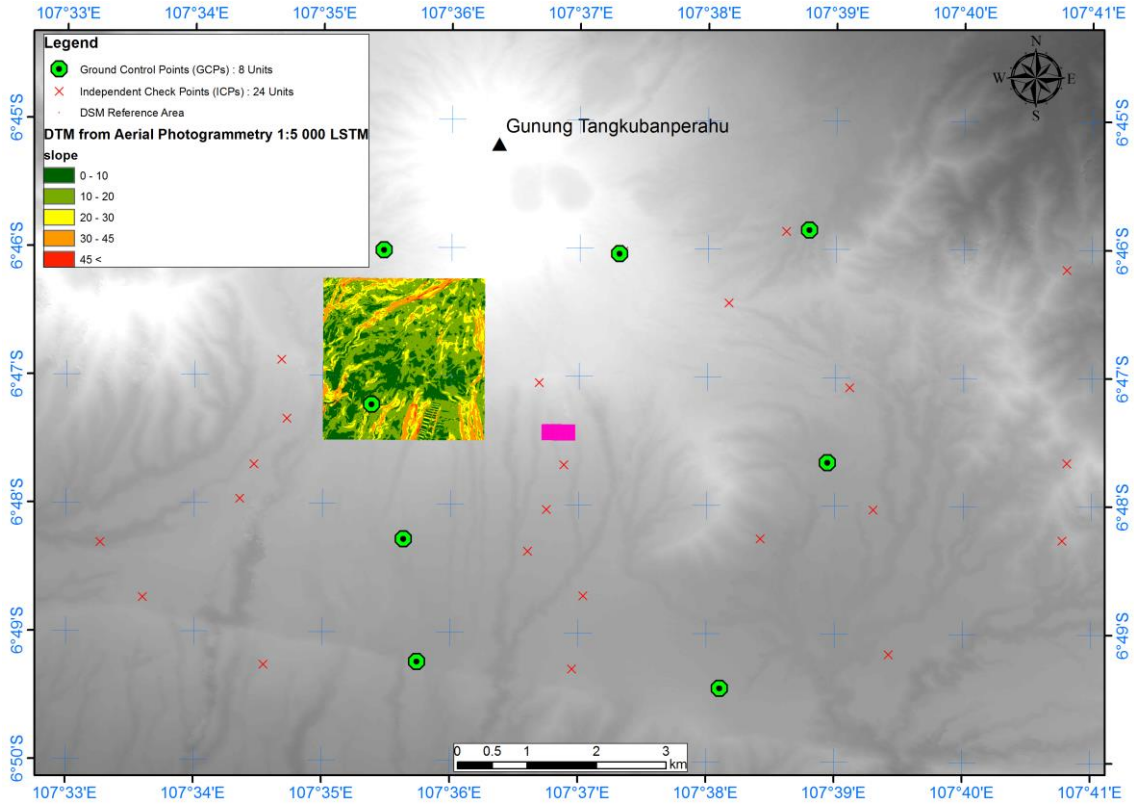

Figure 55: Bandung mountainous area

5.4.1.1 The influences of height references for TanDEM-X height accuracy

A TanDEM-X DEM generated from CoSSC Stripmap data can be improved by the linear model as explained in 4.3.2.2. For the investigations, there are two scenes available (Table 27) with slightly different looking directions and perpendicular baseline values. HOA as inferred in Eq. 5.2 (section 5.2.3) is one important indicator to reflect the geometric accuracy of the generated DEM. Basically from aforementioned equation, the smaller the HOA as represented by larger B_P, smaller wavelength λ, incident angle θ, and slant range R contributes to a higher geometric accuracy.

As explained in 4.3.2.2, HOA is expected to be less than 40 m in order to achieve the geometric accuracy of HRTI Level 3 as targeted by the IDEM. Thereby, it was also planned by the TanDEM-X acquisition at DLR to reach HOA in the range 40-55 m for the first mission year and improved to 35 m for the second mission year (Rossi et al., 2012). Those considerations basically are aimed at a better geometric accuracy as they can be implemented on purpose by DLR. Nonetheless, almost all of the TanDEM-X CoSSC used in this dissertation were not within this expected specification except S02 (HOA=39.178 m) of Borobudur Area (see section 5.2.3) and S02 (HOA=34.090 m) of BIG office area (see section 5.3.2).

To test the effectiveness of the proposed linear model and its applicability for mountainous areas, the DTM reference area must be located outside of the evaluated TanDEM-X Lin-DEM. As shown in Figure 55, the DTM reference has a size of 200 by 500 m while the evaluated TanDEM-X Lin-DEM has a size of one 1:5,000 map tile of 2.3 by 2.3 km (DTM). Differently to the situation in the previous UAV DSM reference area of

Borobudur temple as explained in 5.2.3, only DTM reference from aerial photogrammetric acquisition using Trimble Phase One P65 as explained in 2.2 (1:5,000 LSTM) are available. In this case, there is a discrepancy between the DTM reference and the TanDEM-X Lin-DEM (DSM) for the Bandung test area. In order to minimize the discrepancies, the height reference area must be on the ground or in an open area where there is no difference between DTM and DSM.

Therefore, the selected gridded points from DTM reference data must be as open as possible with sufficient good coherence value i.e. > 0.8. An open area means that the geometric distortion of TanDEM-X data is not significant and classified as on terrain objects. The selection of an open area was intended to ensure that the height reference points from generated TanDEM-X Lin-DEM and reference DTM refers to the same location. In other words, at selected height reference points there is no discrepancy between the generated TanDEM-X Lin-DEM and the DTM reference.

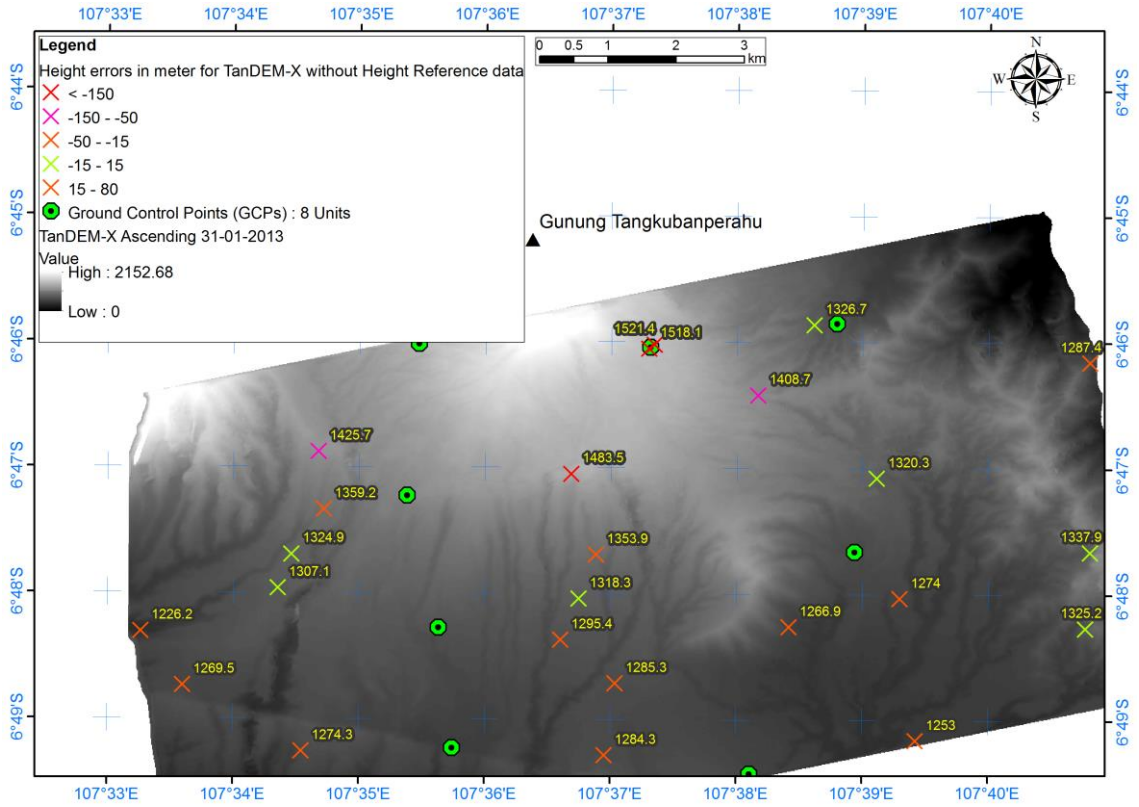

Figure 56: TanDEM-X absolute accuracy without any reference data

Without any height reference data, as detected by 24 ICPs, only some ICPs (cross with green color) had the deviation in the level of -15 – 15 m (Figure 56). The heights for those corresponding GCPs are in the range of 1,300 – 1,340 m (above ellipsoid). Other ICPs (cross with red color) outside the aforementioned range had an unexpected deviation, for some points even in a level more than 100 meter. More detail, the sample mean, standard deviation and RMSE from 24 ICPs are -15.1 m, 82.3 m and 82.0 m respectively. From this result, it is presumably that the Phase to elevation tool in SNAP desktop uses only a few or even only one height reference point to generate an absolute height.

For the Bandung mountainous area, it is also clear that the DEM generation without any reference leads to inaccurate results ranging up to hundred meters deviation (-203.6 – 77.9 m) for 24 ICPs as also shown in Figure 58 (blue line). Therefore, it makes no sense to proceed the DEM generation by relying only on a built-in phase to elevation tool in SNAP desktop.

In addition, the visual inspection of the generated DSM as depicted in Figure 57 indicates that the phase to elevation conversion without any reference data presents an inaccurate DEM distorted by a shift, scale and rotation factors. The accuracy assessments using 1:5,000 GIS vector data showed that the road networks with draped elevation from TanDEM-X DEM (green) without any reference are somehow tilted and shifted in a comparison with the same road networks draped from 1:5,000 GIS vector data (red). The better height accuracy is only visible in the middle of the scene which is marked by the yellow line as also can be detected in the previous accuracy assessment using 24 ICPs. It is now more likely that the phase to elevation conversion in SNAP desktop only take one single point in the middle of the scene as a height reference. For a mountainous area like Bandung, such a single point height reference however is not sufficient enough to generate accurate DEMs without any adjustment in the phase offset and perpendicular baseline value.

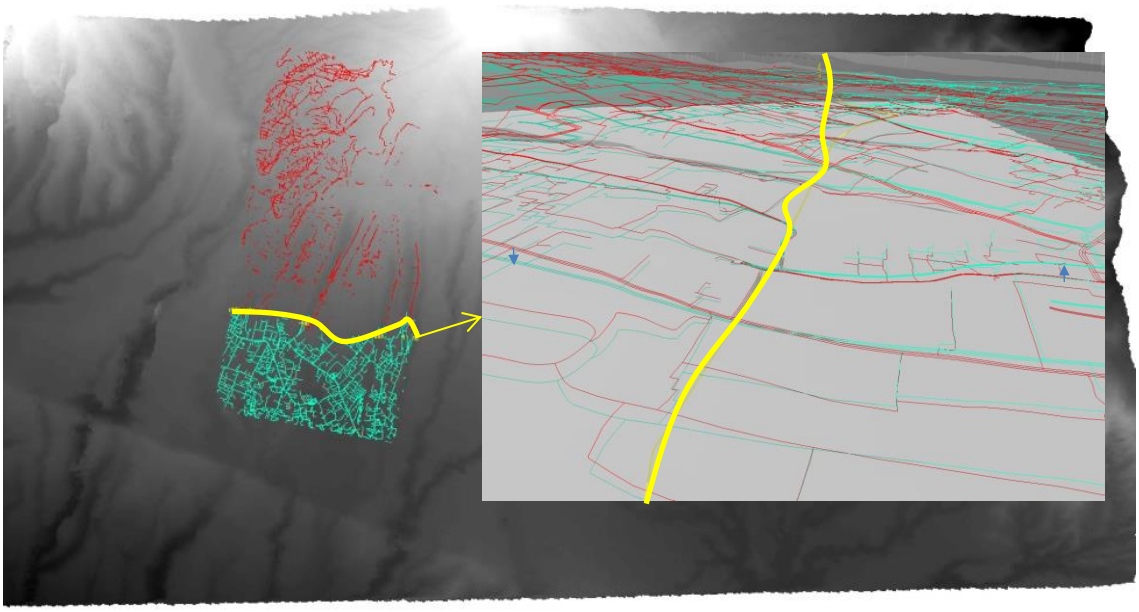

Figure 57: Visualization of DEM orientation problems without any reference data

Differently to the situation for the flat area as investigated in 5.2.3, the absence of the reference data shows clear effects in the DEM orientation as also can be quantitatively seen in Table 28. By just adding only 8 GCPs distributed in the middle part of the scene as shown in Figure 55, the absolute accuracy was improved to a level of 10.8 m (LE90). By purpose, the GCP coverage was distributed only in the middle part of the scene in order to detect the influence of the distribution to the absolute accuracy of the generated DEM. This result is still not exceeding both the IDEM and SRTM absolute accuracy,

and has been improved by the usage of a more accurate 1:5,000 DTM reference in the linear model.

5.4.1.2 Investigation results on the height accuracy for mountainous terrain

For the purpose of the investigations on mountainous terrain, in addition to the ICPs (from GNSS) as used in 5.2.3.2, 1:5,000 GIS vector data (derived from above mentioned airborne data acquisition) are also used to assess the DEM accuracy. Indeed, the scattered ICPs from GNSS measurements are not sufficient to represent the sample points for high elevation, undulated and complex terrains of mountainous areas.

This investigation clearly showed that the usage of GCPs for the mountainous area as a height reference is insufficient to achieve an absolute error less than 6 m as required by the HRTI-4. Well calibrated data as shown by the small amount of μ is also not always in line with the other geometric accuracy descriptors as indicated by the σ and RMSE values. For instance as included in Table 28, the IDEM and B02 (descending) data which have the smallest μ i.e. 0.4 provided less accurate DEM in a comparison with μ = 0.6 m for B01 (ascending) data. In this case B01 (ascending) has the best absolute accuracy in the range less than 5 meter LE90.

Table 28: DEM accuracy (in m) for Bandung mountainous area

Data Sources	**ICPs (24 Units)**				**1:5,000 GIS vector data**			
	μ_z	σ_z	**RMSE$_z$**	**LE90**	μ_z	σ_z	**RMSE$_z$**	**LE90**
IDEM	0.8	5.0	4.9	8.1	0.4	3.8	3.8	6.3
SRTM	1.8	5.2	5.4	8.9	1.5	5.4	5.6	9.2
B01	**TanDEM-X Lin-DEM (ascending)**							
DTM	1.1	3.5	3.6	5.9	0.6	2.8	2.8	4.6
8 GCPs	-1.6	6.5	6.5	10.8	1.6	2.9	3.3	5.4
B02	**TanDEM-X Lin-DEM (descending)**							
DTM	0.5	3.1	3.2	5.2	0.4	3.5	3.6	5.9
8 GCPs	-1.5	8.3	8.5	13.9	-15.0	5.3	15.9	26.2

5.4.1.3 Discussions

The baseline error estimation ($B_P^{'} - B_P$ = 1.19 m**)** of TanDEM-X CoSSC descending data for Bandung mountainous area as included in Table 27 contributed to the height error of 14 m (Cherniakov, 2008 and Krieger et al., 2007). As inferred in Eq. 5.4., even though the value of ΔB_P is not more than 2 m for this dataset (cf.-5.809 m for Borobudur dataset in 5.2.3), the height error is more significant because the influence of the higher topographical height (H) around 1,350 m above MSL. This height error value is approximately the height accuracy of TanDEM-X descending data by using 8 GCPs as height references i.e. 13.9 m (see Table 28).

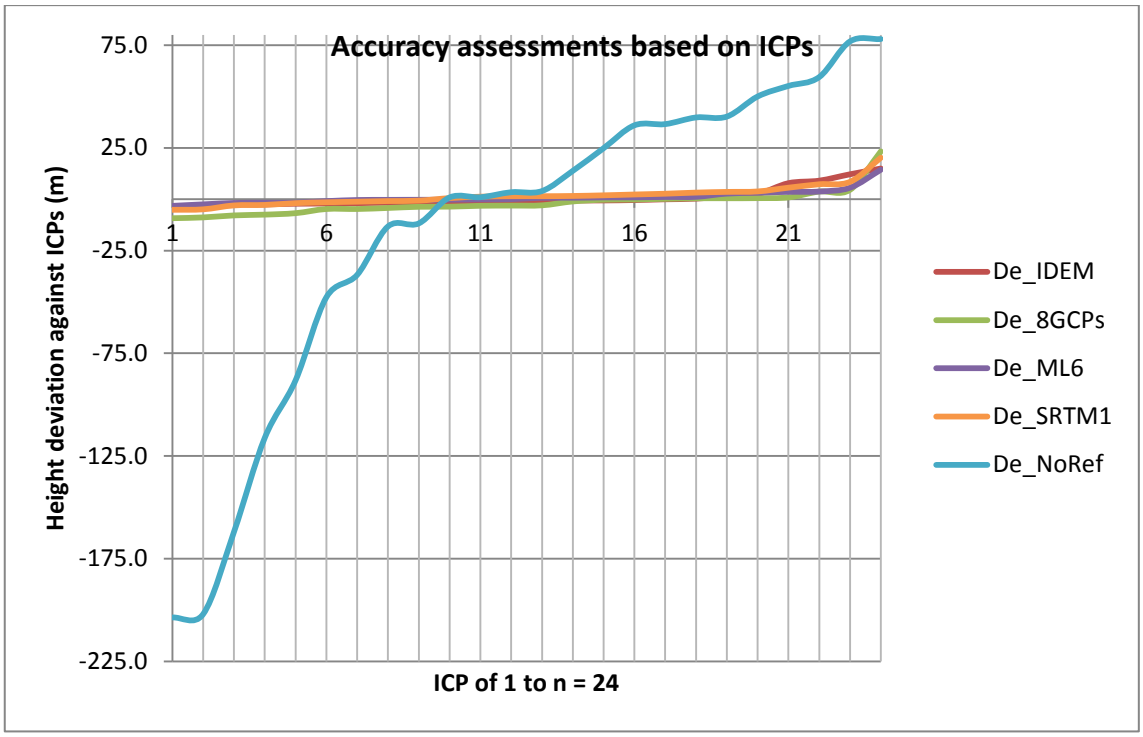

Figure 58: Height deviation for 24 well distributed ICPs

For the height error of 14 m, the DEM tilt component also can be calculated using eq. 5.3 to contribute about 5 m/km from the reference point (middle of the scene), assuming there is no significant slope change (h = 1,300 – 1,340 m above ellipsoid). Again the high topographical height contributes significantly to the generated DEM orientation.

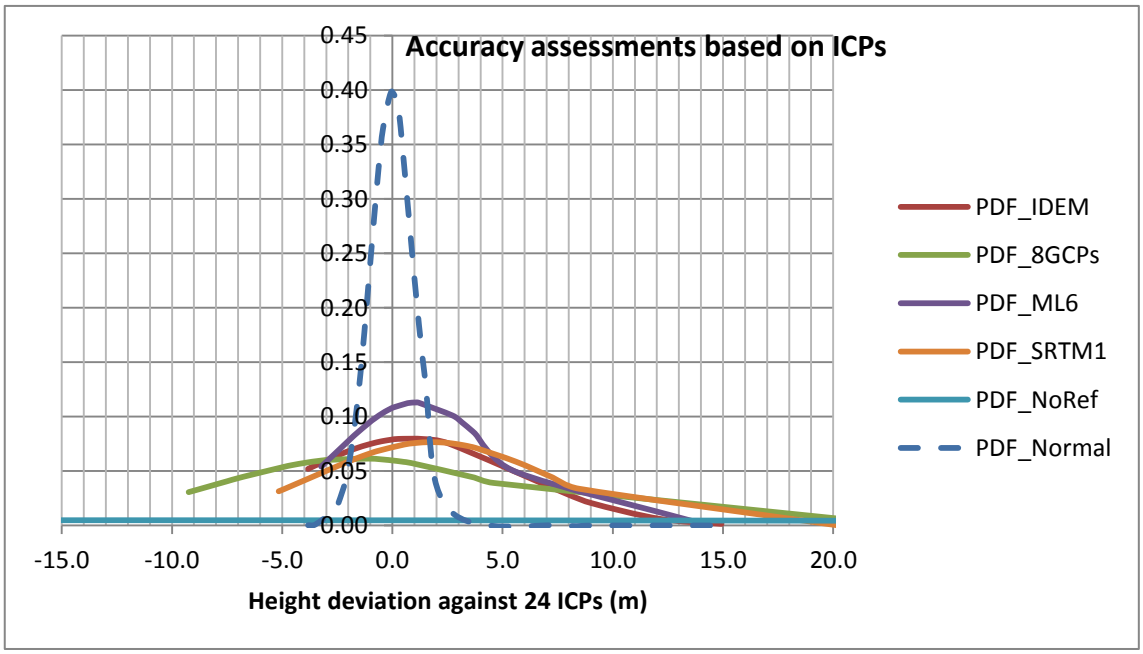

Figure 59: PDF plot on 24 ICPs

Even though Krieger et al., 2007 identified this DEM tilt error in a relative small contribution i.e. for the worst case 3.8 mm/km from the reference point (θ=30°, B_P=260 m, ΔB_{II}=1 mm), the investigation in this section show totally different error results as mentioned above. This unprecedented result indicates that the Eq. 5.3 is valid in the condition where the baseline determination by using double frequency GNSS (Cherniakov, 2008) is accurate enough to minimize the baseline error estimation.

From this difference, it can be stressed out that the precise B_P and the topographical height H play an important role in order to obtain a generated DEM with high geometric accuracy. It is clear that the larger the B_P and the lower the H lead to better geometric accuracy. As explained in other test areas e.g. Borobudur temple and BIG office, the DEM height error and orientation in this section is larger mainly due to the precise B_P and H values. However it is still an open question how big is the influence of the distance to the reference point and how it can determine the DEM orientation as well as the height error components especially for the mountainous area where the accurate reference points are usually not available.

To essentially evaluate the height accuracy, PDF plots for 24 ICPs as depicted in Figure 59 from different DEM visualize the best fit distribution curve to the normal distribution one (blue dotted line). For the DEM generated without any reference, it provides the PDF in an almost flat and not even forming a curvature (blue line). This form of line represents the DEM with poor height accuracy as also depicted beforehand in the blue line of Figure 58.

After all, the PDF plots except the DEM generated without any reference show incomplete normal distribution curves for 24 ICPs (see Figure 59). However, differently to the situation in the moderate area as encountered in Borobudur area (5.2.3), instead adding more ICPs in the accuracy assessment more detail reference data i.e. 1:5,000 GIS vector data are used in order to provide more adequate sample data analysis.

The IDEM (Figure 59: red line) shows a better curve center of the PDF plot as also indicated by the smaller sample mean value μ_Z of 0.8 m. However, TanDEM-X Lin-DEM descending had the smallest sample mean value μ_Z of 0.5 m. Despite their PDF shift reflected by the difference in the sample mean value μ_Z, both SRTM (orange curve) and IDEM (red curve) tend to have the same steepness as visualized in Figure 59. The equal standard deviation σ_Z value for IDEM and SRTM are 5.0 m and 5.2 m respectively (see Table 28) which reflects the aforementioned similar PDF forms.

On the other hand, the TanDEM-X Lin-DEM ascending with Multilooking by factor of 6 (ML6) indicates best height accuracy with the steepest curve indicating a narrower error distribution though its sample mean value μ_Z is 1.1 m. This finding also confirms what ASPRS, 1990 requires for height accuracy for LSTM as already discussed in 5.2.3. In particular, the sample mean value μ_Z itself is not sufficient to evaluate the height accuracy. It must be followed by the lower standard deviation σ_Z as well as the lower $RMSE_Z$. Thus for this Bandung mountainous area, the TanDEM-X Lin-DEM descending with Multilooking by factor of 4 shows the best height accuracy as indicated by μ_Z = 0.5 m, σ_Z = 3.1 m, $RMSE_Z$ = 3.2 m (see Table 28).

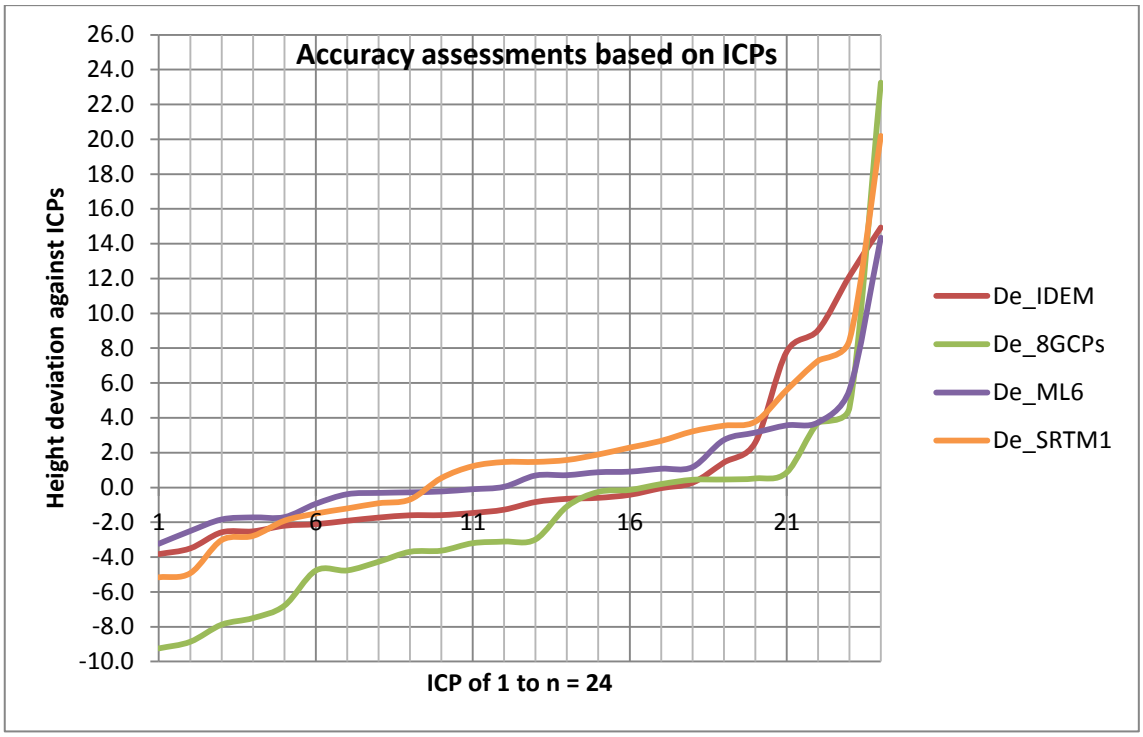

Figure 60: Height deviations for 24 ICPs from GNSS (TanDEM-X DEM without height reference is excluded)

By excluding the height deviation of the generated DEM without a reference in the curve analysis as visualized in Figure 60, a more meaningful comparison on the DEM geometric qualities has been provided. Indeed, it is obvious that TanDEM-X Lin-DEM ascending (B01) with Multilooking 6 by 6 (Figure 60: purple curve) outperformed the IDEM as indicated by the closest fit to zero line and additionally fulfilled the HRTI level 4 specifications i.e. 5.9 m (LE90) as included in Table 28. In addition, TanDEM-X Lin-DEM descending (B02) showed the best geometric accuracy for its height accuracy i.e. 5.2 m (LE90).

All in all, to get a deeper analysis on height accuracies, the height deviations of TanDEM-X Lin-DEM by using 8 GCPs as height references and their corresponding histograms were plotted in Figure 61. For all evaluated 24 ICPs, there were 8 ICPs (small yellow points) which had the lower height deviations (-2 – 2 m) with respect to the aforementioned TanDEM-X Lin-DEM. The height histogram of those aforementioned 8 ICPs was created in the middle part of Figure 61. On the other hand, the height histogram of the 8 GCPs (green points) was also created as depicted in the lower part of Figure 61.

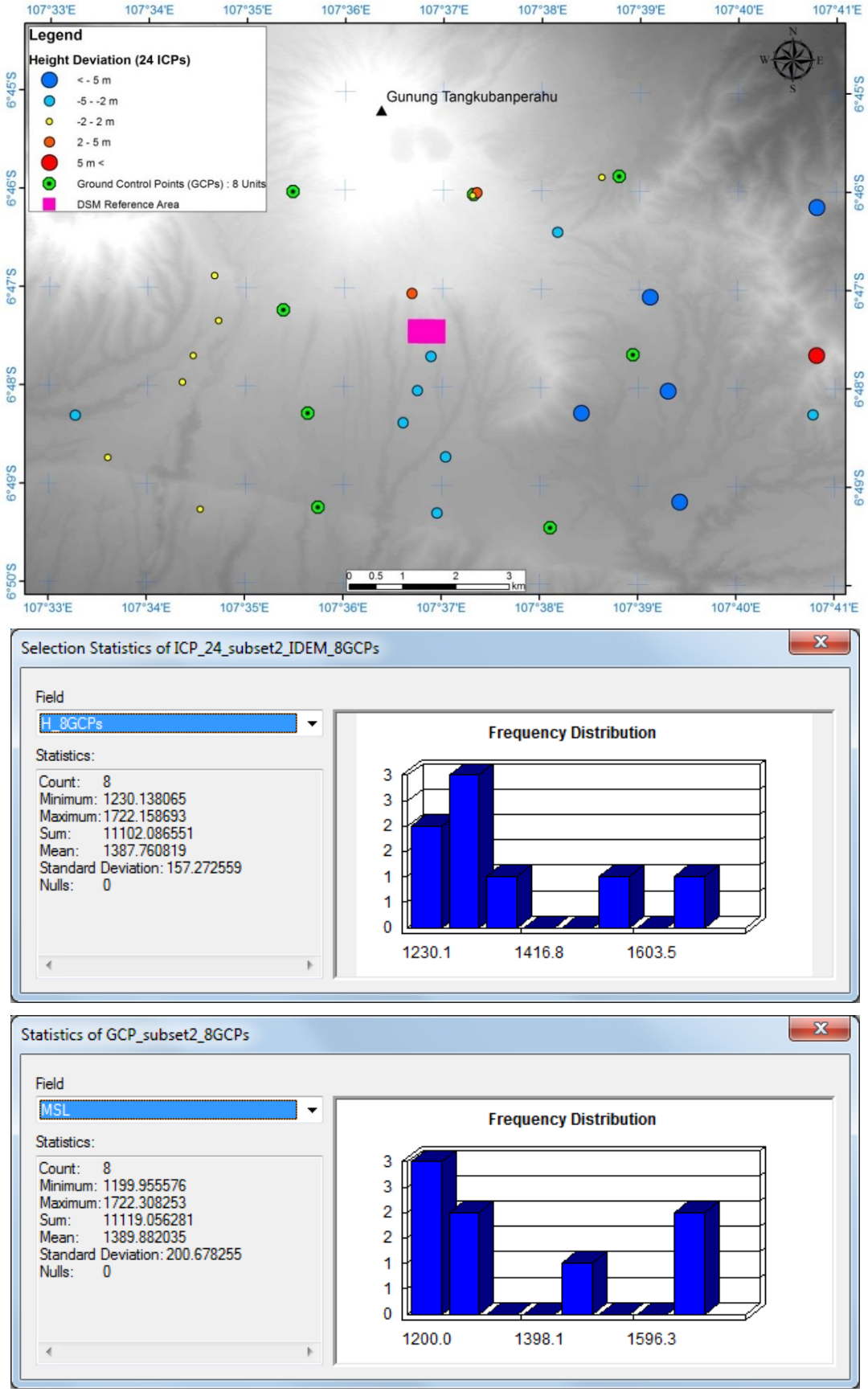

Figure 61: Height deviation for the generated DEM using 8 GCPs against 24 ICPs

As aforementioned, the height calibration by using GCPs has insufficiency to generate a DEM absolute accuracy less than 6 m (LE90). Nevertheless, for a DEM generated by using height references from 8 GCPs as indicated by green curve (Figure 60), there are 8 ICPs which have accurate height deviation in the range of -2 – 2 m (n=14 to n=21). Interestingly as shown in Figure 61, most of those accurate ICPs as visualized by yellow points are not planimetrically located (X,Y) within the coverage of 8 GCPs.

For the Bandung mountainous area, it is also clear that the DEM accuracy assessments using ICPs either from GNSS or 1:5,000 GIS vector data indicate the same results. As an example, the SRTM DEM (green line) has the lowest height accuracy as indicated by high deviation both in using ICP from GNSS (Figure 61) and using ICP from 1:5,000 GIS vector data (Figure 62). The major difference is only about the smoothness of the curve which comes from the different sample numbers used in the assessments.

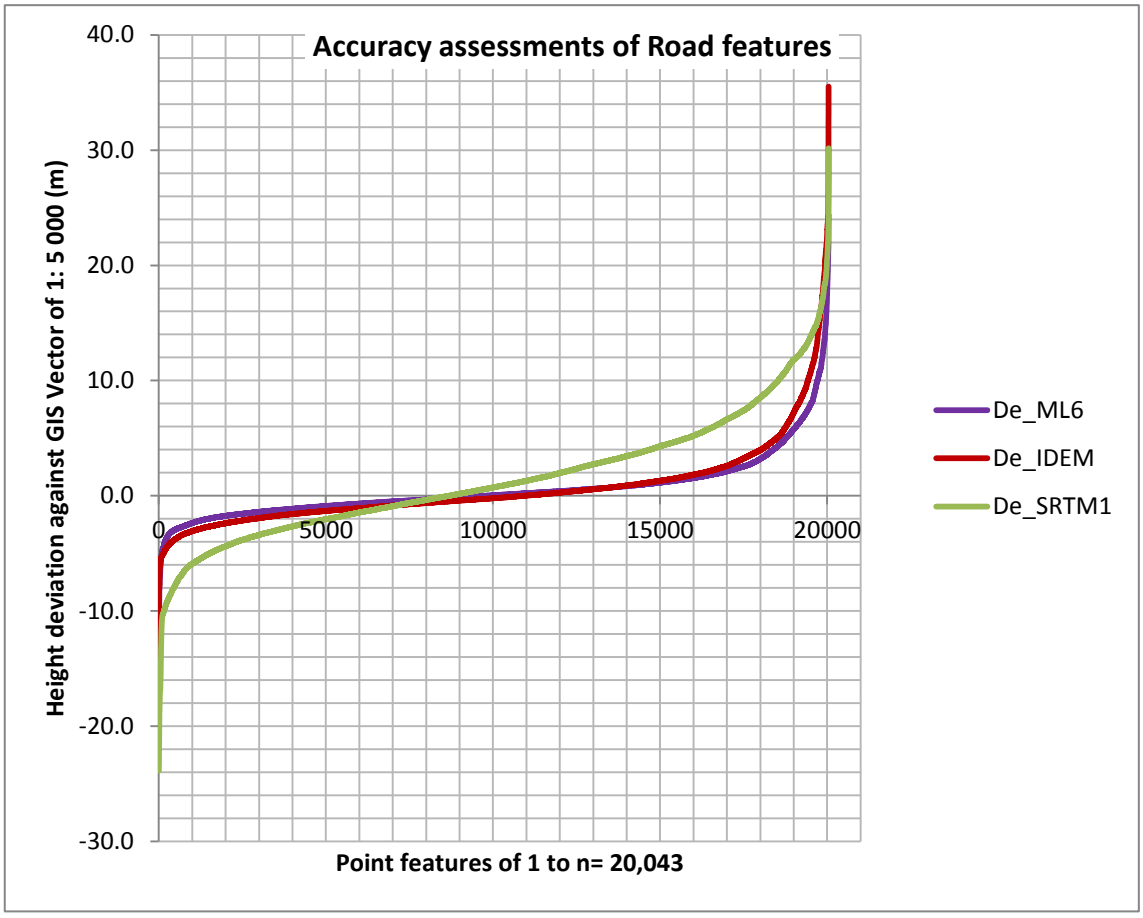

Figure 62: Height deviations for 20,043 ICPs 1:5,000 GIS vector data

In addition, most of the ICPs within the GCP's perimeter have an inaccurate height location as indicated by blue points/circle (negative deviation) and red points/circle (positive deviation) except two of them (yellow points). However, there is one distinct indicator that has clearly shown a correlation between GCPs and accurate ICPs namely the average height. Statistical values in a form of histogram as shown in Figure 61 middle part (ICPs) and lower part (GCPs) indicate the same average (mean) height within -2-2 m tolerance i.e. 1387.8 (ICPs) m and 1389.8 (GCPs) respectively. It means that the dis-

tances to the reference points and the GCP's distribution do not always correlate with the height accuracy as implied in Eq.5.3.

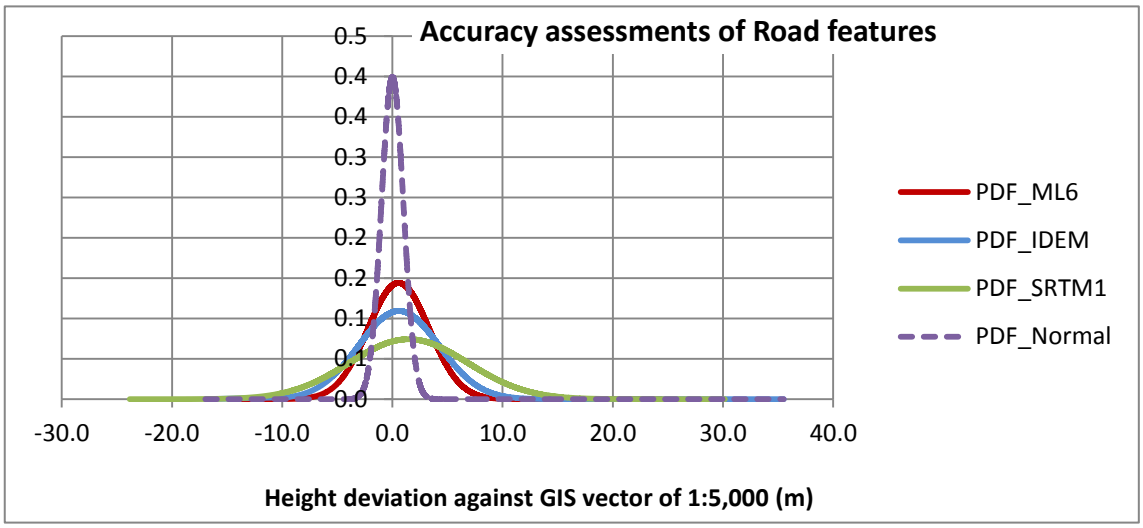

Figure 63: PDF plot on 1:5,000 GIS Vector

By a visual inspection on the different DEMs as shown in Figure 64, it can be seen that the DEM quality of both generated TanDEM-X Lin-DEM descending data (middle-left) and ascending data (middle-right) have more details in comparison with DLR's IDEM (upper-right). Even though the generated DEM from SPOT6 stereo pair was generated in a finer resolution i.e. 1.7 m, there was no significant difference with TanDEM-X DEM data. More details about the height accuracy of the generated DEM from the stereo pair of SPOT6 will be discussed in the next section.

The observation of PDF plots in Figure 63 also confirms that all the errors are consistently normally distributed, with two major types of error. The first is an error towards higher slopes due to the mountainous terrains. The latter is the outlier in conjunction with the PU errors which occurs more frequently than the normal distribution can predict. However in this case, the former height deviations following the Normal Gaussian distribution is the particular interest of the absolute comparison of different DEMs.

All in all, the height deviation of TanDEM-X data i.e. IDEM, TanDEM-X Lin-DEM ascending and descending are mostly in the range of -3 – 3 m without any removal of the outlier data as indicated by yellow points in Figure 64. Nonetheless as indicated by PDF plots (Figure 63) and also confirmed by the statistical values in Table 28, again the generated TanDEM-X Lin-DEM ascending in this section outperforms the height accuracy of IDEM data. The PDF plots of TanDEM-X Lin-DEM ascending (Figure 63: red curve) with multilooking by factor of 6 (ML6) in the same resolution of IDEM i.e. 12 m has better steepness in a comparison with IDEM (Figure 63: blue curve). In line with the PDF, the height error of TanDEM-X Lin-DEM ascending and IDEM are 4.6 m and 6.3 m respectively (see Table 28). Statistical values in Table 28 also confirm that only the generated TanDEM-X Lin-DEMs are complied with LSTM specifications (HRTI level 4) i.e. < 6 m (LE90) or < 3.65 ($RMSE_Z$).

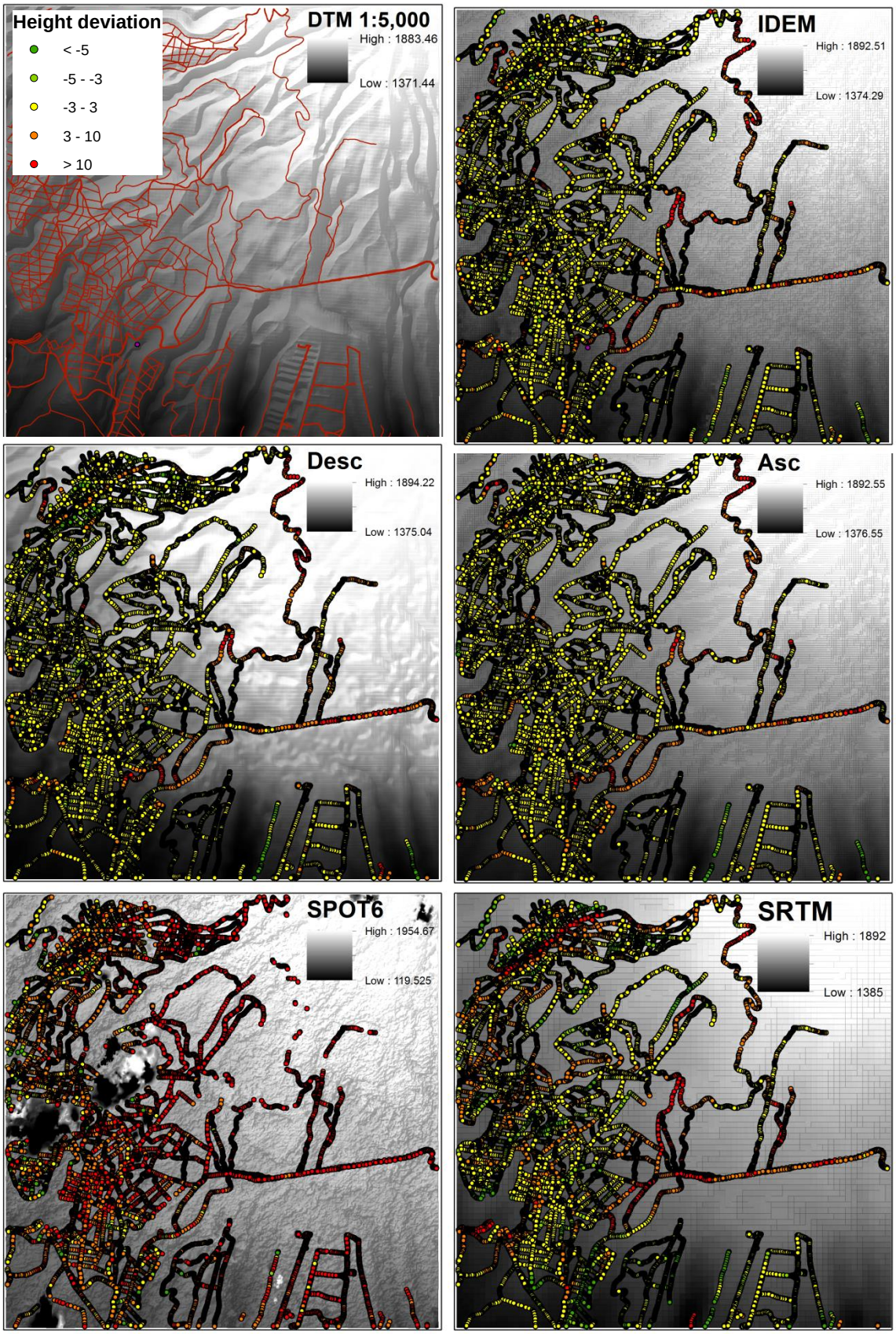

Figure 64: Shaded DEMs for Bandung mountainous area from different data sources

5.4.1.4 Investigation results on the height accuracy of stereo pair DEM

Concerning the generated DEM from stereo pair of SPOT6 data, 8 GCPs as recommended by the QuickBird investigation were used to create the epipolar image using PCI Geomatica. A comprehensive analysis of spatial data accuracy for the corresponding Area of Interest (AOI) has been done by referring to the existing 1,5000 GIS vector data, which has been derived from an air borne campaigns using a medium format digital metric camera Trimble P65.

For this Bandung mountainous area, it is also clear that the DEM accuracy assessments of SPOT6 stereo pair data indicate the poor result as shown in Figure 65. Even though the cloud areas were excluded, the SPOT6 DEM (blue line) has the worst height accuracy as indicated both by the high deviation (Figure 65) and the PDF plot (Figure 66). In some parts, the SPOT6 DEM showed height deviations more than 200 m with scattered distributions over the areas (Figure 64: lower left, red points).

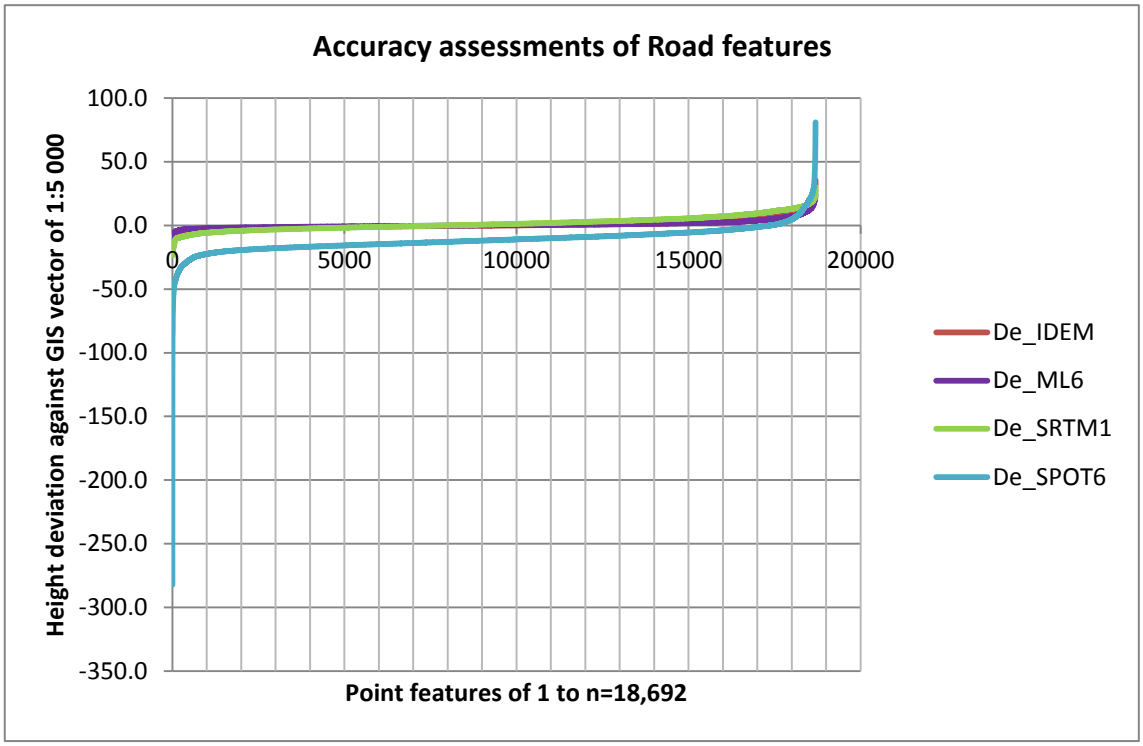

Figure 65: Height deviation for Bandung mountainous area (exclusion of cloud area)

Certainly, a proper topographical map data is required as a valid reference source. Therefore the official large scale topographic map is used as the reference. This 1:5,000 LSTM has been produced in the year 2012 from airborne data acquisition using a medium format digital metric camera. As already demonstrated by (Howard, 1994), in a condition where accurate DEM exists, the statistical error ($RMSE_Z$, μ_Z, σ_Z) can be computed to represent the geometrical accuracy. Nonetheless as indicated by PDF plots (Figure 66) and also confirmed by the statistical values in Table 28, again the generated SPOT6 DEM in this section showed the poor height accuracy compared to other DEMs. The PDF plot of SPOT6 DEM (Figure 66: blue curve) with the exclusion of cloud areas in the resolution of 1.7 m has the lowest steepness and the shifted center in a comparison with other DEMs (Figure 66: red, purple and green curve).

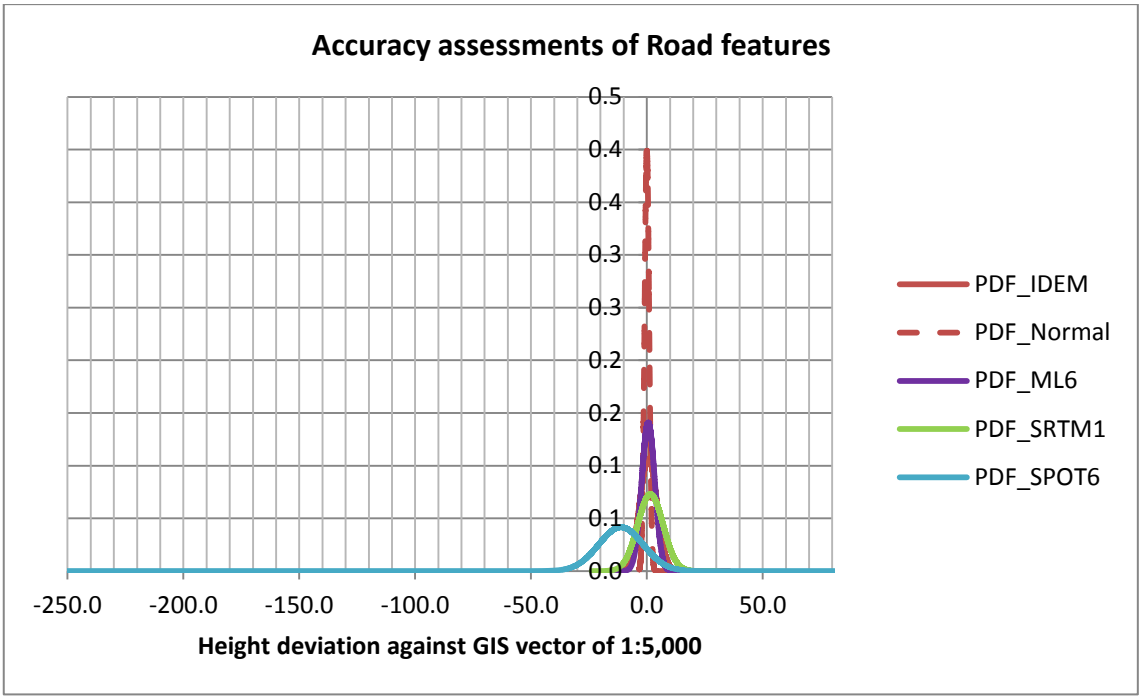

Figure 66: PDF plot for Bandung mountainous area (exclusion of cloud area)

5.4.1.5 Investigations on completeness of VHRS for mountainous area

The aim of this section is to quantify the completeness of GIS vector data derived from VHRS orthoimages (SPOT6) data in a comparison with the orthophoto (Trimble P65) as reference data. As depicted in Figure 67, even though those two orthoimages are not roughly comparable in terms of resolution namely 1.5 m (SPOT6) vis-à-vis 0.1 m (Trimble P65) respectively, the completeness factor can be used to indicate how detailed are the compiled features from VHRS orthoimages with respect to the LSTM specifications.

There are two topographic features used as the most prominent themes in high resolution data of LSTM namely road network and building features (Wegner, 2014). The quantitative indicators (area and length) of those two aforementioned features have been simply derived by performing the GIS operation in order to measure the completeness as discussed in 2.4.1.

Table 29: Completeness for Bandung mountainous area

Features / Sensor	Road networks		Buildings	
	Area (m^2)	Length (m)	Area (m^2)	Length (m)
Trimble Phase P65	57093.66	116147.49	71790.09	22075.03
SPOT6	88776.02	52244.89	65247.09	17663.79
Completeness	**156%**	**45%**	**91%**	**80%**

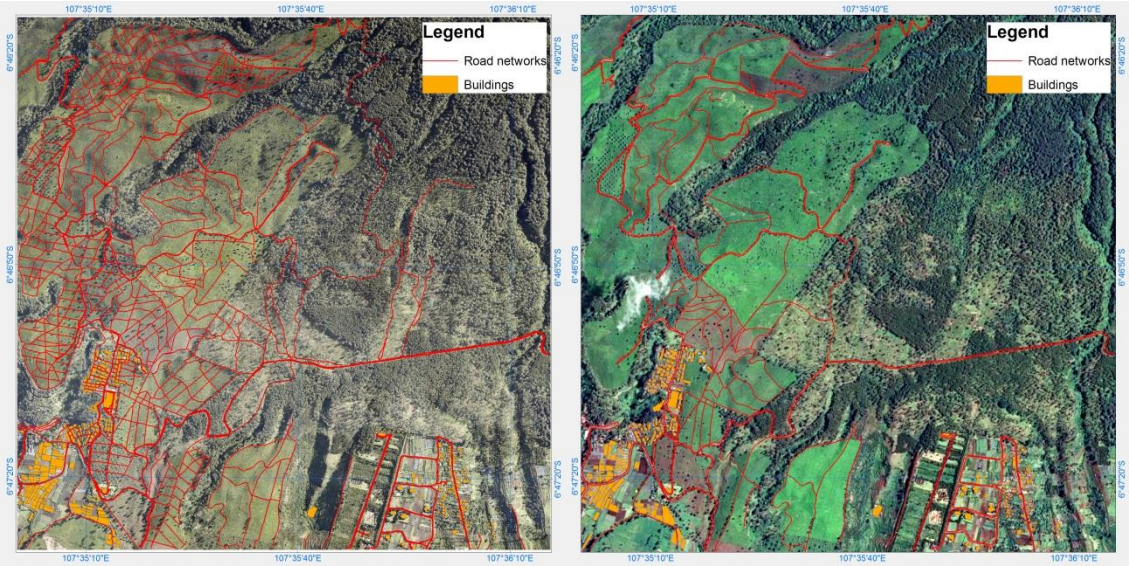

Figure 67: Detail comparison between Trimble Phase One P65 (left) and SPOT6 (right)

5.4.2 Investigation on Bandung urban area

The test area “Lembang” as a representation of an urban area has been selected based on the feature complexity and the reference data availability, including the geodetic reference network infrastructure. In general, the test site covers approximately an area of 2.3 x 2.3 km. The terrain condition of the study area is classified as flat with high elevations.

5.4.2.1 Investigations on the height accuracy of InSAR DEM for urban area

In general, the test site covers approximately an area of 60 x 60 km. It is prioritized by the stakeholders to accomplish the detailed spatial planning over that national strategic area. Therefore in 2012, an airborne data acquisition using a medium format digital metric camera has been done in order to produce the topographical map of the area in a scale of 1:5,000. This data has been used as a reliable reference data for the accuracy assessment in this section.

Nevertheless, for LSTM purposes, the investigations focus on 1 map sheet of 1:5,000 (1209-3136D) with a size approximately 2.3 x 2.3 km on the ground. The AOI has been selected under the assumption that the topographical features have not totally changed yet. Therefore it makes sense to use GCPs from different time series for data production and validation.

5.4.2.2 Investigation results on the height accuracy for urban area

The focus of the accuracy assessments for the hypsographic features i.e. spot heights is to evaluate whether the produced DSM can be sufficiently and properly used for the derivation of contour lines and hydrographic features. As also demonstrated by Soergel, 2013, the comparison between TanDEM-X data and the reference DTM has

shown an accuracy assessment of RMSE = 3.81 and σ = 3.80 for the flat urban area of Hannover. A more proper assessment by selecting only open areas to eliminate the discrepancy between the TanDEM-X Lin-DEM ascending and the reference data (DTM), improves the result to a $RMSE_Z$ = 2.67 and σ = 2.66 respectively (see Table 30).

Table 30: DEM accuracy for Bandung urban area

Data Sources	ICPs (24 Units)				1:5,000 GIS Vectors			
	μ_z	σ_Z	$RMSE_Z$	LE90	μ_z	σ_Z	$RMSE_z$	LE90
IDEM	0.8	5.0	4.9	8.1	-0.5	3.5	3.5	5.8
SRTM 1	1.8	5.2	5.4	8.9	-0.0	5.1	5.1	8.4
B01	**TanDEM-X Lin-DEM (ascending)**							
DTM	1.1	3.5	3.6	5.9	-0.0	2.6	2.6	4.3
8 GCPs	-1.6	6.5	6.5	10.8	-3.4	2.6	4.3	7.1
B02	**TanDEM-X Lin-DEM (descending)**							
DTM	0.5	3.1	3.2	5.2	0.5	2.9	3.0	4.9
8 GCPs	-1.5	8.3	8.5	13.9	-1.7	4.3	4.6	7.6

For the assessments in the Bandung urban area, the height deviations between all the evaluated DEM have more than 5 meter $RMSE_Z$ and standard deviation σ_Z. PDF plot in Figure 68 confirm that there is no significant difference in terms of statistical values for the accuracy assessments using spot height data. Spot height usually is compiled in centimeter precision by using stereo plotting equipment as the raw material to construct the DTM and contour lines as explained in 2.3. But differently to the aforementioned assessments from Soergel, 2013, the open area in this section has been defined by using land cover data also from GIS vector data of 1:5,000. In this case, the evaluated spot heights were overlaid with the potential open area from land cover data i.e. road area (for LSTM not only road segment), paddy field, crop (with vegetation< 2 m height).

5.4.2.3 Discussions

The role of SRTM and/or IDEM as external independent data were also pointed out in order to detect the data inconsistency as found in the spot height case. The height accuracy of SRTM is in the range 5.1 – 5.4 m $RMSE_Z$ whilst IDEM is in the range of 3.5 – 4.9 $RMSE_Z$ (see Table 30). Therefore it is clear that the accuracy assessment using spot heights without open area consideration leads to misleading results as shown in Figure 68.

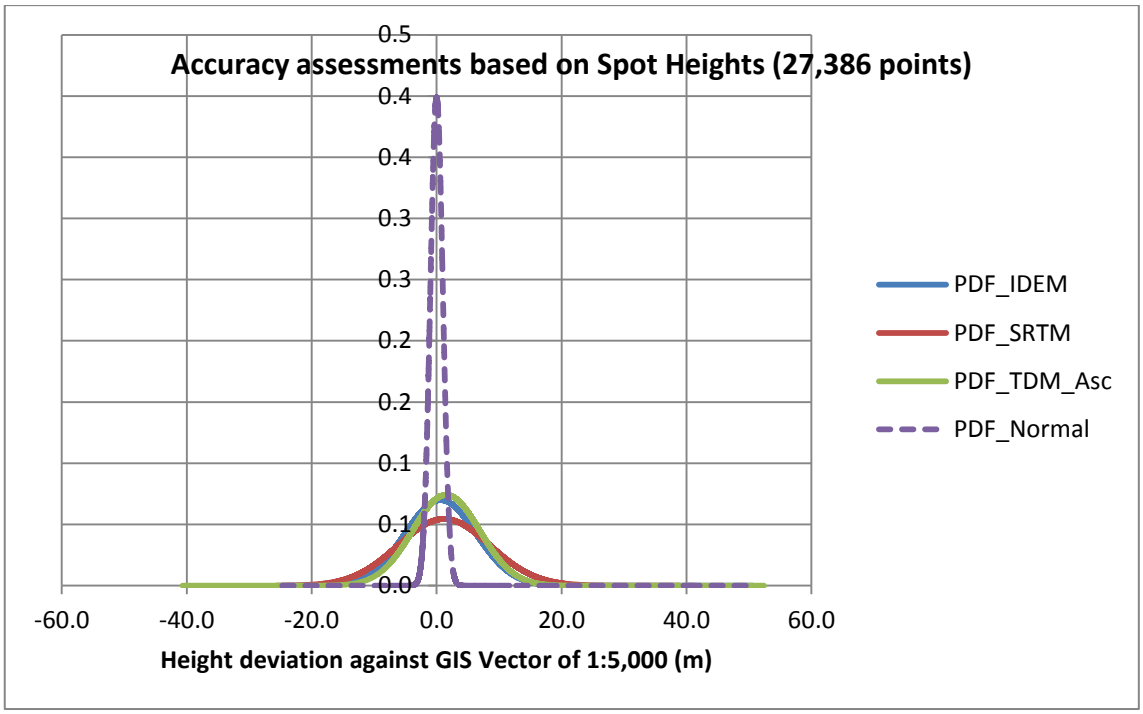

Figure 68: PDF plot for Bandung urban area (all Spot heights)

As shown in Figure 69, the overlaid spot heights for an open area are only 17,054 points, and hence the TanDEM-X Lin-DEM ascending data (using DTM reference) provided the mean value μ_Z = 0.0 m, standard deviation σ_Z = 2.3 m and $RMSE_Z$ = 2.3 m as well. The green line curve of TanDEM-X Lin-DEM ascending was centralized with more steep shape approaching the purple line of the normal distribution curve.

In addition, the TanDEM-X Lin-DEM ascending was very well calibrated and consistent with 1:5,000 spot height data. This results outperformed the IDEM with the mean value μ_Z = -0.8 m, standard deviation σ_Z = 2.7 m and $RMSE_Z$ = 2.8 m. A comparison with road feature assessment also showed consistent results as the $RMSE_Z$ and standard deviation σ_Z are always in the range of 2.3 – 2.6 m (see Table 30).

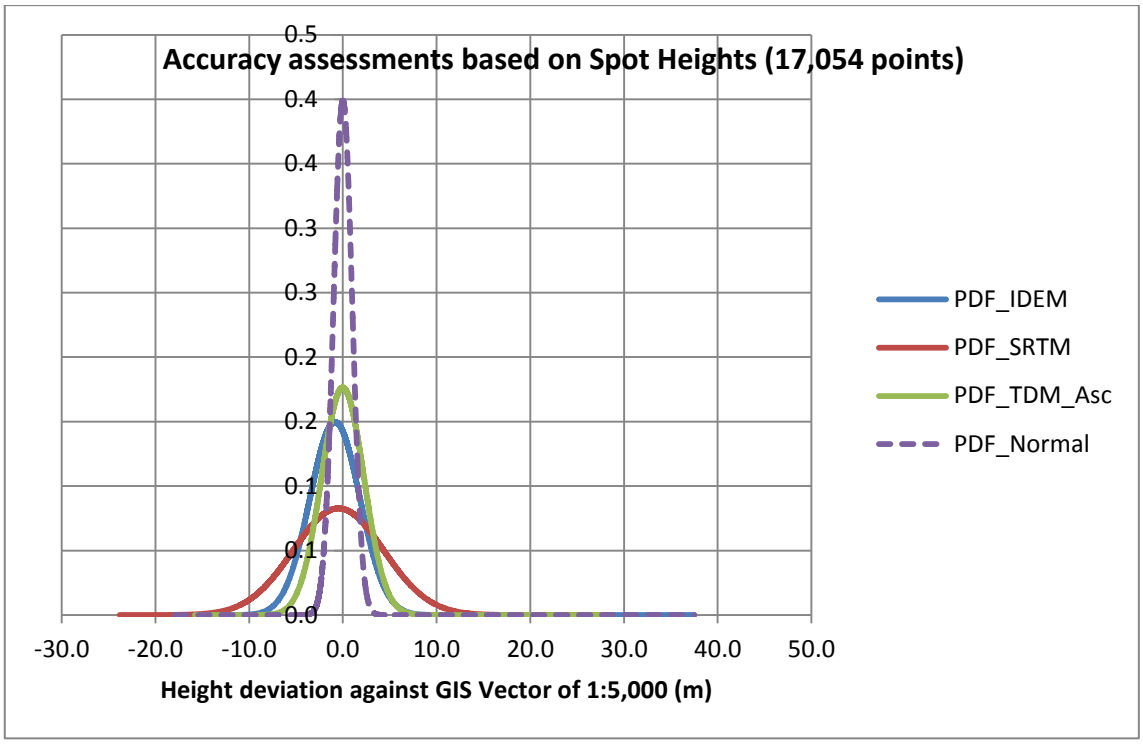

Figure 69: PDF plot for Bandung urban area (open area only)

5.4.2.4 Investigation results on the planimetric accuracy of SPOT6 for urban areas

This section discusses the absolute planimetric accuracy of the final orthorectified SPOT6 data by evaluation of the general (AOI) and the specific test area in 1:5,000 map sheet 12093136D for Bandung urban area (see also Tampubolon and Reinhardt, 2015).

The selection of SPOT6 and TanDEM-X data was intended to test how significant the role of DEM for the orthorectification of an urban area is. As investigated in 5.2.2, for QuickBird imagery in a resolution of 60 cm there are two requirements to fulfill the 1:5,000 LSTM specifications: (1) 8 GCPs and (2) TanDEM-X Lin-DEM. As also investigated in 5.2.4, the QuickBird orthorectified imagery was proven sufficiently to be used as a reference image for UAV data processing to give a geometric accuracy in an order of decimeter accuracy.

From the above mentioned results, as depicted in Figure 70, for half scene of SPOT6 in a size of 60 by 60 km, the investigation was extended for the utilization of SPOT6 data in a resolution of 1.5 m to achieve 1:10,000 LSTM specifications. For that purpose, there were 33 acquired GCPs from GNSS used in the orthorectification by using a generated DEM fromTanDEM-X data.

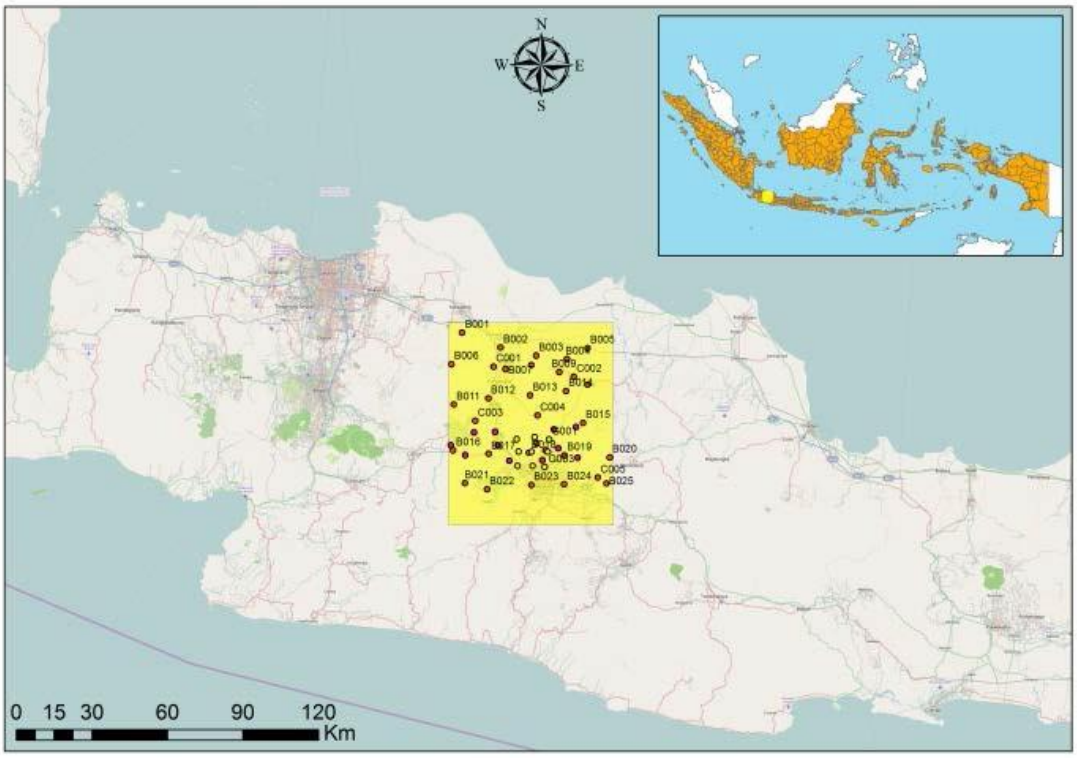

Figure 70: SPOT6 Orthorectification of Bandung area with 33 GCPs

In addition, for one map tile of 1:5,000 (2.3 by 2.3 km), there are 19 ICPs manually selected from the road and building datasets to evaluate the planimetric accuracy. The edge of the building and the center of the road were selected manually both in orthophotos generated from an aerial photogrammetric acquisition using Trimble Phase One (P65) and in orthorectified SPOT6 imagery (Figure 71).

Figure 71: Manual selection of ICP from SPOT6 (left) and Orthophoto (right)

The calculated planimetric accuracy of 19 ICPs from GNSS for big AOI (60x60 km) and for one sheet of 1:5,000 (12093136D) are included in Table 31.

Table 31: Planimetric accuracy for Bandung urban area (SPOT6)

	Ortho using RPC (m)		Ortho by GCP (m)	
	60 x 60 km	**1:5,000**	**60 x 60 km**	**1:5,000**
NSSDA (95%)	6.467	8.150	4.695	4.368
NMAS (90%)	5.760	7.259	4.182	3.890

5.4.2.5 Discussions

The investigation results show that based on GCP measurements, it was possible to achieve the required vertical accuracy in the urban area. In that sense, as investigated by using QuickBird imagery (5.2.2.2), the results by using SPOT6 also indicate that by only using the GCPs the horizontal accuracy has been increased up to 4 times GSD (5 m) regarding the planimetric accuracy.

Hence, topographic maps with an absolute NSSDA (95%) of 5 m (accuracy) can be produced by iterative orthorectification of SPOT6 data with 33 full control GCPs for 60 x 60 km AOI. It provides a SOP that can be extended to the larger map scale in order to generate reliable orthoimages already compliant with LSTM specifications of 1:10,000.

5.5 Summary

The first part of the investigations demonstrated how the quality of many data sources as the potential sources for LSTM must be evaluated properly in a comprehensive way to get the right decision about geospatial data quality. The focus in this case is to improve the algorithm of the TanDEM-X InSAR DEM by using reliable height reference data in order to produce the comparable output to the conventional methods.

VHRS imageries i.e. Quickbird (60 cm resolution) are sufficient on a planimetric (2D) aspect to be used as a geospatial data source for 1:5,000 LSTM within the CE90 accuracy of 2.15 – 3.32 m by only performing orthorectification under certain aspect as follows:

- GCP measurement is still considered as the best solution to establish the reference network both for orthorectification and spatial data accuracy measurements;
- GNSS rapid static positioning or RTK (CORS) can be considered as the necessary solution to establish a GCP network even though it needs heavier efforts viewing from time and resources perspective;
- The medium resolution DEM/DSM such as from ASTER, SRTM in 30 m resolution is sufficient enough to provide object features in 3D, however space borne DSM RADAR such as TerraSAR-X in 7.5 m resolution is providing a better accuracy.

As topographic maps with an absolute NSSDA (95%) of 5 m (accuracy) have been produced by iterative orthorectification of SPOT-6 data with 33 GCPs for 60 x 60 km AOI, it

can be used in order to generate orthoimages sufficient enough for 1:10,000 LSTM requirements in Indonesia.

Also an alternative method to determine the height reference, the absolute phase offset and the baseline has also been presented. The assessment results showed that the implementation of the linearized approach for TanDEM-X InSAR DEM generation has fulfilled the HRTI Level 4 specification (for some test areas) and the HRE08 at most. These results already outperformed the IDEM from DLR.

It is also confirmed that InSAR DEM is a very valuable technique to be utilized in tropical areas though some errors are introduced by layover, foreshortening, shadow, surface decorrelation and the atmospheric signal in the data. GNSS measurement is essential to provide several highly accurate height points for calibrating the residuals in InSAR DEM. Therefore the fusion of GCP and IDEM as an intermediate product is necessary to improve the quality of the on-going InSAR DEM generation. Since the results by using GCPs were not sufficient especially for the mountainous area, the high accuracy DSM or DTM from UAV or Aerial Camera was considered as a mandatory input for the linear adjustment.

Topographic maps with an absolute NSSDA error of 1 m (accuracy) have been achieved with GCPs from a UAV campaign using non-metric consumer grade cameras, providing relatively inexpensive measures in order to generate a DEM sufficient enough for LSTM requirements in Indonesia.

This section has shown that the required RMSE of UAV photo data processing by implementing an integration mechanism with VHRS imagery to fulfill the 1:2,500 (planimetric accuracy) can be reached. However for the DEM quality, it is still necessary to use 8 GCPs / model in order to fulfill the accuracy of 1:5,000 LSTM. On this level of geometric accuracy, GNSS measurement with Precise Point Positioning (PPP) suffices GCP accuracy requirements and hence reduces time, cost and reference station dependency.

As an alternative method to determine the camera exterior orientation parameters has been presented, it is noticeable that the actual tendency in photogrammetry toward SfM is one potential solution for LSTM acceleration in Indonesia. Proven that the determination of camera intrinsic and exterior parameters constitutes the first of the modelling procedure, the solution based on projective geometry aspects can be very useful. The recovered camera exterior parameters, using building structures as a reference model has improved the accuracy of the combined DG and IG method for LSTM purpose. By only using minimum amount of three GCPs, the area outside of the GCP coverage improved significantly by taking into account the building structure model. This low cost approach generated sufficient orthophoto and DSM in compliance with 1:5,000 LSTM requirements.

6 Investigations for Disaster Management (DM)

As already presented in previous chapter 5, the TanDEM-X DEM generation using local or national height reference data namely GCPs and reliable DEM (from UAV or airborne data acquisition) has already provided more accurate DEMs in comparison with the similar IDEM generated using ITP at DLR. Thus, the proposed algorithm to process TanDEM-X CoSSC allows for the generation of DEMs with enhanced spatial resolution and absolute accuracy as well.

This result may contribute to the rapid mapping activities all over the world in the framework of Spatial Data Infrastructures (SDI) for DM. In this case using the thick client approach, it is necessary to have the powerful spatial data processor with the mapping completion as the top priority. However, the data restrictions and security requirements are still problematic in the country, even in the case of high priority situations. In some circumstances, it is even better to initiate additional or new mapping activities right away after the disaster took place.

The focus of this chapter is to demonstrate how the findings of this dissertation can contribute to DM. It must be noted here that only a few examples are presented based on real instances of major disaster situations in Indonesia namely earthquake and volcano eruption.

Some examples in this chapter are selected in order to demonstrate the aforementioned issues in the context of DM. The investigations for DM purposes in this chapter are mainly the application of the improved LSTM method as described in the previous chapter to demonstrate how the role of reliable geospatial data can produce some applicable results. Two major disasters frequently occurred in Indonesia are selected as the background of the proposed use case. The first one is an example from 2013's volcano eruptions in Mount Sinabung (Tampubolon and Reinhardt, 2015) and the second one is an example from 2018's tsunami events in Sunda Strait (Tampubolon and Reinhardt, 2018).

6.1 Research questions and investigation areas

During disaster and emergency situations, geospatial data analysis plays an important role to be used as a mandatory input for DM. As one component of basic geospatial data, large scale topographical maps are mandatory in order to enable geospatial analysis within emergency situations. The importance of DM triggers worldwide cooperation under Services and Applications for Emergency Response (SAFER) projects (Schneiderhan, 2010). Within this context, the geospatial data acquisition takes a major role, in which the utilization of space borne data especially VHRS imagery data collection will be initiated immediately in the period of major disasters around the globe.

Kiefl, 2007 viewed on this issue from the perspective of coordination aspects in terms of quick emergency response and disaster preparedness. Various remote sensing data

produced from different sensors increase the level of accuracy but on the other hand also increase the time delay especially during the geospatial data analysis. Therefore the establishment of an SDI to facilitate the spatial data access is obvious. By establishing this SDI, the coordination among different institutions can be done efficiently without any unnecessary time delay especially during the period of crisis. In disaster and emergency situations, geospatial data must support the DSS with reliable and actual datasets. One fundamental component of the aforementioned geospatial datasets is the DEM in LSTM specification, which sometimes does not exist for the disaster area.

The following sections discuss the investigations for the DM use case based on improved LSTM data derived from above mentioned geospatial data sources. Hence the research questions for the investigations in this chapter were:

1. Is the planimetric accuracy of UAV georeferenced without field GCPs sufficient to perform relevant DM analysis?

   In most disaster situations, it is obviously difficult to perform conventional LSTM due to the field condition. In this case the expected geometric accuracy must not be always compliant with LSTM specification but at least can support rapid mapping activities with high resolution data. As further discussed in section 6.2.1, the Airborne IFSAR Type II (Intermap) data will be used for georeferencing purpose whilst the accuracy assessments will refer to the GCPs from GNSS. Also GCPs (with height) derived from aforementioned IFSAR will be applied and the corresponding achieved accuracy will be presented.

2. Can TanDEM-X data provide reliable DEM for the examples presented by using height reference from IFSAR Airborne Type-II?

   The TanDEM-X InSAR DEM generation for mountainous area as explained in 5.4.1.1 will be applied in the example presented in section 6.2.1 and 6.3.1. However in this case, only the IFSAR Airborne Type II and free SRTM 1 arc second data will be used as a DEM reference. In the disaster situations, it is difficult to conduct a field survey in general. Therefore the usage of GCPs in TanDEM-X data processing will not be treated.

3. Can reliable disaster-related information extracted immediately without any field GCPs?

   As discussed in 5.2.4.2, UAV data processing by using GCPs derived from VHRS and TanDEM-X DEM has delivered accuracy in the order of 0.7-1.1 m (planimetric) and 1-2.2 m (height). For some extent those accuracies already comply with the LSTM specifications in the scale of 1:5,000 – 1:10,000. The combination between DEM and high resolution UAV data in an unsupervised classification to extract features will be discussed in 6.2.3.

4. Can TanDEM-X data provide reliable DEMs by using height reference from free DEM data i.e. SRTM 1 arc second?

   All the LSTM investigations in chapter 5 use only reliable and up-to-date height references. However, for the situation of a disaster in a remote area or an isolated island, a reliable DEM reference does not exist and the phase discontinuities are challenging for an isolated area. However there is an advantage of using a coastline

features that can be used as zero height reference (6.3.1). Not like in previous chapters where SRTM 1 arc second was used only for geocoding purpose, the SRTM 1 arc second in this chapter is extended to be used as a height reference.

5. Can a combination between time series DEM and TanDEM-X D-InSAR provide a quick preliminary analysis as an important input to the Tsunami Early Warning System (TEWS)?

   Time series DEMs as an input to the TEWS are mandatory for an analysis of the impact in advance. In addition, this chapter also describes the role of UAV data acquisition in supporting rapid mapping activities.

As depicted in Figure 72, there are two test areas reflecting different disaster situations. The first test area, mount Sinabung is related with volcano eruptions as further discussed in 6.2. The second test area, the active volcano island of Anak Krakatau which is not only related with an eruption activity but also with the tsunami occurrence as further discussed in 6.3.

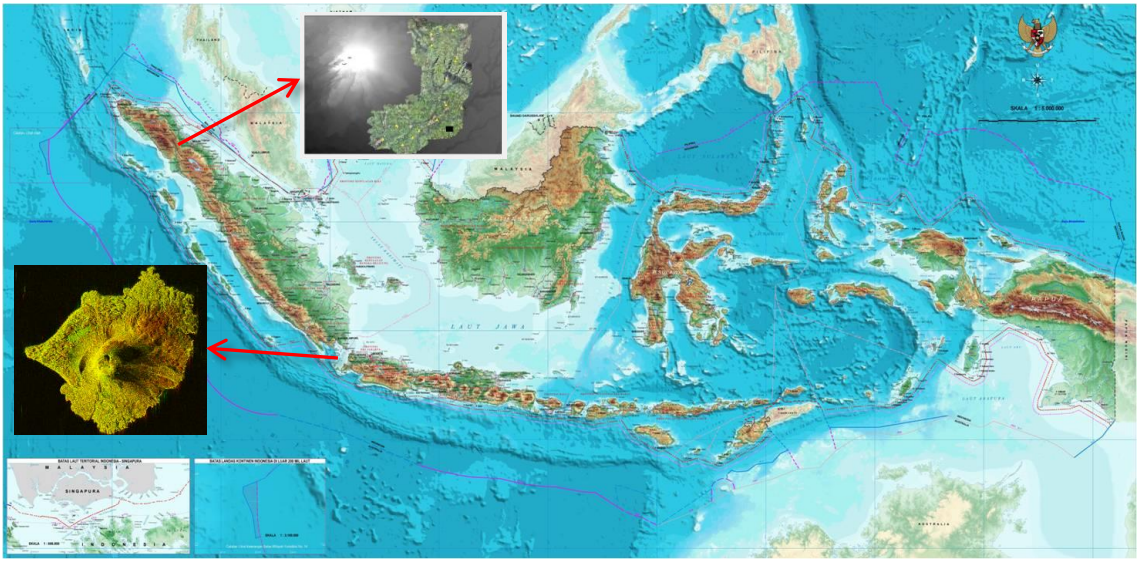

Figure 72: Test areas for DM investigations

6.2 Investigations on volcano eruptions using UAV data

It is their main advantage that UAV platforms enable on-demand very high resolution data collection which can be customized efficiently. UAVs can carry different kind of sensors like non-metric cameras. From the sensor data, different products can derived like point clouds which can be utilized to support decision-making processes within disaster context situations. Moreover, the high resolution data collected from UAV platforms have the capabilities to provide a quick overview of the disaster area. Nevertheless, there are some limitations e.g. flying duration (power system), payload, etc. that shall be taken into account in the UAV data processing for rapid mapping activities.

Unmanned Aerial Vehicle (UAV) is the rising geospatial data platform nowadays that can be attractive for modelling and monitoring the disaster area with a low cost and timely acquisition. Disaster-related object extraction is of special interest for many applications.

Basically, the investigation presented in the following focuses on the geometric accuracy of orthophoto and DEM derived from the UAV data. In order to evaluate the geometric accuracy, it is necessary to use reference data with a proper geometric accuracy. From the UAV data, 2D data like orthophotos as well as 3D data as DEMs have been generated. To some extents, the generation of this different data needs some different inputs and a different evaluation workflow of the 2D and the 3D data.

6.2.1 Investigations on geometric accuracy

Geospatial data collected from a UAV are usually captured from low altitude. In that condition, normally there is no significant occlusion and therefore the data can be used for semi-automatic feature extraction purpose in a similar way as metric airborne data, if suitable tools are used. In this case, it was demonstrated how a UAV platform can deliver geospatial data with sufficient accuracy to be used subsequently for disaster-related object extraction. For this purpose, a proper geo-referencing approach has been defined.

A real disaster occurrence from 2013 in conjunction with Mount Sinabung eruption, Northern Sumatra, Indonesia, is used as a test for the rapid mapping activities presented for DM purposes. After all, this approach includes a proper georeferencing and disaster-object extraction of UAV data to support rapid mapping activities.

The test area of Mount Sinabung has been selected because a real disaster event i.e. volcano eruption occurred there and reference data was available, including the geodetic reference network infrastructure. Mount Sinabung is located in the northern part of Sumatera Island in Indonesia which has been significantly showing volcano activities since 2010.

In the development context of Indonesia, this area is highly prioritized as a strategic area by the stakeholders, and therefore it was a goal to accomplish a detailed spatial planning as soon as possible. As a consequence, an airborne IFSAR data acquisition in 2011 has been done in order to produce topographic maps for the area in a scale of 1:50,000. However, this data set has a sufficient accuracy for 1:10,000 topographic mapping and consequently can be potentially used as a reliable reference data for the accuracy assessment as explained above.

In general, the test site covers approximately a valley area of 1,800 hectares with an elevation approximately between 1,000 – 1,500 meters above MSL (Figure 73). The terrain condition of the affected area such as villages, forests, plantation, etc. is extremely undulated with a lot of valley areas in the bottom of the mountainous regions.

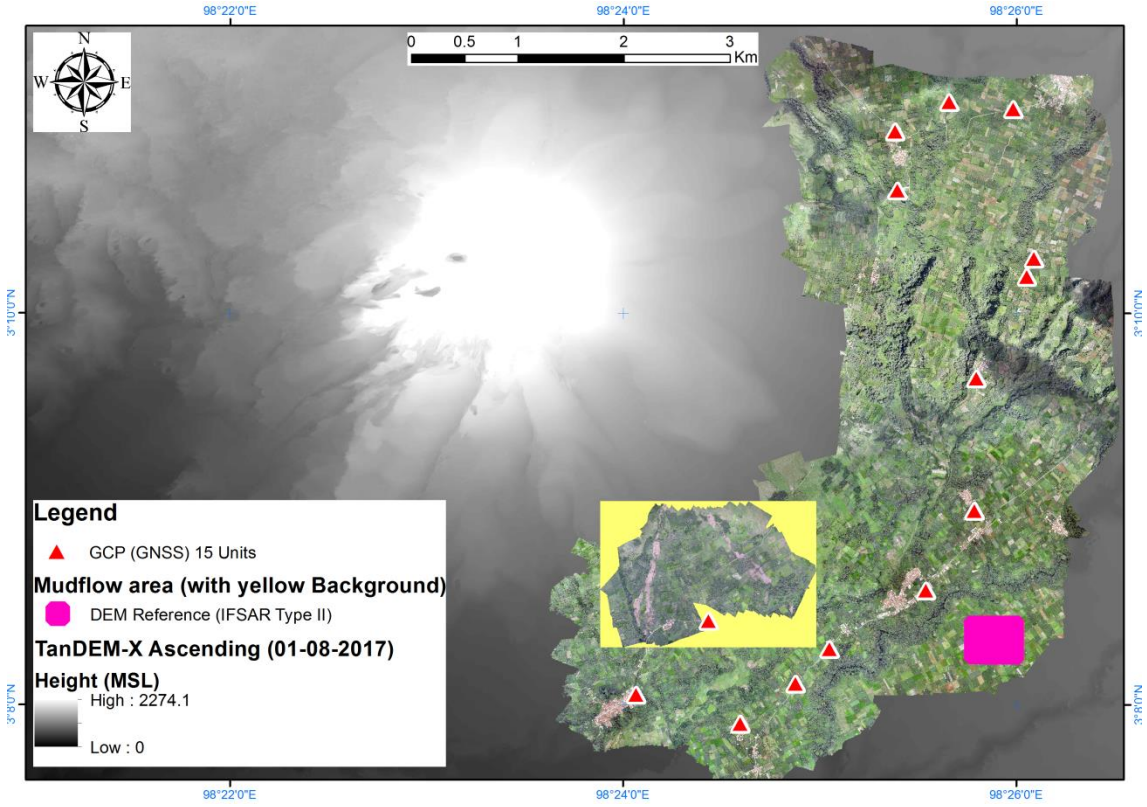

Figure 73: Mount Sinabung area during eruption in December 2013

For this specific use case, the investigation of the role of existing geospatial data e.g. airborne IFSAR data, Microsoft Bing imagery and the SRTM DEM for UAV data processing is used in the context of LSTM specifications.

In the following, the results from different approaches and resolutions are subsequently validated against reference data acquired from field surveys using Global Navigation Satellite System (GNSS) and IFSAR data. Subsequently, this investigation also introduces the combination between unsupervised classification and 3D analysis for the purpose of disaster-related object extraction. In this context, the role of 3D views contributes by providing the seed file data which can improve the unsupervised classification accuracy.

Datasets used The UAV data used in this section was generated by using Canon S-100 camera from a flying height ca. 400 m AGL with a resolution of 11 cm (GSD). UAV data acquisition has been performed immediately after the significant mount eruption in December 8th, 2013 with respect to the area restriction in the period of the disaster declaration status. In addition, there are two TanDEM-X CoSSC datasets available as included in Table 32 for providing the up to date DEM.

Table 32: TanDEM-X CoSSC Data for Sinabung Area (*Height of Ambiguity)

Scenes	HOA* / B_P (m)	Adjusted parameters		Incident angle / Range in DSM Reference Area (°/m)	Looking direction	Acquisition date
		B_P' (m)	ΔΦ (°)			
Si01	-54.862 / 108.484	-117.710	-173.8869	37.4634 / 629325.827	Ascending	01-08-2017
Si02	85.685 / 51.192	95.674	25.3567	29.1454 / 572256.974	Descending	09-09-2017

Reference datasets The airborne data acquired in August 2011 by using IFSAR Type II (Intermap) as explained in 4.4.2 was used as dataset for the TanDEM-X height calibration reference as well as for accuracy investigations and assessment purposes.

For the whole area as depicted in Figure 73, there were 15 GCPs taken by using ArcGIS from Microsoft Bing imagery as done in Tampubolon and Reinhardt, 2014. The height information however were based on two DEMs to be compared namely SRTM DEM and IFSAR Type II DEM. Subsequently, the accuracy assessment for the 2D (planimetric) component has considered 15 ICPs from GNSS survey as also used in the accuracy investigations (2.4.2) covering the whole affected area.

For the mudflow area as depicted in Figure 73 with yellow background, there were also 15 GCPs taken by using Microsoft Bing imagery with the height information either from SRTM DEM or IFSAR Type II DEM. In addition, for the DEM geometric accuracy evaluation the height of all 3,648 grid points of the derived UAV DEM have been compared with the IFSAR DEM including 15 ICPs as well for the mudflow area (see Figure 73).

Table 33: Accuracy assessment for mount Sinabung areas

Area	Planimetric accuracy (m)		Elevation accuracy (m)			
			SRTM DEM		IFSAR Type II DEM	
	$RMSE_r$	LE95	$RMSE_Z$	LE95	$RMSE_Z$	LE95
Whole area	1.7	2.5	5.4	10.6	2.4	4.7
Mudflow	0.9	1.5	4.8	9.4	2.6	5.1

The significant elevation accuracy differences between this investigation area and the previous Borobudur area in section 5.2.4 is presumably caused by the higher altitude (cf. $RMSE_r$ = 0.65, $RMSE_Z$ = 1.14). Since Agisoft PhotoScan is designed for small range photogrammetry, the algorithm is sensitive to the height / distance to the reconstructed object. For instance, in Agisoft PhotoScan, there is a separation between arbitrary and height field reconstruction scheme. This was also confirmed by the previous investigation in the lower altitude i.e. approx. 200 m (AGL) which indicated the better

elevation accuracy of Agisoft PhotoScan. In addition, this result is also confirmed by the visual comparison of orthophotos and DEM outputs as presented in section 5.2.4.2. Not only the DEM details but also the height references are not comparable.

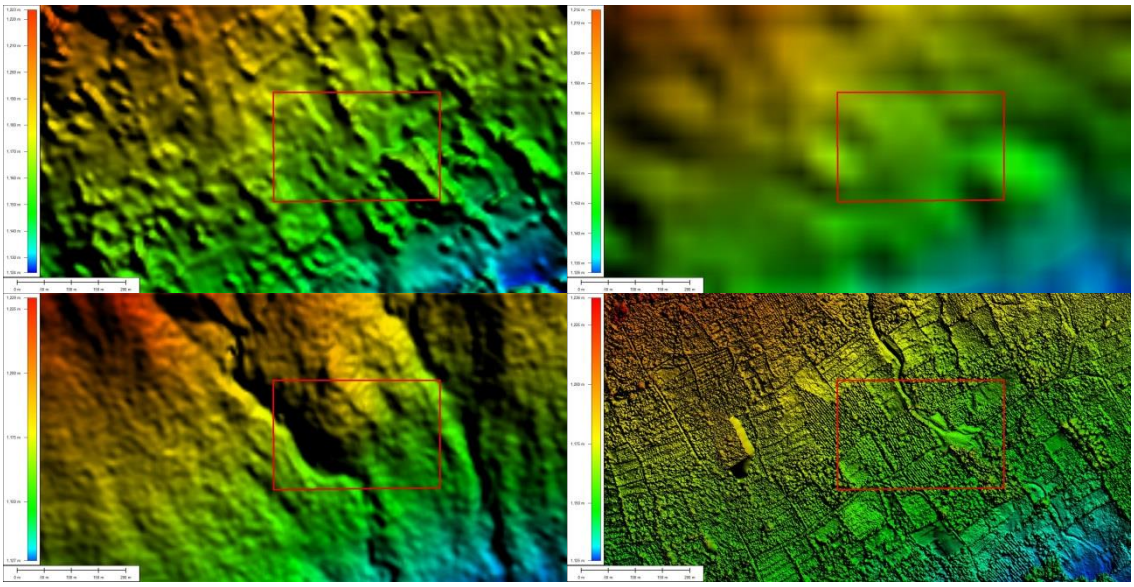

Figure 74: Different shaded relief DEMs of Sukameriah village (upper left: IFSAR in 5 m GSD, lower left: TanDEM-X Ascending in 4.5 m GSD, upper right: SRTM1 in 30 m GSD, lower right: UAV DSM in 20 cm GSD)

6.2.2 Discussions

As TanDEM-X data was taken in 2017 which is more recent to the other datasets, it is not recommended to use that DEM as a height reference for the UAV data (Table 32). Figure 74 shows clearly the significant terrain changes from TanDEM-X DEM (lower left) to the other datasets. In addition, the accuracy assessments will also be mixed with the terrain changes that must be distinguished manually from image interpretation.

By applying time series data analysis, the DEM differences were performed to identify the affected areas with respect to the eruption activity. A comparison between IFSAR Type II DEM and UAV DEM can identify the suspected area of impact i.e.mud flow areas. It is important to reach the geometrical accuracy threshold which comes from the result of elevation accuracy assessment in Table 33, i.e. 2.6 m (RMSE) or 5.1 (LE95% accuracy).

Referring to the aforementioned geometrical accuracy threshold, the deviations between UAV DEM and IFSAR Type II DEM can be grouped into 5 different classes as shown in Figure 75:

1. no changes (-2.593 – 2.593 m) means that the deviation is below the geometric accuracy threshold
2. 95% negative changes (-5 - -2.593 m) means that the deviation is indicating the 95% possibility of negative changes (erosion)
3. 95% positive changes (2.593 – 5 m) means that the deviation is indicating the 95%

possibility of positive changes (dilation)

4. 100% negative changes (< -5 m) means that the deviation is indicating erosion
5. 100 % positive changes (> 5 m) means that the deviation is indicating dilation

Obviously, the accuracy assessment shows that there is a significant improvement if the airborne IFSAR data is used as the elevation reference rather than SRTM DEM. As an example, the DEM difference classification has identified that the disconnected road segment lays within no changes area and therefore not occurred in the period between IFSAR (10 August 2011) and UAV data acquisition (8 December 2013).

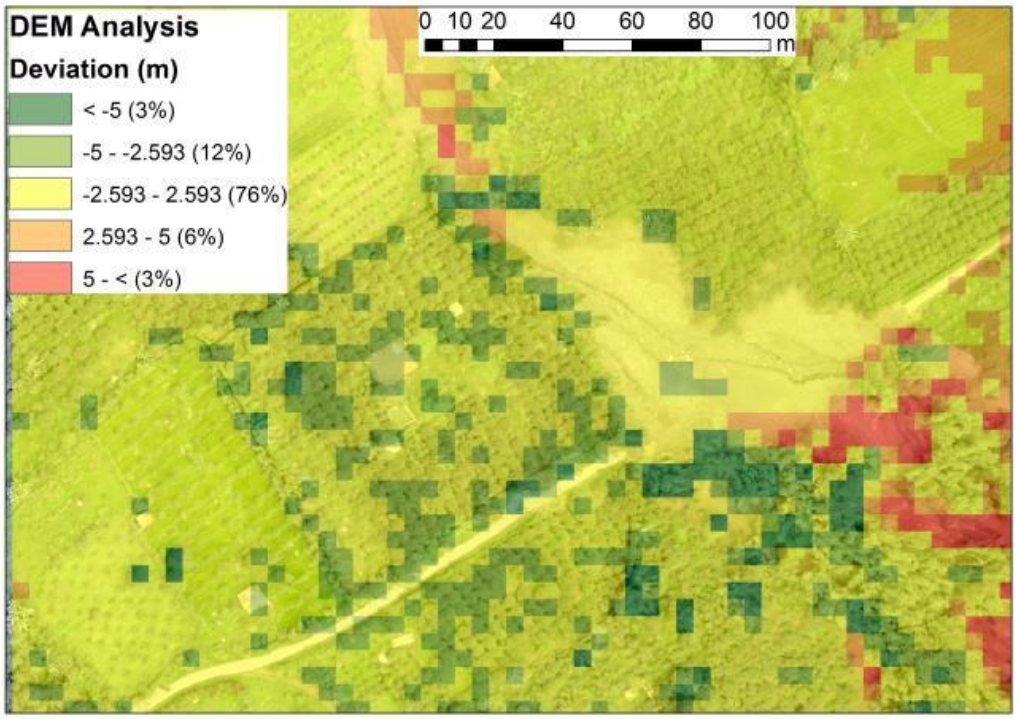

Figure 75: Deviations between UAV DEM and IFSAR DEM in 5 m GSD

6.2.3 Investigations on feature extraction

As already explained in 4.4.2, feature extraction in this dissertation combines the geometrical accuracy investigations and image classification. Geometrical accuracy as discussed in the previous section is the pre-requisite for performing 3D analysis on high resolution time series data.

Another objective of the investigations is to identify a proper classification method for the purpose of disaster-related object extraction from high resolution UAV data. Unsupervised classification has been chosen as an approach to extract features of interest to reduce the processing time and ground truth validation as well.

Based on the DEM differences grouping in previous section, it detected 100% positive changes location where the deviation indicates 3D changes after the disaster as the seed file data i.e. red colors in Figure 75. This area was presumably predicted as the relevant mud flow covered area in post disaster situation.

Before it is possible to proceed further, a visual inspection of the DEM is an initial start by synchronizing the ground truth data to ensure correctness of seed file in the field. In

this step, the blunder errors in the seed file data can be detected and removed manually. As depicted in Figure 76, the visual quality of the UAV orthophoto rendered on its DEM (lower part) is already comparable with the photo from the ground survey (upper part). It reflects also that the optimal alignment from IFSAR Type II as a reference image to the Canon S100 data provide the relative geometric accuracy at most.

Afterwards, the initial unsupervised classification without any seed file data has been performed to classify 7 different classes namely water bodies, crops, grass lands, bare lands, mud flows, road segments and the remaining unclassified area.

This initial unsupervised classification result was also used to check the validity of the seed file data. If the seed file data lay beneath non mud flows area, then it will be removed. At the end, the valid seed data comes as the final result based on the DEM analysis as well as from the first initial unsupervised classification.

The valid seed file data then is submitted to the final unsupervised classification in order to improve the result. From this point, the disaster-related features have been extracted from the final unsupervised classification result.

Figure 76: Disconnected bridge (upper: photo from field survey, lower: animation from UAV data)

Finally, the overlay analysis between unsupervised classification results with the reference data can be performed in order to assess the feature extraction accuracy. In this case, manual interpretation from UAV aerial photographs in 11 cm resolution has been considered as the reference data.

Table 34: Unsupervised classification without Seed file input

Classes / Segments	Manual Interpretation		Fuzzy K-Means		Isodata		K-Means	
	Area (m2)	Acc.(%)	Area (m2)	Acc.(%)	Area (m2)	Acc.(%)	Area (m2)	Acc.(%)
Others	400.09	0.45%	3271.83	12%	4768.98	8%	698.04	57%
Water bodies	382.42	0.43%	2731.63	14%	12754.46	3%	6692.46	6%
Crops	39562.81	44.82%	23717.22	60%	23054.80	58%	26753.21	68%
Grass lands	37121.01	42.06%	36990.16	99.6%	24744.93	67%	38143.33	97%
Bare lands	687.93	0.78%	7743.58	9%	14321.91	5%	12735.81	5%
Mud flows	8938.59	10.13%	12935.65	69%	6692.72	75%	2807.54	31%
Road segments	1170.05	1.33%	857.13	73%	1909.40	61%	416.81	36%
Total	**88262.90**	**100 %**	**Average**	**48%**	**Average**	**40%**	**Average**	**43%**

Each aforementioned class was digitized manually in the UAV orthophoto to provide valid reference data for suspected mud flow area. On the other hand, the three different unsupervised classification methods: Fuzzy K-Means, Isodata and K-Means were performed by using PCI Geomatica 2012 to classify each pixel into 7 aforementioned classes.

Table 35: Unsupervised classification with Seed file input

Classes / Segments	Manual Interpretation		Fuzzy K-Means		Isodata		K-Means	
	Area (m2)	Acc.(%)	Area (m2)	Acc.(%)	Area (m2)	Acc.(%)	Area (m2)	Acc.(%)
Others	400.09	0.45%	4743.63	8%	2838.84	14%	434.03	92%
Water bodies	382.42	0.43%	2641.82	14%	12565.62	3%	6732.35	6%
Crops	39562.81	44.82%	22388.08	57%	23488.31	59%	27464.04	69%
Grass lands	37121.01	42.06%	37575.78	99%	25128.06	68%	37353.61	99%
Bare lands	687.93	0.78%	10217.62	7%	9865.62	7%	9545.96	7%
Mud flows	8938.59	10.13%	9843.11	91%	12580.80	71%	6276.51	70%
Road segments	1170.05	1.33%	853.55	73%	1796.32	65%	457.12	39%
Total	**88262.90**	**100 %**	**Average**	**50%**	**Average**	**41%**	**Average**	**55%**

To detect the influence of the seed file derived from the manual inspection as discussed in the previous section for the accuracy assessments, all of three aforementioned unsupervised classification methods were performed by using the seed file as an input. Finally the area for each class was calculated on its attribute (field) by using ArcGIS.

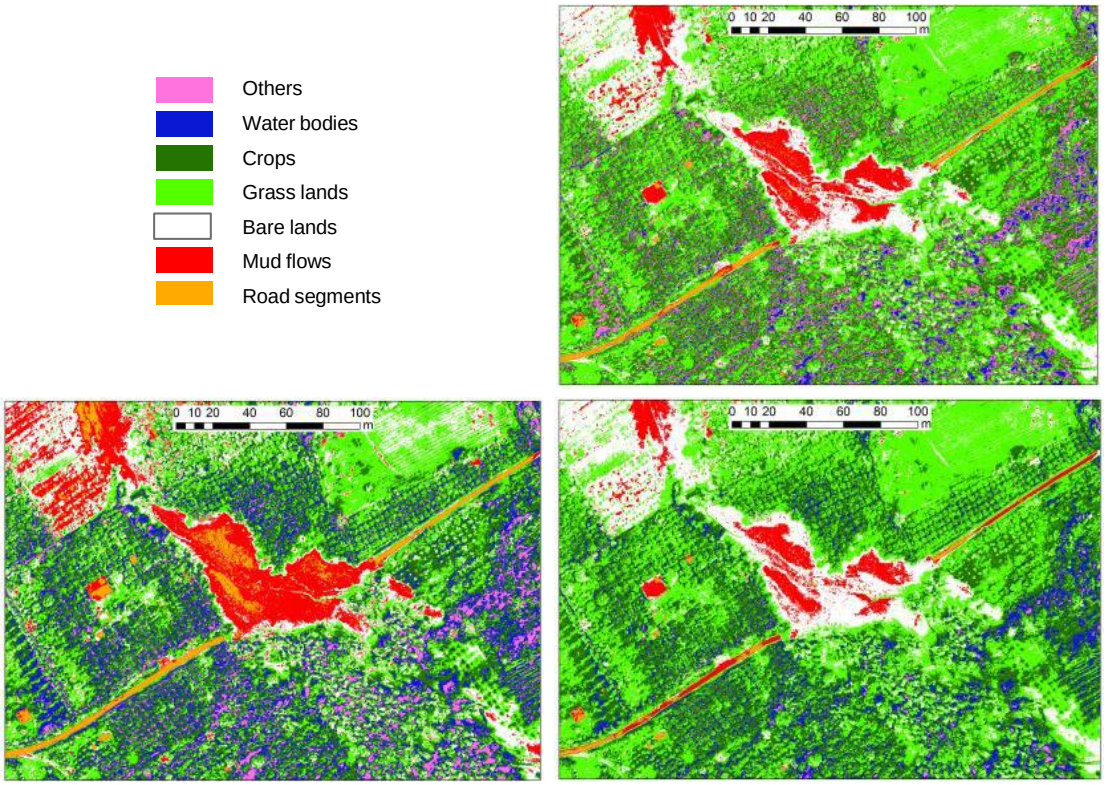

Figure 77: Classification results using seed file data (upper right: Fuzzy K-Means, lower left: Isodata, lower right: K-Means)

6.2.4 Discussions

Without any seed file input, the Isodata presents better results as included in Table 34 where the result of mud flows feature extraction indicates 75% accuracy to the manual inspection from UAV Canon S100 orthophotos. However, since UAV usually generate high resolution data, the exclusion of the seed file data in the unsupervised classification is mostly avoided. Indeed, the seed file from 11 cm UAV orthophoto is usually very accurate to contribute to the unsupervised classification.

From the comparison between Table 34 and Table 35, it can be seen that the seed file information can significantly improve the unsupervised classification accuracy up to 91 % for mud flows feature extraction purpose. On the other hand, the use of seed files also improves the unsupervised classification accuracy especially for road feature extraction which can achieve 73% accuracy using Fuzzy K-Means algorithm.

Fuzzy K-Means classification showed relatively better feature extraction result than others as also can be seen in Figure 77 . Road segments and mud flows regions which are the prominent interest of disaster-related features can be extracted with the most accurate result confirmed by the field verification.

6.3 Investigations on a tsunami event by using TanDEM-X data

The Sunda Strait tsunami swept the coastal area of Java Island in the night of December 22, 2018 local time. The responsible institution i.e. Meteorology and Climatology Agency of Indonesia (BMKG) delivered no immediate tsunami early warning at that time. Therefore people around the west coastal area of Java Island including the touristic area of Tanjung Lesung, Ujung Kulon could not prepare themselves to escape from the tsunami waves reported as 3-4 meter high on the ground. It is still debatable about what is the exact cause of 2018's Sunda Strait tsunami? The major opinion focused on the increasing eruption activity of Anak Krakatau (Child of Krakatoa). A volcanic mudflow material avalanche was suspected as the primary cause to trigger the high sea wave strengthened by the tidal and seasonal wind condition at that time.

In this section, the combination between time series DEM analysis and ground displacement detection is used to try to explain the potential trigger of the Sunda Strait Tsunami. The German TanDEM-X CoSSC is used in order to generate DEMs in a high resolution format comparable to the LSTM specification in Indonesia as already discussed in 5.2.3.

Especially within earthquake / tsunami events it is a challenge to derive an up to date and not too costly terrain representation through actual DEMs. Satellite-based radar data are very well suited to fulfill such needs. A wide coverage and flexible data acquisition modes make radar satellite-based data very interesting also for DEM generation especially for disaster monitoring areas. The main reason for this is the weather independence and high orbit altitudes which can avoid local restrictions and limitations (Percival, 2012). From a technical point of view there is another goal of this section, namely to apply the workflow for deriving a DEM from TanDEM-X Radar Interferometric data as pre-defined in 4.3.2.1.

For the AOI as depicted in Figure 78, there are 3 datasets available as included in Table 36.

Table 36: TanDEM-X CoSSC Data (*Height of Ambiguity).

Scenes	HOA* / Baseline (m)	Looking Direction	Acquisition Date
K01	93.483 / 83.207	Descending	14-10-2015
K02	77.185 / 100.514	Descending	21-01-2016
K03	28.753 / 136.695	Descending	21-02-2019

6.3.1 TanDEM-X DEM generation for the volcanic island

The increasing eruption activities of Anak Krakatau Mountain Island until the end of 2018 make it difficult to perform conventional LSTM. On the other hand, it is mandatory to use DEMs in order to enable GIS analysis within quite a number of societal challenges such as demographic changes, marine research and natural hazards. The massive

exploitation of marine resources develops many new coastal settlement areas with a great danger of natural hazard potential at the same time.

Figure 78: Anak Krakatau and its surrounding island (Source: Bing Imagery, Geospatial Reference System of Indonesia (SRGI), GEOFON Program)

The motivation to identify the potential trigger of the aforementioned disaster by utilizing the radar interferometry techniques was a task for this DM investigation (see chapter 6.3.5 for details). Hence, the main objective is to confirm the contribution of the underwater avalanche to the Sunda Strait tsunami. The TanDEM-X data were used to generate a DEM for the time before the disaster and Sentinel 1A data for a DEM for the time after the disaster (no TanDEM-X data available for this point at the time of writing). Fortunately in this section the recent TanDEM-X data after the tsunami was also available after a while (Table 36). Further the volume estimation through the ground deformation detected was used as the major indication to the tsunami event.

As already explained in 4.3.2.1, the unwrapped phase to elevation step needs either GCPs or a DEM reference in order to determine the absolute phase offset by using a linear model adjustment. Therefore the extension of the model in a linear adjustment is necessary by introducing three important parameters namely perpendicular baseline, height reference and phase offset. This extension was already published in an ISPRS Archives publication in 2018 (Tampubolon and Reinhardt, 2018).

Currently, only one Geodetic Control Point (KTAU) is available at Anak Krakatau volcanic island as depicted in Figure 78. Since it is difficult to conduct the GCP measurements or produce high resolution DEM especially around this active volcano, the alternative strategy in the Unwrapped Phase to Elevation step has been defined. In addition, the phase discontinuities which decrease the height accuracy have to be considered. These phase discontinuities occur due to the sea (waterbody) area.

Basically, as also depicted in Figure 78, there are 3 islands detected surrounding the active volcano i.e. Sertung (West), Krakatau Kecil (East), Krakatau (South). Assuming there is no significant land change in Sertung Island, this area can be used as a reference area for the unwrapped Phase to Elevation step by using linearized model (4.3.2.2). However, as depicted in Figure 79, the effect of phase discontinuities make other islands, including Anak Krakatau, floating away after the height calculation in the generated DSM.

To correct this problem, the preliminary condition about the zero height coastlines is added to the processing scheme. In particular, the role of coastlines as one component of Topographic Maps based on Act of Republic Indonesia, 2011 (see 2.3) was demonstrated. Since the height calculation model is linear as formed in (Tampubolon, Reinhardt, 2018), the height reference can be shifted from one to another area once the relative heights are fixed.

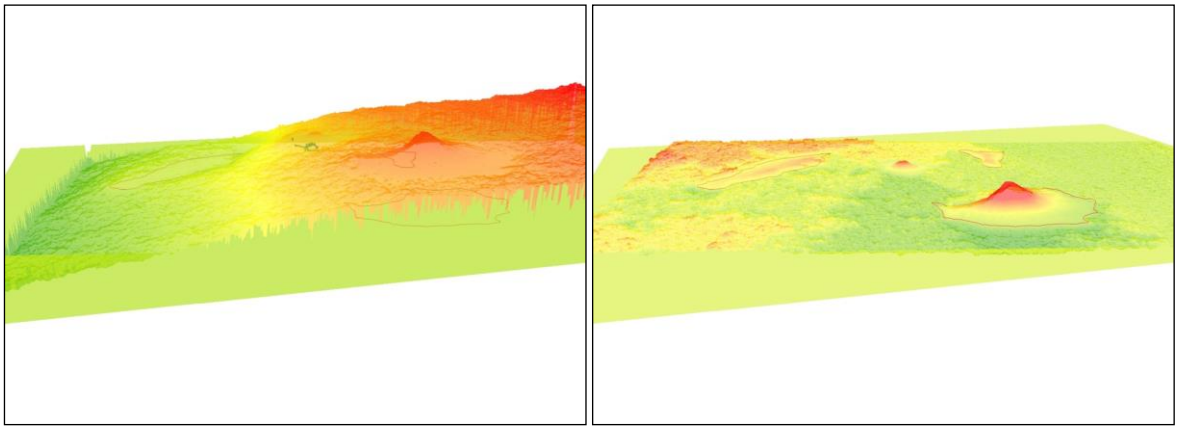

Figure 79: Effect of phase discontinuities (left: not corrected, right: corrected)

6.3.2 Discussions

As explained in 4.3.2.1, the Unwrapped Phase to Elevation step needs either GCPs or a DEM reference in order to determine the absolute phase offset by using a linearized model adjustment. Since there was no available GCP especially during the volcanic eruption, the usage of a DEM reference is applied.

For small islands such as Anak Krakatau, the effect of phase discontinuities was dominant and resulting in an inaccurate DEM because of two major factors. First of all the height reference from one island to another island are different in this case. Therefore it is not possible to provide a unique height reference solution for the whole interferogram. Secondly the adjusted baseline value is also not unique because of the sea water as an obstacle to the phase unwrapping step. Therefore the coastlines features are the

only feasible solution to generate accurate DEM for the case of an interferogram with a lot of small islands such as Anak Krakatau.

6.3.3 Volume calculation on time series DEM

Initially, the volume change estimation of Anak Krakatau volcano was done by using the generated DEMs for the time before and after the disaster using the data sources given in Table 36. For this estimation, TanDEM-X Lin-DEMs of 2015 and 2016 were created by using the SRTM DEM as the height reference.

Subsequently the volume for each DEM was calculated using the Polygon Volume tool in ArcGIS. The results show a growth in volume between 2000 (SRTM) and 2016 (Tan-DEM-X) because of continuous minor volcano activities and a clear loss in volume of more than 100 Mio m^3 between 2016 and 2019 (after the tsunami) as visualized in Figure 80. The volume loss is also confirmed by the recent TanDEM-X data (21-02-2019) which shows a volume of 93 Mio m^3 (Table 37).

Table 37: Volume calculation of Anak Krakatau

DEM	Area (Ha)	Volume (m^3)	Acquisition time
SRTM	270.5	154,118,000	1999-2000
TanDEM-X	313.5	234,408,000	14-10-2015
TanDEM-X	305.3	243,528,000	21-01-2016
Sentinel 1A	318.8	116,250,000	24-01-2019 12-01-2019
Sentinel 1A	243.2	115,806,000	05-02-2019 24-01-2019
TanDEM-X	299.4	93,494,000	21-02-2019

Vector data from Copernicus EMS Rapid Mapping (Copernicus Emergency Management Service, 2018) indicating situations before and after the disaster clearly show that the Anak Krakatau volcano changed his shape enormously after the eruption of December 2018. Part of the former volcano area at the time after the tsunami was covered by water (called underwater avalanche in Figure 81). Using this vector data the lost volume of the volcano were calculated by using the DEM from 2016. It showed that the volcano lost around 44 Mio m^3 (18%) of the volume (Table 38). This is less than the loss calculated from the DEMs, but probably the volcano lost volume also in other areas.

Table 38: Volume calculation of lost volcano area

DEM	Area (Ha)	Volume (m^3)	Acquisition time
SRTM	40.77	33.175,000	1999-2000
TanDEM-X	48.78	44,413,000	14-10-2015
TanDEM-X	43.39	43,868,000	26-01-2016

Also from the Copernicus EMS source mentioned above indicating flood trace for the affected area, the coverage of inundation areas after the tsunami has been investigat-

ed. The volume calculation for these areas show a water inundation volume of around 15 Mio m^3 using the SRTM DEM.

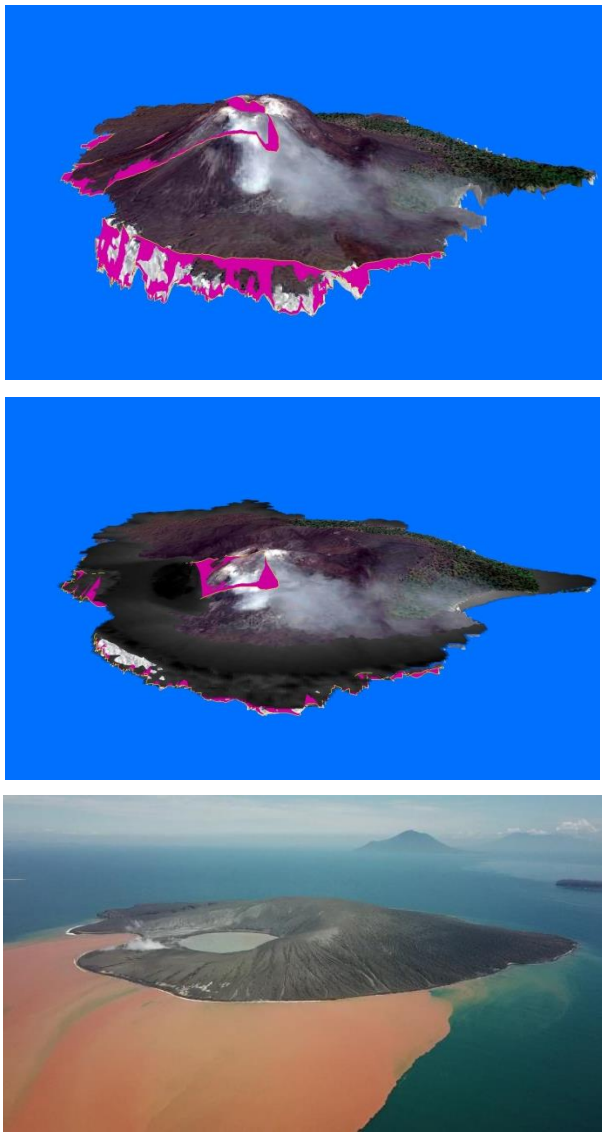

Figure 80: 3 D Visualization of Anak Krakatau (upper part: TanDEM-X 21-01-2016, middle part: TanDEM-X 21-02-2019, lower part: UAV Photo from BNPB)

By comparing the lost volume of the volcano from Table 38 with the total volume of the inundation areas from Table 39, there is a a high probability that the inundation was caused by the loss of mass of the Anak Krakatau. The inundation volume is smaller than the volume lost by the volcano, but parts of the water was surely going elsewhere.

Table 39: Volume of inundation area

Area	Area (Ha)	Volume (m^3)
Tanjung Lesung	90.73	3 627 000
Teluk Lada	79.58	2 246 000
Carita Beach	36.13	715 000
Labuhan South	74.49	1 711 000
Labuhan North	42.00	666 000
Taman Agung	60.56	2 122 000
Kalianda	24.42	457 000
Anyer North	37.97	1 118 000
Anyer South	34.08	808 000
Lampung East	10.26	298 000
Lampung West	24.81	736 000
Sumur	33.87	667 000
TOTAL	**548.90**	**15 171 000**

6.3.4 Discussions

Since, the recent TanDEM-X CoSSC data has HOA of 29 m, the generated DEM was reliably used as the latest DEM to confirm the underwater landslides by a volume loss calculation from the inundation area. From the accuracy investigation in chapter 5, the volume accuracy of TanDEM-X Lin-DEM 2019 can be estimated afterwards by multiplying the island area (Table 37: 299,400 m^2) with the accuracy of HRTI level 4 (6 m) = 1,796,400 m^3.

Therefore, the significant differences between Sentinel 1A DEM (volume: 115,806,000 m^3) compared to the TanDEM-X DEM (volume: 93,494,000 m^3) of the same acquisition time (February 2019) as included in Table 37 show how a lower DEM accuracy can provide inaccurate GIS analysis. In a comparison with the above mentioned volume accuracy of the TanDEM-X Lin-DEM, the volume estimation of Sentinel 1A DEM can provide a misleading result.

By performing some simple GIS Analysis such as Map Overlay and Volume Calculation, the comparison between the volumes of the underwater avalanche from Anak Krakatau with the volume of the inundation area on the coast were presented.

6.3.5 Ground displacement detection

Differential InSAR has been applied by using time series radar data to detect earth surface deformation especially in the situation where accurate DEM reference and/or GCP are not (yet) available. From equation 4.4 as already explained in 4.3.2.4, the differential phase component can be subtracted from the unwrapped phase if the flat earth phase and height phase are known (Richards, 2007). Afterwards the deformation d in meter from multi temporal datasets can be calculated using Eq.4.5.

As the CoSSC format is a co-registered slave data to the master in a bi-static acquisition mode, the identification of the master dataset is mandatory. The TanDEM-X platform consists of two satellites namely TanDEM-X (TDX) and TerraSAR-X (TSX). For the available datasets, it was certain from the included metadata that all the TDX data is a master data set. This important aspect has determined the successful D-InSAR application, otherwise the deformation phase were not feasible to achieve centimeter accuracy. Subsequently, the differential IFSAR techniques are also applied in order to detect the ground deformation.

6.3.6 Investigations results on land deformation of Anak Krakatau

By using multi temporal interferometric data processing between 2015 and 2016, the differential phase has been extracted to calculate the deformation using equation 6.2. As shown in Figure 81, the northern and eastern parts of the volcano have more deformations in the range of 20-30 cm (increase). On the other side of the volcano, the deformations were less detected in the range 0-20 cm.

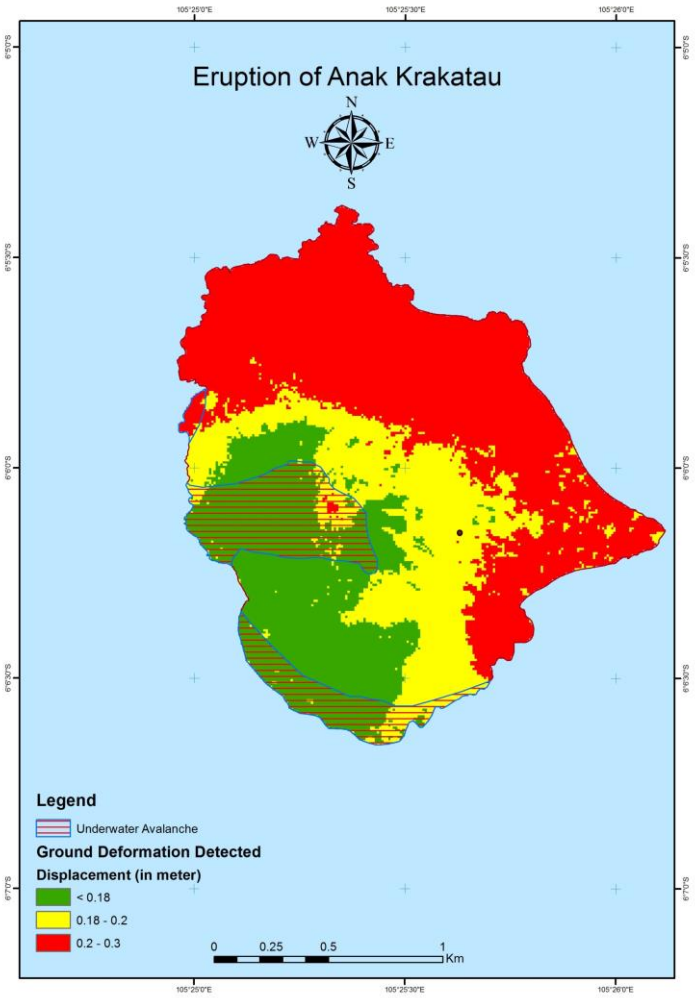

Figure 81: D-InSAR result based on TanDEM-X data 2015-2016

The unequal geodynamic movement of northern and southern parts of Anak Krakatau probably triggered the underwater landslides in the vulnerable area. In addition, the assumption that the underwater landslides resulted from the eruption of Anak Krakatau have a direct contribution to the tsunami wave on the coastal area of Java and Sumatra was confirmed.

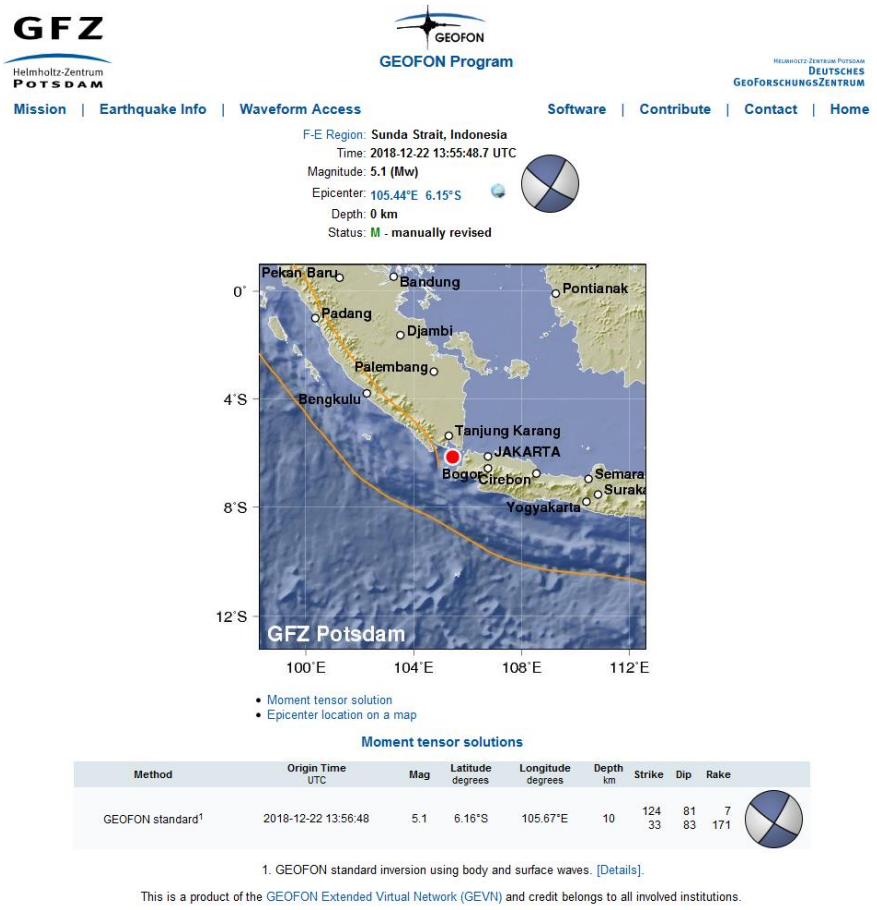

Figure 82: Earthquake occurrence prior to the Sunda Strait Tsunami (Source: Geofon Program)

6.3.7 Discussions

The Sunda Strait tsunami occurred at around 21.00 in the night of December 22, 2018 local time and swept the west coastal area of Java Island as well as the southern coastal area of Sumatra Island. The comparison between lost volume areas (43 Mio m^3) and the volume of the inundation area (15 Mio m^3) clearly showed that there should be a connection between the underwater landslides occurrence prior to the aforementioned tsunami event.

Normally, a tsunami is triggered by the seabed movement following the earthquakes beforehand. Therefore the primary input to be encountered in the InaTEWS is the earthquake detected by the broadband seismometer units. Even though not detected by BMKG, German's GEOFON program published an earthquake occurrence just

around 1 hour before the tsunami hit the coastal area (Figure 82). The epicenter of this earthquake was located in the Krakatau island only 4 km from the erupted volcano with the magnitude of 5.1 (Mw).

In addition, as included in Table 37, the calculated volume for the whole island of Anak Krakatau based on TanDEM-X DEM indicated a sudden loss of approximately 150 Mio m^3 in the period of January 2016 (before the tsunami) to February 2019 (after the tsunami).

6.4 Summary

UAV is of high potential and useful to support rapid mapping activities in terms of accuracy and flexibility. Its high resolution can be turned into higher accuracy by means of integration with existing geospatial data i.e. airborne IFSAR data to map the disaster area immediately. Topographic maps with absolute NSSDA (95%) of 1.5 m (accuracy) can be produced by geo-referencing of UAV data with optical space borne data. It provides relatively inexpensive application in order to generate orthophotos sufficient enough for the 1:5,000 LSTM requirements in Indonesia even in a situation where field GCPs do not exist.

Feature extraction by using photographs taken from UAV has been performed by combining DEM analysis and unsupervised classification in order to get more accurate results. Fuzzy K-Means unsupervised classification indicates a better performance compared to the others for the purpose of disaster-related feature extraction. Hence, the unique combination of UAV and airborne IFSAR data acquisition from different times present rapid mapping activities with a photogrammetric approach in order to provide meaningful result especially in mud flows (lava) object detection.

The second part of the investigation demonstrated how the data sources of UAV and TanDEM-X have provided reliable results for DM purposes. The focus in this case is to extend the applicability of the proposed methodology from the first part of investigations.

It has been shown that up-to-date geo data, in this case TanDEM-X data, play an important role not only in disaster response but also in the analysis of causes. Despite neglecting the tidal and current wave factors in this investigation, it is presumably that the Sunda Strait tsunami was caused by the eruption activity of Anak Krakatau The earthquake occurrence detected by GEOFON was another indication which supports the assumption the tsunami was triggered by the eruption of Anak Krakatau. That means, it is uncertain, but there are clear indicators that the lost masses of the volcano were caused the tsunami. Therefore, the bathymetric survey, as planned for the near future by the responsible institution will probably confirm the underwater terrain changes. Finally, radar interferometry is a potential technology to be used as a support of the Tsunami Early Warning System (TEWS) not only by DEM Generation but also by the differential IFSAR (D-InSAR) technique. D-InSAR can be applied especially in the active volcano island in order to monitor the trend of deformation in advance.

7 Conclusions and further work

As alternative to traditional data collection approaches for Large Scale Topographic Mapping (LSTM) like airborne data acquisition using metric camera sensors and LiDAR, potential data sources namely UAV (with consumer grade camera) data, VHRS imagery and InSAR data were analyzed and combined to support appropriate LSTM for the specific requirements of Indonesia as explained in chapter 2. In a literature study were these data sources examined regarding to the nature and size of its error sources. To increase the geometric quality of these data sources, supporting data, i.e. GCPs and height calibration data, have been identified in chapter 3.

The developed approach has been evaluated and analyzed in chapter 4. Details of the investigations have been presented in chapter 5 and chapter 6 under consideration of the different use cases.

The outcome of the investigations demonstrated the following important findings:

1. The usage of Radar and Optical spaceborne data together with GCP data has improved planimetric and DEM Accuracy. This approach is suitable for 1:10,000 LSTM.
2. DEM Generation by using reference data (GCP for flat area and DEM reference for mountainous area) has improved the TanDEM-X geometric accuracy up to HRTI Level 4 specifications (6 m resolution) for all the LSTM test areas and HRE08 specifications (8 m resolution) for DM test areas at most.
3. UAV acquisition and its GCP requirements (from GNSS or VHRS) for LSTM have been proved as suitable for the range 1:2,500 (planimetric) to 1:5,000 (DEM).
4. The inclusion of building structures in the SfM workflow has improved the external orientation parameters for DEM generation.
5. Disaster-related features have been extracted by combining time series data analysis and unsupervised classification.
6. TanDEM-X data has been used as a potential and essential component for the DSS as an important part of the Tsunami Early Warning System (TEWS).
7. From an economic perspective, even though not investigated in detail, this dissertation has shown how UAV data in a combination with satellite-based data (QuickBird, SPOT6 and TanDEM-X) presented a comparable alternative to the costly airborne data acquisition especially for small AOI (< 50 km^2).

For the future work, there are some suggested topics to be further investigated:

1. The usage of Sentinel 1A/1B data (Copernicus) with lower DEM accuracy and resolution have to be investigated to test the effectiveness of the linear model in DEM generation of other Radar bandwidth i.e. C-Band.
2. The extension introduced to improve the DEM accuracy should be also implemented in the coregistration procedures of TanDEM-X data.
3. The usage of more complex building structures should be further investigated.

The findings in this dissertation can significantly contribute to an enhanced and accelerated provision of large scale topographic maps in Indonesia. However it is the wish of the author that the considered data sources and processing steps contribute as well to the worldwide upgrade of topographical information for the betterment of societal and environmental challenges, especially in third world countries.

References

Act of Republic of Indonesia, 2011. Act No 4 about Geospatial Information. http://www.big.go.id/assets/download/UU_IG/UU%20NO%204%20THN%202011%20TENTANG%20INFORMASI%20GEOSPASIAL.pdf (accessed 5 March 2020)

Agisoft, 2019. Agisoft Metashape User Manual: Professional Edition. Version 1.5. https://www.agisoft.com/pdf/metashape-pro_1_5_en.pdf (accessed 5 March 2020)

Alidoost, F., Azizi, A., Arefi, H., 2015. The Rational Polynomial Coefficients Modification Using Digital Elevation Models. Int. Arch. Photogramm. Remote Sens. Spat. Inf. Sci., 40, 47.

Al-Rousan, N., Cheng, P., Petrie, G., Toutin, Th., Valadan Zoej, M.J., 1997. Automated DEM Extraction and Orthoimage Generation from SPOT Level 1B Imagery, Photogrammetric Engineering & Remote Sensing, Vol.63, No.8, pp. 965-974.

Astrium, 2013. SPOT 6/7 Imagery – User Guide. Toulouse. France

ASPRS, 1990. ASPRS Accuracy Standard for Large-Scale Maps, The American Society for Photogrammetry and Remote Sensing.

Bamler, R., 1997. Digital Terrain Model from Radar Interferometry. In: Photogrammetric Week '97. Wichmann Verlag, Heidelberg.

Bamler, R., and Hartl, P., 1998. Inverse Problems 14 R1.

Bailloeul, T., 2003. Urban digital map updating from satellite high resolution images using GIS data as a priori knowledge. In: 2nd GRSS/ISPRS Joint Workshop on Remote Sensing and Data Fusion over Urban Areas, pp. 283-287.

Bernardo, J., M., 2005. Reference Analysis, in Handbook of Statistics. Dey, D. & Rao, C., eds. Elsevier, pp. 17-90.

BMKG, 2012. Guidance Book of Indonesian Tsunami Early Warning System (InaTEWS) Second edition.

Breit, Helko, et al., 2012. Bistatic and interferometric processing of TanDEM-X data. In: *EUSAR.* 9th European Conference on Synthetic Aperture Radar.

Brown, M., Lowe, D. G., 2005. Unsupervised 3D object recognition and reconstruction in unordered datasets. In Proceedings of the international conference on 3D digital imaging and modelling, pp. 56–63.

Carrivick, J.L., Smith, M.W., Quincey, D.J., 2016. Structure from Motion in the Geosciences, First Edition. John Wiley & Sons, Ltd.

Chen, C., W., and Zebker, H., A., 2002. Phase unwrapping for large SAR interferograms: Statistical segmentation and generalized network models. IEEE Transactions on Geo-

science and Remote Sensing, vol. 40, pp. 1,709-1,719

Cherniakov, Mikhail, 2008. Bistatic Radar: Emerging Technology. New York:Wiley, pp. 2-3.

Copernicus Emergency Management Service, 2018. [EMSR335] Anak Krakatau - INDONESIA: Delineation Map, Monit 01. [Online] Available from: https://emergency.copernicus.eu/mapping/ems-product-component/EMSR335_10ANAKKRAKATAU_01DELINEATION_MONIT01/1 (Accessed 20 Feb. 2019)

Crosetto, M., and Aragues, F.P., 2000. Radargrammetry and SAR Interferometry for DEM generation validation and data fusion. Proceedings of the CEOS SAR Workshop, Toulouse, 26-29 October 1999, ESA SP-450.

D'Errico, M., 2013. Distributed Space Mission for Earth System Monitoring, Springer, New York.

Digital Globe, 2016. Accuracy of WorldView Products, Whitepaper. https://dgv4-cms-production.s3.amazonaws.com/uploads/document/file/154/DG_ACCURACY_WP_V3.pdf (accessed 5 March 2020)

DLR, 2012. TanDEM-X Payload Ground Segment CoSSC Generation and Interferometric Consideration (version 1.0), Oberpfaffenhofen, Germany, TD-PGS-TN-3129, pp. 20-21.

DLR, 2015. TerraSAR-X/TanDEM-X Ground Segment Bandwidth Consideration for Interferometric Application (version 1.0), Oberpfaffenhofen, Germany, TD-GS-TN-4279.

DLR, 2018. TanDEM-X Ground Segment DEM Products Specification Document (version 3.2), Oberpfaffenhofen, Germany, TD-GS-PS-0021.

ESA, 2007. InSAR Principle: Guidelines for SAR Interferometry Processing and Interpretation, Noordwijk, The Netherlands, pp. 18-19.

Federal Geographic Data Committee, 1998. Geospatial Positioning Accuracy Standards Part 3: National Standard for Spatial Data Accuracy (version 2.0), FGDC-STD-001- 1998: Federal Geographic Data Committee, pp.3-4 Washington, D.C.

Fiedler, H., Krieger, G., Werner, M., Hajnsek, I., Moreira, A., Zink, M., 2008. The TanDEM-X Mission Concept, European Conference on Synthetic Aperture RADAR (EUSAR), Friedrichshafen, Germany.

Foch, H., 2009. EXPRESSMaps: Emergency Mapping Service One Click, One Day, One Map, GIM International June, Netherlands.

Forlani, G., Asta, E.D., Diotri, F., Morra di Cella, U., Roncella, R., Santise, M., 2018. Quality Assessment of DSMs Produced from UAV Flights Georeferenced with On-Board RTK Positioning. MDPI Remote Sensing Journal, 10, 311.

Goudarzi, M. A., Landry, R. J., 2017. Assessing horizontal positional accuracy of Google Earth imagery in the city of Montreal, Canada, Geodesy and Cartography, 43(2), pp.

56–65.

Gutjahr, K., Perko, R., Raggam, H., Schardt, M., 2014. The Epipolarity Constraint in Stereo-radargrammetric DEM Generation, IEEE Transaction on Geoscience and Remote Sensing, Vol. 52, No.8.

Haklay, M., 2010. How good is volunteered geographical information? A comparative study of OpenStreetMap and Ordnance Survey datasets, Environment and Planning B: Planning and Design 2010, volume 37, pp. 682-703.

Heady, B., Kroenung, G., Rodarmel, C., 2009. High resolution elevation data (HRE) specification overview. In Proceedings of the Digital Mapping—From Elevation to Information, San Antonio, ASPRS-MAPPS Fall Conference, San Antonio, TX, USA.

Höchle, J., 2012. Medium-Format Cameras and Their Use in Topographic Mapping. The International Annals of the Photogrammetry, Remote Sensing and Spatial Information Sciences. Vol. I-4, pp. 77–82.

Hoffmann, J., Walter, D., 2006. How complementary are SRTM-X and –C band digital elevation models?, Photogrammetric Engineering & Remote Sensing, 72(3), pp. 261-268.

Holland, D.A., Boyd, P., Marshall, P., 2006. Updating topographic mapping in Great Britain using imagery from high-resolution satellite sensors, ISPRS Journal of Photogrammetry & Remote Sensing 60, pp. 212-223.

Howard. A., 1994. Accuracy of Topographic Maps Derived from ERS-1 Interferometric Radar. IEEE Transaction on Geoscience and Remote Sensing Vol. 32, No.4, pp. 823-836.

Infoterra, 2009. 3D Topographic Mapping with TerraSAR-X: Unique Mapping Concepts Using High-Resolution Spaceborne SAR, Germany.

ISO, 2013. Geographic information – Data quality measures. (ISO 19157:2013). https://www.iso.org/standard/32575.html (accessed 5 March 2020).

Jacobsen, K., 2013. DEM Generation from High Resolution Satellite Imagery, PFG No. 5, Stuttgart, DOI: 10.1127/1432-8364/2013/0194.

Jacobsen, K., 2018. Systematic Geometric Image Errors of Very High Resolution Optical Satellites. The International Archives of the Photogrammetry, Remote Sensing and Spatial Information Sciences, Volume XLII-1, ISPRS TC I Mid-term Symposium ”Innovative Sensing – From Sensors to Methods and Applications”, Karlsruhe.

Javernick, L., Brasington, J., Caruso, B., 2014. Modeling the topography of shallow braided rivers using Structure-from- Motion Photogrammetry. Geomorphology 213. pp. 166-282.

Kidd, R., McCallum, I., Fritz, S., Kraxner, F., Obersteiner, M., 2009. GEO Information For Disaster Recovery - Case Study: The use of Orthophotos in Aceh, Indonesia. Interim Report. International Institute for Applied System Analysis, Austria.

Kiefl, N., Koppe, W., Hennig, S.D., 2010. TerraSAR-X Stereo Digital Elevation Models for

Complex Terrain Conditions in Alpine Regions and its suitability for Orthorectification Purposes of Optical and SAR Imagery. In: Wagner W., Székely, B. (eds.): ISPRS TC VII Symposium – 100 Years ISPRS, Vienna, Austria, July 5–7, 2010, IAPRS, Vol. XXXVIII, Part 7B.

Kiefl, R., Kemper, T., Mehl, H., Riedlinger, T., Scholte, K., Voigt, S., 2007. Satellite Image Analysis for Disaster and Crisis-Management Support. IEEE Transactions on Geoscience and Remote Sensing Vol. 45 No.6 June 2007.

Klonus, S., Ehlers, M., 2008. Pansharphening with TerraSAR-X and Optical Data. In: proceedings of the 3rd TerraSAR-X Science Team Meeting. Darmstadt, Germany: German Aerospace Center, pp. 25-26.

Konecny, G., Breitkopf, U., Radtke, A., Lee, K., 2015. The Status of Topographic Mapping in the World, Final Report, UNGGIM - ISPRS.

Krieger, G., Fiedler, H., Moreira, A., 2004. Bi and multistatic SAR: Potential and challenges. In Proc. EUSAR, 2004.

Krieger, G., Moreira, A., Fiedler, H., Hajnsek, I., Werner, M., Younis, M., Manfred, Z., 2007. TanDEM-X: A Satellite Formation for High-Resolution SAR Interferometry. IEEE Transactions on Geoscience and Remote Sensing Vol. 45 No.11.

Lachaise, M., Fritz, T., and Eineder, M., 2014. Dual-baseline phase unwrapping challenges in the TanDEM-X mission. In EUSAR 2014; 10th European Conference on Synthetic Aperture Radar;Proceedings of, pages 1–4. VDE.

Langaas, S., and Tveite, H., 1995. To Characterise and Measure Completeness of Spatial Data: A Discussion Based on the Digital Chart of the World (DCW). In: Bjørke, J.T., (ed) Proceedings from the 5th Scandinavian Research Conference on Geographical Information Systems, Trondheim, Norway, pp. 155-161.

Li, Y., 2008. Vehicle extraction using histogram and genetic based fuzzy image segmentation from high resolution UAV aerial imagery. The International Archives of the Photogrammetry, Remote Sensing and Spatial Information Sciences. Vol. XXXVII. Part B3b., pp. 529–533.

Maiyo, L., Kerle, N. and Köbben, B., 2009. Collaborating via GIS and Geo-Web Services: Disaster Mapping 2.0, GIM International June 2009, Netherlands.

Mercer, B., 2009. Countrywide Coverage of RADAR DTMs – The Intermap Approach. Photogrammetric Week, Stuttgart, Germany.

Mura, J.C., Pinheiro, M., Rosa, R., Moreira, J.R., 2012. A Phase-Offset Estimation Method for InSAR DEM Generation Based on Phase-Offset Functions. Remote Sensing Journal, ISSN 2072-4292, pp. 745-761.

Neitzel, F., 2011. Mobile 3D Mapping with a Low-cost UAV System. International Archives of the Photogrammetry, Remote Sensing and Spatial Information Sciences, Zurich, Switzerland, Vol. XXXVIII-1/C22.

Perko, R., Raggam, H., Schardt, M., and Roth, P.M., 2018. Very High Resolution Mapping with the Pléiades Satellite Constellation, American Journal of Remote Sensing, Vol. 6, No.2, pp. 89-99, doi: 10.11648/j.ajrs.20180602.14.

Percivall, G., Alameh, N., Moe, K., and Evans, J., 2012. Strengthening disaster management using Earth Observations - GEOSS and CEOS activities, Geoscience and Remote Sensing Symposium (IGARSS), IEEE International, pp. 3,525-3,528.

Rahmani, M. K., Pal, N., and Arora, K., 2014. Clustering of Image Data using K-Means and Fuzzy K-Means. International Journal of Advanced Computer Science and Applications. Vol. 5. No.7., pp. 160-163.

Richards, Mark A. A., 2007. A Beginner's guide to Interferometric SAR Concepts and Signal Processing. IEEE A&E Systems Magazine Vol.22 No.9.

Rodriguez, E., Morris, C., and Belz, J., 2006. A global assessment of the SRTM performance. Photogrammetric Engineering & Remote Sensing, 72(3), pp. 249–260.

Rossi, C., Rodriguez Gonzalez, F., Fritz, T., Yague Martinez, N., Eineder, M., 2012. TanDEM-X calibrated Raw DEM generation. ISPRS Journal of Photogrammetry and Remote Sensing, 73, pp. 12-20. DOI: http://dx.doi.org/10.1016/j.isprsjprs.2012.05.014 (accessed 5 March 2020).

Schneiderhan, Tobias, et al., 2010. Insights to the Emergency Mapping Service within the GMES project SAFER – Highlights, main achievements and challenges. In: Living Planet Symposium, Bergen, Norway.

Shen, X., Li, Q., Wu, G., Zhu, J., 2017. Bias compensation for rational polynomial coefficients of high-resolution satellite imagery by local polynomial modeling. Remote Sens., 9, 200.

Singh, S., 2003. Simple random sampling in Advanced Sampling Theory with Applications. Springer Netherlands, pp. 71-36.

Snavely, N., Seitz, S.N., Szeliski, R., 2008. Modeling the world from internet photo collections. International Journal of Computer Vision 80: 189-210.

Soergel, U, Jacobsen, K., Schack, L., 2013. The TanDEM-X Mission: Data collection and deliverables. In Photogrammetric Week, Institute for Photogrammetry, Stuttgart, Germany, pp. 193–203. https://phowo.ifp.uni-stuttgart.de/publications/phowo13/170Soergel.pdf (accessed 5 March 2020).

Tampubolon, W., and Hendrayana, E., 2012. Orthorectification of Very High Resolution Satellite Imagery in the context of Detail Spatial Planning Purposes (study area: National Strategic Region of Borobudur Temple-Indonesia), In: Proceedings of Applied Geoinformatics for Society and Environment, Vol. 1, 2nd edition, pp. 45-51.

Tampubolon, W., and Reinhardt, W., 2014. UAV Data Processing for Large Scale Topographical Mapping, The International Archives of Photogrammetry, Remote Sensing and Spatial Information Science, XL-5, ISPRS Technical Commission V Symposium.

Tampubolon, W., and Reinhardt, W., 2015. Analysis of Radar and Optical Space Borne

Data for Large Scale Topographical Mapping, The International Archives of Photogrammetry, Remote Sensing and Spatial Information Science, XL-3/W2, PIA15+HRIGI15 - Joint ISPRS Conference.

Tampubolon, W., and Reinhardt, W., 2015. UAV Data Processing for Rapid Mapping Activities, The International Archives of Photogrammetry, Remote Sensing and Spatial Information Science, XL-3/W3, 371-377.

Tampubolon, W., and Reinhardt, W., 2018. Quality Assessment of an Extended Interferometric Radar Data Processing Approach, The International Archives of Photogrammetry, Remote Sensing and Spatial Information Science, XLII-4, 615-621.

Tampubolon, W. and Reinhardt, W., 2019. Utilization of TanDEM-X data to identify the potential trigger of 2018's Sunda Strait Tsunami in Indonesia. In: Kyriakidis, P., Hadjimitsis, D., Skarlatos, D., & Mansourian, A. (Eds.), 2019. Accepted Short Papers from the 22nd AGILE Conference on Geo-Information Science.

Toutin, T., 2012. Radarsat-2 DSM Generation With New Hybrid, Deterministic, and Empirical Geometric Modeling Without GCP, IEEE Transaction On Geoscience and Remote Sensing, Vol. 50, No.5.

Veci, L., 2016. Interferometry Tutorial. Array Sytems Computing Inc., http://step.esa.int/docs/tutorials/S1TBX%20Stripmap%20Interferometry%20with%20Sentinel-1%20Tutorial.pdf (accessed 5 March 2020).
Wang, B.-C., 2008. Digital Signal Processing Techniques and Applications in Radar Image Processing. Wiley, Hoboken.

Weber, M., and J. Herrmann, 2006. TerraSAR-X and TanDEM-X: Global mapping in 3D using radar. Proc. Second Int. Workshop "The Future of Remote Sensing," Antwerp, Belgium, ISPRS Intercommission Working Group I/V Autonomous Navigation, 36–1/W44.

Wegner, J.D., Ziehn, J.R., Soergel, U., 2014. Combining High-Resolution Optical and InSAR Features for Height Estimation of Buildings with Flat Roofs. IEEE Transactions of Geoscience and Remote Sensing, Vol. 52, No. 9, pp. 5840-5854. DOI: 10.1109/TGRS.2013.2293513.

Westoby, M.J., Brasington, J., Glasser, N.F., Hambrey, M.J., Reynolds, J.M., 2012. Structure-from-Motion photogrammetry: a low-cost, effective tool for geoscience applications. Geomorphology 179, pp. 300-314.

Willis, J.N., Griffiths, H.D., 2007. Advances in Bistatic Radar. SciTech Publishing, Inc., pp. 411-423.

Zhang, Y., Zhang, L.N., Yang, C.D., Bao, W.D., Yuan, X.X., 2011. Surface area processing in GIS for different mountain regions. For. Ecosyst., 13, pp. 311–314.

Zhang, Z., Wu, J., Zhang, Y., Zhang, Y. And Zhang, J., 2004. Multi-View 3D City Model Generation with Image Sequences. International Archives of Photogrammetry and Remote Sensing, Istanbul, Turkey, Vol. 34, Part 5, pp. 351-356.

Zhou, Y., Zhou, C., E, D., Wang, Z., Tian, X., 2011. InSAR DEM Reconstruction with ICE-

SAT GLAS Data of the Grove Mountains Area. Fringe 2011 Workshop, Frascati, Italy.